

**BEHAVIOUR AND STRENGTH OF FULLY ENCASED  
COMPOSITE COLUMNS**

**MD. SOEBUR RAHMAN**

**DOCTOR OF PHILOSOPHY  
(CIVIL & STRUCTURAL)**



**DEPARTMENT OF CIVIL ENGINEERING  
BANGLADESH UNIVERSITY OF ENGINEERING AND TECHNOLOGY  
DHAKA, BANGLADESH**

**DECEMBER, 2016**

**BEHAVIOUR AND STRENGTH OF FULLY ENCASED  
COMPOSITE COLUMNS**

by

**Md. Soebur Rahman**

A thesis submitted to the Department of Civil Engineering of Bangladesh University of Engineering and Technology, Dhaka, in partial fulfillment of the requirements for the degree

of

**DOCTOR OF PHILOSOPHY**

**(CIVIL & STRUCTURAL)**



DEPARTMENT OF CIVIL ENGINEERING  
**BANGLADESH UNIVERSITY OF ENGINEERING AND TECHNOLOGY**  
**DHAKA, BANGLADESH**

December, 2016

## CERTIFICATE OF APPROVAL

The thesis titled “**Behaviour and Strength of Fully Encased Composite Columns**”, by Md. Soebur Rahman, Student Number 0412044001 (F) Session: April/2012 has been accepted as satisfactory in partial fulfillment of the requirements for the degree of Doctor of Philosophy (Civil & Structural) on 04 December, 2016.

### BOARD OF EXAMINERS

---

Dr. Mahbuba Begum  
Professor  
Department of Civil Engineering  
BUET, Dhaka-1000

Chairman  
(Supervisor)

---

Dr. Raquib Ahsan  
Professor  
Department of Civil Engineering  
BUET, Dhaka-1000

Member  
(Co-Supervisor)

---

Dr. Abdul Muqtadir  
Professor and Head  
Department of Civil Engineering  
BUET, Dhaka-1000

Member  
(Ex-officio)

---

Dr. Syed Fakhrul Ameen  
Professor  
Department of Civil Engineering  
BUET, Dhaka-1000

Member

---

Dr. Ahsanul Kabir  
Professor  
Department of Civil Engineering  
BUET, Dhaka-1000.

Member

---

Dr. Md. Nazrul Islam  
Professor  
Department of Civil Engineering  
DUET, Gazipur.

Member  
(External)

## DECLARATION

Except for the contents where specific reference have been made to the work of others, the studies embodied in this thesis is the result of investigation carried out by the author. No part of this thesis has been submitted to any other University or other educational establishment for a Degree, Diploma or other qualification (except for publication).

A handwritten signature in black ink, appearing to read 'Md. Soebur Rahman', written in a cursive style.

(Signature of the Student)

Md. Soebur Rahman

## **ACKNOWLEDGEMENT**

In the name of Allah, the most Gracious and the most Merciful

The author sincerely expresses his deepest gratitude to the Almighty.

First and foremost, the author would like to express thank to his supervisor Dr. Mahbuba Begum, Professor, Department of Civil Engineering, BUET. It has been an honour to be her first Ph.D. student. Her guidance on the research methods, deep knowledge, motivation, encouragement and patience in all the stages of this research work has been made the task of the author less difficult and made it possible to complete the thesis work.

The author also wishes to express his deepest gratitude to his co-supervisor Dr. Raquib Ahsan, Professor, Department of Civil Engineering, BUET for his constant guidance, invaluable suggestions, motivation in difficult times and affectionate encouragement, which were extremely helpful in accomplishing this study.

The author also grateful to all the most respected members of Doctoral Committee for their valuable and constructive advice and suggestions throughout this research works.

The author also takes the opportunity to pay his heartfelt thanks to all the staff members of Concrete Laboratory and Strength of Materials Laboratory for their consistent support and painstaking contributions to the research and experimental work.

The author also appreciatively remembers the assistance and encouragement of his friends and well wishers and everyone related to carry out and complete this study. Finally, the author wishes to express his deep gratitude to his family members, wife and two daughter (Sumya and Safika) for their constant support, encouragement and sacrifice throughout the research work.

## ABSTRACT

This study presents experimental as well as extensive numerical investigations on fully encased composite (FEC) columns under concentric and eccentric axial loads. The experimental program consisted of thirteen (13) FEC columns of two different sizes with various percentages of structural steel and concrete strength. These FEC columns were tested for concentrically and eccentrically applied axial loads to observe the failure behaviour, the ultimate load carrying capacity and axial deformation at the ultimate load. Numerical simulations were conducted on FEC columns under axial compression and bending using ABAQUS, finite element code. Both geometric and material nonlinearities were included in the FE model. A concrete damage plasticity model capable of predicting both compressive and tensile failures, was used to simulate the concrete material behaviour. Riks solution strategy was implemented to trace a stable peak and post peak response of FEC columns under various conditions of loading. To validate the model, simulations were conducted for both concentrically and eccentrically loaded FEC test specimens from current study and test specimens from published literatures, encompassing a wide variety of geometries and material properties. Comparisons were made between the FE predictions and experimental results in terms of peak load and corresponding strain, load versus deformation curves and failure modes of the FEC columns. In general, the FE model was able to predict the strength and load versus displacement behaviour of FEC columns with a good accuracy.

A parametric study was conducted using the numerical model to investigate the influences of geometric and material properties of FEC columns subjected to axial compression and bending about strong axis of the steel section. The geometric variables were percentage of structural steel, column slenderness ( $L/D$ ), eccentricity ratio ( $e/D$ ) and spacing of ties ( $s/D$ ). The compressive strength of concrete ( $f_{cu}$ ) and yield strength of structural steel were used as the material variables in the parametric study. The strength of the materials were varied from normal to ultra-high strength. In general,  $L/D$  ratio,  $e/D$  ratio, strength of steel and concrete were found to greatly influence the overall capacity and ductility of FEC columns. The effects of ultra-high strength concrete (120 MPa) and ultra-high strength steel of 913 MPa on the FEC column behaviour was also explored. Use of ultra-high strength structural steel in FEC column increased the overall capacity by 40% accompanied by a reduction in the ductility by 17 %. However the ductility was regained when the tie spacing was reduced by 50%. Finally, the experimental as well as the numerical results were compared with the code (ACI 2014, AISC-LRFD 2010 and Euro code 4) predicted results. The equations given by the three codes can safely predict the capacity of FEC columns constructed with UHSM (concrete 120 MPa and structural steel 913 MPa) for concentric axial load. For concentrically loaded FEC columns the material limits specified in these codes may be extended to cover the range of ultra-high strength materials. However, the simplified plastic stress distribution proposed in AISC-LRFD (2010) was found to be unsafe for predicting the load and moment capacities of eccentrically loaded FEC columns with ultra-high strength structural steel and concrete.

## TABLE OF CONTENTS

ACKNOWLEDGEMENT	iv
ABSTRACT	v
TABLE OF CONTENTS	vi
LIST OF FIGURES	xi
LIST OF TABLES	xiv
LIST OF SYMBOLS	xvi
LIST OF ABBREVIATIONS	xix
CHAPTER 1 INTRODUCTION	
1.1 General	1
1.2 Objectives and Scope of the Study	3
1.3 Organization of the Thesis	5
CHAPTER 2 LITERATURE REVIEW	
2.1 Introduction	7
2.2 Types of Composite Columns	8
2.3 Research on Steel-Encased Concrete Columns	9
2.3.1 Experimental investigations	9
2.3.2 Numerical and analytical investigations	15
2.3.3 Comparison of codes	18
2.4 Conclusions	22
CHAPTER 3 REVIEW OF DESIGN CODES ON COMPOSITE COLUMNS	
3.1 Introduction	23
3.2 ACI-318 (2014)	23
3.2.1 Axial compressive strength	23
3.2.2 Flexural and axial loads	25
3.3 AISC-LRFD (2010)	26
3.3.1 Axial compressive strength	26
3.3.2 Axial loads and flexure (P-M)	28
3.4 Euro Code 4 (2005)	31
3.4.1 Resistance of cross sections	31
3.4.2 Axial load and bending moment (P-M)	32
3.5 Material Properties and Detailing Criteria	38
3.6 Conclusions	41

CHAPTER 4	EXPERIMENTAL INVESTIGATIONS OF FEC COLUMNS	
4.1	Introduction	42
4.2	Test Program	42
4.2.1	Description of test specimens	42
4.2.2	Explanation of test parameters	45
4.3	Column Fabrication	46
4.3.1	Steel section fabrication	46
4.3.2	Concrete mix design	47
4.3.3	Concrete placement	48
4.4	Material Properties	49
4.4.1	I-Shaped structural steel	49
4.4.2	Steel reinforcement	50
4.4.3	Concrete	51
4.5	Test Setup and Data Acquisition System	53
4.5.1	Setup and instrumentation of concentrically loaded FEC columns	54
4.5.2	Setup and instrumentation of eccentrically loaded FEC columns	55
4.6	Observations and Failure Mode	55
4.6.1	Failure of concentrically loaded columns	56
4.6.1.1	Column in Group SCN4A	57
4.6.1.2	Column in Group SCN4B	59
4.6.1.3	Column in Group SCH6A	61
4.6.1.4	Column in Group SCH6B	63
4.6.2	Failure of eccentrically loaded columns	64
4.6.2.1	Column Group SCN4E	64
4.6.2.2	Column Group SCH6E	65
4.7	Load versus Deformation Relationship	66
4.7.1	Concentrically loaded columns	66
4.7.2	Eccentrically loaded columns	70
4.8	Conclusions	71
CHAPTER 5	FINITE ELEMENT MODEL OF FEC COLUMNS	
5.1	Introduction	73
5.2	Properties of Test Specimens	73
5.2.1	Test specimens from current study	74
5.2.1.1	Normal strength concrete FEC columns	74



5.2.1.2 High strength concrete FEC columns	75
5.2.2 Test specimens from published literature	76
5.3 Geometric Properties of the Finite Element Model	83
5.3.1 Element selection	83
5.3.2 Mesh description	84
5.3.3 Modeling of steel-concrete interactions	85
5.3.4 End boundary conditions	85
5.4 Material Properties	86
5.4.1 Steel	86
5.4.2 Concrete	87
5.4.2.1 Stress-Strain relationship for concrete in compression	89
5.4.2.2 Stress-Strain relationship for concrete in tension	92
5.5 Load Application and Solution Strategy	93
5.5.1 Newton Raphson and Modified Newton Raphson Methods	93
5.5.2 The Riks Method	94
5.6 Conclusions	96
<b>CHAPTER 6 COMPARISON OF NUMERICAL RESULTS WITH EXPERIMENTAL DATA</b>	
6.1 Introduction	97
6.2 Performance of Finite Element Model	97
6.2.1 Axial load versus axial deformation	97
6.2.1.1 Test specimens from current study	98
6.2.1.2 Test specimens from published literature	102
6.2.2 Axial capacity and axial strain	107
6.2.2.1 Test specimens from current study	107
6.2.2.2 Test specimens from published literature	108
6.2.3 Failure Modes	112
6.2.3.1 Test specimens from current study	112
6.2.3.2 Test specimens from published literature	114
6.3 Contributions of Steel and Concrete in the Capacity of FEC Columns	119
6.4 Effect of Concrete Strength on Axial Capacity of FEC Column	121
6.5 Conclusions	121
<b>CHAPTER 7 PARAMETRIC STUDY</b>	
7.1 Introduction	123

7.2 Design of Parametric Study	124
7.2.1 Percentage of I-shaped structural steel	124
7.2.2 Column slenderness ratio, $L/D$	126
7.2.3 Load eccentricity ratio, $e/D$	126
7.2.4 Concrete compressive strength, $f_{cu}$	126
7.2.5 Transverse reinforcement spacing-to-depth ratio, $s/D$	126
7.3 Material Properties of Parametric Columns	128
7.4 Results and Discussion	129
7.4.1 Effect of structural steel percentages	129
7.4.1.1 Load versus axial deformation response	130
7.4.1.2 Axial capacity of FEC columns	131
7.4.1.3 Ductility index for FEC columns	133
7.4.1.4 Modes of failure	134
7.4.2 Effect of overall column slenderness ratio	135
7.4.2.1 Load versus axial deformation response	136
7.4.2.2 Peak load and corresponding moment	137
7.4.2.3 Load versus lateral displacement response	138
7.4.2.4 Load versus moment response	139
7.4.2.5 Modes of failure	140
7.4.3 Effect of load eccentricity ratio	142
7.4.3.1 Load versus average axial deformation response	142
7.4.3.2 Peak load and corresponding moment	143
7.4.3.3 Load versus lateral displacement responses	144
7.4.3.4 Axial load versus moment	145
7.4.4 Effect of concrete compressive strength	146
7.4.4.1 Load versus average axial deformation	147
7.4.4.2 Peak load and corresponding moment	148
7.4.4.3 Behaviour of FEC columns with UHSM	149
7.4.5 Effect of transverse reinforcement spacing	150
7.4.5.1 Load versus axial deformation	151
7.4.5.2 Peak load for different tie spacing	152
7.4.5.3 Effect of tie spacing with UHSM	152
7.5 Conclusions	154

CHAPTER 8	COMPARISONS OF FEC COLUMN STRENGTH WITH DESIGN CODES	
8.1	Introduction	156
8.2	Ultimate Axial Capacity for Concentric Load	156
8.2.1	Test specimens from current experimental study	157
8.2.2	Test specimens from published literature	158
8.2.3	Specimens from parametric study	159
8.2.4	Specimens with UHSM	160
8.3	Eccentrically Loaded FEC Columns	162
8.3.1	Load versus moment (P-M) curves	163
8.3.2	Comparison between numerical and code predicted capacities	166
8.4	Conclusions	167
CHAPTER 9	CONCLUSIONS AND RECOMMENDATIONS	
9.1	Summary	168
9.2	Conclusions	169
9.2.1	Experimental and numerical study	169
9.2.2	Parametric study	169
9.2.3	Review of code provisions	171
9.3	Recommendations for Future Research	171
REFERENCES		173

## LIST OF FIGURES

Figure 1.1 Typical X-sections of composite columns	2
Figure 2.1 Detail X-sections of different composite columns	8
Figure 3.1 Interaction diagram (P-M) for composite columns	28
Figure 4.1 Geometry of FEC columns	44
Figure 4.2 Reinforcement for FEC columns	46
Figure 4.3 I-shaped structural steel sections	47
Figure 4.4 Structural steel with reinforcement in FEC columns	47
Figure 4.5 Concrete placement in FEC columns	49
Figure 4.6 Structural steel plate samples for tension test	50
Figure 4.7 Reinforcement samples for tension test	50
Figure 4.8 Typical 3-D view of concrete cylinders	51
Figure 4.9 Schematic diagram of test set up	53
Figure 4.10 Test set up for concentric axial load in the laboratory	54
Figure 4.11 Test set up for eccentric axial load in the laboratory	55
Figure 4.12 Local failure of a column during test	56
Figure 4.13 Failure modes of column Group SCN4A	57-58
Figure 4.14 Failure modes of column Group SCN4B	59-60
Figure 4.15 Failure modes of column Group SCH6A	61-62
Figure 4.16 Failure modes of column Group SCH6B	63-64
Figure 4.17 Failure modes of column SCN4E	65
Figure 4.18 Failure modes of column SCH6E	66
Figure 4.19 Axial load versus axial deformation for columns in Group SCN4A	67
Figure 4.20 Axial load versus axial deformation for columns in Group SCN4B	68
Figure 4.21 Axial load versus axial deformation for columns in Group SCH6A	69
Figure 4.22 Axial load versus axial deformation for columns in Group SCH6B	69
Figure 4.23 Axial load versus axial deformation for column SCN4E	70
Figure 4.24 Axial load versus axial deformation for column SCH6E	71
Figure 5.1 Typical cross section of FEC columns (Chen and Yeh 1996)	76
Figure 5.2 Typical cross section of FEC columns (Morino et al. 1984)	78
Figure 5.3 Typical cross section of FEC columns (Matsui 1979)	79
Figure 5.4 Typical cross section of FEC columns (Dundar et al. 2008)	79
Figure 5.5 Typical cross section of FEC columns (Kim et al. 2012)	81
Figure 5.6 Column test set-up used (Kim et al. 2012)	82

Figure 5.7 Finite elements used in the numerical simulation	84
Figure 5.8 Axial load versus aspect ratio	84
Figure 5.9 Finite element mesh for FEC columns	85
Figure 5.10 End boundary conditions in FE models for concentric and eccentric load	86
Figure 5.11 Stress-strain curve for steel used in the numerical analysis	87
Figure 5.12 Uniaxial compressive and tensile behaviour of concrete used by damage plasticity model in ABAQUS	89
Figure 5.13 Stress-strain curves for concrete in uniaxial compression	92
Figure 5.14 Stress-strain curve for concrete in uniaxial tension	93
Figure 5.15 Newton-Raphson iterative method	94
Figure 5.16 Modified Newton-Raphson iterative method	94
Figure 5.17 Riks solution strategy	95
Figure 6.1 Experimental and numerical load versus deformation for Group SCN4A	99
Figure 6.2 Experimental and numerical load versus deformation for Group SCN4B	99
Figure 6.3 Experimental and numerical load versus deformation for Group SCH6A	100
Figure 6.4 Experimental and numerical load versus deformation for Group SCH6B	101
Figure 6.5 Experimental and numerical load versus deformation for column SCN4E	102
Figure 6.6 Experimental and numerical load versus deformation for column SCH6E	102
Figure 6.7 Experimental and numerical load versus deformation for column SRC1	103
Figure 6.8 Experimental and numerical load versus deformation for column SRC2	103
Figure 6.9 Experimental and numerical load versus deformation for column SRC3	104
Figure 6.10 Experimental and numerical load versus deformation for column SRC4	104
Figure 6.11 Experimental and numerical load versus deformation for column SRC5	104
Figure 6.12 Experimental and numerical load versus deformation for column SRC6	105
Figure 6.13 Experimental and numerical load versus deformation for column SRC7	105
Figure 6.14 Experimental and numerical load versus deformation for column C1	106
Figure 6.15 Experimental and numerical load versus deformation for column C2	106
Figure 6.16 Failure of column SCN4B1 (a) Experimental (b) Numerical	113
Figure 6.17 Stress-contour in structural steel at failure (a) SCH6B and (b) SCH6E	113-114
Figure 6.18 Experimental failure of column for column (Kim et al. 2012)	114
Figure 6.19 Numerical failure of column C1	115
Figure 6.20 Numerically determined yielding of transverse reinforcement	116
Figure 6.21 Numerically determined yielding of transverse reinforcement	117
Figure 6.22 Experimental failure of columns CC3 and CC4 (Dundar et al. 2008)	118

Figure 6.23 Numerical failure of columns CC3 and CC4	118
Figure 6.24 Contribution of individual elements in FEC columns in ultimate capacity	119-120
Figure 6.25 Load versus percentage of structural steel in columns	120
Figure 6.26 Effects of concrete strength on load-deformation of FEC columns	121
Figure 7.1 Typical cross section and elevation of parametric FEC column	125
Figure 7.2 Effect of structural steel on load- deformation response curve (Group 1)	130
Figure 7.3 Effect of structural steel on load- deformation response curve (Group 2)	131
Figure 7.4 Effect of structural steel on load- deformation response curve (Group 3)	131
Figure 7.5 Effect of structural steel on axial capacity increment	133
Figure 7.6 Stress contour of concrete at failure	135
Figure 7.7 Stress contour of structural steel at failure	135
Figure 7.8 Effect of L/D ratio on axial load versus axial deformation (Group 4)	136
Figure 7.9 Effect of L/D ratio on axial load versus axial deformation (Group 5)	136
Figure 7.10 Effect of L/D ratio on axial load	138
Figure 7.11 Effect of (L/D) ratio on axial load versus lateral displacement (Group 4)	138
Figure 7.12 Effect of (L/D) ratio on axial load versus lateral displacement (Group 5)	139
Figure 7.13 Effect of L/D ratio on axial load versus moment (Group 4)	139
Figure 7.14 Effect of L/D ratio on axial load versus moment (Group 5)	140
Figure 7.15 Deformed shape and stress contour of concrete at failure	141
Figure 7.16 Deformed shape and stress contour of structural steel at failure	142
Figure 7.17 Effect of e/D ratio on load versus axial deformation (Group 6)	143
Figure 7.18 Effect of (e/D) ratio on load versus axial deformation (Group 7)	143
Figure 7.19 Effect of (e/D) ratio on axial load versus lateral displacement (Group 6)	145
Figure 7.20 Effect of (e/D) ratio on load versus lateral displacement (Group 7)	145
Figure 7.21 Effect of e/D ratio on load versus moment (Group 6)	146
Figure 7.22 Effect of e/D ratio on load versus moment (Group 7)	146
Figure 7.23 Effect of concrete compressive strength on load vs deformation (Group 8)	147
Figure 7.24 Effect of concrete compressive strength on load vs deformation (Group 9)	147
Figure 7.25 Stress-strain relationships of high-strength steel and concrete (Kim et al. 2012)	149
Figure 7.26 Effect of transverse reinforcement spacing on axial load versus deformation	151
Figure 7.27 Effect of transverse reinforcement spacing on axial load vs deformation UHSM	153
Figure 8.1 Load versus moment curves for FEC columns with normal strength material	164
Figure 8.2 Load versus moment curves for FEC columns with high strength concrete	165
Figure 8.3 Load versus moment curve for FEC columns with UHSM	166

## LIST OF TABLES

Table 3.1 Plastic capacities for rectangular FEC column major axis bending AISC (2010)	29
Table 3.2 Plastic capacities for rectangular FEC column minor axis bending AISC (2010)	30
Table 3.3 Stress distribution at each point of FEC column major axis bending EC4 (2005)	35
Table 3.4 Stress distribution at each point of FEC column minor axis bending EC4 (2005)	37
Table 3.5 Comparison on material strength and design criteria of different codes	38
Table 4.1 Geometric properties of test specimens with normal strength concrete (28 MPa)	45
Table 4.2 Geometric properties of test specimens with high strength concrete (42MPa)	45
Table 4.3 Concrete mix design at saturated surface dry (SSD) conditions	48
Table 4.4 Tensile properties of structural steel plate	50
Table 4.5 Tensile properties of steel reinforcement	51
Table 4.6 Designation of concrete cylinder in different strength	52
Table 4.7 Concrete cylinder strength	52
Table 4.8 Peak load and strain for concentrically loaded columns	67
Table 4.9 Peak load and strain for eccentrically loaded columns	70
Table 5.1 Material properties of concrete and reinforcement	74
Table 5.2 Material properties of structural steel plate	75
Table 5.3 Material properties of concrete and reinforcement	75
Table 5.4 Material properties of structural steel plate	75
Table 5.5 Geometric properties of test specimens (Chen and Yeh 1996)	77
Table 5.6 Materials properties of concrete and reinforcement (Chen and Yeh 1996)	77
Table 5.7 Materials properties of structural steel (Chen and Yeh 1996)	77
Table 5.8 Geometric properties of reference specimens	80
Table 5.9 Material properties of concrete and reinforcement	80
Table 5.10 Material properties of structural steel plate	80
Table 5.11 Geometric properties of test specimens (Kim et al. 2012)	81
Table 5.12 Materials properties of concrete and reinforcement (Kim et al. 2012)	82
Table 5.13 Materials properties of structural steel (Kim et al. 2012)	82
Table 6:1 Comparison of numerical and experimental results from current study	108
Table 6:2 Comparison of numerical and experimental results for concentric loads	109
Table 6.3 Comparison of numerical and experimental results for eccentrically loaded columns	110

Table 6.4 Comparison of numerical and experimental results of FEC columns with high strength materials	111
Table 6.5 Ductility index of FEC columns with high strength materials	112
Table 7.1 Columns for investigating the effect of structural steel ratio	127
Table 7.2 Columns for investigating the effect of slenderness ratio (L/D)	127
Table 7.3 Columns for investigating the effect of eccentricity ratio (e/D)	127
Table 7.4 Columns for investigating the effect of concrete compressive strength ( $f_{cu}$ )	128
Table 7.5 Columns for investigating effect of transverse reinforcement spacing (s/D)	128
Table 7.6 Effect of structural steel ratio on axial load capacity	132
Table 7.7 Ductility index of column Group 1	134
Table 7.8 Ductility index of column Group 2	134
Table 7.9 Ductility index of column Group 3	134
Table 7.10 Effect of structural steel ratio at peak load	137
Table 7.11 Effect of eccentricity ratio on peak load and moment	144
Table 7.12 Effect of concrete compressive strength on peak load and moment	148
Table 7.13 Effect of UHSM on peak load of FEC columns	150
Table 7.14 Ductility index of column Group 10	151
Table 7.15 Effect of transverse reinforcement spacing at peak load	152
Table 7.16 Ductility index of column with normal and high strength of materials	153
Table 8.1 Comparison between test results and predicted values using code guidelines	158
Table 8.2 Comparison between test results and code predicted results	158
Table 8.3 Comparison between numerical results and code predicted results (Normal concrete and normal strength structural steel)	159
Table 8.4 Comparison between numerical results and code predicted results (Medium strength concrete and normal strength structural steel)	160
Table 8.5 Comparison between numerical results and code predicted results (High strength concrete and normal strength steel)	160
Table 8.6 Comparison between numerical results and code predicted results (High strength structural steel and concrete)	161
Table 8.7 Statistical results for the 41 FEC columns listed in Tables (8.1–8.6) for concentric axial load	162
Table 8.8 Comparison between numerical and code predicted axial loads	166
Table 8.9 Comparison between numerical and code predicted bending moments	167



## LIST OF SYMBOLS

$A_c$	Area of concrete
$A_g$	Gross area of concrete section
$A_{mi}$	Area of one reinforcing bar within $2h_n$ region
$A_r$	Area of longitudinal reinforcement
$A_{ri}$	Area of one reinforcing bar
$A_s$	Area of structural steel section
$A_{sx}$	Area of steel shape, pipe, or tubing in a composite section
$b_f$	Full flange width
$C_c$	Clear cover of FEC columns
$D$	Depth of the column cross-section
$d$	Depth of I-shaped structural steel
$d_c$	Compression damage parameter for concrete
$d_t$	Tensile damage parameter for concrete
$E_c$	Modulus of elasticity of concrete
$E_{cm}$	Secant modulus of elasticity of concrete
$E_r$	Modulus of elasticity of reinforcing steel
$El$	Flexural rigidity
$El_{eff}$	Effective moment of inertia rigidity of composite section
$E_{it}$	Initial tangent modulus
$E_s$	Modulus of elasticity of steel
$e$	Eccentricity
$e/D$	Eccentricity ratio
$e_x$	Initial load eccentricity for bending about strong axis
$e_y$	Initial load eccentricity for bending about the weak axis
$F_{sh}$	Stress at the onset of strain hardening of steel
$F_u$	Ultimate strength of structural steel plate
$F_y$	Yield strength of structural steel shape
$F_{yr}$	Yield strength of longitudinal reinforcement
$f_c$	Compressive stress of concrete
$f_{cd}$	Design value of concrete compressive strength
$f_{yd}$	Design value of the yield strength of structural steel

$f_t$	Tensile stress of concrete
$f_{tu}$	Uniaxial tensile strength of concrete
$h_n$	Distance from centroidal axis to neutral axis
$h_1$	Overall thickness of composite column cross-section
$h_2$	Width of composite column cross-section
$I_c$	Moment of inertia of concrete section
$I_r$	Moment of inertia of reinforcing steel
$I_s$	Moment of inertia of structural steel
$I_{sr}$	Moment of inertia of reinforcing bars
$I_{sx}$	Moment of inertia of structural steel shape, pipe or tube
$k_1, k_2$	Factors used to define the post-peak descending branch of the stress-strain curve of high strength concrete
$K$	Effective length factor
$KL$	Effective length;
$L/D$	Overall column slenderness ratio
$L_e$	Effective length of the column
$L_u$	Unsupported length of column
$M_E$	Moment capacity for neutral axis located $h_E$ from centroid axis
$\Delta M_E$	Plastic moment of cross-section resulting from region $2h_E$
$M_{max}$	Maximum internal moment
$M_{pl}$	Plastic resistance moment of the composite section
$M_{pn}$	Plastic moment of cross-section resulting from region $2h_n$
$M_u$	Moment at the peak load of the parametric column
$M_1$	Lesser factored end moment on a compression member
$M_2$	Greater factor end moment on a compression member
$N_{pl.ed}$	Plastic resistance to compression
$N_{pm}$	Axial force resistance of concrete portion of cross-section
$P_c$	Critical load of column
$P_{exp}$	Experimental peak load
$P_{num}$	Numerical peak load
$P_n$	Nominal compressive strength of column
$P_o$	Column capacity under uniaxial compression
$r$	Radius of gyration

$s$	Tie spacing
$s/D$	Tie spacing-to-depth ratio
$t_f$	Thickness of flange
$t_w$	Thickness of web
$U_{1u}$	Maximum lateral displacement for strong axis bending
$w_c$	Weight of concrete per unit volume
$Z_c$	Plastic modulus of overall concrete cross-section
$Z_{cE}$	Plastic section modulus of concrete within $2h_E$ region
$Z_{cn}$	Plastic section modulus of concrete within $2h_n$ region
$Z_r$	Plastic section modulus of reinforcing steel
$Z_{rE}$	Plastic section modulus of reinforcing steel within $2h_E$ region
$Z_s$	Plastic modulus of steel cross-section
$Z_{sE}$	Plastic section modulus of steel section within $2h_E$ region
$Z_{sn}$	Plastic section modulus of steel section
$\beta$	Parameter to control the shape of the compressive stress-strain curve of concrete
$\varepsilon_c$	Compressive strain of concrete
$\varepsilon_{cu}, \varepsilon_o$	Axial strain of concrete
$\varepsilon_c^{\sim pl}$	Effective plastic strain in compression
$\varepsilon_t^{\sim pl}$	Effective plastic strain in tension
$\varepsilon_{ln}^{pl}$	Logarithmic plastic strain of steel
$\varepsilon_L$	Concrete strain corresponding to a stress value of $0.8f_{cu}$
$\varepsilon_{sh}$	Strain at the onset of strain hardening of steel
$\varepsilon_u$	Strain at the ultimate strength of steel
$\varepsilon_y$	Yield strain of steel
$\sigma_{nom}$	Nominal stress
$\sigma_{true}$	True stress
$\nu$	Poisson's ratio for concrete
$\delta_{exp}$	Axial deformation at peak load in experimental
$\delta_{num}$	Axial deformation at peak load in numerical
$\beta_{dns}$	The ratio of maximum factored sustained shear within a story to the maximum factored shear in that story associated with the same load combination
$\mu$	Ductility index

## LIST OF ABBREVIATIONS

CC	Concrete crushing
CFT	Concrete filled tube
COV	Coefficient of variation
FEC	Fully encased composite
FEM	Finite element model
FRP	Fiber reinforced polymer
HSC	High strength concrete
NSC	Normal strength concrete
PEC	Partially encased composite
SCH	Short column with high strength concrete
SCN	Short column with normal strength concrete
SD	Standard deviation
SHSC	Super high strength concrete
SRC	Steel reinforced column
UHSM	Ultra-high strength material

## CHAPTER 1

### INTRODUCTION

#### 1.1 General

Composite column is a structural member that uses a combination of structural steel shapes, pipes or tubes with or without reinforcing steel bars and concrete to provide adequate load carrying capacity to sustain either axial compressive loads alone or a combination of axial loads and bending moments. In a composite column both the steel and the concrete sections resist the external loading by interacting together by bond and friction. Composite columns are constructed providing structural steel inside concrete or concrete inside the structural steel. These columns are being used worldwide for the construction of high rise buildings since it can reduce the size of the columns in the building and increase the usable space of the floor plan. In addition, composite column enhances the overall rigidity of the building and provides significant shear resistance to strong earthquakes and other lateral loads.

Composite column sections used in high-rise construction can be classified into three types, (a) Fully encased composite column (FEC); (b) Partially encased composite column (PEC); and (c) Concrete filled tube (CFT). Typical cross-sections of these three types of composite columns are shown in Figure 1. As shown in Figure 1(a), in FEC columns the structural steel section is fully encased by surrounding concrete whereas in PEC columns (Figure 1(b)) the steel section is partially encased by concrete. On the other hand in concrete filled tubular composite columns (Figure 1(c)) the concrete is fully confined by the surrounding steel section. These composite sections have evolved to take the best out of the two materials i.e. concrete and steel. In these composite sections concrete provides compressive strength, stability, stiffness, improved fire proofing and better corrosion protection whereas steel provides tensile strength, ductility and high speed of construction. Among these three sections FEC column renders better fire proofing and corrosion protection since the steel section is fully encased by concrete. The cost for fire proofing and corrosion resistance is not required for FEC columns as compared to PEC and CFT columns. Hence, for the moist weather condition of Bangladesh FEC columns can be the best solution for high rise constructions from strength, ductility and economy considerations.

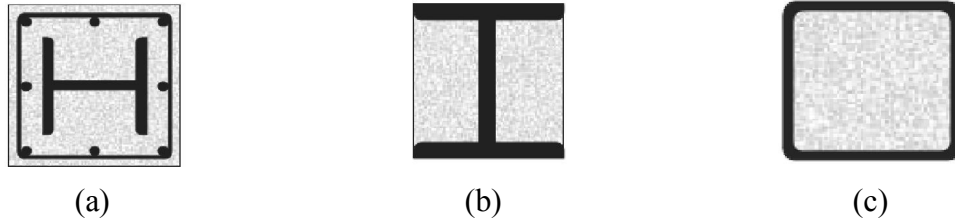


Figure 1.1 Typical X-sections of composite columns, (a) FEC; (b) PEC; and (c) CFT

Composite construction system first appeared in the United States of America in 1894. However the design guidelines were established in 1930 (Gajanan and Sabnis 1979; Eggemann 2003). During the past few decades, steel concrete composite structural systems have been used in many tall buildings all over the world. Extensive experimental and theoretical studies were carried out by Bridge Roderic (1978), Burr (1912), Viridi and Dowling (1973), Munoz and Hsu (1997), Mirza and Skrabek (1992), Chen and Yeh (1996), Tsai et al. (1996), Tawil and Deierlein (1999), Chen et al. (1999), Dundar et al. (2007), Dundar and Tokgoz (2008), Kim et al. (2012, 2013) and Cristina et al. (2014). An extensive review (from year 1965 to 1999) was carried out by Shanmugam and Lakshmi (2001) on steel concrete composite columns. Most of the experimental studies on composite columns were carried out for concentric and eccentric axial loads having different slenderness ratios, different structural steel sections and different concrete and structural steel strength. Analytical and theoretical studies were conducted by Chen and Lin (2006), Shih et al. (2013) and Samanta and Paul (2013). In addition, Chen and Lin (2006) carried out extensive analytical studies on FEC columns constructed with various shapes of structural steel sections using fibre section model.

Current design rules for composite structures are specified in AISC-LRFD (2010), ACI 318 (2014), Euro code-4 (2005), Architectural Institute of Japan (AIJ 2005), Egyptian code (2012) and Canadian Standard Association, CSA (2009). Out of these ACI-318, AISC-LRFD and Euro code-4 are being used widely all over the world for the design of FEC columns. However, up-to-date, limited studies were found on comparison of strength for FEC columns among these three codes. Studies on code comparison were conducted by Furlong (1976), Tawil and Deierlein (1999), Weng and Yen (2002), Ellobody et al. (2011), Soliman et al. (2012), Moniem et al. (2016), and Lu (2016) to identify the differences of the specifications used for the design of FEC columns. However, most of these studies were conducted for FEC columns constructed with concrete strength less than 70 MPa and steel strength less than 500 MPa.

Numerical analysis takes comparatively less time and is cost effective than experimental study. It is also more realistic than analytical and theoretical studies. Moreover, finite element (FE) analysis is able to predict the experimental behaviour and isolate the contributions of the individual elements of FEC column. Studies on FEC columns using FE analysis varying different parameters of FEC columns are very limited. Recently, Ellobody and Young (2011), Ellobody et al. (2011) and Mote and Vijay (2013) developed finite element models to investigate the behaviour of concentrically and eccentrically loaded FEC columns with normal and medium strength concrete. Limited studies were found on the development of full scale finite element model on FEC columns with various percentages of structural steel, slenderness ratios, eccentricity, spacing of transverse reinforcement and with high strength materials.

Fully encased composite (FEC) column is a competitive solution for seismic and non-seismic zones due to excellent seismic performances and also because of improved fire protection. This is a relatively new system for the construction industry of Bangladesh. In the upcoming version of Bangladesh National Building Code (BNBC 2010) the design of FEC columns has been included. Most of the guidelines have been adopted from AISC-LRFD (2005). The applicability of these design provisions in the construction environment of Bangladesh need to be explored. Moreover, limited studies have been found on the development of full scale finite element model for this column subjected to monotonic as well cyclic loading conditions. This study aims to perform extensive experimental as well as numerical investigations on FEC columns under concentric and eccentric conditions of loading. Attempts have been made in this study to develop a full scale 3D FE model for FEC columns to explore the behavior and strength of FEC columns encompassing a wide variety of geometry and material properties. Behaviour and strength of FEC columns with high strength concrete and high strength steel also need to be explored.

## **1.2 Objectives and Scope of the Study**

The objectives of the present study are,

- i) To conduct experimental investigations on FEC columns under concentric and eccentric axial loads.
- ii) To develop a nonlinear 3D finite element model of FEC columns using ABAQUS finite element code.

- iii) To perform parametric study with a view to explore the effect of several geometric and material variables on the strength and failure behaviour of FEC columns.
- iv) To compare the strength of FEC columns obtained from the experimental and FE analysis with the strength obtained from the design equations proposed in ACI 318 (2014), AISC-LRFD (2010), and Euro code 4 (2005).

To achieve the objectives mentioned above experimental and extensive numerical studies were conducted. Experimental program consisted of thirteen (13) square FEC columns with two different sizes, concrete strength and percentages of structural steel. Seven of these columns with a size of 100 mm  $\times$  100 mm were constructed with normal strength concrete (28 MPa). Another, six specimens with a size of 150 mm  $\times$  150 mm were constructed with higher strength concrete (42 MPa). All the test columns had a length of 900 mm. The percentages of structural steel were varied from 2% to 3.75% in these columns. The columns were tested for concentric and eccentric axial loads.

The ABAQUS/Standard, finite element code (HKS 2013) was used to construct the numerical model for FEC columns. Both geometric and materials nonlinearities were included in the FE model. A concrete damage plasticity model capable of predicting both compressive and tensile failures, was used to model the concrete material behaviour. Riks solution strategy was implemented to trace a stable peak and post peak response of FEC columns under various conditions of loading. To validate the model, simulations were conducted for both concentrically and eccentrically loaded FEC test specimens from current study and test specimens from published literatures, encompassing a wide variety of geometries and material properties. Comparisons were made between the FE predictions and experimental results in terms of peak load, peak strain, load versus deformation curves and failure modes of the FEC columns.

An extensive parametric study was conducted using the numerical model to investigate the influences of some key parameters affecting the behaviour of FEC columns under concentric and eccentric axial loads. The key parameters selected in the present study are percentage of structural steel, column slenderness ( $L/D$ ), eccentricity ratio ( $e/D$ ) and spacing of ties ( $s/D$ ). The compressive strength of concrete and yield strength of structural steel in FEC columns were used as the material variables in the parametric study. The cross-section of the parametric columns have selected as 500 mm  $\times$  500 mm. The effects of ultra-high strength concrete (120 MPa) and high strength structural steel of 913 MPa on the FEC column



behaviour was also explored. Finally, the experimental as well as the numerical results were compared with the code (ACI 2014, AISC-LRFD 2010 and Euro code 4) predicted results.

### **1.3 Organization of the Thesis**

This thesis is divided into eight chapters. An introduction to the study is presented in Chapter 1. It includes the research background, objectives and the scope of the study. Chapter 2 presents a brief review on the literature related to FEC columns and explores in relative detail the experimental and analytical research works carried out on FEC columns.

The design guide lines along with the capacity prediction equations for FEC columns according to ACI-318 (2014), AISC-LRFD (2010) and Euro code-4 (2005) is presented in Chapter 3. The comparison between the design guidelines and detailing rules for composite columns as provided in these codes are also included.

Chapter 4 presented the experimental test program along with the FEC column parameters to be examined. It also includes a description about fabrication of structural steel and placement of the concrete used in the columns. A description of the instrumentation, end fixtures and loading condition was included. The experimental results and observation for different loading conditions were also included in this chapter.

The detailed description of the finite element model for FEC columns, along with the properties of the test specimens from published literature are given in Chapter 5. The selected element types, mesh configuration, material mechanical properties for steel and concrete and the solution strategy implemented in the finite element model were also presented.

The results of the numerical simulations of the test specimens used to validate the developed finite element model under concentric and eccentric loading conditions are presented in Chapter 6. Discussions are included on the comparison between the experimental and numerical failure modes, peak axial loads, axial strains at peak load, load versus axial deformation curves, for different test groups. In addition, the effects of transverse reinforcement spacing on the column behaviour, percentage of structural steel and the contributions of steel and concrete individually on the overall load carrying capacity of this composite system are demonstrated.

Chapter 7 presents the detailed parametric study conducted with the developed finite element model to cover the range of several geometric and material parameters on the behaviour of FEC columns. The findings of this parametric study are demonstrated and discussed in detail.

Chapter 8 includes the comparison of experimental and numerical results with the three design codes ACI-318 (2014), AISC-LRFD (2010) and Euro code-4 (2005). The applicability of these codes for FEC columns with high strength concrete and steel are also demonstrated.

A summary of the methodology and conclusions regarding the achievements of this research work were included in Chapter 9, along with the recommendations for future research.

## CHAPTER 2

### LITERATURE REVIEW

#### 2.1 Introduction

Composite columns are constructed using various combinations of structural steel and concrete in an attempt to utilize the beneficial properties of each material. The interactive and integral behavior of concrete and the structural steel elements makes the composite column a very stiff, more ductile, cost effective and consequently a structurally efficient member in building and bridge constructions. Mainly three types of composite column sections are used in high-rise building construction. In early 1900's, concrete was used to encase steel columns and beams, and as a filler material for floor systems. The first experimental test was carried out by Emperger in the year 1907 on built up composite columns under concentric load. Author also proposed formulas to predict the strength of composite columns (Bridge and Roderick, 1978; Eggemann, 2003). Experimental investigations on concrete encased steel composite columns have been conducted by different researchers since long before. Analytical method was developed in early 1900 to investigate the behaviour of FEC columns. On the other hand numerical simulations of reinforced concrete structures using finite element method, witnessed a remarkable advancement since 1990. Though, experimental research is costly and time consuming than numerical research, yet the progress in numerical studies are comparatively less. Recently, a nonlinear finite element models investigating the behaviour of concentric and eccentric axial load of FEC columns was developed by different researchers. The design of composite columns has been addressed by a large number of design specifications. Among these, ACI-318, AISC-LRFD, and Euro code 4 have been widely using around the world for the design of composite structure.

Initially, American Institute of Steel Construction (AISC) and the American Concrete Institute (ACI) provided rules for the design of these structural elements. In the United States of America a joint Structural Specifications Liaison Committee (SSLC) was organized in 1978 to evaluate the acceptability of composite column design procedure. Successively, the numbers of versions on AISC-LRFD specifications and ACI-318 were issued in different time. Other specifications or codes that provided the rules for design of composite structure were the Euro code (ENV 1994), the Architectural Institute of Japan (AIJ, 1997), the Building Code of Australia (BCA, 2005), and the New Zealand building code (the

NZBC1992) standards. However, ACI-318, AISC-LRFD, and Euro code 4 are being widely used around the world for the design of composite structure. Before describing the experimental, numerical and codes comparison a short notes about composite columns are given below.

## 2.2 Types of Composite Columns

Composite column sections used in high-rise construction can be classified into three types based on construction, (a) Fully encased composite column (FEC); (b) Partially encased composite column (PEC); and (c) Concrete filled tube (CFT). Typical cross-section of these three types of composite columns is given in Figure 2.1. These three types of columns can be constructed varying the position and shape of structural steel. As shown in Figure 2.1(a) to 2.1(c) steel sections are surrounded by concrete in all three cases whereas in PEC columns Figure 2.1(d) to 2.1(e) the steel sections is partially encased by concrete with or without shear stud and reinforcement. On the other hand in concrete filled tubular columns Figure 2.1(f) to 2.1(j) the concrete is fully confined by the surrounding steel section. These composite sections were evolved to make the best out of the two materials i.e. concrete and steel.

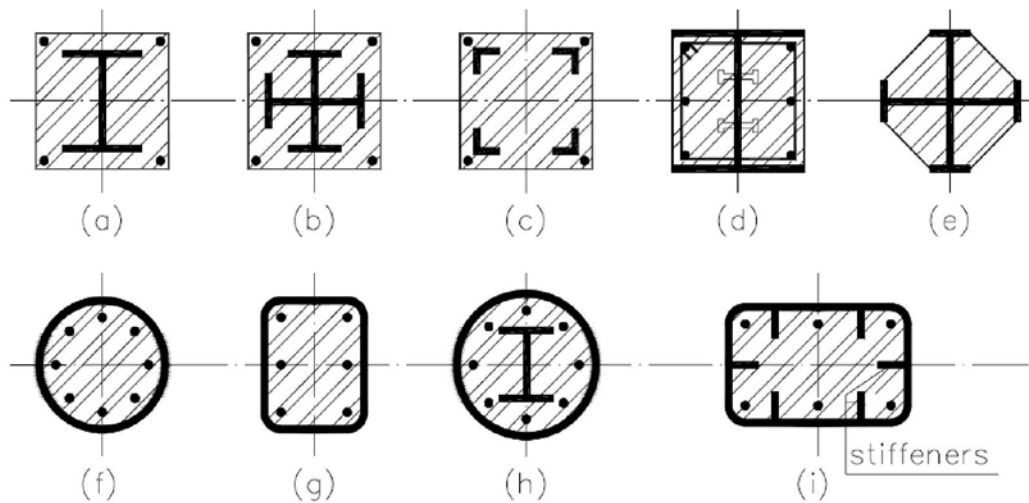


Figure 2.1 Detail X-sections of different composite columns, (i) FEC columns (a)-(c); (ii) PEC columns (d)-(e); (iii) CFT columns (f)-(i), Euro code 4 (2005)

Concrete provides compressive strength, stability, stiffness, whereas steel provides tensile strength, ductility and high speed of construction. Among these three sections FEC column renders better fire proofing and corrosion protection since the steel section is fully encased by concrete. The cost for fire proofing and corrosion resistance is not required for FEC

columns as compared to PEC and CFT columns. Hence, for the moist weather condition of Bangladesh FEC columns can be the best solution for high rise constructions from strength, ductility and economy considerations.

### **2.3 Research on Steel-Encased Concrete Columns**

Extensive experimental and analytical, and a few numerical research works were carried out on FEC columns by previous investigators. Experimental study on composite columns started in the year of 1905 for concentric axial load. Analytical and theoretical studies started from the year of 1976. Recently, the numerical models were developed to determine the behaviour and strength of FEC columns. Successive sections will focus on the experimental, analytical and numerical investigations on FEC columns under various conditions of loading. Comparison between various design guides as performed by previous researchers are also summarized below.

#### **2.3.1 Experimental investigations**

Extensive experimental researches were carried out on FEC columns, by several research groups (Virdi and Dowling, 1973; Bridge and Roderick 1978; Matsui, 1979; Morino et al., 1984; Munoz et al., 1991; Chen and Yeh, 1996; Tsai et al., 1996; Weng et al., 2001; Eggemann, 2003; Dundar et al., 2006, 2008; Kim et al., 2012, 2013; Shih et al., 2013; Cristina et al., 2014; Attar et al. 2015) to investigate the behaviour of columns under various loading conditions. A large number of tests were performed on short FEC columns constructed with normal strength concrete subjected to concentric, eccentric and biaxial load. A few long column tests were carried out using normal strength under static loading conditions. Findings of these experimental investigations are presented below:

Bridge and Roderick (1978) and Eggemann (2003) reported that Emperger (1907) tested three steel columns to determine their buckling loads in year 1907. Successively, he carried out more than 1000 tests on composite columns in Europe and about 570 tests in North America from 1907 to 1932. He also distinguished different types of composite columns. Finally, the researchers published a design formula to determine the ultimate capacity of composite columns.

Virdi and Dowling (1973) investigated experimentally nine square FEC columns for eccentric axial load. The objective of the test was to determine the experimental and analytical ultimate load carrying capacity of these FEC columns. The columns had a 254 mm × 254 mm square cross section reinforced with a 152.4 mm × 152.4 mm × 23.4 kg/m

structural steel section encased in 50.8 mm of concrete and four 12.7 mm diameter rebar's, one at each corner and with a 19.05 mm clear cover. The variables were the length, eccentricity along major and minor axis. These columns were pin-ended composite columns tested under axial loads and biaxial bending. Authors reported that the analytical results could predict the experimental results with good accuracy.

Matsui (1979) conducted research work on the behaviour of concrete-encased columns subjected to eccentric axial load. The objective of this study was to observe the effects of slenderness on ultimate capacity and failure modes. Three specimens were constructed with normal strength concrete with square cross-section (160 mm × 160 mm). The length of these columns was 924 mm, 2309 mm and 3464 mm. The structural steel section was H-shaped 100 × 100 × 6 × 8 mm used in all the FEC columns. The specimens had concrete cube strengths 18.5, 21.4 and 22.5 MPa and structural steel yield stresses were 306, 298, 304 MPa, in these columns, respectively. The longitudinal reinforcement bars were 6 mm in diameter and the transverse reinforcement bars were 4 mm in diameter. The yield stress of the reinforcing bars ( $f_{yr}$ ) was 376 MPa in all the columns. The relative slenderness ratios of the specimens were 0.26, 0.66 and 1.29. The author determined that the experimental capacity of these columns were 996, 974 and 874 kN, respectively. He reported that the ultimate capacity of these columns decreased with the increase of slenderness ratio. Author also presented the failure modes of these columns and reported that comparatively less slender columns failed due to concrete crushing, followed by structural steel yielding and more slender columns failed by flexural buckling.

Morino et al. (1984) experimentally investigated the elasto-plastic behaviour of steel reinforced concrete (SRC) columns subjected to biaxial eccentric compression load. The purposes of this study were to observe the reduction of ultimate capacity and failure behaviour due to changes in eccentricity angle and slenderness of FEC columns. The column specimens had a 160 mm × 160 mm concrete square cross section encasing rolled steel H-section of 100 × 100 × 6 × 8 mm. The columns were divided in four groups as per slenderness ratios and designated as A4, B4, C4 and D4. The load was applied for two different eccentricities (40 mm and 75 mm) on these columns. Each eccentric axial load was applied from five different angles ( $0^0$ ,  $30^0$ ,  $45^0$ ,  $60^0$  and  $90^0$ ). Three experimental parameters varied for the test columns were, the slenderness ratio, the eccentricity and the angle location of the applied load. Effect of eccentricity, angle between load point and major axis, and slenderness ratio on the load-deflection behaviour and the maximum load carrying capacity

were investigated. The ultimate load carrying capacities of these columns are reduced by about 35% when eccentricity is changed from minor axis to major axis. Authors reported that a sharp peak appears on the load-deflection curve of a short column because of concrete crushing. The P-delta effect was more pronounced in a long column and a gradual unloading took place.

Munoz et al. (1997) carried out experimental study on the behaviour of biaxially loaded concrete- encased composite columns. The composite column specimens were one short and three slender, with square cross section,(63.5 mm × 63.5 mm). Each specimen consisted of I-shaped structural steel section encased by concrete and additionally reinforced with four longitudinal reinforcements as corner bars. The slenderness ratio of the column with  $L/r = 42.7$  was designated as MC1. The slenderness ratios of other three columns were  $L/r = 64$ , was designated as MC2, MC3 and MC4, respectively. The overall length of the specimens was 8130 mm for the short column (MC1) and 12200 mm for the long columns (MC2, MC3 and MC4). The average concrete compressive strength were 36.77, 30.97, 25.83 and 27.51 MPa for columns MC1, MC2, MC3 and MC4, respectively. Strain gauges were fixed at the surface of these test specimens to determine the axial strain and the curvatures with respect to the main bending axis of the column. The main variables considered in the experimental investigation were concrete compressive strength  $f_{cu}$ , tensile strength of reinforcing steel, slenderness ratio, and eccentricity of the applied load. The effects of the eccentrically applied axial compressive force, load-deflection and moment-curvature behavior on the maximum load capacity of a composite column were examined. The axial load capacities were 28.17, 26.48, 29.06 and 22.03 kN for these columns MC1, MC2, MC3 and MC4, respectively. The failure modes of these columns were observed during the experimental test. Hairline cracks were started on these columns MC1, MC2, MC3 and MC4 at 50%, 30%, 40% and 40% of the maximum load, respectively. The test results were compared with the analytical results of the maximum load capacity obtained from a numerical analysis. The comparative results indicated that the analytical method and computer program used to model and analyze the composite column specimens (i.e numerical analysis) could accurately predict the maximum load capacity and deformation behavior of a pin-ended biaxially loaded concrete-encased steel column with axial compressive load in single curvature bending.

Chen and Yeh (1996) carried out extensive experimental studies to determine the ultimate capacity of FEC columns with different shaped structural steel. Ten short columns were

constructed with three different shapes of the structural steel section with normal strength concrete. The shapes of the structural steel sections used in the specimens were I, H and cross shaped. All the H-shaped steel section were more similar to the wide-flange section, while the I-shaped section had a narrow flange. The specimens had square cross-sections of 280 mm × 280 mm and a constant nominal length of 1200 mm. The specimens had concrete cylinder strengths varying from 26.4 to 29.8 MPa and a structural steel yield stress of 296 to 345 MPa. The longitudinal and transverse reinforcement bars were 16 mm and 8mm in diameter. Three different spacings of transverse reinforcement (35 mm, 75 mm and 140 mm) were used to observe the effect of transverse spacing on overall capacity of columns. The author reported that the columns constructed with cross-shaped structural steel sections took comparatively more load than the other shaped ones. This happened as the confining effect was more in the FEC columns constructed with cross shaped structural steel. The ultimate load carrying capacity also increased when the transverse reinforcement spacing decreased. The rates of load increment for the closer spacing of transverse reinforcement were comparatively higher in the columns constructed with H-shaped structural steel.

Tsai et al. (1996) experimentally determined the behavior of axially loaded steel reinforced concrete columns. Ten short columns were constructed with cross shaped structural steel section with normal strength concrete. These ten (10) specimens were labeled from SRC1 to SRC10. The specimens had square cross-sections of 280 mm × 280 mm and a constant nominal length of 1200 mm. The specimens had concrete cylinder strengths varying from 21.3-26.3 MPa and a steel yield stress of 296-345 MPa. The longitudinal and transverse reinforcement bars were 16 mm and 8 mm in diameter. Three different spacing of transverse reinforcement (100 mm, 140 mm and 190 mm) were used to observe the effect of transverse spacing on overall capacity of columns. The author reported that the ultimate load carrying capacity increased when the transverse reinforcement spacing decreased. The rate of the load increment was about 2%.

Dundar et al. (2006) conducted an experimental study on the behaviour of reinforced and concrete-encased composite columns subjected to biaxial bending and axial load. The primary objective of this investigation was to examine the ultimate strength capacity and load-deflection behaviour of short and slender reinforced concrete columns. The experimental results were compared with the ultimate capacities obtained theoretically. Theoretical results were calculated using various stress-strain models for the materials done by previous authors. The experimental program included fifteen (15) reinforced concrete



columns. Five specimens were short square (100 mm × 100 mm) tied columns (C1–C5) with 870 mm length. Seven specimens were slender square tied columns (C11–C14, C21–C23) with two different sizes. Other three specimens were L-shaped section slender tied columns (LC1–LC3). The columns groups (C11–C14) and (C21–C23) were 100 mm × 100 mm and 150 mm × 150 mm square in sizes, respectively. Ultimate capacity of these reinforced concrete columns were determined experimentally for eccentric axial load and compared with calculated theoretical results. A computer program was developed based on these theoretical calculations. The ultimate capacity was determined using this computer program for the tested FEC columns. The authors reported that the theoretical results could predict the experimental results for different cross section of reinforced and composite column members with good accuracy.

Dundar and Tokgoz (2008) carried out experimental tests on biaxially loaded concrete-encased composite columns. The main objective of this study was to observe the load-deflection behaviour and load carrying capacities of short and slender FEC columns. The researchers also, compared these experimental results with theoretical results. The theoretical results were calculated considering the flexural rigidity ( $EI$ ) and slenderness ratio of these composite columns. The slenderness effect due to the additional eccentricity of the applied axial load was considered by the moment magnification method. The main variables in the tests were eccentricity of applied axial load, concrete compressive strength, cross section, and slenderness effect. This experimental study consisted of ten composite column specimens. Two specimens were square section short composite columns (CC1–CC2), four specimens of square section slender composite columns (CC3–CC6) and the other four specimens were of L-shaped section slender composite columns (LCC1–LCC4). The complete experimental load-deflection behaviour of the composite column specimens were determined. An interactive theoretical method including slenderness effect was suggested to perform the ultimate strength analysis and to determine the complete load-deflection behaviour of composite columns. Good agreement was achieved between the complete experimental and the theoretical load-deflection diagrams in the study. In addition, the flexural rigidity was significant effect on the slenderness of composite columns.

Kim et al. (2012) carried out experimental study for eccentric axial load of concrete-encased steel column using high strength steel and concrete. Seven concrete-encased steel columns using high-strength structural steel (nominal yield strength  $f_{ys} = 913$  and  $806$  MPa) and high strength concrete (cylinder compressive strength  $f_{cu} = 94$  MPa) were tested to investigate the

eccentric axial load-carrying capacity and the deformation capacity. Out of seven, four were fully encased square composite columns and designated as C1 to C4 with cross section 260 mm × 260 mm. The test parameters of the fully encased composite columns were the eccentricity of the axial load, and the effect of lateral reinforcement. These columns were tested experimentally for two different eccentricity (120 mm and 60 mm) and lateral reinforcement spacing (50 mm and 130 mm). Since the yield strain (0.004) of the high-strength steel was greater than the ultimate compressive strain (0.003) of the concrete subjected to short-term loads, the current study focused on the effect of early concrete crushing on the behavior of the composite columns. The test results showed that in the case of inadequate lateral confinement, the load-carrying capacity was limited by the early crushing of concrete. However, because of the high-strength steel section, all test specimens showed ductile flexural behavior after the delamination of the concrete. The test results were compared with the predictions by nonlinear numerical analysis and current design codes.

Shih et al. (2013) carried out study on axial strength and ductility of square composite columns with two interlocking spirals. The axial compressive capacity and load–displacement behaviour of composite columns confined by two interlocking spirals were experimentally and analytically investigated. The innovative spiral cage used for a square column was fabricated by interlocking a circular spiral and a star-shaped spiral to enhance the confinement effect for the core concrete. Eight full-scale square composite columns were tested under monotonically increased axial compression. Experimental results demonstrated that, with significant savings of the transverse reinforcement, the composite columns confined by two interlocking spirals achieved excellent axial compressive strength and ductility. It revealed that the spirally reinforced concrete column achieved better load-carrying capacity and behaviour than the rectilinearly tied reinforced concrete column, although the amount of the spirals was less than that of the rectilinear hoops. Moreover, an analytical model was developed to take into account the concrete confinement due to the structural steel in addition to the transverse reinforcement and distributions of the longitudinal bars. The analytical results accurately predicted the axial compressive capacity and load–displacement behaviour of the specimens.

### 2.3.2 Numerical and analytical investigations

Analytical methods were developed parallel to experimental study in early 1900 to determine the strength and behaviour of FEC columns. Successively, computer analysis method was developed to determine the nonlinear behaviour of FEC columns under different loading conditions. Numerical analyses for FEC columns using FE model started very recently as compared to other methods. It has numbers of advantages over experimental research. However, it was found that very limited research on numerical simulation of FEC column has been conducted. Extensive analytical studies were carried out by Wang and Hsu (1992), Tsao and Hsu (1993), Munoz (1994) and Chen and Lin (2005). Numerical studies on FEC columns were developed by Ellobody et al (2011), Ellobody and Young (2011), Kim et al. (2012, 2013) under various loading conditions.

Munoz (1994) developed a computer program to compare experimental results. The analytical method used to develop the computer program was based on the numerical integration technique originally developed by Hsu (1974) with modifications and adaptations introduced by Wang and Hsu (1992), Tsao and Hsu (1993), and finally by Munoz (1994) to study the behavior of composite columns. A segmental subdivision of the column length was used to determine the complete load-deflection and moment-curvature for both short and slender columns. The load-deformation behavior included the ascending and descending branches of the loaded column under study. The column cross section was divided into a number of small square or rectangular areas for which the conditions of equilibrium and strain compatibility was satisfied at the nodal points using the secant modulus of elasticity for the concrete elements. The second order effects due to the deformed shape of the composite column under load were included in the analysis. The author validated the experimental results carried out by previous researchers. (Viridi et al. 1973; Morino et al. 1984; Bridge et al. 1978; and Taylor et al. 1983). All the columns were constructed with normal strength concrete and structural steel and were square in size. The columns were tested for concentric and eccentric axial loads. The ultimate loads obtained from the tests ( $P_{Test}$ ) and the computer analyses ( $P_{Com}$ ) were compared. It was found that a good agreement existed between test and finite element results for most of the columns. The mean value of  $P_{Test}/P_{Com}$  ratios were 1.041, 1.055, 1.006 and 1.01 for the test specimens of Viridi et al. (1973), Morino et al. (1984), Bridge et al. (1978) and Taylor et al. (1983) respectively. The corresponding standard deviations were 0.086, 0.055, 0.126 and 0.0382, respectively.

Chen and Lin (2006) developed analytical models for predicting axial capacity and behavior of twenty six (26) concrete encased steel composite stub columns from previous authors (Chen and Yeh 1996; Tsai et al. 1996 and Chen et al. 1999). Analytical models were mainly developed to validate the experimental results and to prepare constitutive relationships for materials used in the composite cross section. These columns were constructed with different shape of structural steel (I, H, T and cross shaped) with normal strength structural steel and concrete. A comparison was carried out between experimental tests results ( $P_{Test}$ ) and analytical results ( $P_{Analy.}$ ). A maximum difference of about 6% was observed between the experimental and analytical results for this specimen. The average ratios of the experimental to analytical capacities, ( $P_{Test}/P_{Analy.}$ ) were 1.01, 1.02 and 1.00 for three series of tests (Chen and Yeh 2005; Tsai et al. 1996, Chen et al. 1999), respectively. Similarly, the corresponding coefficients of variation were 0.02, 0.06 and 0.02, respectively. The analytical models were able to predict the experimental capacity with good accuracy. Constitutive relationships were established for materials used in the composite cross section, which included unconfined concrete, partially ( $K_p$ ) and highly ( $K_h$ ) confined concrete, structural steel section, and longitudinal reinforcing bar. The strength of the confined concrete was influenced by the tie spacing, volumetric ratio of the lateral reinforcement, and the distribution of the longitudinal reinforcing bar. The value of partial confinement factor for concrete,  $K_p$  was determined for these FEC columns and varied from 1.04 to 1.50. Similarly, the values of high confinement factor for concrete,  $K_h$  determined for these FEC columns individually and were observed to vary from 1.23 to 1.97. The cross-shaped steel section was found to provide the highest confinement effect on concrete.

Ellobody and Young (2011) investigated the behaviour of pin-ended axially loaded concrete encased steel composite columns. The main objective of the study was to understand the structural response and modes of failure of the columns and to assess the composite column strengths against current design codes. The study covered slender, non-slender, stub and long concrete encased steel composite columns. The concrete strengths varied from normal to high strength (20-110 MPa). The steel section yield stress was also varied from normal to high strength (275-690 MPa). A nonlinear 3-D finite element model was developed to analyse the inelastic behaviour of steel, concrete, longitudinal and transverse reinforcing bars as well as the effect of concrete confinement on concrete encased steel composite columns. The finite element model was validated against published experimental results. The ultimate loads obtained from the tests ( $P_{Test}$ ) and finite element analyses ( $P_{FE}$ ) were compared. The

mean value of  $P_{FE}/P_{Test}$  ratios was 0.97 with the corresponding coefficient of variation (COV) of 0.055. A good agreement between tests and finite element results for most of the columns were obtained. A maximum difference of 11% was observed between experimental and numerical results for column specimens. Furthermore, the variables that influence the composite column behaviour and strength comprising different slenderness ratios, concrete strength and steel yield stress were investigated in a parametric study. The authors reported that the increase in structural steel strength had a small effect on the composite column strength for the columns having higher relative slenderness ratios due to the flexural buckling failure mode.

Ellobody et al. (2011) carried out numerical simulations of eccentrically loaded concrete encased steel composite columns. The primary objectives were to validate the FE models against existing test results and to carry out parametric studies with varying eccentricity. All the experimental columns were constructed with normal strength concrete. A nonlinear 3-D finite element model were developed and simulated for eccentric load acting along the major axis. The eccentricities were varied from 0.17 to 0.3 of the overall depth (D) of the column sections. The developed finite element model for eccentrically loaded concrete encased steel composite columns was verified against the test results. The eccentric ultimate loads obtained from the tests ( $P_{Test}$ ) and finite element analyses ( $P_{FE}$ ) were compared. A good agreement was obtained between the test and finite element results for most of the eccentrically loaded columns. The mean value of  $P_{FE}/P_{Test}$  ratio was 0.95 with the coefficient of variation (COV) of 0.077. The failure mode predicted from the finite element analysis for the eccentrically loaded concrete encased steel composite columns was flexural buckling.

Kim et al. (2012 and 2013) carried out numerical studies on FEC columns with high strength steel and concrete with varying eccentricity and structural steel shapes. Total eight (8) FEC columns were numerically investigated using fiber section analysis in these studies. A computer program for fiber model analysis was developed using MATLAB (The Math works Inc. 2010) for this purpose. The contributions of the steel and concrete were determined to perform nonlinear numerical analysis for the critical section of the specimens. The analysis results were compared with the test results, in terms of the axial load-strain relationship and the moment-curvature relationship. In the model, a composite section was divided into layers and the force-equilibrium, linear strain distribution, and constitutive relationships of the materials were considered. In material models for the high-strength concrete the tensile stress of the concrete was ignored. The concrete area in the composite

section was divided into three regions according to confinement level: unconfined (concrete cover), partially confined (confined by lateral rebar's), and highly confined (confined by lateral rebar's and steel section) concrete zones. Authors reported that the nonlinear numerical analysis showed good agreement with the test results. But, it is observed from the study that the difference between experimental and numerical results of mentioned columns were 5% to 12%.

Mote and Vijay (2013) investigated the behaviour of pin-ended axially loaded concrete encased steel composite columns. A non-linear 3-D finite model was developed to analyse the inelastic behaviour of steel, concrete, longitudinal and transverse reinforcing bars as well as the effect of concrete confinement of the concrete encased steel composite columns. The experimental investigation on concrete encased steel composite columns was conducted with different slenderness ratio, different steel sections and different concrete and steel strength. The authors used various shape of structural steel in this study.

### **2.3.3 Comparison of codes**

AIC-318 (2014), AISC-LRFD (2010) and Euro code 4 are being used widely around the world for the construction of steel concrete composite structures. Extensive comparative studies were carried out between ACI-318 and AISC-LRFD for FEC column by Task Group 20 (1973), Furlong (1976), Tawil and Deierlein (1999), Weng and Yen (2000) and Soliman et al. (2012). Few studies were carried out on comparison between AISC-LRFD and Euro code 4 on FEC columns (Ellobody et al., 2011; Ellobody and Young 2011). Recently, Kim et al. (2012 and 2013), Samanta and Paul (2013), carried out comparative studies among these codes. These studies were based on comparatively older versions of the codes or specifications. Details of these three codes ACI-318 (2014), AISC-LRFD (2010) and Euro code 4 (2005) are given in Chapter 3.

Task Group 20 (1973) has designated composite columns in a standing committee of the Structural Stability Research Council (formerly called the Column Research Council). The Council recognized that the strength and stiffness of the structural steel alone were several times greater than the strength and stiffness of the structural concrete and ordinary reinforced concrete column. Design concepts traditionally applied to structural steel involved fundamental differences from those generally applied to reinforced concrete. The consequences of unequal results from the different design concepts required reconciliation within a rational statement of recommended practice for composite column. In subsequent

years the Council received reports from this task group, identified the major differences between the structural steel (AISC) and reinforced concrete (ACI-318) approach to regulations each felt should govern the design of composite columns.

Furlong (1976) published rules for composite column design based on the AISC column design method. Author compared the design provisions given by the ACI code with the test results and the AISC design method. Again, Furlong (1977) proposed equations for the evaluation of allowable service loads on composite columns. He attempted to provide for a continuous transition between the existing AISC design provisions applicable to the structural steel and the existing ones recommended by the ACI Building Code for reinforced concrete. Furlong (1978) also proposed interaction design equations for composite columns.

Tawil and Deierlein (1999) reviewed design criteria for concrete encased composite columns with emphasis on seismic behavior and the use of high-strength concrete. Strength and ductility of composite columns have been studied using a fiber analysis technique that accounts for the inelastic stress-strain response of steel and concrete. The change in composite column behavior as a function of the ratio of structural steel to gross column area, the nominal compression strength of concrete and concrete confinement by reinforcing bars have also been studied. The author limited the discussion to short columns where slenderness effects were not considered. The author had shown large differences in the nominal strengths for combined axial compression and bending calculated according to the ACI-318 and the AISC-LRFD specifications for concrete encased composite columns, and this discrepancy increased as the concrete strength is increased.

Weng and Yen (2000) carried out comparisons of concrete-encased composite column strength provisions for design in ACI-318 code (1999) and AISC-LRFD specification (1993). The calculated member strengths based on these two design provisions showed significant difference in some cases. The objective of this study was to investigate the difference between these two approaches and to evaluate the accuracy of their strength predictions. The authors compared the predicted strengths by using the ACI-318 and the AISC-LRFD approaches with 78 physical test results of encased composite column done by previous researchers. These columns were constructed with normal strength concrete and different percentages of structural steel. The statistical results showed that the ACI - 318-to-experimental capacity ratio had a mean value of 0.90 with a coefficient of variation (COV) of 15% and the AISC-to-experimental capacity ratio had a mean value of 0.73 with a COV

of 21%. This comparative study indicates that the ACI-318 approach generally gave closer predictions than the AISC-LRFD method.

Ellobody and Young (2011) conducted comparative study between AISC-LRFD and Euro code 4 for concentric axial load. These columns were different in sizes, lengths, and materials properties. Columns were experimentally investigated by previous authors. These columns were constructed with normal strength concrete (30 MPa) and structural steel (275 to 460 MPa). The unfactor load capacity of these columns were determined using equations given by these two codes. The composite column strengths obtained from AISC-LRFD ( $P_{AISC}$ ) and Euro code 4 ( $P_{EC4}$ ) were compared with the test results ( $P_{Test}$ ). The mean values of  $P_{Test}/P_{AISC}$  and  $P_{Test}/P_{EC4}$  ratios were 1.33 and 1.21, respectively, with the corresponding coefficients of variation (COV) of 0.211 and 0.117, respectively. The authors reported that the design strength predicted by the two specifications were conservative for the tested specimens. The AISC-LRFD (2005) predications were more conservative than the Euro code 4.

Ellobody et al. (2011) presented a study on numerical simulations of eccentrically loaded FEC columns. The objective of this study was to compare numerical results with the Euro code 4. The finite element models were validated against existing test results. Numerical models were developed considering the variables that influence the eccentrically loaded composite column behaviour and strength comprising different eccentricities, column dimensions, structural steel sizes, concrete strengths, and structural steel yield stresses. The concrete strengths varied from normal to high strength (30-110 MPa). The steel section yield stresses also varied from normal to high strength (275-690 MPa) with 5% structural steel. The strength of composite columns obtained from the finite element analysis were compared with the design strengths calculated using the Euro code 4 for composite columns. The authors reported that the Euro code 4 accurately predicted the eccentrically loaded composite columns, while over estimated the moment.

Soliman et al. (2012) carried out an experimental study to determine the ultimate load carrying capacity, axial deformation and failure pattern of the FEC columns. The columns were constructed with I-shaped steel section, round steel pipes, round plastic pipes and I-shaped wood as structural materials. The aim of this study was also to observe the failure behaviour and compare the experimental load with the strength obtained from different codes. Ten FEC columns were constructed to investigate the effect of these parameters. The columns were constructed with normal strength concrete (25 MPa) and structural steel



(240 MPa). All the columns were square in cross section of size 200 mm × 200 mm with entire height as 1400 mm. The experimental ultimate load capacities were compared with the current state of design provisions for composite columns from the Egyptian codes ECP203 (2007) and ECP-SC-LRFD (2012), as well as, American Institute of Steel Construction, AISC-LRFD (2010), American Concrete Institute, ACI-318 (2008), and British Standard BS-5400-5. Authors reported that ACI-318 gives the closest prediction with an average of 4% lower than the test results and ECP-SC-LRFD (2012) gives the most conservative results with an average of 29% lower than the test results.

Samanta and Paul (2012) conducted a study on evaluation of current design practices on estimation of axial capacity of concrete encased steel composite stub columns. The design assessment of concrete encased I-section composite column was based on approaches given in Euro code 4, ACI-318, BS Code and AISC-LRFD. This study included comparison of various design parameters and evaluation of design strength based on the procedures predicted in the various codes of practices. A practical example has been considered to determine the ultimate capacities using various procedures to compare among them. The obtained results based on the methods varied widely, because of the different design considerations adopted by the different codes. As such, they hardly considered the effect of confinement of the concrete due to the presence of longitudinal reinforcements as well as lateral ties.

Kim et al. (2012) carried out a study to evaluate the applicability of the current design codes for the composite sections with high-strength materials. The P-M interaction curves resulting from the test were compared with the predictions by numerical analysis and the current design codes of ACI 318 (2008), Euro code 4 (2005), AISC-LRFD (2010) and AIJ (2001). The author reported that ACI 318-08 method under estimated the load carrying capacity of the specimens by neglecting the lateral confinement effect. On the other hand, Euro code 4, using full plastic capacity of the steel section, overestimated the test results. Thus, current design provisions need to be modified to accurately predict the load-carrying capacity of the composite members with high-strength steel and concrete. From the test results, the effective flexural stiffness  $EI_{eff}$  was evaluated. Generally, the current design codes, except Euro code 4, under estimated the test results. AISC-LRFD (2010) gave the best predictions for flexural stiffness of composite columns as reported by Kim et al. (2012)

## **2.4 Conclusions**

From the review of literature presented in this chapter it has become clear that extensive experimental investigations were carried out on strength and failure modes of short and slender FEC columns with normal strength of concrete (21 MPa to 35 MPa) and structural steel (250 MPa to 350 MPa) for concentric, eccentric and biaxial loading conditions. Studies on FEC columns using various percentages of structural steel are limited. Behaviour of FEC columns with high and ultra-high strength materials has not been explored completely. Effects of several geometric parameters such as column slenderness ratio, structural steel ratio, load eccentricity ratio and tie spacing on the strength and ductility of high strength FEC columns need to be explored. Most of the available codes on composite columns do not include the capacity prediction equations for high strength materials. In most of the codes, the upper limit for the strength of concrete is 70 MPa and for structural steel is 525 MPa. Therefore, the code specified guidelines and design equations for composite columns need to be extended to incorporate the effects of high and ultra-high strength materials. Experimental investigations on FEC columns with various structural steel percentages and concrete strength are therefore required. However, it is not possible to get a complete understanding of the influences of various components from experimental investigations only due to the high cost and time requirement for full scale testing. Therefore, finite element models are also required that can accurately predict the behaviour of FEC columns under various combinations of geometric and material properties.

## CHAPTER 3

### REVIEW OF DESIGN CODES ON COMPOSITE COLUMNS

#### 3.1 Introduction

Numerous different structural systems are used today to meet the performance or functional requirements in structures. Composite construction is widely used in structural systems to provide additional lateral stiffness for long span structures. FEC column construction uses the structural and constructional advantages of both concrete and steel. Concrete has low material costs, good fire resistance, and easy to place. Steel has high ductility and high strength-to-weight and stiffness-to-weight ratios. When properly combined, steel and concrete can produce synergetic savings in initial and life-cycle costs. The current state of design provisions for composite structural system are American Institute of Steel Construction AISC-LRFD (2010), American Concrete Institute ACI 318 (2014), European standard (Euro code 4), Canadian Standard Association (CSA 2009), Egyptian code ECP-SC-LRFD (2012), and British Standard (BS-5400) available in the world. Among above mentioned codes, AISC-LRFD (2010), ACI-318 (2014) and Euro code 4 are widely used for the design of steel concrete composite structures. This Chapter will present the design specifications and capacity prediction equations along with the detailing rules for FEC columns in ACI-318 (2014), AISC-LRFD (2010) and Euro code 4 (2005).

#### 3.2 ACI-318 (2014)

ACI-318 uses the limit state design format with load factors and capacity reduction factors. The strength of a composite column is computed as for reinforced concrete members. The expression for equivalent stiffness includes a creep factor, and cracked concrete stiffness is considered. Minimum eccentricities are specified to cover construction tolerances. The following sections briefly introduce the concerned strength provisions for the concrete-encased composite columns as recommended in the ACI-318 building code (2014).

##### 3.2.1 Axial compressive strength

Under uniaxial compression, the nominal compressive strength,  $P_n$  of a concrete-encased composite column can be found by summing up the axial-load capacities of the materials that make up the cross section. This leads to

$$P_n = 0.8P_o \quad (3.1)$$

$$P_o = 0.85f_{cu}A_c + F_{yr}A_r + F_yA_s \quad (3.2)$$

where,

$P_o$  = column capacity under uniaxial compression

$f_{cu}$  = compressive strength of concrete

$A_c$  = area of concrete

$F_{yr}$  = yield strength of longitudinal reinforcement

$A_r$  = area of longitudinal reinforcement

$F_y$  = yield strength of steel shape

$A_s$  = area of structural steel shape

The nominal axial compressive strength  $P_n$  for an encased composite column is limited to  $0.8P_o$  owing to a minimum eccentricity under axial load for all designed columns. Slenderness effects can be neglected for non sway frame if (a) or (b) is satisfied:

(a) For columns not braced against side sway

$$\frac{kl_u}{r} \leq 22 \quad (3.3)$$

(b) For columns braced against side sway

$$\frac{kl_u}{r} \leq 34 + 12(M_1/M_2) \quad (3.4)$$

and

$$\frac{kl_u}{r} \leq 40 \quad (3.5)$$

where,

$M_1/M_2$  is negative if the column is bent in single curvature, and positive for double curvature.

For composite columns, the radius of gyration,  $r$ , shall not be taken greater than:

$$r = \sqrt{\frac{(E_c I_g / 5) + E_s I_{sx}}{\left(\frac{E_c A_g}{5}\right) + E_s A_{sx}}} \quad (3.6)$$

Equation (3.6) is provided for estimating the radius of gyration for members with enclosed structural shapes.

where,

$I_{sx}$  = moment of inertia of structural steel shape, pipe, or tubing about centroidal axis of composite member cross section,  $\text{mm}^4$

$A_g$  = gross area of concrete section,  $\text{mm}^2$

$A_{sx}$  = area of steel shape, pipe, or tubing in a composite section,  $\text{mm}^2$ .

$E_c$  = modulus of elasticity of concrete, MPa

$E_s$  = modulus of elasticity of reinforcement and structural steel, MPa

The critical buckling load  $P_c$  shall be calculated

$$P_c = \frac{\pi^2(EI)_{eff}}{(kl_u)^2} \quad (3.7)$$

For composite columns,  $(EI)_{eff}$

$$(EI)_{eff} = \frac{(0.2E_c I_g)}{1 + \beta_{dns}} + E_s I_{sx} \quad (3.8)$$

For composite columns in which the pipe or structural shape makes up a large percentage of the cross section, the load transfer due to creep is insignificant. Accordingly, only the  $EI$  of the concrete in Equation (3.8) is reduced for sustained load effects.

where,

$\beta_{dns}$  = the ratio of maximum factored sustained shear within a story to the maximum factored shear in that story associated with the same load combination

$E_c$  = modulus of elasticity of concrete, MPa

$E_s$  = modulus of elasticity of reinforcement and structural steel, MPa

$I_{sx}$  = moment of inertia of structural steel shape, pipe, or tubing about centroidal axis of composite member cross section, mm<sup>4</sup>.

### 3.2.2 Flexural and axial load

The ACI-318 provisions for the strength interaction between axial and flexural loads for concrete-encased composite columns are essentially the same as those for ordinary reinforced concrete columns. It was based on a strain compatibility analysis at the limit state to develop a thrust versus moment ( $P-M$ ) interaction relation. The following assumptions are made in the analysis:

- Plane section remains plane.
- The maximum concrete compressive strain is limited to 0.003.
- The Whitney stress block, having a magnitude of  $0.85f_{cu}$ , is used for the concrete.
- Tensile strength of the concrete is neglected.
- Strain hardening of steel shape and rebar is neglected.

### 3.3 AISC-LRFD (2010)

The AISC-LRFD (2010) defines a composite column as a steel column fabricated from rolled or built up steel shapes and encased in structural concrete or fabricated from steel pipe or tubing and filled with structural concrete. In this specification the design method for composite columns is based on the ultimate strength of the materials part of the cross section and takes into account the inelastic material properties with the required design loads as factored service loads. It contains the latest design approach of structural steel based on the ultimate strength concept. The nominal strength of a composite cross section is calculated from the ultimate resistance to load, and reduction capacity factors related to material properties and characteristics of member failure are applied to the nominal strength of the cross section.

The strength provisions for concrete-encased composite columns as recommended in Chapter I of the AISC-LRFD (2010). In order for dissimilar materials to act in a composite manner, forces must be transferred between the materials so that they achieve a state of internal equilibrium with one another. Previous editions of the AISC-LRFD specification briefly address load transfer; however, these provisions are quite limited in scope and clarity. The AISC-LRFD (2010) specification significantly expands load transfer requirements in a new section. Clear guidance is now provided for the allocation of forces between steel and concrete sections as well as for force transfer mechanisms used for composite members.

#### 3.3.1 Axial compressive strength

In AISC-LRFD (2010) the design of composite column is based on the design equations for steel columns. The slenderness and area parameters are modified for the presence of concrete. Load transfer should be provided by direct bearing at the connections.

(a) When  $\frac{P_{no}}{P_e} \leq 2.25$

$$P_n = P_{no} \left[ 0.658^{\left(\frac{P_{no}}{P_e}\right)} \right] \quad (3.9)$$

(b) When  $\frac{P_{no}}{P_e} > 2.25$

$$P_n = 0.877P_e \quad (3.10)$$

where

$$P_{no} = [f_y A_s + f_{ysr} A_{sr} + 0.85 f_{cu} A_c] \quad (3.11)$$

$$P_e = \pi^2 (EI)_{eff} / (KL)^2 \quad (3.12)$$

$$EI_{eff} = E_s I_s + 0.5 E_s I_{sr} + C_1 E_c I_c \quad (3.13)$$

$$C_1 = 0.1 + 2 \left( \frac{A_s}{A_c + A_s} \right) \leq 0.3 \quad (3.14)$$

where

$A_c$  = area of concrete, mm<sup>2</sup>

$A_{sr}$  = area of continuous reinforcing bars, mm<sup>2</sup>

$A_s$  = area of steel section, in<sup>2</sup>

$E_c$  = modulus of elasticity of concrete, MPa

$E_s$  = modulus of elasticity of steel, MPa.

$EI_{eff}$  = effective moment of inertia rigidity of composite section, kip-mm<sup>2</sup>

$f_{cu}$  = specified minimum concrete compressive strength, MPa

$f_y$  = yield stress of the steel section, MPa

$f_{ysr}$  = specified minimum yield stress of reinforcing bars, MPa

$I_c$  = moment of inertia of the concrete section, mm<sup>4</sup>

$I_s$  = moment of inertia of the steel shape, mm<sup>4</sup>

$I_{sr}$  = moment of inertia of reinforcing bars, mm<sup>4</sup>

$K$  = effective length factor

$L$  = laterally unbraced length of the member, mm.

$w_c$  = weight of concrete per unit volume

Equation (3.11), for encased sections, comprises three terms. The first term is related to the structural steel section and the second term is related to the reinforcing bars. Both the structural steel and the reinforcement bars are assumed to reach their full capacity, which means that the coefficients for the first and the second term are 1.0. The third term is related to concrete strength. A uniform compressive stress of  $0.85f_{cu}$  is assumed. Equation (3.11), for the stiffness of the cross section, also has three parts. The structural steel is considered to contribute its full capacity, but the reinforcing bars are considered to contribute only half of their capacity as the bars on the tension side of the section will probably have yielded well before the section attains its ultimate strength. The effectiveness of the concrete part is

reduced using the coefficient  $C_1$ , because the concrete is not well confined (AISC-LRFD (2010)).

### 3.3.2 Axial loads and flexure (P-M)

Design for combined axial force and flexure may be accomplished using either the strain compatibility method or the plastic-distribution method. Several different procedures for employing the plastic-distribution method are given for concrete encased members. To assist in developing the interaction curves illustrated within the design examples, a series of equations are provided in AISC-LRFD (2010). These equations define selected points on the interaction curve, without consideration of slenderness effects. Tables 3.1 and 3.2 outline specific cases, and the applicability of the equations to a cross-section that differs should be carefully considered. As an example, the equations in Table 3.1 are appropriate for the case of side bars located at the centerline, but not for other sidebar locations. In contrast, these equations are appropriate for any amount of reinforcing at the extreme reinforcing bar location. In Table 3.2, the equations are appropriate only for the case of reinforcing bars at the corners of the encased section. When design cases deviate from those presented the appropriate interaction equations can be derived from first principles. The interaction diagram AECBD shown in Figure 3.1 is approximated by the polygon ACDB. Point A and Point B are the pure axial strength and flexural strength of the section, respectively. Point C corresponds to a plastic neutral axis location that results in the same flexural strength as Point B, but including axial compression. Point D corresponds to an axial compressive strength of one half of that determined for Point C. An additional Point E is included (between points A and C) for encased W-shapes bent about its weak axis (AISC-LRFD, 2010).

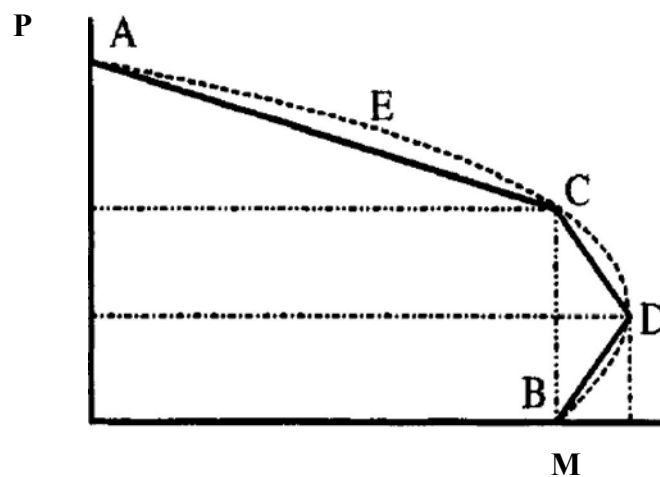


Figure 3.1 Interaction diagram (P-M) for composite columns



Table 3.1 Plastic capacities for rectangular FEC column major axis bending (AISC 2010)

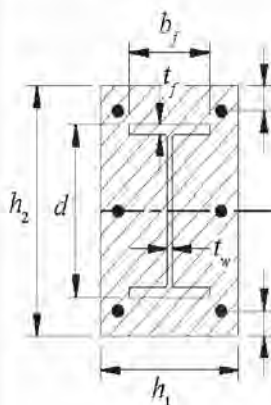
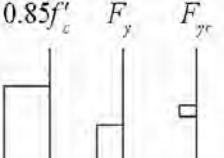


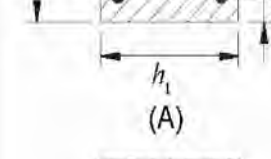
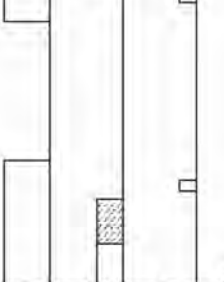
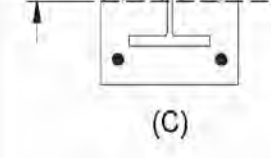
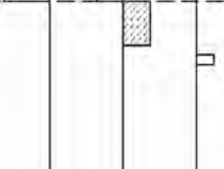
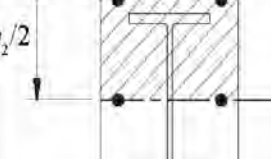
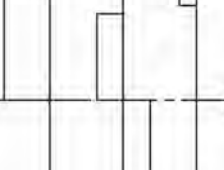
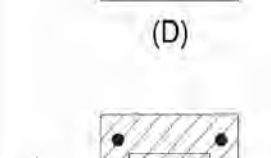
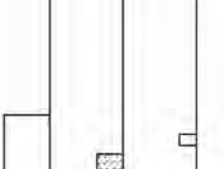
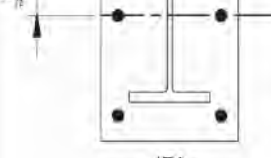
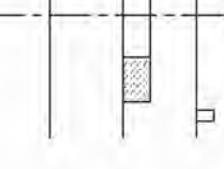
Section	Stress Distribution	Point	Defining Equations
 <p>(A)</p>		A	$P_A = A_s F_y + A_{sr} F_{yr} + 0.85 f'_c A_c$ $M_A = 0$ <p> <math>A_s</math> = area of steel shape  <math>A_{sr}</math> = area of all continuous reinforcing bars  <math>A_c = h_2 h_1 - A_s - A_{sr}</math> </p>
 <p>(C)</p>		C	$P_C = 0.85 f'_c A_c$ $M_C = M_B$
 <p>(D)</p>		D	$P_D = \frac{0.85 f'_c A_c}{2}$ $M_D = Z_s F_y + Z_r F_{yr} + \frac{Z_c}{2} (0.85 f'_c)$ <p> <math>Z_s</math> = full x-axis plastic section modulus of steel shape  <math>A_{sr}</math> = area of continuous reinforcing bars at the centerline  <math>Z_r = (A_{sr} - A_{sr,c}) \left( \frac{h_2}{2} - c \right)</math>  <math>Z_c = \frac{h_1 h_2^2}{A} - Z_s - Z_r</math> </p>
 <p>(C)</p>		CL PNA	$P_B = 0$ $M_B = M_D - Z_{cr} F_y - \frac{1}{2} Z_{cr} (0.85 f'_c)$ $Z_{cr} = h_1 h_n^2 - Z_{cr}$ <p>For <math>h_n</math> below the flange <math>\left( h_n \leq \frac{d}{2} - t_f \right)</math></p>
 <p>(D)</p>		PNA	$h_n = \frac{0.85 f'_c (A_s + A_{sr,c}) - 2 F_y A_{sr,c}}{2 [0.85 f'_c (h_1 - t_w) + 2 F_y t_w]}$ $Z_{cr} = t_w h_n^2$
 <p>(D)</p>		B	<p>For <math>h_n</math> within the flange <math>\left( \frac{d}{2} - t_f &lt; h_n \leq \frac{d}{2} \right)</math></p> $h_n = \frac{0.85 f'_c (A_s + A_{sr} - db_f + A_{sr,c}) - 2 F_y (A_s - db_f) - 2 F_y A_{sr,c}}{2 [0.85 f'_c (h_1 - b_f) + 2 F_y b_f]}$ $Z_{cr} = Z_s - b_f \left( \frac{d}{2} - h_n \right) \left( \frac{d}{2} + h_n \right)$
 <p>(B)</p>		PNA CL	<p>For <math>h_n</math> above the flange <math>\left( h_n &gt; \frac{d}{2} \right)</math></p> $h_n = \frac{0.85 f'_c (A_s + A_{sr} + A_{sr,c}) - 2 F_y A_s - 2 F_y A_{sr,c}}{2 (0.85 f'_c h_1)}$ $Z_{cr} = Z_{s,c} = \text{full x-axis plastic section modulus of steel shape}$

Table 3.2 Plastic capacities for rectangular FEC column minor axis bending (AISC 2010)

Section	Stress Distribution	Point	Defining Equations
<p>(A)</p> <p>(E)</p> <p>(C)</p> <p>(D)</p> <p>(B)</p>	<p><math>0.85f'_c</math> <math>F_y</math> <math>F_{yr}</math></p>	A	$P_A = A_s F_y + A_c F_{yr} + 0.85 f'_c A_c$ $M_A = 0$ $A_s$ = area of steel shape $A_w$ = area of continuous reinforcing bars $A_c = h_1 h_2 - A_s - A_w$
		E	$P_E = A_s F_y + (0.85 f'_c) \left[ A_c - \frac{h_1}{2} (h_2 - b_f) + \frac{A_w}{2} \right]$ $M_E = M_D - Z_{ys} F_y - \frac{1}{2} Z_{is} (0.85 f'_c)$ $Z_{is} = Z_{ys}$ = full y-axis plastic section modulus of steel shape $Z_{is} = \frac{h_1 b_f^2}{4} - Z_{ys}$
		C	$P_C = 0.85 f'_c A_c$ $M_C = M_D$
		D	$P_D = \frac{0.85 f'_c A_c}{2}$ $M_D = Z_{is} F_y + Z_{ys} F_{yr} + \frac{1}{2} Z_{cs} (0.85 f'_c)$ $Z_{is}$ = full y-axis plastic section modulus of steel shape $Z_{ys} = A_w \left( \frac{h_2 - c}{2} \right)$ $Z_{cs} = \frac{h_1 h_2^2}{4} - Z_{is} - Z_{ys}$
		B	$P_B = 0$ $M_B = M_D - Z_{ms} F_y - \frac{1}{2} Z_{ms} (0.85 f'_c)$ $Z_{ms} = h_1 h_n^2 - Z_{ms}$ For $h_n$ below the flange $\left( \frac{t_w}{2} < h_n \leq \frac{b_f}{2} \right)$ $h_n = \frac{0.85 f'_c (A_c + A_s - 2t_f b_f) - 2F_y (A_s - 2t_f b_f)}{2 [4t_f F_y + (h_1 - 2t_f) 0.85 f'_c]}$ $Z_{ms} = Z_{ys} - 2t_f \left( \frac{b_f}{2} + h_n \right) \left( \frac{b_f}{2} - h_n \right)$ For $h_n$ above the flange $\left( h_n > \frac{b_f}{2} \right)$ $h_n = \frac{0.85 f'_c (A_c + A_s) - 2F_y A_s}{2 [0.85 f'_c h_1]}$ $Z_{ms} = Z_{ys}$ = full y-axis plastic section modulus of steel shape

### 3.4 Euro Code 4 (2005)

The Euro Code 4 column design assumes that concrete and steel interact fully with each other until failure. Design by the Euro Code method uses the full plastic axial and moment capacity of the cross-section. Reduction factors are applied to these values based on the column slenderness and other considerations. The Euro Code composite design considers all material properties of the cross-section, including partial safety factors for the different materials. The Euro Code uses partial safety factors to reduce steel yield stress, concrete compressive strength, and yield stress of reinforcing bar, while AISC-LFRD uses a single resistance factor. It is observed that Euro code procedures are more complex than the AISC-LFRD composite column design.

#### 3.4.1 Resistance of cross sections

The plastic resistance to compression  $N_{pl,Rd}$  of a composite cross-section is calculated by adding the plastic resistances of its components:

$$N_{pl,Rd} = A_a f_{yd} + 0.85 A_c f_{cd} + A_s f_{sd} \quad (3.15)$$

Thus, the un-factored design strengths ( $P_{EC4}$ ) for axially loaded concrete encased steel composite columns is calculated using the simplified method of design Clause 6.7.3 of the Euro code-4 (2005) based on the relative slenderness ( $\bar{\lambda}$ ) as follows:

$$P_{EC4} = \chi N_{pl} \quad (3.16)$$

where

$$\chi = \frac{1}{\phi + [\phi^2 - \bar{\lambda}^2]^{0.5}} \leq 1 \quad (3.17)$$

with

$$\phi = 0.5 [1 + \alpha (\bar{\lambda} - \bar{\lambda}_o) + \bar{\lambda}^2] \quad (3.18)$$

and

$$\bar{\lambda} = \frac{L_e}{\pi} \left( \frac{A_s f_{ys} + 0.85 A_c f_c + A_r f_{yr}}{E_s I_s + 0.6 E_{cm} I_c + E_r I_r} \right)^{\frac{1}{2}} \quad (3.19)$$

where

$E_{cm}$  = is the secant modulus of elasticity of concrete in MPa,

$L_e$  = is the effective length of the column,

$\alpha$  and  $\bar{\lambda}_o$  are the factors given in Table 5.3 (EC-3) of the specification and taken as 0.49 and 0.21, respectively for the concrete-encased steel composite columns investigated.

$E_s$  = modulus of elasticity of steel, MPa

$E_c$  = modulus of elasticity of concrete, MPa

$E_r$  = modulus of elasticity of reinforcing steel, MPa

$I_s$  = moment of inertia of steel, mm<sup>4</sup>

$I_c$  = moment of inertia of concrete (assumed to be uncracked), mm<sup>4</sup>

$I_r$  = moment of inertia of reinforcing steel, mm<sup>4</sup>

The modulus of elasticity for concrete was previously defined in the Euro code-4 as

$E_c = 600f_{cu}$  but is now defined as  $E_c = 0.8E_{cm}/\gamma_c$  where  $E_{cm}$  is the secant modulus of concrete, and  $\gamma_c$  is taken as 1.35.

### 3.4.2 Axial load and bending moment (P-M)

The resistance of the cross-section subjected to axial load and bending moment can be calculated by utilizing a full plastic stress distribution assumption. In the steel beam-column interaction curve, the moment resistance reduces with increasing axial load. However, in the composite beam-column interaction curve, the moment resistance increases up to the “balance point” due to the presence of axial load because of the pre-stressing effect of the compressive forces. The interaction curve can be drawn by determining the stress block at numerous levels of axial load. This calculation is easily performed by computer routines. An approximation of the full interaction curve can be determined by calculating several points on the curve and connecting those points with straight lines. These points may be calculated by assuming rectangular stress blocks (Euro code 4, 2005).

#### *Approximation by a Polygonal Path*

As proposed in Euro code 4 (2005) the interaction curve of the cross-section can be approximately drawn by connecting four or five key points related to the resistance to combined compression and bending. The stress distribution at each point from point A to D of the interaction curve for major axis bending. Five points from A to E are required as shown in the stress distribution and interaction curve for minor axis bending. The maximum internal moment at point D is:

$$M_{max} = Z_s f_{yd} + \frac{1}{2} Z_c f_{cd} + Z_r f_{rd} \quad (3.20)$$

where,

$Z_s$  = plastic modulus of steel cross-section, mm<sup>3</sup>

$Z_c$  = plastic modulus of overall concrete cross-section, mm<sup>3</sup>

$Z_r$  = plastic modulus of reinforcement, mm<sup>3</sup>

The 1/2 factor for the concrete term is based on neglecting tension in the concrete. Thus, only half of the cross-section is considered. The plastic modulus of the reinforcement can be expressed as:

$$Z_r = \sum_{i=1}^n A_{ri} e_i \quad (3.21)$$

where

$A_{ri}$  = area of one reinforcing bar, in.<sup>2</sup>

$e_i$  = distance to the bending axis considered, in.

The plastic moment of the composite cross-section resulting from for the region  $2h_n$  can be calculated as:

$$M_{pn} = Z_{sn} f_{yd} + \frac{1}{2} Z_{cn} f_{cd} + Z_{rn} f_{rd} \quad (3.22)$$

The sub index n indicates that the stresses within  $2h_n$  are used for this calculation. The distance  $h_n$  and the region  $2h_n$  are shown in Table 3.3. The equations for  $h_n$  are different depending on the type of cross-section and the location of the neutral axis. The equations needed to get obtain  $h_n$  are given below.

### ***Concrete-Encased I-sections Major Axis***

The plastic modulus of the structural steel I-section about its major axis can be obtained from the design tables, or it can be calculated as:

$$Z_s = \frac{(d-2t_f)t_w^2}{4} + b_f t_f (d - t_f) \quad (3.23)$$

The plastic modulus of the concrete is:

$$Z_c = \frac{h_1 h_2}{4} - Z_s - Z_r \quad (3.24)$$

There are three regions to consider for the position of the neutral axis. The procedure for finding the position is iterative. First, a distance  $h_n$  located on a particular region is assumed. Again,  $h_n$  is calculated by substituting value into the appropriate equation (Equations 3.25 to 3.29). If the value for  $h_n$  is within the assumed region, the distance  $h_n$  has been determined. If not, another region is chosen and the procedure is repeated. The distance  $h_n$  and plastic modulus of the steel for each position of neutral axis are:

(a) Neutral axis in the web:  $h_n \leq \frac{d}{2} - t_f$

$$h_n = \frac{N_{pm} - A_m(2f_{rd} - f_{cd})}{2h_1f_{cd} + 2t_2(2f_{yd} - f_{cd})} \quad (3.25)$$

$$Z_{sn} = t_w h_n^2 \quad (3.26)$$

(b) Neutral axis in flange:  $\frac{d}{2} - t_f \leq h_n < \frac{d}{2}$

$$h_n = \frac{N_{pm} - A_m(2f_{rd} - f_{cd}) + (b_f - t_w)(d - 2t_f)(2f_{yd} - f_{cd})}{2h_1f_{cd} + 2t_2(2f_{yd} - f_{cd})} \quad (3.27)$$

$$Z_{sn} = b_f h_n^2 - \frac{(b_f - t_w)(d - 2t_f)^2}{4} \quad (3.28)$$

(c) Neutral axis outside the steel section:  $\frac{d}{2} \leq h_n \leq \frac{h_2}{2}$

$$h_n = \frac{N_{pm} - A_m(2f_{rd} - f_{cd}) - A_s(2f_{yd} - f_{cd})}{2h_1f_{cd}} \quad (3.29)$$

$$Z_{sn} = Z_s \quad (3.30)$$

where  $A_m$  is the sum of reinforcement areas within the  $2h_n$  region, and the plastic modulus of the concrete in the region  $2h_n$  is

$$Z_{cn} = h_1 h_n^2 - Z_{sn} - Z_{rn} \quad (3.31)$$

The neutral axis is in the web for most I-type composite sections under major axis bending.

Table 3.3 Stress distribution at each point of FEC column major axis bending (EC4 2005)

	Section	Stress Distribution	Equation
<b>A</b>			$N = P_{pl} = A_c \cdot f_{cd} + A_s \cdot f_{yd} + A_r \cdot f_{rd}$ $f_{cd} = 0.85 \cdot f_c' / \gamma_c, f_{yd} = F_y / \gamma_s, f_{rd} = F_{yR} / \gamma_c$ <p><math>\gamma_c, \gamma_s, \gamma_r</math> : partial safety factors</p> $A_c = h_1 \cdot h_2 - A_s - A_r$ $M = 0$
<b>B</b>			$N = 0$ $h_n \rightarrow h_1 \cdot a \cdot f_{cd} = (h_2 - 2a) \cdot t_w \cdot f_{yd}$ $M = M_{pn} = Z_{sn} \cdot f_{yd} + \frac{1}{2} \cdot Z_{cn} \cdot f_{cd} + Z_{rn} \cdot f_{rd}$ $Z_{sn} = t_w \cdot h_n^2 ; Z_{cn} = h_1 \cdot h_n^2 - Z_{sn} - Z_{rn}$
<b>C</b>			$N = N_{pm} = A_c \cdot f_{cd}$ $h_n \rightarrow h_1 \cdot a \cdot f_{cd} = (h_2 - 2a) \cdot t_w \cdot f_{yd}$ $M = M_{pm} = Z_{sn} \cdot f_{yd} + \frac{1}{2} \cdot Z_{cn} \cdot f_{cd} + Z_r \cdot f_{rd}$
<b>D</b>			$N = \frac{1}{2} \cdot N_{pm} = \frac{1}{2} \cdot A_c \cdot f_{cd}$ $M = M_{max} = Z_s \cdot f_{yd} + \frac{1}{2} \cdot Z_c \cdot f_{cd} + Z_r \cdot f_{rd}$ $Z_s = \frac{(d - 2 \cdot t_f) \cdot t_w^2}{4} + b_f \cdot t_f \cdot (d - t_f)$ $Z_c = \frac{h_1 \cdot h_2^2}{4} - Z_s - Z_r$

### Concrete Encased I-shapes Minor-Axis

The plastic modulus of the steel I-section about its minor axis can be taken from a table or calculated as:

$$Z_s = \frac{(d-2t_f)t_w^2}{4} + \frac{2t_f b_f^2}{4} \quad (3.32)$$

The plastic modulus of the concrete is obtained given by:

$$Z_c = \frac{h_1 h_2}{4} - Z_s - Z_r \quad (3.33)$$

There are two regions to consider for the location of the neutral axis for minor axis bending. The same procedure is followed to find the location of the neutral axis as for major axis bending.

(a) Neutral Axis in the web:  $\frac{t_w}{2} \leq h_n \leq \frac{b_f}{2}$

$$h_n = \frac{N_{pm} - A_m(2f_{rd} - f_{cd}) - t_w(2t_f - d)(2f_{yd} - f_{cd})}{2h_1 f_{cd} + 4t_4(2f_{yd} - f_{cd})} \quad (3.34)$$

$$Z_{sn} = 2t_f h_n^2 - \frac{(d-2t_f)^2}{4} \quad (3.35)$$

(b) Neutral Axis in flange:  $\frac{t_w}{2} \leq h_n \leq \frac{h_2}{2}$

$$h_n = \frac{N_{pm} - A_m(2f_{rd} - f_{cd}) - A_s(2f_{yd} - f_{cd})}{2h_1 f_{cd}} \quad (3.36)$$

$$Z_s = Z_s \quad (3.37)$$

$$Z_{cn} = h_1 h_n^2 - Z_{sn} - Z_{rn} \quad (3.38)$$

Because the interaction diagram for weak axis bending bulges significantly between points A and C, an additional point E is calculated in the region between point A and C (Table 3.4). This position can be calculated by arbitrarily choosing a neutral axis between  $h_n$  and the edge of the cross-section. It is convenient to choose the edge of the steel shape when making this choice. The result of the axial force calculation at point E is

$$N_E = h_2(h_E - h_n)f_{cd} + 2t_f(h_E - h_n)(2f_{yd} - f_{cd}) + A_{rE}(2f_{rd} - f_{cd}) + N_{pm} \quad (3.39)$$

where

$A_{rE}$  = reinforcement area which eventually exists in the additionally compressed region between the distances  $h_n$  and  $h_E$

Finally, the moment  $M_E$  is obtained from the difference between  $M_{max}$  and  $\Delta M_E$ .

$$M_E = M_{max} - \Delta M_E \quad (3.40)$$

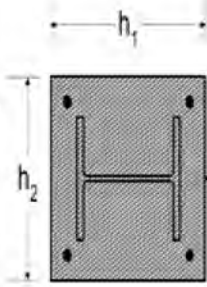
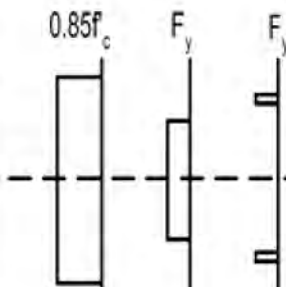
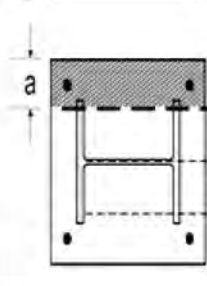
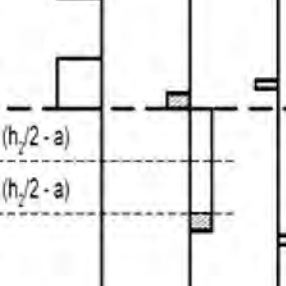
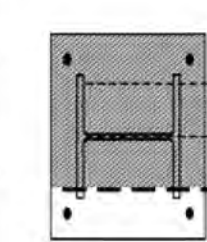
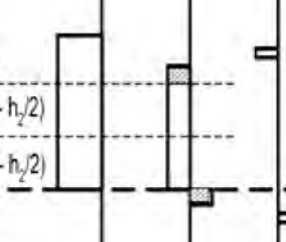
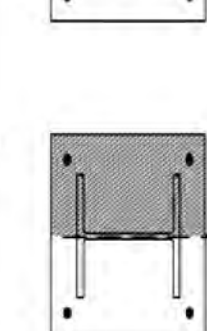
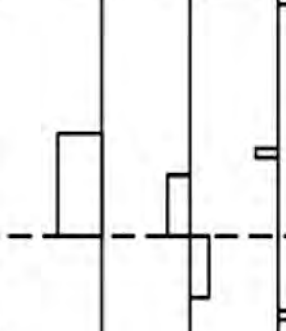
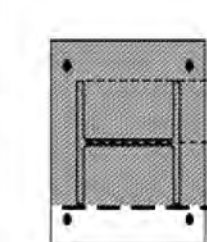
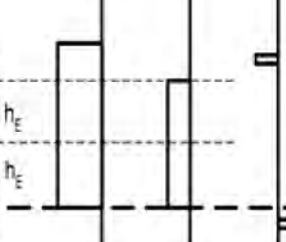
where

$$\Delta M_E = Z_{sE}f_{yd} + \frac{1}{2}Z_{cE}f_{cd} + Z_{rE}f_{rd} \quad (3.41)$$

The terms  $Z_{sE}$ ,  $Z_{cE}$  and  $Z_{rE}$  can be calculated from the appropriate above equations by substituting  $h_E$  instead of  $h_n$ .



Table 3.4 Stress distribution at each point of FEC column minor axis bending (EC4 2005)

	Section	Stress Distribution	Equation
A			$N = P_{pl} = \Lambda_c \cdot f_{cd} + \Lambda_s \cdot f_{yd} + \Lambda_r \cdot f_{rd}$ $\Lambda_c = h_1 \cdot h_2 - \Lambda_s - \Lambda_r$ $f_{cd} = 0.85 \cdot f_c / \gamma_c, f_{yd} = F_y / \gamma_s, f_{rd} = F_{yr} / \gamma_r$ $M = 0$
B			$N = 0$ $h_n \rightarrow h_1 \cdot a \cdot f_{cd} = 2 \cdot (h_2 - 2a) \cdot t_f \cdot f_{yd} + (d - 2 \cdot t_f) \cdot t_w \cdot f_{yd}$ $M = M_{pn} = Z_{sn} \cdot f_{yd} + \frac{1}{2} \cdot Z_{cn} \cdot f_{cd} + Z_m \cdot f_{rd}$ $Z_{sn} = 2 \cdot t_f \cdot h_n^2 + \frac{(d - 2 \cdot t_f) \cdot t_w^2}{4}$ $Z_{cn} = h_1 \cdot h_n^2 - Z_{sn} - Z_m$
C			$N = N_{pm} = \Lambda_c \cdot f_{cd}$ $M = M_{pn} = Z_{sn} \cdot f_{yd} + \frac{1}{2} \cdot Z_{cn} \cdot f_{cd} + Z_r \cdot f_{rd}$
D			$N = \frac{1}{2} \cdot N_{pm} = \frac{1}{2} \cdot \Lambda_c \cdot f_{cd}$ $M = M_{max} = Z_s \cdot f_{yd} + \frac{1}{2} \cdot Z_c \cdot f_{cd} + Z_r \cdot f_{rd}$ $Z_s = \frac{(d - 2 \cdot t_f) \cdot t_w^2}{4} + \frac{1}{2} \cdot t_f \cdot b_f^2$ $Z_c = \frac{h_1 \cdot h_2^2}{4} - Z_s - Z_r$
E			$N = \frac{1}{2} \cdot (P_{pl} + N_{pm})$ $M = M_{max} - \Delta M_E, \Delta M_E = Z_{sE} \cdot f_{yd} + \frac{1}{2} \cdot Z_{cE} \cdot f_{cd} + Z_{rE} \cdot f_{rd}$ $Z_{sE} = 2 \cdot t_f \cdot h_E^2 + \frac{(d - 2 \cdot t_f) \cdot t_w^2}{4}$ $Z_{cE} = h_1 \cdot h_E^2 - Z_{sE} - Z_{rE}$

### 3.5 Materials Properties and Detailing Criteria

Material strength and detailing play a vital role on the strength and durability of FEC columns. In these three standard (ACI-318, AISC-LRFD and Euro code 4) limits have been given on different material strength and detailing criteria for the construction of FEC column. A comparison has been carried out among these three codes on limit of different material strength and detailing criteria for FEC columns. The materials used in FEC columns are structural steel, longitudinal and transverse reinforcement and concrete. The detailing criteria are clear cover, spacing of transverse reinforcement, longitudinal reinforcement, and shear connector provisions etc. The following Table 3.5 contains the comparison on materials strength and design criteria of FEC column.

Table 3.5 Comparison on material strength and design criteria of different codes

Items	AISC-LRFD (2010)	ACI-318 (2014)	Euro code 4 (EC4 2005)
Concrete (normal weight)	Concrete compressive strength Min. $f'_c = 21$ MPa (3.0 ksi) Max. $f'_c = 70$ MPa (10.0 ksi)	Min. $f'_c = 17$ MPa (2.5 ksi)	Min. $f'_{ck} = 20$ MPa (2.9 ksi) Max. $f'_{ck} = 50$ MPa (7.3 ksi)
	Concrete compressive strength (lightweight) Min. $f'_c = 21$ MPa (3.0 ) $f'_c = 42$ MPa (6 Ksi)	Min. $f'_c = 17$ MPa (2.5 Ksi)	Not permitted.
	Structural steel core limitations	The cross-sectional area of the structural steel core shall comprise at least 1% of the total composite section.	No requirement.
Concrete cover for encased steel member	No requirement.	No requirement.	Min. of 40 mm (1.6 in.) or one-sixth times steel core flange width, whichever is greater. A max. of 0.4 times the composite column width in the strong direction or 0.3 times the composite column depth in the weak direction may be used for calculations.
Yield strength	Max. $F_y = 525$ MPa (75 ksi)	Max. $F_y = 345$ MPa (50 ksi)	Max. $F_y = 460$ MPa (67 ksi) With more restrictive strength limits for $F_y = 420$ MPa (61 ksi)

	Items	AISC-LRFD (2010)	ACI-318 (2014)	Euro code 4 (EC4 2005)
Transverse reinforcement	Transverse reinforcement area/diameter	Min. tie diameter 10 mm (No 3) bar and may 12 mm (No 4) bar	Min. tie diameter No 3 bar and max No. 5 bar.	Min. tie diameter shall be no less than 0.25 times the longitudinal bar diameter or 6 mm (0.24 in.), whichever is greater.
	Intermediate transverse reinforcement requirements	General reference made to ACI 318 (2005).	No specific requirement for composite members. General rules for compression members require that every corner and alternate longitudinal bar shall have lateral support. Additionally, no longitudinal bar shall be farther than 150 mm (6in.) clear from a laterally supported bar.	No bar within a compression zone shall be located further than 150 mm (6.0 in.) from a restrained bar.
	Transverse reinforcement spacing	Lateral ties are used, a minimum of either a No. 3 (10 mm) bar spaced at a maximum of 12 in. (305 mm) on center, or a No. 4 (13 mm) bar or larger spaced at a maximum of 16 in. (406 mm) on center shall be used. Deformed wire or welded wire reinforcement of equivalent area are permitted. Maximum spacing of lateral ties shall not exceed 0.5 times the least column dimension.	Max. spacing of lateral ties is the least of $16d_b$ , $48d_{stirrup}$ , or 0.5 times the least column dimension.	Max. spacing of lateral ties is the least of $20d_b$ , the least column dimension, or 400 mm (15.75 in.). At beam-column intersections and lapped joints, spacing is limited to 60% of the above requirement (EC2).
	Spiral transverse reinforcement requirements	General reference made to ACI-318(2014).	Volumetric spiral reinforcement ratio ( $\rho_s$ ) $\rho_s = 0.45 \left( \frac{A_g}{A_{ch}} - 1 \right) \frac{f_c}{f_{yt}}$	No specific requirement.
Longitudinal reinforcement	Longitudinal reinforcement ratio	$0.004A_g \leq A_{sr}$	$0.01A_c \leq A_{sr} \leq 0.08A_c$	$0.003A_c \leq A_{sr} \leq 0.06A_c$
	Concrete cover for longitudinal reinforcement	Min. reinforcement clear cover = 38 mm (1.5 in.)	Min. reinforcement clear cover = 38 mm (1.5 in.), or more for special conditions.	Min. reinforcement cover ranges from 10 mm. (0.4 in) to 55 mm (2.2 in.) with a minimum of one bar diameter based on exposure condition, bond, and fire resistance(EC2).
	Min. diameter of longitudinal reinforcement	No requirement.	No requirement.	Min. dia. = 8 mm (0.3 in.)

Items	AISC-LRFD (2010)	ACI-318 (2014)	Euro code 4 (EC4 2005)
Location and number of longitudinal reinforcement bars	At least four continuous bars shall be used in encased composite columns (presumably at corners although not specifically stated).	Vertical bars must be located at each corner, with longitudinal bars spaced not farther apart than one-half the least side dimension of the composite member. Four bar min. for circular ties, six bar min. for spirals.	Min. of one bar per corner for any column shape, and four bars for a circular shape.
Longitudinal reinforcement spacing	General reference made to ACI 318.	Min. clear distance is $1.5d_b$ or 33 mm (1.5 in.), whichever is greater.	Min. spacing is the longitudinal bar diameter, the diameter of aggregate +5 mm (0.2 in), or 20 mm (0.8 in.), whichever is greater. However, rebar may be directly attached to the steel shape provided the bond surface is reduced by one-half or three quarters, depending upon the location of the reinforcement with respect to the embedded steel shape (EC2).
Shear Transfer (Load Introduction)	Load transfer between concrete encasement and steel core Shear connectors must be placed symmetrically at least two sides of the steel core. Shear connectors must be distributed above and below the load transfer region for a distance equal to at least 2.5 times the column depth. Max. connector spacing may not exceed 400 mm (16 in.).	Any axial load strength assigned to concrete of a composite member shall be transferred to the concrete by members or brackets in direct bearing on the composite member concrete.	Need not be used if the design bond/friction strength is sufficient. If required, must be distributed in the region equal to 2.0 times the minimum transverse column dimension (or one-third of the column length, whichever is greater. Concrete confinement effects may be considered in computation of shear resistance for members with studs connected to the web.
General Reinforcement	Development length Lap splices	General reference made to ACI. General reference made to ACI 318.	Various requirements are contained in ACI 318 Requirements for tension lap splices, compression lap splices, and general provisions are contained in ACI318
Miscellaneous	Connection of multiple encased shapes	When two or more steel shapes are encased, they must be interconnected with lacing, tie plates, batten plates, or otherwise, to avoid individual shape buckling prior to concrete hardening.	No requirement. No requirement.

### **3.6 Conclusions**

AISC-LRFD (2010), ACI-318 (2014) code and Euro Code 4 (2005) were reviewed in this chapter for FEC columns. This review was mainly carried out on design equations for the capacity prediction and design criteria given by these three standards. The ACI-318 design equations originally developed for reinforced concrete columns may not be appropriate for the design of concrete-encased composite columns. For instance, the nominal strength of a composite column specified in the ACI-318 Code is based on the assumption of strain compatibility. However, the influence of residual stress in the steel section and confinement effect in concrete are neglected. On the other hand, the AISC-LRFD column equations were developed to considering the full capacity structural steel and the half effect of longitudinal reinforcement. In EC4 full interaction between the steel and concrete sections has been considered until the failure occurs. Geometric imperfections and residual stresses were also taken into account in the calculation. The effect of confinement of the concrete due to the presence of longitudinal reinforcements, structural steel as well as lateral ties were not considered by any of the codes. The detailing criteria and the materials properties for the construction of FEC columns were reviewed. It was observed that none of the standards give guide lines for the use of high strength or ultra high strength materials in FEC columns.

## CHAPTER 4

### EXPERIMENTAL INVESTIGATIONS OF FEC COLUMNS

#### 4.1 Introduction

An experimental investigation, to determine the complete failure modes and load deflection behaviour of FEC columns is presented in this study. The main variables considered in the test program were, the applied axial load positions, concrete compressive strength, cross sectional dimensions, and percentage of structural steel. The loads were applied concentrically and eccentrically on top of the columns. The failure modes, peak load, peak strain and experimental load-deflection behaviour of the specimens were examined for these two types of loads (concentric and eccentric) in this study. The composite column specimens were tested in the Solid Mechanics Laboratory of Bangladesh University of Engineering and Technology (BUET), Dhaka, Bangladesh during the month of January in 2015. The description of the test specimens, test setup, loading conditions and results obtained are presented in the following sections.

#### 4.2 Test Program

The test program consisted of thirteen (13) FEC columns of two different sizes with various percentages of I-shaped structural steel and concrete strength. These FEC columns were square in size and constructed with normal and high strength concrete. The columns were tested for concentric and eccentric loads, to observe the failure behaviour and the ultimate load carrying capacity of FEC columns. The load versus deflection behaviour of these FEC columns were also observed.

##### 4.2.1 Description of test specimens

In the experimental study, eleven columns were tested for concentrically applied axial load and two columns for eccentrically applied axial load. Two types of square columns with different sizes were constructed in this study. Seven specimens were square short composite columns constructed with normal strength concrete. These seven columns were divided into three groups. These groups were SCN4A (SCN4A1, SCN4A2 and SCN4A3), SCN4B (SCN4B1, SCN4B2 and SCN4B3) and SCN4E. The columns of group SCN4A, SCN4B and SCN4E had a square cross-section of 100 mm × 100 mm. The length of these columns were fixed at 900 mm. The columns included in group SCN4A and SCN4B were tested for concentric axial load and group SCN4E for eccentric axial load.

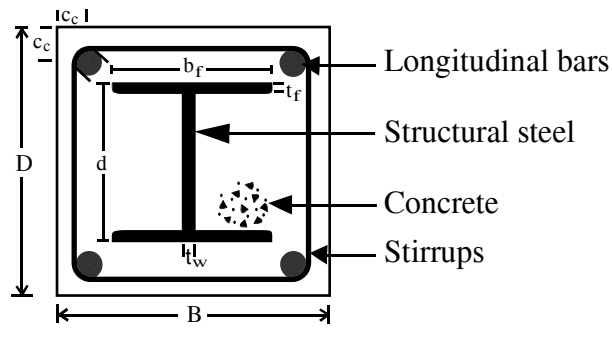
Another six columns constructed with higher strength concrete (42 MPa) were divided in three groups. These three groups were SCH6A (SCH6A1, SCH6A2 and SCH6A3), SCH6B (SCH6B1 and SCH6B2) and SCH6E. The columns of group SCH6A, SCH6B and SCH6E had square cross-sections of 150 mm × 150 mm and length of 900 mm. The columns included in group SCH6A and SCH6B were tested for concentric axial load and group SCH6E for eccentric axial load. The diameters of the main and transverse reinforcements were 8 mm and 6 mm respectively in these columns. The column sizes 100 mm × 100 mm and 150 mm × 150 mm were constructed with stirrup spacing of 50 mm and 75 mm, respectively. The first stirrup was fixed at a distance of 25 mm from the face of the column. The concrete compressive strength ( $f_{cu}$ ) for normal and high strength concrete are 28 MPa and 42 MPa, respectively. Figure 4.1 shows the cross-section and elevations of a typical FEC test column. The geometric parameters illustrated in the plan view (Figure 4.1(a)) are the column depth (D), the overall breadth (B) and other elements used for construction of FEC columns. Typical 3-D views of the FEC columns are illustrated in Figure 4.1(b). The elements used in FEC columns are longitudinal and transverse reinforcement, concrete and I-shaped structural steel. The overall dimensions of I-shaped structural steel were, the flange width,  $b_f$ , the total depth,  $d$ , and the flange thickness,  $t_f$  and web thickness,  $t_w$ . Parameters illustrated in the elevation view in Figure 4.1(c) are the column length,  $L$ , and the centre-to-centre spacing of the stirrups,  $s$ , of 100 mm × 100 mm and 150 mm × 150 mm sections respectively. The yield strength of reinforcement and I-shape structural steel are 470 MPa and 350 MPa, respectively. The overall length ( $L$ ) of all sizes of FEC test columns are 900 mm. The column Groups SCN4A, SCN4B, SCH6A and SCH6B were tested for concentric axial load. The columns SCN4E and SCH6E were tested for eccentric axial loads. The geometric properties of the test specimens for normal and high strength concrete are given in Tables 4.1 and 4.2, respectively. The sizes of I-shape structural steel sections were selected considering all the limitations of available codes for composite columns. The flange and web plate compactness for I-shaped structural steel sections are as follows:

Flange Compactness (I-section)

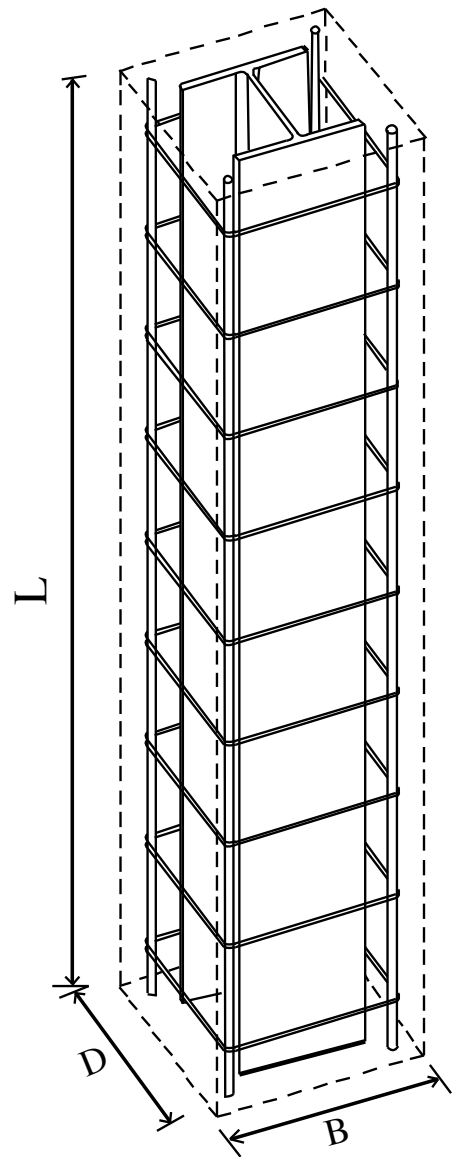
$$\frac{b_f}{2t_f} \leq \frac{95}{\sqrt{f_y}} \quad (4.1)$$

Web Compactness (I- section)

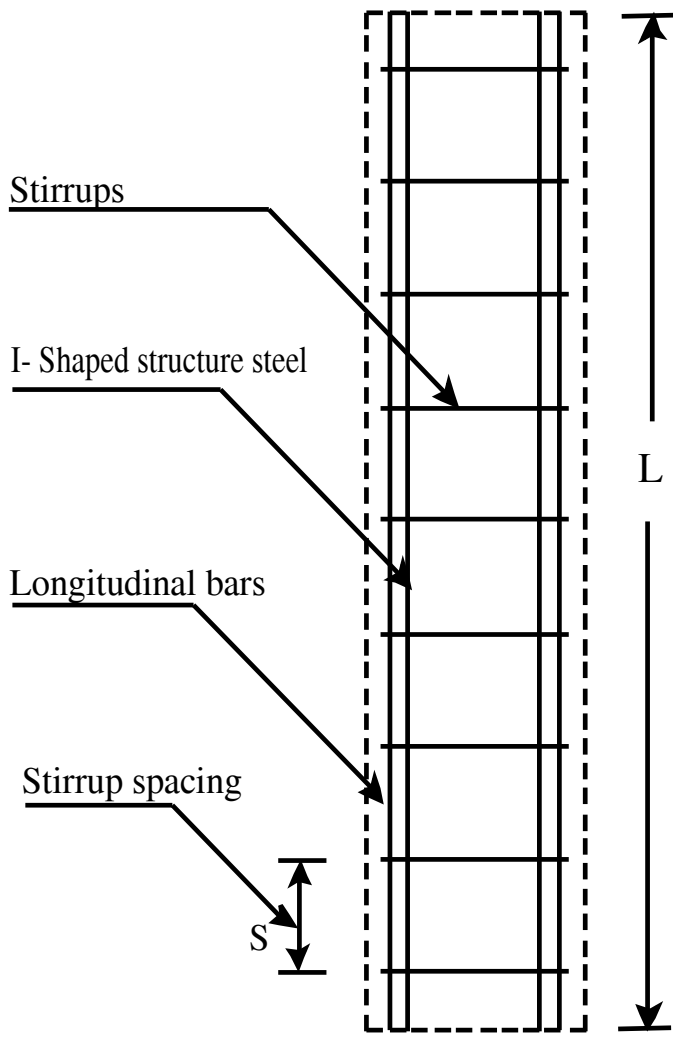
$$\frac{d}{t_w} \leq \frac{235}{\sqrt{f_y}} \quad (4.2)$$



(a) Plan View



(b) 3-D View



(c) Elevation

Figure 4.1 Geometry of FEC columns in (a) Plan View (b) 3-D View and (c) Elevation



Table 4.1 Geometric properties of test specimens with normal strength concrete (28 MPa)

Sl. no.	Specimen designation	Structural steel size $b_f \times d \times t_f \times t_w$ (mm)	Reinforcement		Steel ratio	
			Longitudinal reinforcement	Tie rebar (mm)	Structural steel (% $A_s$ )	Rebar (% $A_{sr}$ )
1	SCN4A1	20×30×5×5	4- $\phi$ 8mm	$\phi$ 6mm@50mm	3	2
2	SCN4A2	20×30×5×5	4- $\phi$ 8mm	$\phi$ 6mm@50mm	3	2
3	SCN4A3	20×30×5×5	4- $\phi$ 8mm	$\phi$ 6mm@50mm	3	2
4	SCN4B1	25×35×5×5	4- $\phi$ 8mm	$\phi$ 6mm@50mm	3.75	2
5	SCN4B2	25×35×5×5	4- $\phi$ 8mm	$\phi$ 6mm@50mm	3.75	2
6	SCN4B3	25×35×5×5	4- $\phi$ 8mm	$\phi$ 6mm@50mm	3.75	2
7	SCN4E	25×35×5×5	4- $\phi$ 8mm	$\phi$ 6mm@50mm	3.75	2

Table 4.2 Geometric properties of test specimens with high strength concrete (42 MPa)

Sl. No.	Specimen designation	Structural steel size $b_f \times d \times t_f \times t_w$ (mm)	Reinforcement		Steel ratio	
			Longitudinal reinforcement	Tie rebar (mm)	Structural steel (% $A_s$ )	Rebar (% $A_{sr}$ )
1	SCH6A1	30×40×5×5	4- $\phi$ 8mm	$\phi$ 6mm@75mm	2	1
2	SCH6A2	30×40×5×5	4- $\phi$ 8mm	$\phi$ 6mm@75mm	2	1
3	SCH6A3	30×40×5×5	4- $\phi$ 8mm	$\phi$ 6mm@75mm	2	1
4	SCH6B1	45×55×5×5	4- $\phi$ 8mm	$\phi$ 6mm@75mm	3	1
5	SCH6B2	45×55×5×5	4- $\phi$ 8mm	$\phi$ 6mm@75mm	3	1
6	SCH6E	45×55×5×5	4- $\phi$ 8mm	$\phi$ 6mm@75mm	3	1

#### 4.2.2 Explanation of test parameters

The primary parameters varied in the test were size of the column, structural steel ratio, concrete compressive strength and eccentricity of applied axial load. Test specimens of column group SCN4A and SCN4B were designed to examine the behaviour and strength of FEC columns for normal strength of concrete subjected to concentric axial load. These columns were fabricated with different percentages of structural steel to observe the variation in ultimate load carrying capacity of the columns. Similarly, another two groups of test specimens SCH6A and SCH6B were constructed with high strength concrete with two different percentages of structural steel.

FEC column specimen SCN4E (100 mm × 100 mm) and SCH6E (150 mm × 150 mm) were constructed with concrete compressive strength of 28 MPa and 42 MPa, respectively. The parameters varied between these two columns SCN4E and SCH6E were loading eccentricity and the column orientation. Column SCN4E and SCH6E were oriented about the weak and

strong axis bending, respectively. The column SCN4E and SCH6E were designed to have eccentricities of 33 mm and 50 mm, respectively. These two test specimens were designed to examine the ultimate load carrying of these columns against the weak and strong axis bending for normal and high strength of concrete. All the above mentioned experimental studies were designed to validate the numerical model to be developed in the present study.

### **4.3 Column Fabrication**

There are mainly two parts in FEC columns i.e. steel cage and concrete (as shown in Figure 4.1). The steel cage consists of I-shaped structural steel, longitudinal and transverse reinforcements. The structural steel sections were fabricated by The Modern Structures Limited, in Savar, Dhaka, Bangladesh. The steel cage consisting of steel I-section and longitudinal and transverse reinforcements were constructed in the Solid Mechanics Laboratory, BUET, Bangladesh. Finally, concrete was placed around the steel cage for the construction of FEC columns.

#### **4.3.1 Steel section fabrication**

The Modern Structures Limited constructed the I-shaped structural steel section according to the design drawings. Firstly, the web and the flanges were cut from the same steel plate so that the mill rolling direction of the plate matches the longitudinal axis of the steel section. Secondly, they were fillet welded continuously on both sides of the web along both web-flange junctions. There were four different sizes of I-shaped structural steel sections made for constructing the thirteen FEC test columns. The longitudinal and transverse reinforcements are shown in Figure 4.2. Figure 4.3 shows the I-shaped structural steel section. Before the placement of concrete the steel I section was placed along the center line of the rebar cage as shown in Figure 4.4.



Figure 4.2 Reinforcements for FEC columns



Figure 4.3 I-shaped structural steel sections



Figure 4.4 Structural steel with reinforcement in FEC columns

#### 4.3.2 Concrete mix design

The main properties of interest during the mix design were strength and workability. Trial batches of all mixes were made to ensure the desired properties. To cast all the FEC columns, two types of concrete were used: normal-strength (28 MPa) and high-strength (42 MPa). The mix designs are presented in Table 4.3 where the total amounts were calculated for the two different strength of concrete. Seven FEC columns (100 mm × 100 mm × 900 mm) and six cylinders were cast with 28 MPa concrete strength. Another, six FEC columns (150 mm × 150 mm × 900 mm) and six cylinders were cast with 42 MPa concrete strength. The two different strength of concrete were constructed with locally available materials. Twenty (20) millimeters down grade crushed stone chips were used as a coarse aggregate.

The Sylhet sand of 2.60 fineness module (FM) was used as fine aggregate. The cement used in concrete mix was CEM-I type A of Seven Rings Gold Brand.

Table 4.3 Concrete mix design at saturated surface dry (SSD) conditions

Material	Concrete test strength	
	28 MPa concrete	42 MPa concrete
	Weight (kg)/cum	Weight(kg)/cum
Water	17	29
Cement	39	90
Fine aggregate (Sylhet sand)	63	105
Coarse aggregate (stone chips)	88	157

A slump value of 75 mm to 100 mm was assumed for this mix design. From completed mix design, the obtained ratio of cement, fine aggregate and coarse aggregate were 1:1.62:2.25 (SSD weight) and 1:1.17:1.75 (SSD weight) for 28 MPa and 42 MPa concrete, respectively.

### 4.3.3 Concrete placement

All concrete was produced in the batching facility of the Concrete Material Laboratory in BUET. Due to the casting convenience, columns with 100 mm × 100 mm cross-section and six cylinders for 28 MPa concrete strength were cast in the morning. The other six columns of 150 mm × 150 mm cross-section and six cylinders of 42 MPa concrete strength were cast in the afternoon on the same day. The column specimens were cast horizontally inside a formwork. The formwork was made of 1" thick pieces of wood. They were put together and connected by black nails. There were thirteen formwork prepared for the construction of these columns. The whole bare sections of FEC columns were put inside the formwork after placement of small quantities of concrete at the bottom of the form works shown in Figure 4.5. Twelve concrete cylinders (100 mm diameter, 200 mm height) were cast in order to determine the material properties of the concrete. A good standard in batching, placing, and vibration techniques were followed during concrete placement in all FEC columns. Proper curing (cover the surface with gunny bags) was done for fourteen days after concrete placement.

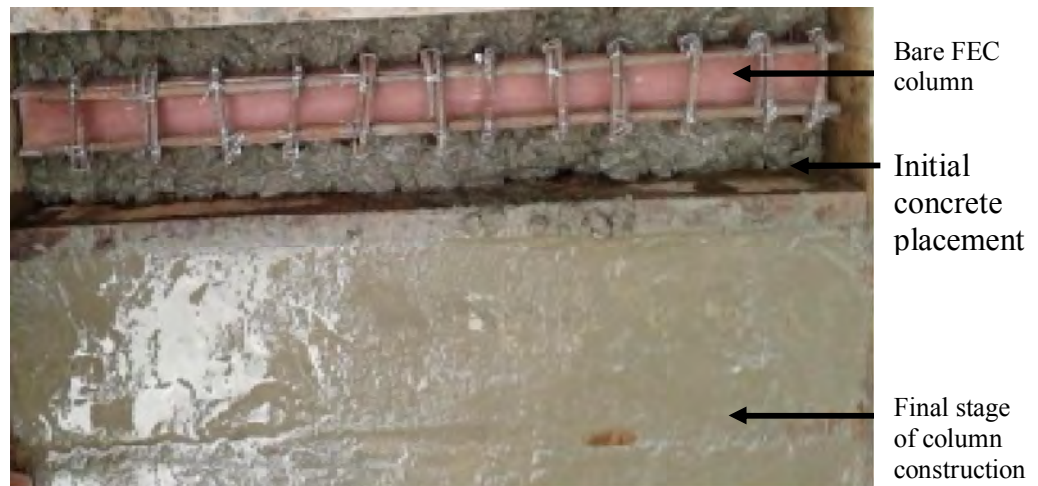


Figure 4.5 Concrete placements in FEC columns

#### 4.4 Material Properties

The FEC columns consist of I-shape structural steel, longitudinal reinforcement, stirrups, and concrete. To determine the stress-strain characteristics of the steel plate and longitudinal reinforcement in tension, tensile coupons were conducted on steel plates and on different diameter rebar's used in the test specimens. Concrete cylinders were cast and tested to ascertain the characteristic compressive strength of the concrete. In total twelve cylinders were tested for the two types of concrete strength (28 MPa and 42 MPa) used in this study.

##### 4.4.1 I-Shaped structural steel

All the plates used in web and flange of structural steel section were tested in the laboratory. Three steel plate samples, as shown in Figure 4.6 were tested to determine the material properties of steel. The plate samples were cut from the same steel plate by which I- shaped structural steel column was constructed. The tension tests on plates were conducted in the universal testing machine (UTM), with a tensile capacity of 2000 kN, in the Structural Mechanics laboratory of BUET. Load measurements were taken using the internal load cell of the UTM. The results of the steel-plate tension tests are given in Table 4.4. The average yield strength of the steel plate was 350 MPa. All the I-shaped steel columns were constructed as built up sections. Webs and flanges were connected through fillet welding.



Figure 4.6 Structural steel plate samples for tension test

Table 4.4 Tensile properties of structural steel plate

Coupon Flat Bar	Yield stress ( $F_y$ ) (MPa)	Ultimate stress ( $F_u$ ) (MPa)	Elastic modulus ( $E_s$ ) (MPa)	Yield strain ( $\epsilon_y$ ) (mm/mm)	Ultimate strain ( $\epsilon_u$ ) (mm/mm)
1	350	530	200000	0.00374	0.1263
2	352	534	200000	0.00396	0.1354
3	348	514	200000	0.003888	0.1278
<b>Mean</b>	<b>350</b>	<b>526</b>	<b>200000</b>	<b>0.00386</b>	<b>0.1298</b>

#### 4.4.2 Steel reinforcement

Two different diameters of reinforcements were used for the construction of composite columns i.e. main reinforcement and stirrups. Main reinforcement was used at the four corners of each columns and stirrups along the length of the columns. The size and arrangements of the rebars are described in section 4.2.1 and shown in Figure 4.1. The sizes of main reinforcement and stirrups were 8 mm and 6 mm, respectively. Three samples were tested from each size of reinforcement. The rebar samples, as shown in Figure 4.7.

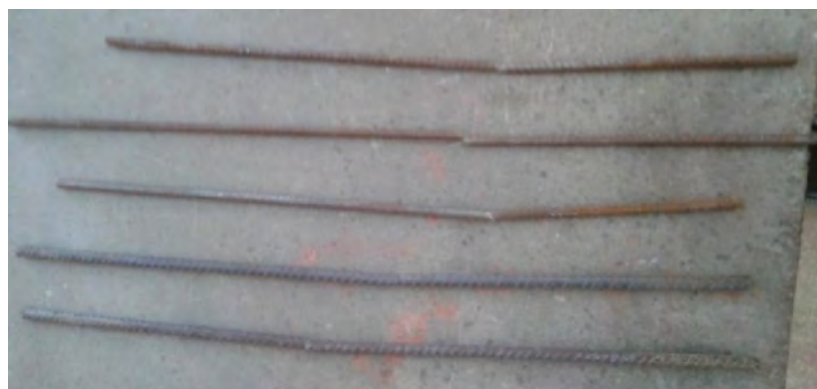


Figure 4.7 Reinforcement samples for tension test

Similarly, coupon test were conducted in UTM, with a tensile capacity of 2000 kN, in the Structural Mechanics laboratory of BUET. Load measurements were taken using the internal load cell of the UTM 2000 kN. The results of the tension coupon tests for rebars are given in Table 4.5.

Table 4.5 Tensile properties of steel reinforcement

Coupon	Yield stress ( $F_y$ ) (MPa)	Ultimate stress ( $F_u$ ) (MPa)	Elastic modulus ( $E_s$ ) (MPa)	Yield strain ( $\epsilon_y$ ) (mm/mm)	Ultimate strain ( $\epsilon_u$ ) (mm/mm)
6 mm dia bar					
1	473	635	200000	0.00325	0.14932
2	464	632	200000	0.00313	0.14462
3	467	633	200000	0.00316	0.14286
<b>Mean</b>	<b>468</b>	<b>634</b>	<b>200000</b>	<b>0.00318</b>	<b>0.1456</b>
8 mm dia bar					
1	473	633	200000	0.003225	0.13155
2	468	630	200000	0.003199	0.13895
3	474	639	200000	0.003236	0.13615
<b>Mean</b>	<b>470</b>	<b>634</b>	<b>200000</b>	<b>0.00322</b>	<b>0.13555</b>

#### 4.4.3 Concrete

A total of two mixes were required to batch the thirteen FEC columns. Two different strength of concrete (28 MPa and 42 MPa) were cast for constructing these columns. In order to determine the material properties, a total of twelve concrete cylinders with 100 mm diameter and 200 mm in height were cast from each mix shown in Figure 4.8. Six cylinders were cast for each strength of concrete. The designation of the individual cylinder for two different strength of concrete is shown in Table 4.6.



Figure 4.8 Typical 3-D view of concrete cylinders

Table 4.6 Designation of concrete cylinder for different strength

Concrete strength	Cylinder designation					
28 MPa Column group (SCN4A,SCN4B & SCN4E)	4NSC 1	4NSC 2	4NSC 3	4NSC 4	4NSC 5	4NSC 6
42 MPa Column group (SCH6A, SCH6B & SCH6E)	6HSC 1	6HSC 2	6HSC 3	6HSC 4	6HSC 5	6HSC 6

Twenty four hours after casting, cylinders were removed from molds and kept in the lime water. Six concrete cylinders (three from first mix and three from second mix) were brought out from the lime water after 28 days to determine the compressive strength of concrete and the other six cylinders were tested during the day of column testing. All cylinders were capped with a high strength capping compound prior to testing to ensure uniform bearing in the testing machine. Cylinders were tested in the concrete Materials Laboratory at BUET. The compressive strength of all twelve cylinders are given in Table 4.7.

Table 4.7 Concrete cylinder strength

Concrete Type	Column	Designation of cylinders		Strength		Strength Increase (28 day to test day)	
		28 day	Test day	28 day (MPa)	Test day (MPa)	(MPa)	(%)
Normal Strength (28 MPa)	SCN4A1						
	SCN4A2						
	SCN4A3	4NSC1	4NSC4	28.9	29.8	+ 0.9	3.0
		4NSC2	4NSC5	28.8	29.5	+ 0.7	2.5
	SCN4B1	4NSC3	4NSC6	27.9	28.7	+ 0.8	2.8
	SCN4B2						
	SCN4B3						
	SCN4E						
<b>Mean</b>				<b>28.5</b>	<b>29.3</b>	<b>+0.8</b>	<b>2.8</b>
High Strength (42 MPa)	SCH6A1						
	SCH6A2						
	SCH6A3	6HSC1	6HSC4	43.4	44.1	+0.7	1.6
		6HSC2	6HSC5	41.5	42.6	+1.1	2.7
	SCH6B1	6HSC3	6HSC6	42.6	43.9	+1.3	3.0
	SCH6B2						
	SCH6E						
<b>Mean</b>				<b>42.5</b>	<b>43.55</b>	<b>1.04</b>	<b>2.44</b>



Average compressive strength of three cylinders (4NSC1-4NSC3) after 28 days was found to be 28.5 MPa. Remaining three cylinders (4NSC4-4NSC6) were tested at the same day of testing FEC columns and their average compressive strength was found to be 29.3 MPa. Average compressive strength of three cylinders (6HSC1-6HSC3) from other group after 28 days was found to be 42.5 MPa. Remaining three cylinders (6HSC4-6HSC6) were tested at the same day of testing FEC columns and their average compressive strength was found to be 43.5 MPa. This value is slightly greater than 28 days compressive strength. This variation was due to the reason that concrete gains strength with time.

#### 4.5 Test Setup and Data Acquisition System

All tests were performed using a Universal Testing machine (UTM) that has a loading capacity of 2000 kN. The UTM actuator, which is attached to a moveable crosshead, applies a compressive force from above and has flexibility of changing stroke rate. The base of the UTM sits on a high platform. The data acquisition system used a PC running Horizon data acquisition software. A schematic diagram of UTM is shown in Figure 4.9. The test set-up highlights the end conditions, which were provided to ensure a uniform loading surface to the columns. Axial load was applied to the composite columns specimens at the rate of 5 kN/sec. The digital reading of axial load and axial deformation were collected by using an electronic data acquisition system during testing of each specimen.

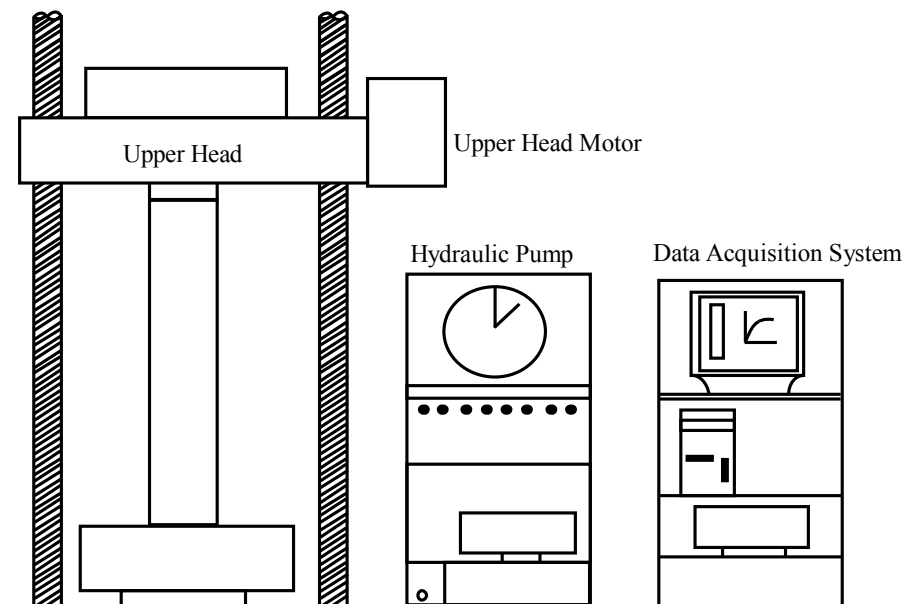


Figure 4.9 Schematic diagram of test set up

UTM load and stroke rates were verified before each test to ensure correct readings. The UTM instruments are frequently calibrated and verified according to a regular

schedule. Real-time graphs of the key data were displayed during loading to assist in controlling the tests. Laboratory safety regulations do not permit personnel near the UTM while it is operating, so a digital camera was used to take photographs of the specimens during the tests. The tests were carried out for concentrically and eccentrically applied axial load.

#### **4.5.1 Setup and instrumentation of concentrically loaded FEC columns**

The test setup was similar for the column group SCN4A, SCN4B, SCH6A and SCH6B. The columns included in these groups were tested for concentric axial load. The columns were so placed in the UTM to provide uniform bearing and a fixed end condition. Figure 4.10 shows the concentric axial load test setup in the laboratory.



Figure 4.10 Test set up for concentric axial load in laboratory

Firstly, the specimen was centered underneath the UTM actuator. Secondly, the column was aligned vertically. Thirdly, the column height was so adjusted to facilitate the concentric loading. Before the application of loads a sufficient gap between column top and machine was provided. Considering all types of effects including failure of columns, a uniform load rate of 5 kN/sec was used throughout the loading for these columns.

#### **4.5.2 Setup and instrumentation of eccentrically loaded FEC columns**

The test setup was similar for the two eccentrically loaded columns designated as SCN4E and SCH6E. The columns were so placed in the UTM that top end of the columns could move about major axis and minor axis bending but the bottom end of these columns were fixed. The eccentric load test setup of FEC columns are shown in Figure 4.11. To apply eccentric axial load, a steel bar was put on the top of each column. The column SCH6E was subjected to strong axis bending, by applying the axial load at 50 mm from the strong axis of the steel I section in the column. Similarly, for column SCN4B the axial was load applied at 33 mm eccentricity from the weak axis of the structural steel section in the column. Considering all types of effects including failure of columns, a uniform rate of 5 kN/sec was used throughout the loading in all columns.



Figure 4.11 Test set up for eccentric axial load in laboratory

#### **4.6 Observations and Failure Modes**

Thirteen columns were tested under pure compression (concentric) and eccentric loads, thus failures were essentially a primary compression mode. The local failure was observed in a specimen during test which occurred at the top and bottom of the column under axial load. This local failure was prevented by using FRP at the top and bottom of the columns. The

FRP sheet (2 mm thick) was wrapped at the top and bottom of the FEC columns. The wrap length was  $h/4$  ( $h$  = height of the column) distance from the top and bottom of the test columns. The cracks were observed to occur at or near the middle of the test columns after the use of FRP wrapper at the ends of the columns. The cracks were visible about 80% to 90% of ultimate capacity of the test columns. These cracks widened and propagated as the applied load increased resulting in crushing of concrete (CC) at the ultimate failure load of the test columns. In the test columns the primary mode of failure was crushing of concrete. The photographs highlighting the failure mode of the test columns are shown in following sections.

#### 4.6.1 Failure of concentrically loaded columns

Eleven columns were tested for concentric load in the laboratory. Six columns of 100 mm × 100 mm in size were constructed with normal strength and other five columns of 150 mm × 150 mm size were constructed with high strength of concrete. Local failures at the ends were prevented by fixing FRP at the top and bottom of the test columns. The failure modes of different column groups are described in following sections.

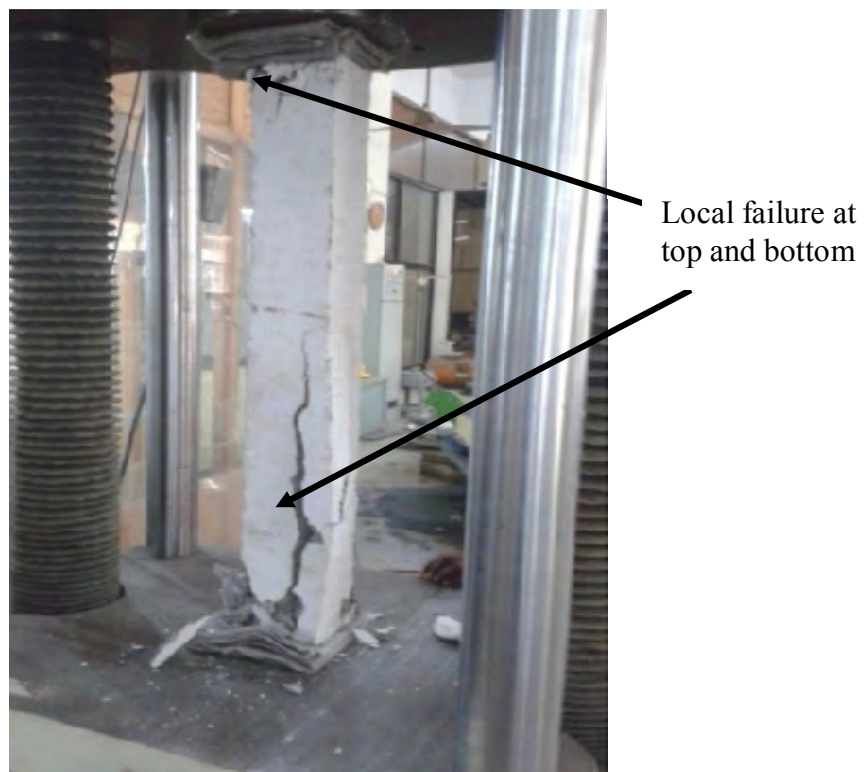
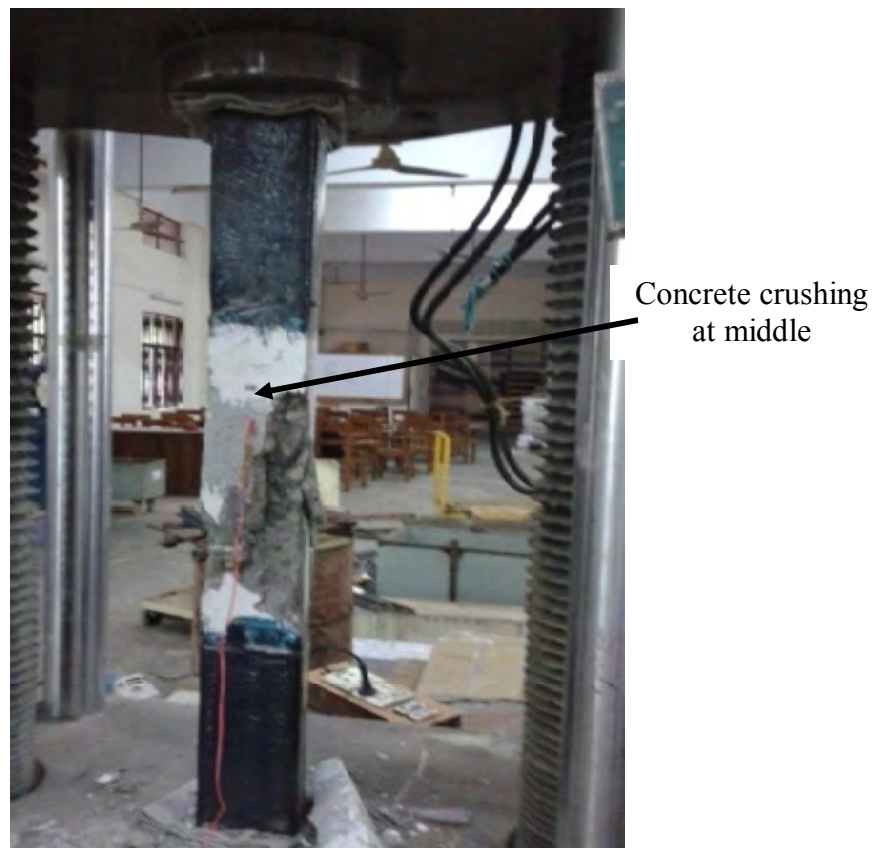


Figure 4.12 Local failure of a column during test for concentric load

#### 4.6.1.1 Column Group SCN4A

This group consists of three columns (SCN4A1, SCN4A2, SCN4A3) details of which were given in section 4.2.1 and Table 4.1. All data acquisition processes were found to be working properly during the pre-test verification. The cracks started at about 85 percentage of ultimate load carrying capacity of the columns. The failure modes of these three columns SCN4A1, SCN4A2 and SCN4A3 showed similar pattern. All columns failed due to crushing of concrete at the middle region which is shown in Figure 4.13.



(a) SCN4A1

Figure 4.13 Failure modes of column Group SCN4A



Concrete crushing  
at middle

(b) SCN4A2



Concrete crushing  
at middle

(c) SCN4A3

Figure 4.13 (cont.) Failure modes of column Group SCN4A

#### 4.6.1.2 Column Group SCN4B

This group consisted of three columns (SCN4B1, SCN4B2, SCN4B3) which were constructed of same materials. The difference between column group SCN4A and SCN4B were in the percentage of structural steel as mentioned in section 4.2.1. It was found that the cracks started at an elevation of about 175 mm from the bottom. The failure modes of these columns (SCN4B1 to SCN4B3) were of similar patterns. All the columns of this group failed due to crushing of concrete. Crushing occurred at the mid height of these columns which are shown in Figure 4.14.



(a) SCN4B1

Figure 4.14 Failure modes of column Group SCN4B



Concrete crushing  
at middle

(b) SCN4B2



Concrete crushing  
at middle

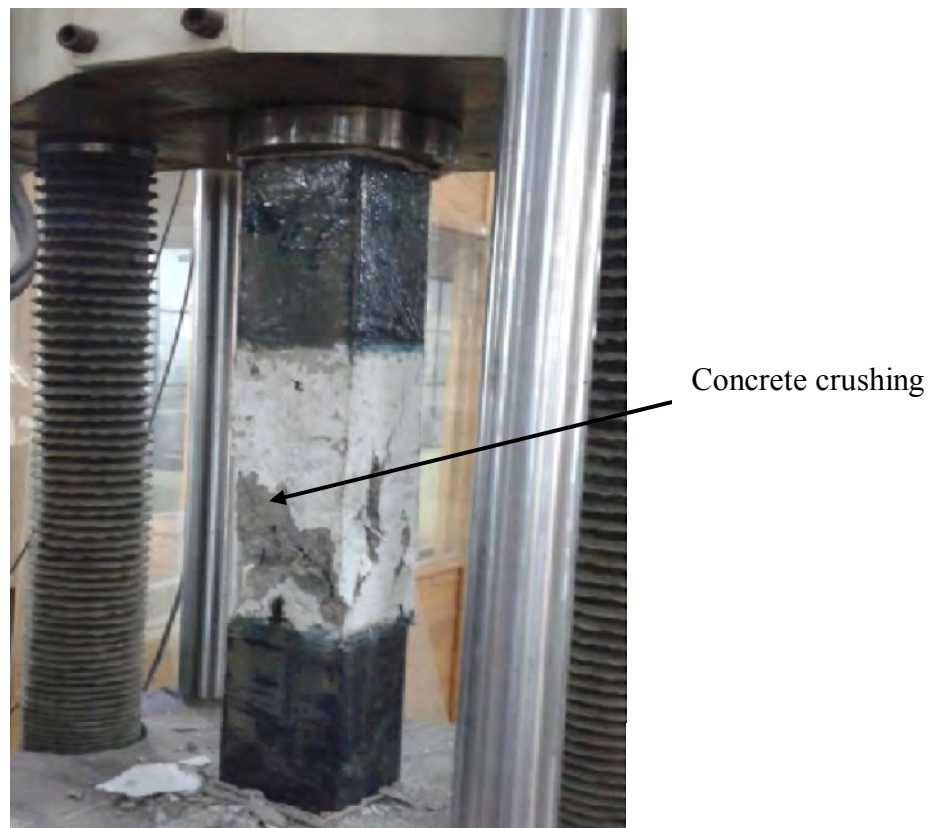
(c) SCN4B-3

Figure 4.14 (cont.) Failure modes of column Group SCN4B



#### 4.6.1.3 Column Group SCH6A

This group was formed with three columns (SCH6A1, SCH6A2, SCH6A3) which were constructed with similar geometric and material properties. The sizes and the material properties of these columns are shown in section 4.2.1 and in Tables 4.2. These columns were tested under concentric axial load. The difference of this column group from above mentioned groups (SCN4A and SCN4B) was in sizes, concrete strength and percentage of structural steel which are mentioned in section 4.2.1 and Tables 4.1 and 4.2. It was found that the cracks started at an elevation of about 300 mm from the bottom. The cracks were found on all the sides of the columns. The three columns (SCH6A1 to SCH6A3) showed similar failure patterns. All the columns of this group were failed due to concrete crushing which is shown in Figure 4.15. The depth of cracks in columns SCH6A1 and SCH6A3 were comparatively less than column SCH6A2.



(a) SCH6A1

Figure 4.15 Failure modes of column Group SCH6A



Concrete crushing  
at middle

(b) SCH6A2



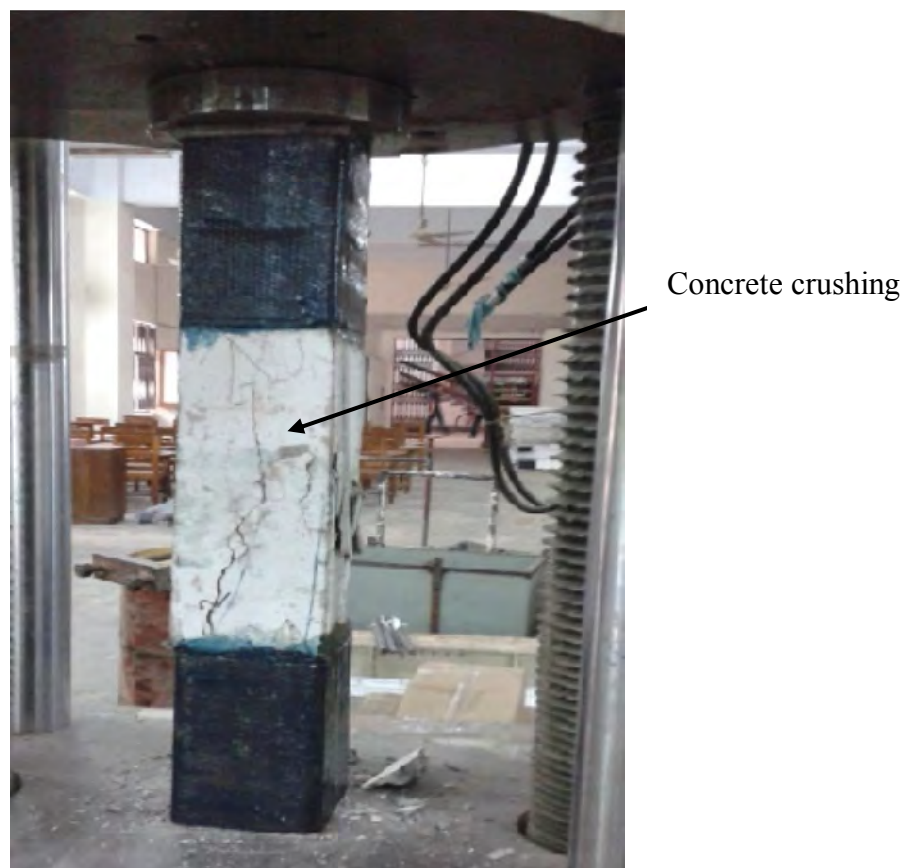
Concrete crushing  
at middle

(c) SCH6A3

Figure 4.15 (cont.) Failure modes of column Group SCH6A

#### 4.6.1.4 Column Group SCH6B

This group consisted of two columns (SCH6B1 and SCH6B2) of similar geometric and material properties. The main difference of this group of columns from SCH6A is the percentage of structural steel. The sizes and the materials properties of these columns are shown in Section 4.2.1 and in Table 4.2. These columns were tested under concentric axial load. It was found that the cracks started at mid height of the columns. The cracks were found in all sides of the columns in similar pattern. All the columns of this group failed due concrete crushing which is shown in Figure 4.16. The depth of all the cracks in column SCH6B1 is comparatively very less than column SCH6B2. No spalling of concrete was observed during the failure of column, SCH6B1.



(a) SCH6B1

Figure 4.16 Failure modes of column Group SCH6B



(b) SCH6B2

Figure 4.16 (cont.) Failure modes of column Group SCH6B

#### 4.6.2 Failure of eccentrically loaded columns

Two identical FEC columns (SCN4E and SCH6E) were loaded eccentrically according to the test setup and procedures described in section 4.5.2. The columns SCN4E and SCH6E were tested under eccentric axial loads. The load on column SCN4E was applied at an eccentricity of 33 mm from weak axis of the steel I section producing axial compression and bending about weak axis of the I section. On the other hand, column SCH6E was loaded at an eccentricity of 50 mm from the strong axis of the I section producing axial compression and bending about the strong axis of the column. The failure modes of the columns were observed during the test. The load was applied axially on the top surface of the columns at equal rate (5 kN/sec). The failure patterns of these columns are noted in following sections.

##### 4.6.2.1 Column SCN4E

This column was constructed with equal geometric and materials properties of column group SCN4B. All data acquisition processes were found to be working properly during the pre-test verification. For the convenience of providing eccentric load, a 25 mm dia steel bar was placed on the top of column at 33 mm distance from weak axis. Load was applied in such a

way so that the steel bar cannot slip during the test. The concrete at the top of compression side crushed initially. The columns failed due to crushing of concrete



Concrete crushing  
at compression

Figure 4.17 Failure modes of column SCN4E

at compression side in the middle of the column as shown in Figure 4.17. The test was stopped when the column reached at steady load condition.

#### 4.6.2.2 Column SCH6E

This column was constructed with equal geometric and materials properties of column group SCH6B. All data acquisition processes were found to be working properly during the pre-test verification. For the convenience of providing eccentric load, a 25 mm dia steel bar was placed on the top of column at 50 mm distance from the strong axis. Load was applied in such a way so that the steel bar cannot slip during the test. It was observed that failure occurred at the compression side of the column as shown in Figure 4.18.



Concrete crushing  
at compression side

Figure 4.18 Failure modes of column SCH6E

#### **4.7 Load versus Axial Deformation Relationship**

The axial load and axial shortening of the test columns were recorded. The point of ultimate failure was usually characterized by the concrete crushing and softening. All the specimens were tested under concentric and eccentric axial load. The FEC column was found to have larger stiffness, as well as larger ultimate load capacity as compared to RC column. Furthermore, in FEC columns the apparent ductility was found to be quite adequate with a significant post peak reserve of strength being displayed. Load versus deformation curves for the test columns are presented in the following sections.

##### **4.7.1 Centrally loaded columns**

Four groups of column were tested under concentric axial load to determine the load versus deflection behaviour of FEC columns. These columns were constructed with variable cross sectional size, materials properties and percentage of structural steel. Axial compressive strength and axial shortening at the ultimate load (peak load) were observed and recorded for each FEC column specimens experimentally for concentric load given in Table 4.8.

Table 4.8 Peak load and corresponding strain for concentrically loaded columns

Sl No.	Specimen designation	Concrete $f_{cu}$ (MPa)	Strength of steel		Peak load $P_{expt}$ (kN)	Mean $P_{expt}$ (kN)	Strain at peak load ( $\mu\epsilon$ )	Mean strain ( $\mu\epsilon$ )
			$F_u$ (MPa)	$F_{ys}$ (MPa)				
1	SCN4A 1	28	470	350	493		2707	
2	SCN4A 2	28	470	350	510	491	2727	2708
3	SCN4A 3	28	470	350	470		2690	
4	SCN4B 1	28	470	350	521		3241	
5	SCN4B 2	28	470	350	530	516	3210	3202
6	SCN4B 3	28	470	350	497		3155	
7	SCH6A 1	42	470	350	1103		4428	
8	SCH6A 2	42	470	350	1149	1117	4553	4486
9	SCH6A 3	42	470	350	1099		4577	
10	SCH6B 1	42	470	350	1247		4398	
11	SCH6B 2	42	470	350	1233	1240	4226	4314

### Column Group SCN4A

This group consisted of three FEC columns constructed with equal cross section and similar materials properties. The axial load versus axial deformation response for these three identical columns is very close shown in Figure 4.19. Columns SCN4A1 and SCN4A3 are in excellent agreement whereas the peak axial load of column SCN4A2 was found to be 8% higher as compared to the other two columns (SCN4A1 and SCN4A3). This slight variation may be attributed to the variability in the concrete material properties in these test specimens. However, the average ultimate capacity or peak load for this group (SCN4A) of specimens was 491 kN as included in Table 4.8.

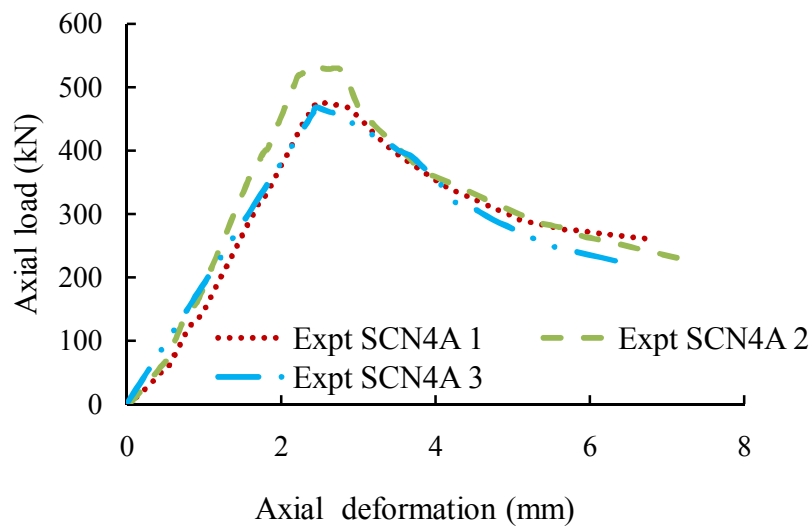


Figure 4.19 Axial load versus axial deformation for columns in Group SCN4A

### **Column Group SCN4B**

This group consisted of three FEC columns constructed with equal cross section and similar materials properties. Figure 4.20 showed the experimental axial load versus axial deformation of the column Group SCN4B (SCN4B1, SCN4B2 and SCN4B3). The ascending branch of the load deformation curves were in excellent agreement among these columns. Columns SCN4B1 and SCN4B3 are in excellent agreement whereas the peak axial load of column SCN4B2 was found to be 6% higher as compared to the other two columns (SCN4B1 and SCN4B3). This slight variation may be attributed to the variability in the concrete material properties in these test specimens. However, the average ultimate capacity or peak load for this group (SCN4B) of specimens was 516 kN as included in Table 4.8.

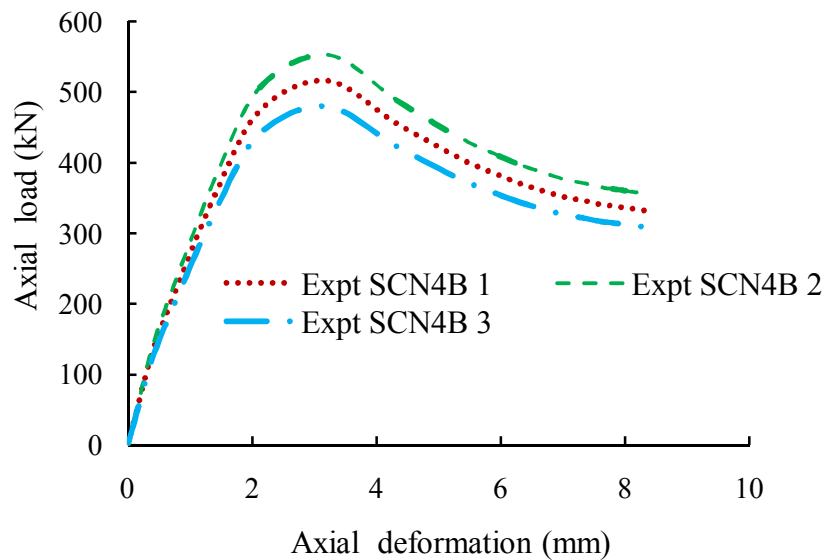


Figure 4.20 Axial load versus axial deformation for columns in Group SCN4B

### **Column Group SCH6A**

This group consisted of three FEC columns constructed with equal cross section and similar materials properties. Figure 4.20 showed the experimental axial load versus axial deformation of the column group SCH6A (SCH6A1, SCH4A2 and SCH4A3). These columns were constructed with high strength concrete (42 MPa). Columns SCH6A2 and SCH6A3 are in excellent agreement whereas the peak axial load of column SCH6A1 was found to be 3% higher as compared to the other two columns (SCH6A2 and SCH6A3). This slight variation may be attributed to the variability in the concrete material properties in these test specimens. However, the average ultimate capacity or peak load for this group (SCH6A) of specimens was 1117 kN as included in Table 4.8.



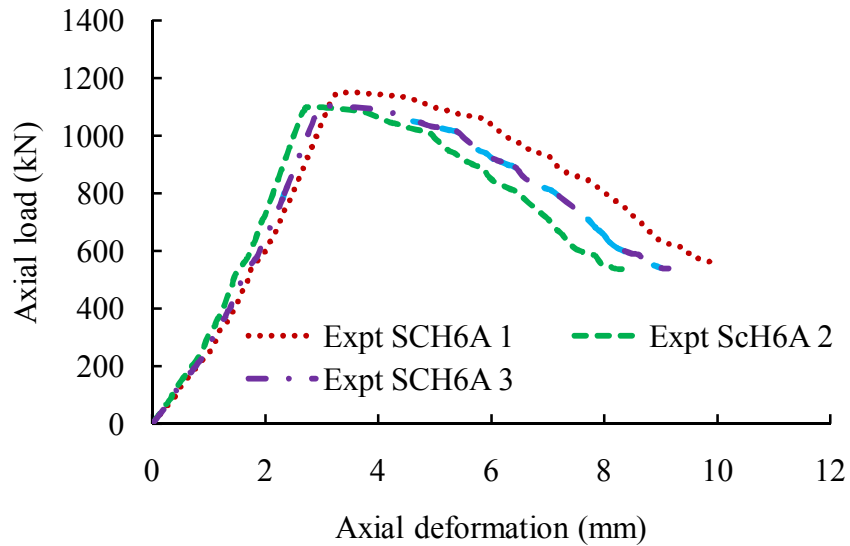


Figure 4.21 Axial load versus axial deformation for columns in Group SCH6A

**Column Group SCH6B**

This group consisted of two FEC columns (SCH6B1 and SCH6B2) constructed with equal cross section and similar materials properties. The ascending branch of the curves is in excellent agreement between them. The peak load of columns SCH6B1 and SCH6B2 are very close with negligible difference between them. Figure 4.22 showed the axial load versus axial deformation of column group SCH6B. Peak load of columns SCH6B1 and SCH6B2 fall gradually. The slope of the curves at descending branch was in very good agreement between them. However, the average ultimate capacity or peak load for this group (SCH6B) of specimens was 1240 kN as included in Table 4.8.

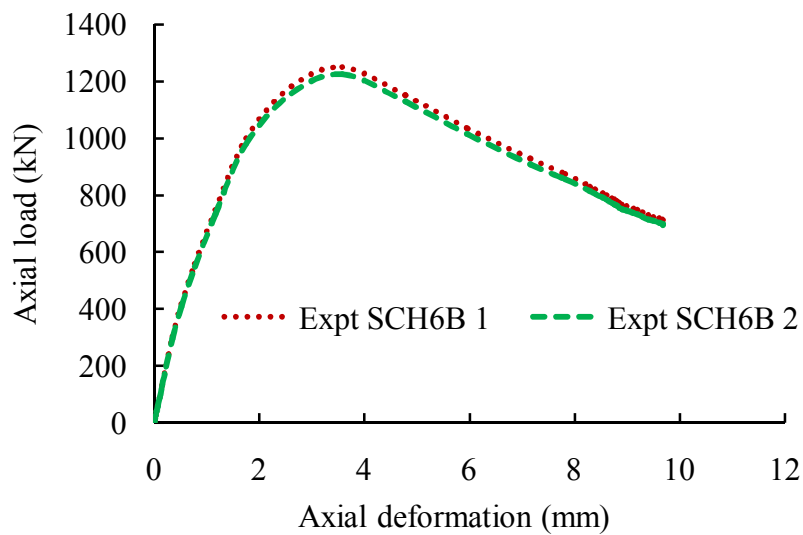


Figure 4.22 Axial load versus axial deformation for columns in Group SCH6B

#### 4.7.2 Eccentrically loaded columns

Two columns (SCN4E and SCH6E) were tested to determine behaviour of FEC columns under eccentric loading. Details geometric properties of these columns were given in section 4.2.1. Axial compressive strength and axial shortening were observed and recorded for these FEC columns during the test. The ultimate load capacity and corresponding average axial strain of these columns were determined during the test and listed in Table 4.9. The load carrying capacity of column SCH6E ( $e_y/D = 0.3$ ) were reduced by 62% than column SCH6B ( $e/D = 0$ ). Column SCH6E was subjected to eccentric load producing bending about the strong axis of the steel section. The axial load versus average axial deformation curves for column SCN4E and SCH6E are shown in Figure 4.23 and Figure 4.24, respectively. These test results will be used for the validation of the numerical model in present study.

Table 4.9 Peak load and strain for eccentrically loaded columns

Sl no	Specimens designation	Concrete	Rebar's	Structural	Location of load		Load capacity (kN)	Axial strain at peak load ( $\mu\epsilon$ )
		$f_{cu}$ (MPa)	$f_{yt}$ (MPa)	steel $f_{ys}$ (MPa)	$e_x$	$e_y$		
1	SCN4E	28	470	350	33	-	178	1780
2	SCH6E	42	470	350	-	50	460	1945

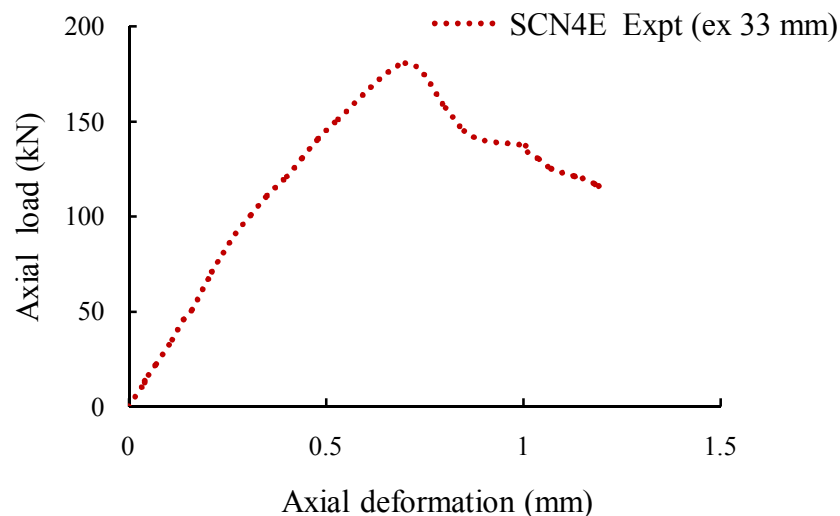


Figure 4.23 Axial load versus axial deformation of column SCN4E

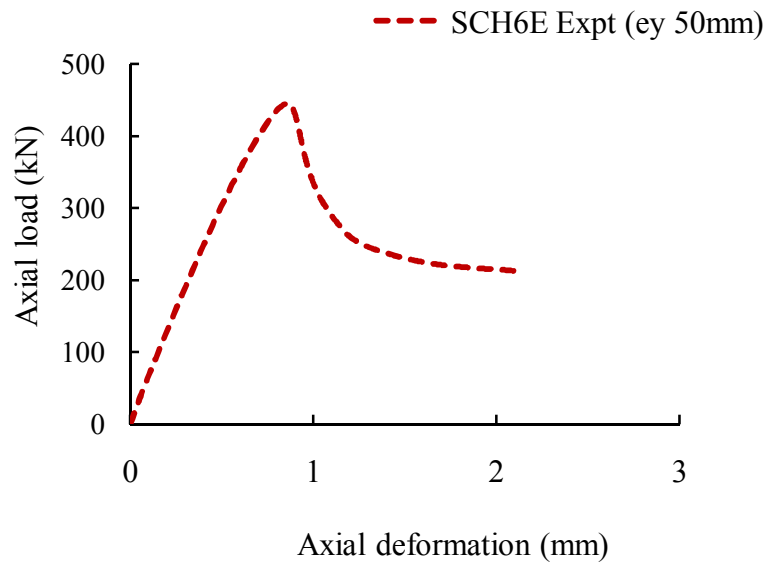


Figure 4.24 Axial load versus axial deformation of column SCH6E

#### 4.8 Conclusions

An experimental research project was undertaken to study the strength and behaviour of FEC columns. Total thirteen FEC column specimens were tested under concentric and eccentric axial loads. These columns were divided into six groups based on the concrete strength and loading conditions during the test. All the FEC columns were short and square in section with two different sizes. First series of test specimens consisted of seven columns constructed with normal strength concrete. Another, six columns were constructed with high strength concrete in the second series of specimens. The concrete compressive strength ( $f_{cu}$ ) for normal and high strength concrete were 28 MPa and 42 MPa, respectively. The column sizes were 100 mm  $\times$  100 mm and 150 mm  $\times$  150 mm. The structural steel ratio in these groups of columns varied from 2% to 4%. The columns were tested for concentric and eccentric axial loads, to observe the failure behaviour, the ultimate load carrying capacity and deformation at ultimate load for these FEC columns. The failure in the test specimens were attained by crushing of concrete. The load carrying capacity of FEC columns increased with the increase of structural steel ratio. The axial capacity of the FEC columns were increased by 7% and 10% for the variation of structural steel ratio of 1% when the columns were constructed with concrete strength of 28 MPa and 42 MPa, respectively. The load carrying capacity of FEC columns were also determined for eccentric axial load about minor and major axis bending. The load carrying capacity of column SCH6E ( $e_y/D = 0.3$ ) were reduced by 62% than column SCH6B ( $e/D = 0$ ). Column SCH6E

was subjected to eccentric load producing bending about the strong axis of the steel section. Similarly, the load carrying capacity of column SCN4E ( $e_x = 0.3$ ) were reduced by 65% than column SCN4B ( $e/D = 0$ ). Column SCN4E was subjected to eccentric load producing bending about the weak axis of the steel section.

## CHAPTER 5

### FINITE ELEMENT MODEL OF FEC COLUMNS

#### 5.1 Introduction

Experimental research on full scale composite test specimen is costly and time consuming. Computer aided analysis of FEC columns using finite element methods are therefore, required to broaden the current knowledge about the behavior of these columns. Finite element analysis can also be used to improve the understanding of the influences of various parameters on the strength and behaviour of these columns. The primary objective of this part of the work was to develop a complete finite element (FE) model that can be applied for a variety of geometries of FEC columns, subjected to various loading conditions, and provide accurate simulations of the behaviour of composite columns. The ABAQUS/Standard, finite element code (HKS 2013) was used to construct the numerical model for FEC columns. Both geometric and materials nonlinearities were included in the FE model.

A concrete damage plasticity model capable of predicting both compressive and tensile failures, was used to model the concrete material behaviour. The steel-concrete interface in the composite column was modelled using the embedded option (algorithm) in ABAQUS/Standard. Riks solution strategy was implemented to trace a stable peak and post peak response of FEC columns under various conditions of loading. To validate the model, simulations were conducted for both concentrically and eccentrically loaded FEC test specimens from current study and twenty two test specimens from published literatures, encompassing a wide variety of geometries and material properties. This chapter includes the description of the test specimens along with the tests used for the validation of the FE model as well as the geometric and material properties of the columns used for FE analysis. The load application technique and solution strategy implemented in the numerical analysis are also presented.

#### 5.2 Properties of Test Specimens

Experimental results of FEC test specimens from current study (as described in Chapter 4) and from published literatures (Chen and Yeh 1996; Morino et al. 1984; Dundar et al. 2008; Matsui 1979 and Kim et al. 2012) were used to evaluate the performance and accuracy of the FE model for FEC columns. The FEC test columns were constructed with normal and high strength concrete, reinforcement and I-shaped structural steel. The properties of the test

columns used in the finite element (FE) analysis are given in the following section. These properties are followed by description of the finite element model geometry used to simulate the various tests, the material model parameters, as well as the loading and solution strategy.

### 5.2.1 Test Specimens from current study

The test specimens of current study consisted of thirteen short FEC columns constructed with normal and high strength concrete and tested under different loading conditions. All the FEC columns were short and square in section with two different sizes. First series of test specimens consisted of seven columns constructed with normal strength concrete whereas six columns were constructed with high strength concrete in the second series of specimens. The detail of these test specimens are already described in Chapter 4 section 4.2.1. These columns were numerically simulated for concentric and eccentric loading conditions.

#### 5.2.1.1 Normal strength concrete FEC columns

The columns constructed with normal strength concrete were divided into three groups. These groups were SCN4A (SCN4A1, SCN4A2 and SCN4A3), SCN4B (SCN4B1, SCN4B2 and SCN4B3) and SCN4E. The columns of group SCN4A, SCN4B and SCN4E had cross-sections of 100 mm × 100 mm. The length of these columns was 900 mm. The diameter of the main and transverse reinforcements were 8 mm and 6 mm respectively in these columns. The spacing of the transverse reinforcement was 50 mm along the length of the columns. The test columns included in groups SCN4A and SCN4B were modelled for concentric axial load and column SCN4E for eccentric axial load. The material properties for concrete, reinforcement and structural steel section used in the finite element analysis of these FEC columns are given in Tables 5.1 and 5.2, respectively. All these columns were fabricated with 350 MPa structural steel plate, and 28 MPa (normal strength) concrete.

Table 5.1 Material properties of concrete and reinforcement

Specimen designation	Properties of concrete				Properties of reinforcement					
	$f_{cu}$ (MPa)	$E_c$ (MPa)	$\epsilon_{cu}$ ( $\mu\epsilon$ )	$\nu$	$F_y$ (MPa)	$F_{sh}$ (MPa)	$F_u$ (MPa)	$\epsilon_y$ (%)	$\epsilon_{sh}$ (%)	$\epsilon_u$ (%)
SCN4A	28	24467	1862	0.18	470	470	634	0.322	1.92	13.55
SCN4B	28	24467	1862	0.18	470	470	634	0.322	1.92	13.55
SCN4E	28	24467	1862	0.18	470	470	634	0.322	1.92	13.55

Table 5.2 Material properties of structural steel plate

Specimen designation	Properties of structural steel					
	$F_y$ (MPa)	$F_{sh}$ (MPa)	$F_u$ (MPa)	$\epsilon_y$ (%)	$\epsilon_{sh}$ (%)	$\epsilon_u$ (%)
SCN4A	350	350	526	0.386	2.23	12.98
SCN4B	350	350	526	0.386	2.23	12.98
SCN4E	350	350	526	0.386	2.23	12.98

### 5.2.1.2 High strength concrete FEC columns

The columns constructed with high strength concrete were divided into three groups. These three groups were SCH6A (SCH6A1, SCH6A2 and SCH6A3), SCH6B (SCH6B1 and SCH6B2) and SCH6E. The columns of group SCH6A, SCH6B and SCH6E modelled numerically, had square cross-sections of 150 mm  $\times$  150 mm and length of 900 mm. The diameters of main and transverse reinforcement were 8 mm and 6 mm, respectively. The spacing of the transverse reinforcement was 75 mm along the length of the columns.

Table 5.3 Material properties of concrete and reinforcement

Specimen designation	Properties of concrete				Properties of reinforcement					
	$f_{cu}$ (MPa)	$E_c$ (MPa)	$\epsilon_{cu}$ ( $\mu\epsilon$ )	$\nu$	$F_y$ (MPa)	$F_{sh}$ (MPa)	$F_u$ (MPa)	$\epsilon_y$ (%)	$\epsilon_{sh}$ (%)	$\epsilon_u$ (%)
SCH6A	42	28416	2146	0.18	470	470	634	0.322	1.92	13.55
SCH6B	42	28416	2146	0.18	470	470	634	0.322	1.92	13.55
SCH6E	42	28416	2146	0.18	470	470	634	0.322	1.92	13.55

Table 5.4 Material properties of structural steel plate

Specimen designation	Properties of structural steel					
	$F_y$ (MPa)	$F_{sh}$ (MPa)	$F_u$ (MPa)	$\epsilon_y$ (%)	$\epsilon_{sh}$ (%)	$\epsilon_u$ (%)
SCH6A	350	350	526	0.386	2.23	12.98
SCH6B	350	350	526	0.386	2.23	12.98
SCH6E	350	350	526	0.386	2.23	12.98

The test columns included in group SCH6A and SCH6B were modelled for concentric axial load and column SCH6E for eccentric axial load. The material properties for concrete, reinforcement and structural steel section used in the numerical simulations of these FEC columns are given in Tables 5.3 and 5.4, respectively. All these columns were fabricated with 350 MPa structural steel plate and 42 MPa concrete.

### 5.2.2 Test specimens from published literatures

Experimental results of twenty two FEC column specimens from published literature (Chen and Yeh 1996; Morino et al. 1984; Dundar et al. 2008; Matsui 1979 and Kim et al. 2012) were considered for validating the finite element code developed in the study. These test specimens represented a wide variety of geometric as well as material properties. These specimens varied in compressive strength of concrete, tensile strength of structural steel and the percentage of structural steel ratio. These columns were numerically simulated for concentric, eccentric and biaxial loads. The description of the test specimens are given in the following sections.

#### *Chen and Yeh (1996)*

Chen and Yeh (1996) conducted extensive experimental investigations on FEC columns with various structural steel shapes. Ten test specimens as shown Table 5.5, from this test data base were selected for numerical simulations using the current FE model. Three different shapes of the structural steel sections were used in these specimens i.e., H, cross and I-shaped structural steel sections (Figure 5.1). The H-shaped steel section was more like the wide-flange section, while the I-shaped section had a narrow flange as illustrated in Figure 5.1. The specimens had square cross-sections of 280 mm × 280 mm and a length of 1200 mm. The cylinder strength of concrete in these specimens varied from 26.4 to 29.8 MPa and the structural steel yield stress from 296 to 345 MPa. The longitudinal and transverse reinforcing bars were 16 mm and 8 mm in diameter, respectively. The spacings of transverse reinforcement in these specimens were 35 mm, 75 mm and 140 mm. Experimentally, the effects of tie spacings on load carrying capacity of these columns, were observed . These columns were tested experimentally for concentric axial load. Plastic properties of steel and concrete were incorporated in the FE models based on coupon test as shown in Tables 5.6 and 5.7.

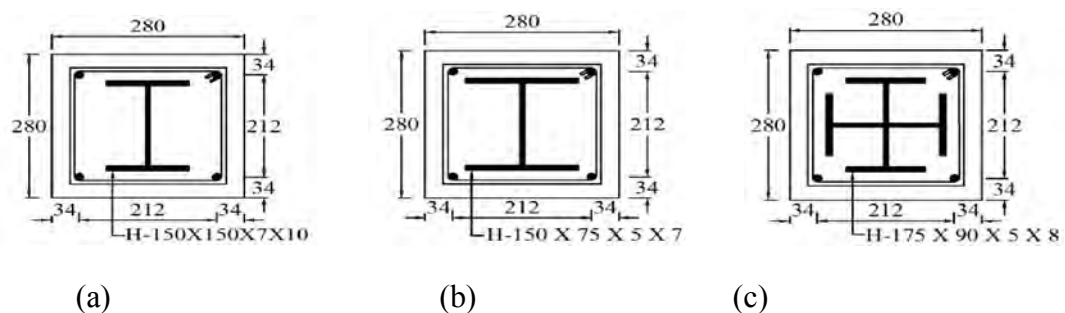


Figure 5.1 Typical cross sections of FEC columns (Chen and Yeh 1996)

(a) I (b) H and (c) Cross-shaped structural steel sections



Table 5.5 Geometric properties of test specimens (Chen and Yeh 1996)

Specimen designation	Size		Length of	Structural steel		Reinforcement	
	B (mm)	D (mm)	Column (mm)	Shape	Size ( $b_f \times d \times t_w \times t_f$ ) (mm)	Longitudinal	Tie spacing (mm)
SRC1	280	280	1200	H	H150×150×7×10	12-φ16mm	φ-8mm @140
SRC2	280	280	1200	H	H150×150×7×10	12-φ16mm	φ-8mm @ 75
SRC3	280	280	1200	H	H150×150×7×10	12-φ16mm	φ-8mm @ 35
SRC4	280	280	1200	Cross	Two H175×90×5×8	12-φ16mm	φ-8mm @140
SRC5	280	280	1200	Cross	Two H175×90×5×8	12-φ16mm	φ-8mm @ 75
SRC6	280	280	1200	Cross	Two H175×90×5×8	12-φ16mm	φ-8mm @ 35
SRC7	280	280	1200	I	H150×75×5×7	12-φ16mm	φ-8mm @140
SRC8	280	280	1200	I	H150×75×5×7	12-φ16mm	φ-8mm @ 75
SRC9	280	280	1200	I	H150×75×5×7	12-φ16mm	φ-8mm @ 140
SRC10	280	280	1200	I	H150×75×5×7	12-φ16mm	φ-8mm @ 75

Table 5.6 Materials properties of concrete and reinforcement (Chen and Yeh 1996)

Specimen designation	Properties of concrete				Properties of reinforcement					
	$f_{cu}$	$E_c$	$\epsilon_{cu}$	$\nu$	$F_y$	$F_{sh}$	$F_u$	$\epsilon_y$	$\epsilon_{sh}$	$\epsilon_u$
	(MPa)	(MPa)	( $\mu\epsilon$ )		(MPa)	(MPa)	(MPa)	(%)	(%)	(%)
SRC1	29.5	24932	1896	0.18	350	350	438	0.175	1.8	18
SRC2	28.1	24499	1868	0.18	350	350	438	0.175	1.8	18
SRC3	29.8	25023	1902	0.18	350	350	438	0.175	1.8	18
SRC4	29.8	25023	1902	0.18	350	350	438	0.175	1.8	18
SRC5	29.8	25023	1902	0.18	350	350	438	0.175	1.8	18
SRC6	29.5	24932	1896	0.18	350	350	438	0.175	1.8	18
SRC7	28.1	24499	1868	0.18	350	350	438	0.175	1.8	18
SRC8	26.4	24997	1834	0.18	350	350	438	0.175	1.8	18
SRC9	28.1	24449	1868	0.18	350	350	438	0.175	1.8	18
SRC10	29.8	25023	1902	0.18	350	350	438	0.175	1.8	18

Table 5.7 Materials properties of structural steel (Chen and Yeh 1996)

Specimen designation	Properties of structural steel plate					
	$F_y$	$F_{sh}$	$F_u$	$\epsilon_y$	$\epsilon_{sh}$	$\epsilon_u$
	(MPa)	(MPa)	(MPa)	(%)	(%)	(%)
SRC1	296	296	373	0.148	1.48	15
SRC2	296	296	373	0.148	1.48	15
SRC3	296	296	373	0.148	1.48	15
SRC4	345	345	431	0.173	1.73	17
SRC5	345	345	431	0.173	1.73	17
SRC6	345	345	431	0.173	1.73	17
SRC7	303	303	379	0.152	1.52	17
SRC8	303	303	379	0.152	1.52	15
SRC9	303	303	379	0.152	1.52	15
SRC10	303	303	379	0.152	1.52	15

### ***Morino et al (1984)***

The columns tested by Morino et al. (1984) were 160 mm × 160 mm in size and constructed with normal strength concrete. These columns were tested under eccentric load about major and minor axis bending. The test columns were fabricated with 8 mm thick steel plates (b/t ratio of 12.5). The length of the test columns were 960 mm. Transverse rebar's with 4 mm diameter were spaced at 150 mm along the length of the columns. Three columns (A4-00, A4-45, and A4-90) were taken from this experimental study for the numerical simulation. The lists of these specimens, along with their geometric properties, are given in Table 5.8. Typical cross sections of these columns are given in Figure 5.2. The material properties of concrete, structural steel and reinforcement used in the numerical simulations are given in Table 5.9 and Table 5.10.

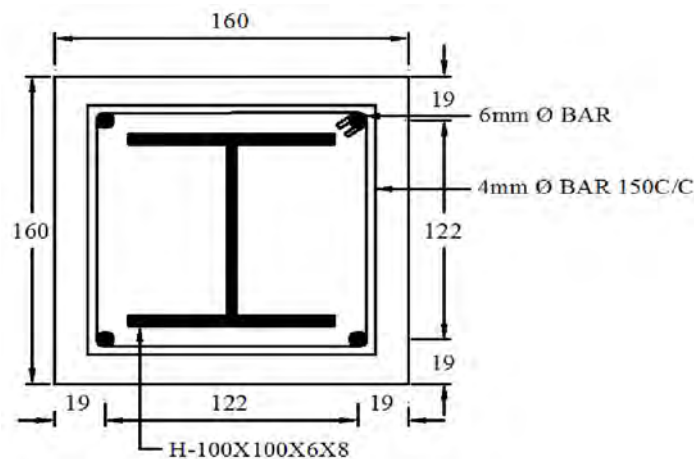


Figure 5.2 Typical cross section of FEC columns (Morino et al. 1984)

### ***Matsui (1979)***

Matsui (1979) conducted experimental investigations on FEC columns subjected to concentric axial load. The specimens were square in cross-section of 160 mm × 160 mm with various lengths (924 mm, 2304 mm and 3464 mm). These three columns were designated as 1, 2, and 3. The structural steel section was H-shaped 100 × 100 × 6 × 8 mm. The specimens had concrete cube strengths varying from 18.5-22.5 MPa and structural steel yield stresses varying from 298-306 MPa. The geometric properties of these specimens are given in Table 5.8. Typical cross sections of these columns are given in Figure 5.3. The longitudinal and transverse reinforcements were 6 mm and 4 mm in diameter, respectively. Transverse reinforcement were spaced at 75 mm along the length of the columns. The material

properties of concrete, structural steel and reinforcement used in the numerical simulations are given in Tables 5.9 and 5.10.

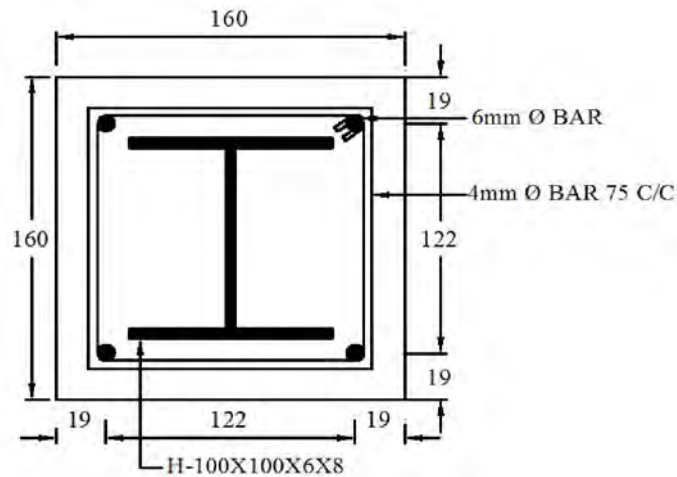


Figure 5.3 Typical cross section of FEC columns (Matsui 1979)

**Dundar et al. (2008)**

Dundar et al. (2008) conducted experimental investigations on short and slender concrete encased composite columns subjected to short-term axial load and biaxial bending. From this study two square shaped slender composite columns were selected for analysis using the current FE model. The cross sectional details and other geometric properties of these columns (designated as CC3 and CC4) are provided in Table 5.8. T shaped structural steel section as shown in Figure 5.4, was used for the construction of these FEC columns. The material properties of concrete, structural steel and reinforcement used in the numerical simulations are given in Tables 5.9 and 5.10.

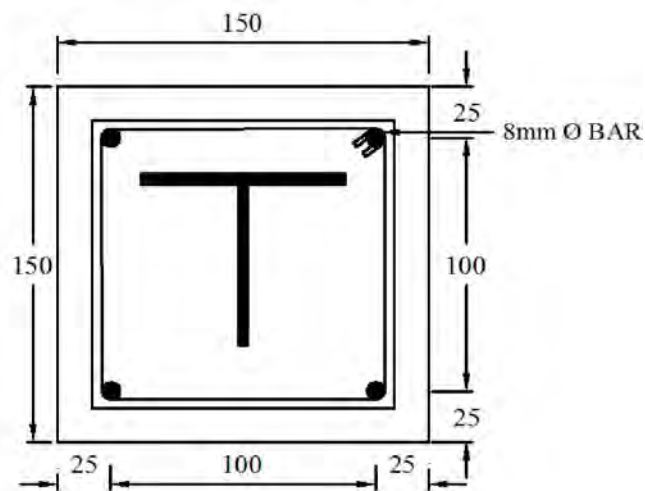


Figure 5.4 Typical cross section of FEC columns (Dundar et al. 2008)

Table 5.8 Geometric properties of reference test specimens

References	Specimen designation	Size		Length of column (mm)	Steel plate size $b_f \times d \times t_w \times t_f$ (mm)	Reinforcement	
		B	D			Longitudinal	Tie spacing
		(mm)	(mm)				
Morino et al. (1984)	A4-00	160	160	960	H100×100×6×8	4-φ 6mm	φ-4mm @150
	A4-45	160	160	960	H100×100×6×8	4-φ 6mm	φ-4mm @150
	A4-90	160	160	960	H100×100×6×8	4-φ 6mm	φ-4mm @150
Dundar et al. (2008)	CC3	150	150	1300	T 50×50×5	4-φ 8mm	φ-6mm @100
	CC4	150	150	1300	T 50×50×5	4-φ 8mm	φ-6mm @100
Matsui (1979)	1	160	160	924	H100×100×6×8	4-φ 6mm	φ-4mm @75
	2	160	160	2309	H100×100×6×8	4-φ 6mm	φ-4mm @75
	3	160	160	3464	H100×100×6×8	4-φ 6mm	φ-4mm@75

Table 5.9 Material properties of concrete and reinforcement

Specimen designation	Properties of concrete				Properties of reinforcement					
	$f_{cu}$	$E_c$	$\epsilon_{cu}$	$\gamma$	$F_y$	$F_{sh}$	$F_u$	$\epsilon_y$	$\epsilon_{sh}$	$\epsilon_u$
	(MPa)	(MPa)	( $\mu\epsilon$ )		(MPa)	(MPa)	(MPa)	(%)	(%)	(%)
A4-00	21.1	22150	1728	0.18	380	380	495	0.19	1.9	19
A4-45	21.1	22150	1728	0.18	380	380	495	0.19	1.9	19
A4-90	21.1	22150	1728	0.18	380	380	495	0.19	1.9	19
CC3	22.69	22714	1760	0.18	500	500	625	0.25	2.24	22
CC4	45.4	29270	2214	0.18	500	500	625	0.25	2.24	22
1	18.5	22828	1766	0.18	376	376	489	0.188	1.88	19
2	21.4	23829	1826	0.18	376	376	489	0.188	1.88	19
3	22.5	24468	1866	0.18	376	376	489	0.188	1.88	19

Table 5.10 Material properties of structural steel

Specimen designation	Structural steel plate					
	$F_y$	$F_{sh}$	$F_u$	$\epsilon_y$	$\epsilon_{sh}$	$\epsilon_u$
	(MPa)	(MPa)	(MPa)	(%)	(%)	(%)
A4-00	344.8	344.8	431	0.173	1.73	16
A4-45	344.8	344.8	431	0.173	1.73	16
A4-90	344.8	344.8	431	0.173	1.73	16
CC3	235	235	294	0.117	1.12	11
CC4	235	235	294	0.117	1.12	11
1	306	306	386	0.153	1.53	15
2	298	298	378	0.149	1.49	14
3	304	304	383	0.153	1.53	15

**Kim et al. (2012)**

Kim et al. (2012) conducted experimental as well as numerical investigations on fully or partially encased composite columns using higher strength structural steel ( $F_y = 913$  and  $806$  MPa) and high strength concrete ( $f_{cu} = 94$  and  $113$  MPa) under eccentric load. From this test database four fully encased square composite columns designated as C1, C2, C3 and C4

were selected for the validation of the developed FE model for high strength materials. The geometric and material details for these high strength test specimens are listed in Tables 5.11 and 5.12, respectively. These specimens had cross-sections of 260 mm × 260 mm and a constant length of 900 mm. The longitudinal and transverse reinforcements were 13 mm and 10 mm in diameter, respectively. The transverse reinforcements were spaced at 50 mm along the height of the columns for C1, C2 and C4 specimens. Column C3 had a larger tie spacing of 130 mm as shown in Table 5.11. Typical cross-section of the columns is shown in Figure 5.5.

Table 5.11 Geometric properties of test specimens (Kim et al. 2012)

Specimen designation	Size		Length of specimens (mm)	Structural steel plate	Reinforcement	
	B (mm)	D (mm)		$b_f \times d \times t_w \times t_f$ (mm)	Longitudinal	Tie spacing (mm)
C1	260	260	2620	H150×100×17.6×17.6	6-φ 13mm	φ-10mm @50
C2	260	260	2620	H150×100×17.6×17.6	6-φ 13mm	φ-10mm @50
C3	260	260	2620	H150×100×17.6×17.6	6-φ 13mm	φ-10mm @130
C4	260	260	2620	H150×100×17.6×17.6	6-φ 13mm	φ-10mm @50

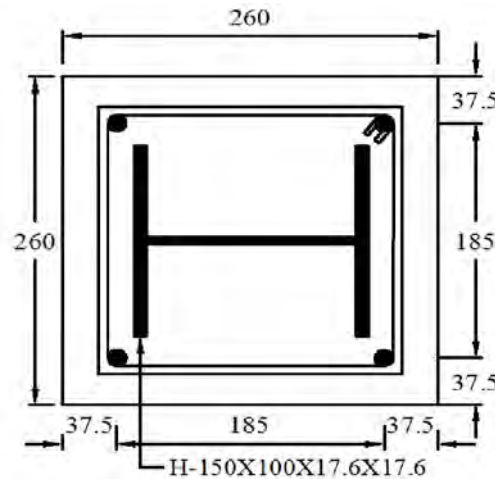


Figure 5.5 Typical cross section of FEC columns (Kim et al. 2012)

All of the four columns were constructed with high strength concrete (91.3 MPa) and high strength structural steel (913 MPa) as listed in Table 5.12. The strength of the longitudinal and transverse rebars were 525 MPa, except column C4. High strength (703 MPa) transverse rebars were used in column C4.

Table 5.12 Materials properties of concrete and reinforcement (Kim et al. 2012)

Specimen designation	Properties of concrete				Properties of reinforcement					
	$f_{cu}$	$E_c$	$\epsilon_{cu}$	$\nu$	$F_y$	$F_{sh}$	$F_u$	$\epsilon_y$	$\epsilon_{sh}$	$\epsilon_u$
	(MPa)	(MPa)	( $\mu\epsilon$ )		(MPa)	(MPa)	(MPa)	(%)	(%)	(%)
C1	91.3	38100	2600	0.184	525	525	656	0.263	2.68	12.39
C2	91.3	38100	2600	0.184	525	525	656	0.263	2.68	12.39
C3	91.3	38100	2600	0.184	525	525	656	0.263	2.68	12.39
C4	91.3	38100	2600	0.184	525	525	656	0.263	2.68	12.39

Table 5.13 Materials properties of structural steel (Kim et al. 2012)

Specimen designation	Properties of structural steel plate					
	$F_y$	$F_{sh}$	$F_u$	$\epsilon_y$	$\epsilon_{sh}$	$\epsilon_u$
	(MPa)	(MPa)	(MPa)	(%)	(%)	(%)
C1	913	913	988	0.454	2.11	7
C2	913	913	988	0.454	2.11	7
C3	913	913	988	0.454	2.11	7
C4	913	913 </td <td>988</td> <td>0.454</td> <td>2.11</td> <td>7</td>	988	0.454	2.11	7

These columns were tested under eccentric axial loads producing bending about major axis of the steel section. The eccentricity ratio ( $e/D$ ) used for column C1, C3 and C4 was 0.4 (120 mm) and for column C2 the eccentricity ratio was 0.23 (60 mm). The experimental set-up showing the loading platens of these columns are shown in Figure 5.6.

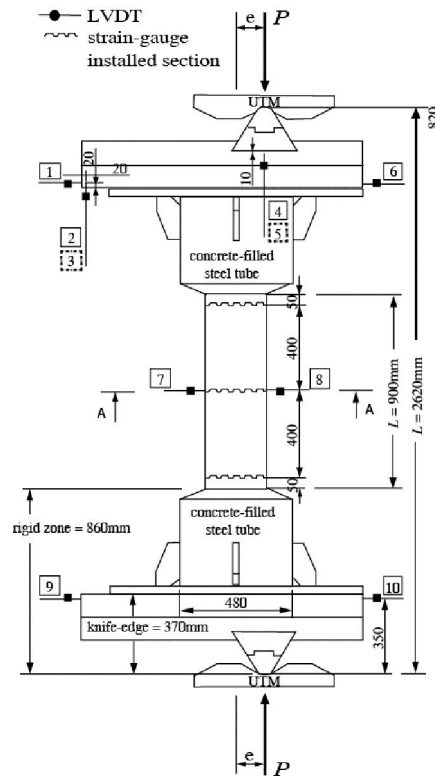


Figure 5.6 Column test set-up used (Kim et al. 2012)

### **5.3 Geometric Properties of the Finite Element Model**

A complete 3D finite element model was developed in this study to investigate the behavior and strength of FEC columns encompassing a wide variety of geometry and material properties. Both material and geometric nonlinearities were incorporated in the FE model. ABAQUS/Standard (HKS 2013) finite element code was used to develop the nonlinear FE model for FEC columns in this study. Descriptions of the mesh and elements used in the finite element models of the test specimens, along with the boundary conditions including steel-concrete interaction are presented in the subsequent sections.

#### **5.3.1 Element selection**

The FEC columns investigated in this study comprised of four components, such as structural steel section, longitudinal reinforcement, transverse reinforcement and concrete. The structural steel section in FEC column was modeled with S4R shell element (as shown in Figure 5.7 (a)). Each node of the S4R shell element has six degrees of freedom: three translations and three rotations. This element uses one integration point on its mid-surface to form the element internal force vector. The default number of integration points through the thickness of this element were five, which were considered sufficient for modelling the nonlinear material behaviour of the current problem under monotonic loading. The concrete of FEC column was simulated using solid C3D8R (as shown in Figure 5.7 (b)) element. It is a continuum three dimensional eight node reduced integration brick element with three translational degrees of freedom at each node. In ABAQUS/Standard, the updated Lagrangian formulation is used for all continuum and shell elements. In this formulation the nodal coordinates are updated at the beginning of each increment. The shape functions and derivatives are then re-evaluated using the updated nodal coordinates. Three dimensional 2-node truss elements designated as T3D2 (Figure 5.7 (c)) were used to model the longitudinal bars and transverse reinforcement. To ensure bonding between the concrete and the reinforcing bars, the rebar's were defined as "embedded" reinforcement in the concrete blocks, which effectively couples the longitudinal behavior of the rebar with that of the adjacent concrete.

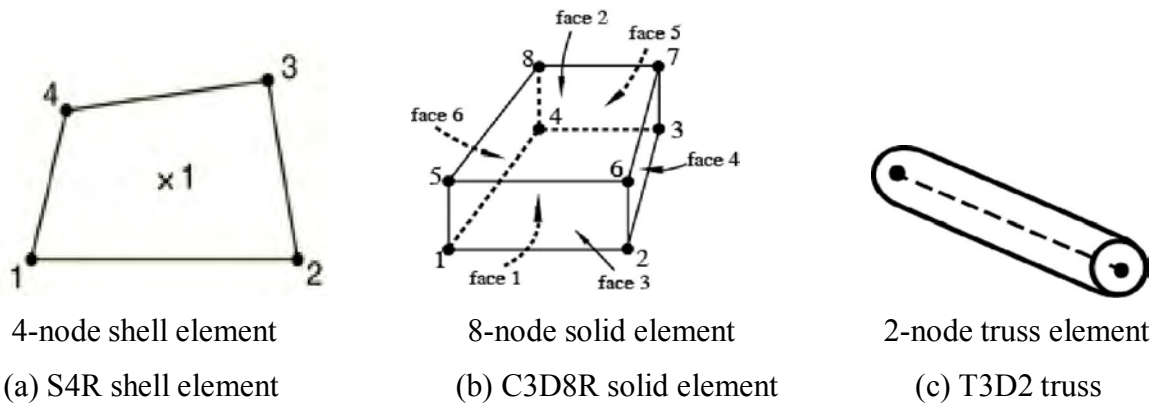


Figure 5.7 Finite elements used in the numerical simulation

### 5.3.2 Mesh description

A sensitivity analysis was performed on the FE model to optimize the mesh size in order to produce the accurate behaviour of FEC column with less computational time. Column SCN4B1 was modelled using different mesh sizes. The trail aspect ratios (length: width: height) for finite elements were 1:1:0.8, 1:1:1, 1:1:1.5, 1:1:2, 1:1:2.5 and 1:1:3. The geometric details and materials properties of this column are given in Tables 4.1 and 4.4. The comparison of the axial capacity for this column with the selected mesh sizes are shown in Figure 5.8. It was observed from the graph that the element aspect ratio of 1:1:2 or 1:1:2.5 can be considered as the optimum mesh size for the FE model of FEC columns in the current study. The entire model mesh for FE analysis is shown in Figure 5.9.

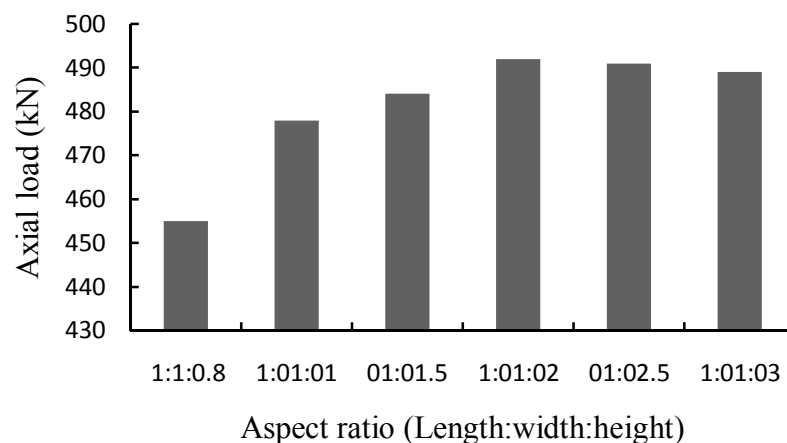


Figure 5.8 Axial load versus aspect ratio



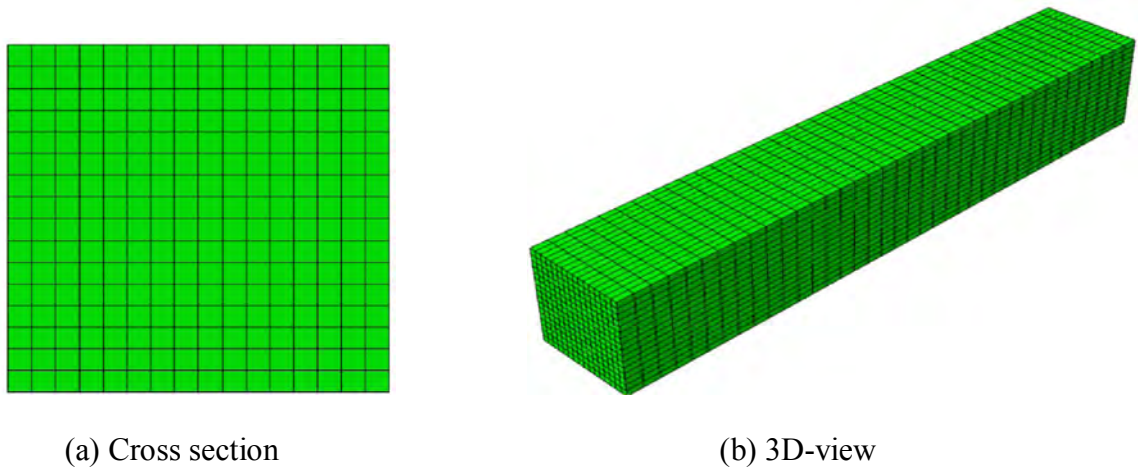


Figure 5.9 Finite element mesh for FEC columns

### 5.3.3 Modeling of steel-concrete interactions

The elements used for rebars and the structural steel shape of the FEC columns were defined using embedded element option in ABAQUS/Standard (HKS 2013). This option ensures bonding between concrete and steel part of the column. The embedded element technique is used to specify an element or groups of elements embedded in host elements. In FEC columns, the concrete was defined as the host element whereas the structural steel section and reinforcement were defined as the embedded elements. If a node of an embedded element lies within a host element, the translational degrees of freedom at the node are eliminated and the node becomes an “embedded node”. The translational degrees of freedom of the embedded node are constrained to the interpolated values of the corresponding degrees of freedom of the host element. Embedded elements are allowed to have rotational degrees of freedom, but these rotations are not constrained by the embedding.

### 5.3.4 End boundary conditions

Symmetry boundary conditions were applied along the planes of symmetry of the models. The end boundary conditions in the FE model was defined in such a way to comply with that applied in the experimental setup. The boundary conditions applied in the FE model to simulate the conditions for concentrically and eccentrically loaded specimens are shown in Figure 5.10. In concentrically loaded column tests, the bottom end of the column was fixed and the axial load was applied through rigid body reference node at the

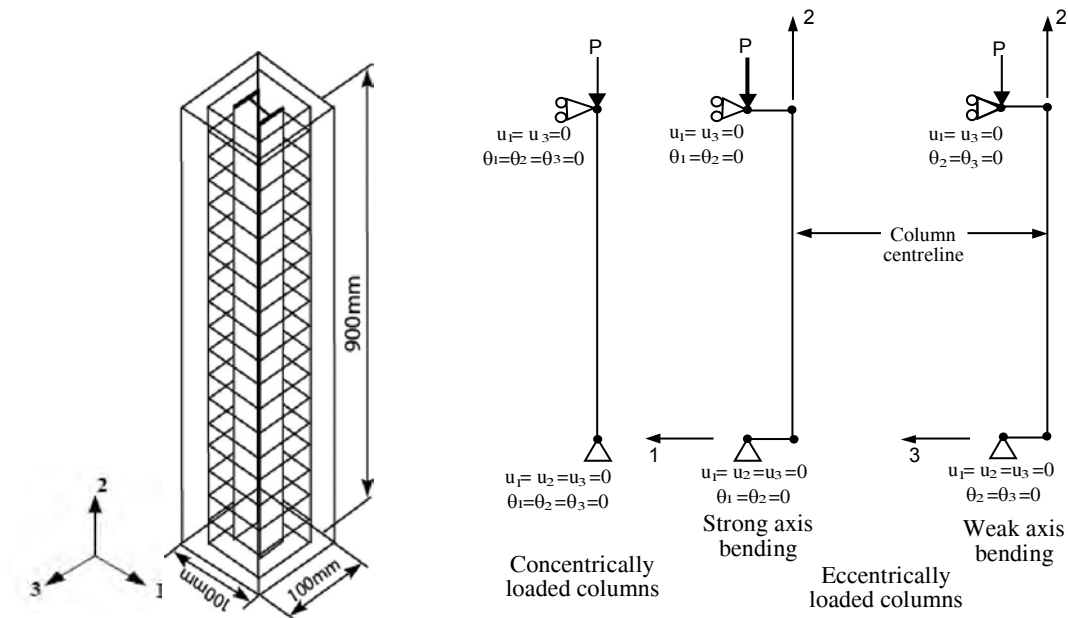


Figure 5.10 End boundary conditions in FE model for concentric and eccentric load

center of the top end of the column. The rotations and horizontal translations at the top surface were fixed. Since the load is applied at the top the vertical restraint was released. The axial load was applied using a displacement control technique. In the finite element model for eccentrically loaded test specimens, pinned-pinned end conditions were applied at the end eccentric points located on the end rigid planes. For strong axis bending, rotations about the strong axis were released at these points. Similarly, rotations about the weak axis were released for weak axis eccentricity. A rigid body reference node is defined on the top of the column to apply displacement.

## 5.4 Materials Properties

Steel and concrete are the main materials used in construction of FEC columns. The nonlinear behaviour of these two materials were incorporated in the FE model using the appropriate material models for steel and concrete available in the ABAQUS (HKS 2013) finite element code. The description of the material models for steel and concrete along with their mechanical properties (stress versus strain relationship) used in the FE model is described in the following sections.

### 5.4.1 Steel

The steel material properties for the I-shaped structural steel and longitudinal and transverse reinforcements were modelled with an elasto-plastic model. Steel is a ductile material which experiences large inelastic strain beyond the yield point. So the true stress and logarithmic

strain graph which is also called hardening curve, as shown in Figure 5.11, is considered for modeling the material behavior of steel. Point A in the stress-strain curve is the yield point, point B refers to the onset of strain hardening and point C is the ultimate stress point. The material data used to define this tri-linear curve for the steel plate materials were obtained from the tensile tests on steel coupons from the test specimens of current study as well as for the reference test specimens (Tables 5.1 to 5.13). The stress and strain data obtained from the uniaxial tension tests are converted to true stress,  $\bar{\sigma}_{true}$ , and logarithmic plastic strain,  $\varepsilon_{ln}^{pl}$ , for FE analysis using the following relationships:

$$\sigma_{true} = \sigma_{nom} (1 + \varepsilon_{nom}) \quad (5.1)$$

$$\varepsilon_{ln}^{pl} = \ln (1 + \varepsilon_{nom}) - \frac{\sigma_{true}}{E_s} \quad (5.2)$$

Where,  $E_s$  is the modulus of elasticity of steel,  $\sigma_{nom}$  is the nominal or engineering stress and  $\varepsilon_{nom}$  is the nominal or engineering strain obtained from material tests. The value of the Poisson's ratio for steel used in the numerical analysis is 0.3.

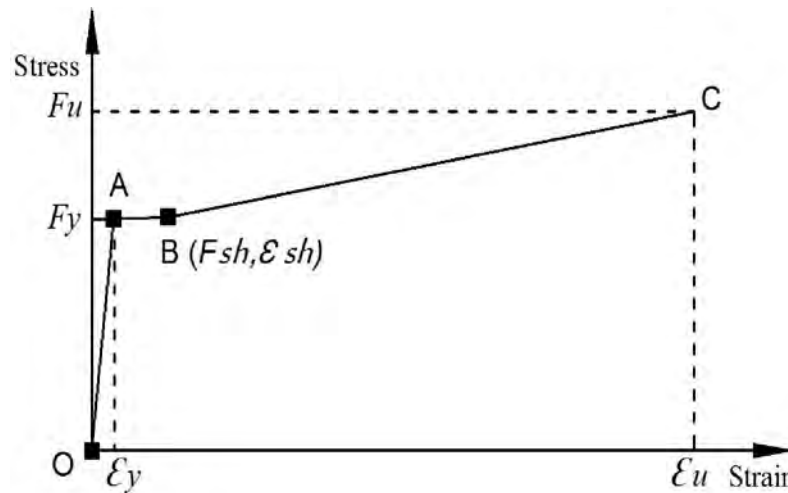


Figure 5.11 Stress-strain curve for steel used in the numerical analysis

#### 5.4.2 Concrete

The damage plasticity model in ABAQUS (HKS 2013) was used to simulate the concrete material behaviour in the FEC columns. The model is a continuum, plasticity-based damage model for concrete (Lubliner et al. 1989) that is capable of predicting both compressive and tensile behaviour of the concrete material under low confining pressures. The model was verified by Begum et al. (2007) against published triaxial compressive test results (Sfer et al. 2002) for concrete cylinders under different levels of confinement. To represent the inelastic behaviour of concrete the damage plasticity model uses the concept of isotropic damaged elasticity, in combination with isotropic tensile and compressive plasticity. The model is

capable of taking into consideration the degradation of elastic stiffness (or “damage”) induced by reversible cycles as well as high temperatures both in tension and compression. The concrete damage plasticity model uses a non-associated plastic flow rule in combination with isotropic damage elasticity. The Drucker-Prager hyperbolic function is used to define the plastic flow potential. The dilation angle defines the plastic strain direction with respect to the deviatoric stress axis in the meridian plane. The volumetric expansion of concrete can be controlled by varying the dilation angle. In this study, a value of 15 degrees is defined for the dilation angle of concrete as for concrete material (Begum et al. 2007). Complete stress-strain curves for concrete under uniaxial compression and tension are necessary to predict the structural response of the composite column using the damage plasticity model for concrete.

The uniaxial compressive and tensile responses (Figures 5.12 (a) and 5.12 (b), respectively) of concrete used in this model are simplified to capture the main features of the response (Begum et al. 2007). Under uniaxial compression, the stress-strain response (as shown in Figure 5.12(a)) is assumed to be linear up to the initial yield stress, which is assumed to be  $0.30f_{cu}$  in the current study. The plastic region is characterized by stress hardening, followed by strain softening after reaching the ultimate strength,  $f_{cu}$ . The uniaxial compression hardening curve is defined in terms of the inelastic strain,  $\varepsilon_c^{-in}$ , which is calculated using Equation (5.3). The damage plasticity model automatically calculates the compressive plastic strains,  $\varepsilon_c^{-pl}$ , Equation (5.3), using a damage parameter,  $d_c$ , that represents the degradation of the elastic stiffness of the material in compression.

$$\varepsilon_c^{-in} = \varepsilon_c - \frac{f_c}{E_c} \quad (5.3)$$

$$\varepsilon_c^{-pl} = \varepsilon_c^{-in} - \frac{d_c}{(1-d_c)} \frac{f_c}{E_c} \quad (5.4)$$

Since, the current study includes only monotonic loading conditions, no stiffness degradation or recovery is considered. Hence, the plastic strain expression becomes:

$$\varepsilon_c^{-pl} = \varepsilon_c^{-in} \quad (5.5)$$

Figure 5.12(b) shows the uniaxial tensile behaviour of concrete used in the damage plasticity model. The stress-strain curve in tension is assumed to be linearly elastic until the failure stress,  $f_{tu}$ , is reached. After this point strain softening represents the response of the cracked concrete that is expressed by a stress versus cracking displacement curve. The values of the

plastic displacements calculated by the damage model are equal to the cracking displacements since the tensile damage parameter,  $d_t$ , is zero for current study (Begum et al. 2007).

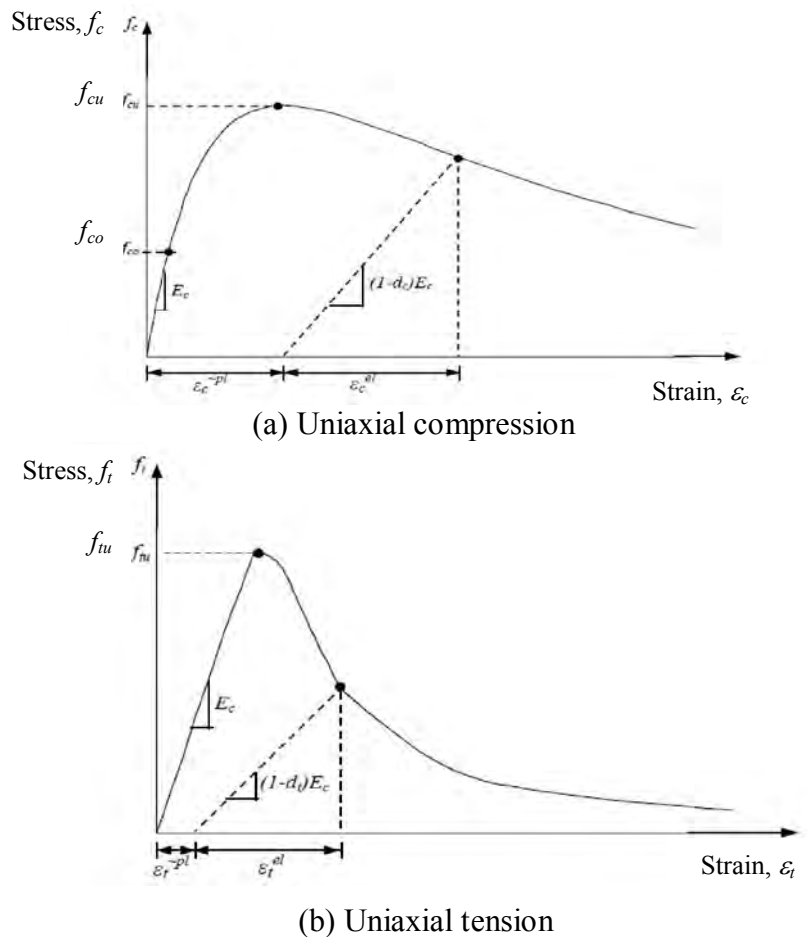


Figure: 5.12 Uniaxial compressive and tensile behaviour of concrete used by damage plasticity model in ABAQUS (after HKS 2013)

#### 5.4.2.1 Stress-strain relationship for concrete in compression

Extensive experimental and theoretical research has been conducted and several empirical models have been proposed (Wang et al. 1978; Carreira and Chu 1985; Tsai 1988; Hsu and Hsu 1994; Almusallam and Alsayed 1995; Gysel and Taerwe 1996; Wee et al. 1996; Barr and Lee 2003 and Lu and Zhao 2010) for the development of the stress-strain relationship of normal, medium and high strength concrete under uniaxial compression. For normal strength concrete (up to 60 MPa), the relationships (as shown in Equation 5.6) proposed by Carreira and Chu (1985), are used in the current study to define the complete stress-strain relationship for concrete beyond the elastic limit where  $\beta$  is a material parameter that depends on the

shape of the stress-strain diagram. The parameter  $\beta$  is calculated using equation (5.7) as proposed by Carriera and Chu (1985).

$$f_c = f_{cu} \left[ \frac{\beta \left( \frac{\varepsilon}{\varepsilon_{cu}} \right)}{\beta - 1 + \left( \frac{\varepsilon}{\varepsilon_{cu}} \right)^\beta} \right] \quad (5.6)$$

$$\beta = \left[ \frac{f_{cu}}{32.4} \right]^3 + 1.55 \quad (5.7)$$

The compressive behavior of concrete up to linear elastic portion is defined using the modulus of elasticity in compression. The proportional limit or elastic limit for normal strength concrete is assumed to be 30% of its compressive strength. In the plastic regime, the effective stress–plastic strain curve is developed using the stress strain function proposed by Carriera and Chu (1985) in uniaxial compression. The material properties used to generate the concrete stress strain curve for the test specimens are listed in Tables 5.1 to 5.10. The Carriera and Chu (1985) model can reasonably predict the stress-strain curve for normal strength concrete up to strength of 60 MPa.

Wee et al. (1996) reported that the equations given by Carriera and Chu (1985) can give good prediction of the complete stress strain curves for normal strength concrete and ascending branch of stress strain curve for high strength concrete. However, for high strength concrete the descending branch and the post-peak residual strength at high strains are not adequately represented by the Carreira and Chu (1985) model. The equations for descending branch from Carreira and Chu (1985) was modified by Wee et al. (1996) for high strength of concrete. Therefore, two modification factors,  $k_1$  and  $k_2$ , were introduced into Equation (5.8) by Wee et al. (1996) for modelling the descending branch of the stress-strain response of high strength of concrete. The expression for the descending branch becomes:

$$f_c = f_{cu} \left[ \frac{k_1 \left( \frac{\varepsilon}{\varepsilon_{cu}} \right)}{k_1 \beta - 1 + \left( \frac{\varepsilon}{\varepsilon_{cu}} \right)^{\beta}} \right] \quad (5.8)$$

The factors  $k_1$  and  $k_2$ , were determined empirically by Wee et al (1996) based on their experimental investigations on high strength concrete behaviour (with  $f_{cu}$  ranging from 60 to 100 MPa):

$$k_1 = \left( \frac{50}{f_{cu}} \right)^{3.0} \quad (5.9)$$

$$k_2 = \left( \frac{50}{f_{cu}} \right)^{1.3} \quad (5.10)$$

For the numerical simulations of high strength concrete (60 MPa to 100 MPa) the model proposed by Wee et al. (1996) was implemented in the current FE analysis. However, for concrete with strength greater than 100 MPa the descending branch and the post-peak residual strength at high strains are not adequately represented by this model.

In current study the model suggested by Lu and Zhao (2010) was used for high strength concrete with  $f_{cu}$  greater than 100 MPa. Lu and Zhao (2010) used the stress-strain relationships originally proposed by Gysel and Taerwe (1996) with some modifications in the descending branch. Two equations are proposed to describe the stress strain relationship for two ranges of concrete strains. For  $0 \leq \varepsilon \leq \varepsilon_L$ , where  $\varepsilon_L$  = concrete strain corresponding to a stress value of  $0.8f_{cu}$  on the descending branch of the stress-strain curve.

$$f_c = f_{cu} \left[ \frac{(E_{it}/E_0)(\varepsilon/\varepsilon_0) - (\varepsilon/\varepsilon_0)^2}{1 + (E_{it}/E_0 - 2)(\varepsilon/\varepsilon_0)} \right] \quad (5.11)$$

in which

$$\varepsilon_L = \varepsilon_0 \left[ \left( \frac{1}{10} \frac{E_{it}}{E_0} + \frac{4}{5} \right) \sqrt{\left( \frac{1}{10} \frac{E_{it}}{E_0} + \frac{4}{5} \right)^2 - \frac{4}{5}} \right] \quad (5.12)$$

and for  $\varepsilon > \varepsilon_L$ , a correction factor,  $\lambda$  is introduced in the model of Van Gysel and Taerwe (1996) for decreasing the steepness of the descending part of the stress-strain curve. The continuity of the complete stress-strain curves implies that for the predefined value  $\varepsilon = \varepsilon_L$ ,  $f_c$  in equation (5.13) will be equal to the  $0.8f_{cu}$ .

$$f_c = \frac{f_{cu}}{1 + \lambda \left[ (\varepsilon/\varepsilon_0) - 1 / (\varepsilon_L/\varepsilon_0) - 1 \right]^{2(1-\lambda)}} \quad (5.13)$$

Therefore,  $\lambda$  can be determined as  $\lambda = 1/4$ . It is obvious that the most important parameters used to define the stress strain relationship include the concrete compressive strength  $f_{cu}$ , the initial tangent modulus  $E_{it}$ , secant modulus at peak stress  $E_0$  and the strain at peak stress  $\varepsilon_0$ . All of these parameters are obtained experimentally as shown in Table 5.1 to 5.13. Typical stress-strain curves used in the current FE model for concrete with strength ranging from 28 MPa to 120 MPa is shown in Figure 5.13. The concrete stress strain curves for strength up to 60 MPa were generated using the Carriera and Chu (1985) model. Similarly, the stress strain curves for concrete strength from 61 MPa to 100 MPa were generated using the equations proposed by Wee et al. (1996). On the other hand the curves for 120 MPa concrete were developed using the model proposed by Lu and Zhao (2010).

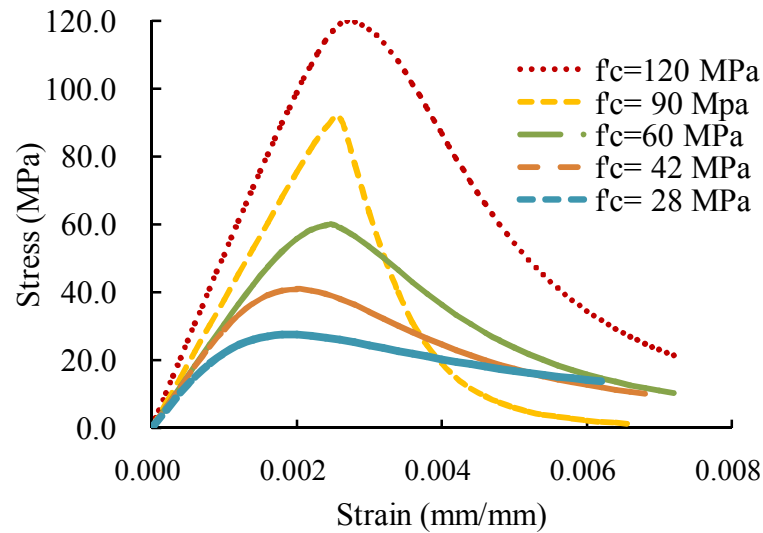


Figure 5.13 Stress-strain curves for concrete in uniaxial compression

#### 5.4.2.2 Stress-strain relationship for concrete in tension

Concrete tension properties for damage model are defined in two stages i.e. the linear elastic portion up to the tensile strength and the nonlinear post peak portion which is called the tension stiffening. The first part is defined using the modulus of elasticity of concrete and the uniaxial tensile strength of concrete. The uniaxial tensile strength of concrete  $f_{tu}$  was set at 10% of the uniaxial compressive strength for the normal strength concrete and 5% for the high strength concrete as used by Begum et al. (2007) in the FE analysis of partially encased composite column. To generate the tension stress-strain diagrams for normal strength concrete the following equation as proposed by Carreira and Chu (1985) was used.

$$f_c = f_{tu} \left[ \frac{\beta \left( \frac{\epsilon}{\epsilon_{tu}} \right)}{\beta - 1 + \left( \frac{\epsilon}{\epsilon_{tu}} \right)^\beta} \right] \quad (5.14)$$

The value  $\beta$  was used in this study equation proposed by Carreira and Chu (1985).



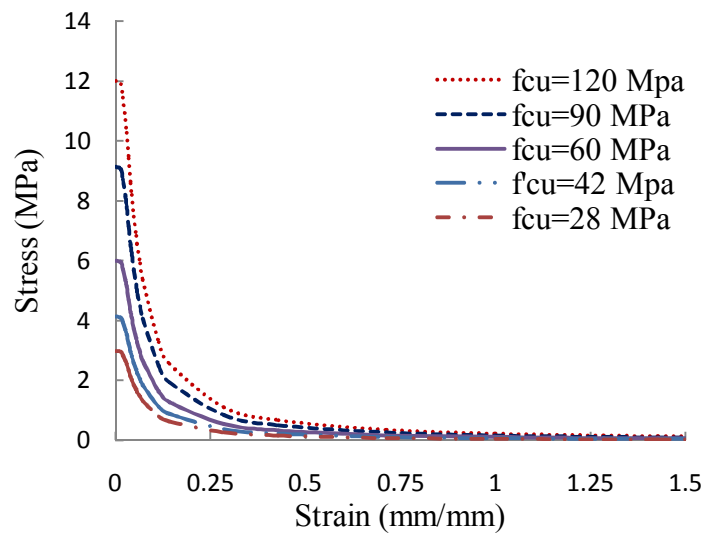


Figure 5.14 Stress-strain curve for concrete in uniaxial tension

## 5.5 Load Application and Solution Strategy

In this study the load was applied using displacement control technique on the top surface of the column. The nodes at top and bottom surfaces of the columns were made rigid. The displacement was applied at the rigid body reference node. The base of the column is fixed in all directions during concentric axial load. Rotation was allowed in different directions during eccentric and biaxial loads based on the positions of the applied loads or displacement. Riks solution strategy has been implemented to trace stable post peak behavior of the composite column up to failure.

### 5.5.1 Newton Raphson and Modified Newton Raphson Methods

The basic approach used in ABAQUS/Standard to solve nonlinear equations is Newton-Raphson iterative method. The solution procedure is shown in Figure 5.15. The solution seeks equilibrium through a horizontal path at a constant load vector. In this method the stiffness matrix ideally is updated at the end of every iteration. Since the major computational cost per iteration in Newton-Raphson iterations lies in the calculation decomposition of the tangent stiffness matrix developed at the beginning of a time step for all iterations within the time step, the solution path followed in a modified Newton-Raphson iterative method as illustrated in Figure 5.16. However, both methods failed to converge in the neighborhood of unstable responses such as near the ultimate load point.

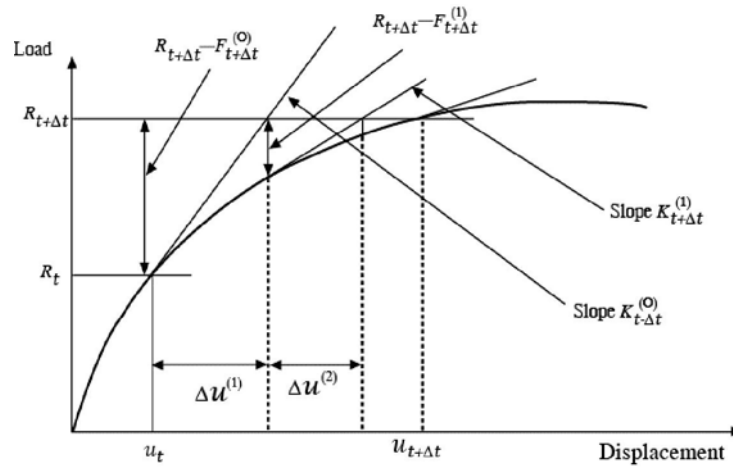


Figure 5.15 Newton-Raphson iterative method

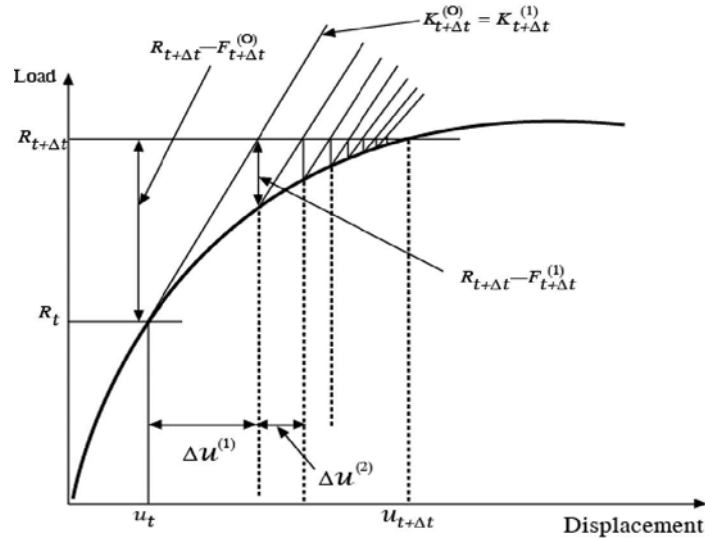


Figure 5.16 Modified Newton-Raphson iterative method

### 5.5.2 The Riks Method

To allow tracking of system response past limiting points the so-called “arc length control” (Figure 5.17) can be used. The technique was first developed by Riks (1979) and was later modified by (Ramm 1981). In the Riks solution algorithm both the load level and displacements are treated as unknown. The basic algorithm remains the Newton-Raphson iteration method, but the search for equilibrium is based on an iterative path perpendicular to a tangent plane taken in the equilibrium surface at the previously converged point. In this method the perpendicular solution path is easily controlled to intersect the equilibrium surface and converges well past limiting points (HKS 2013). A load whose magnitude is defined in the Riks step is referred to as a “reference” load. All prescribed loads are ramped

from the initial (dead load) value to the reference values specified. The loading during a Riks step is always proportional. The current load magnitude,  $P_{total}$ , is defined by

$$P_{total} = P_0 + \lambda(P_{ref} - P_0) \quad (5.15)$$

where  $P_0$  is the “dead load,”  $P_{ref}$  is the reference load vector, and  $\lambda$  is the “load proportionality factor.” The load proportionality factor is found as part of the solution. Abaqus/Standard prints out the current value of the load proportionality factor at each increment.

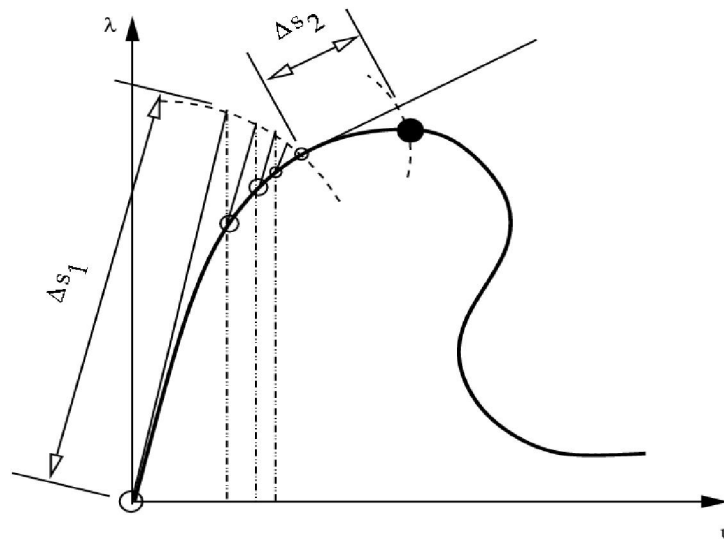


Figure 5.17 Riks solution strategy

Abaqus/Standard uses Newton's method to solve the nonlinear equilibrium equations. The Riks procedure uses only a 1% extrapolation of the strain increment. The initial increment in arc length along the static equilibrium path,  $\Delta l_{in}$ . The initial load proportionality factor  $\Delta\lambda_{in}$ , is computed as

$$\Delta\lambda_{in} = \frac{\Delta l_{in}}{l_{period}} \quad (5.16)$$

where  $l_{period}$  is a user-specified total arc length scale factor (typically set equal to 1). This value of  $\Delta\lambda_{in}$  is used during the first iteration of a Riks step. For subsequent iterations and increments the value of  $\lambda$  is computed automatically. The value of  $\lambda$  is part of the solution. Minimum and maximum arc length increments,  $\Delta l_{min}$  and  $\Delta l_{max}$  can be used to control the automatic incrementation. Direct user control of the increment size is also provided; in this case the incremental arc length,  $\Delta l$ , is kept constant. This method is not recommended for a Riks analysis since it prevents Abaqus/Standard from reducing the arc length when a severe

nonlinearity is encountered. Since the loading magnitude is part of the solution, a method to specify when the step is completed. A maximum value of the load proportionality factor,  $\lambda_{end}$  or a maximum displacement value at a specified degree of freedom. The step will terminate when either value is crossed. If neither of these finishing conditions is specified, the analysis will continue for the number of increments specified in the step definition (HKS 2013).

## **5.6 Conclusions**

The development of the 3D finite element model for the nonlinear simulations of the behaviour of FEC columns is presented in this Chapter. Both geometric and materials nonlinearities are included in the FE model. The selection of the element types and mesh size are based on the behaviour of these columns which is obtained from experimental investigations. The structural steel and rebars in FEC column are simulated using elasto-plastic material model whereas the damage plasticity model is used for concrete. Carreira and Chu (1985), Wee et al. (1996) and Lu and Zhao (2010) equations are used to model concrete stress strain behaviour under uniaxial compression and tension for normal (30 to 60 MPa), medium (61 MPa to 100 MPa) and high (>100 MPa) strength of concrete, respectively. Riks solution strategy is implemented to trace stable post peak behavior of the composite column up to failure.

## CHAPTER 6

### COMPARISON OF NUMERICAL RESULTS WITH EXPERIMENTAL DATA

#### 6.1 Introduction

A comparative study is carried out to verify the numerical results with the experimental results which has been presented in this chapter. Numerical results were obtained from 3D nonlinear finite element analysis using ABAQUS finite element code. The numerical simulations were performed on a wide variety of FEC columns with different geometric and material properties. A total of 35 FEC test columns were analyzed to validate the numerical results with the experimental findings for eccentric and concentric loads. The finite element analysis was conducted on thirteen short FEC columns from current study and twenty two FEC column specimens from published literature (Morino et al. 1984, Chen and Yeh 1996, Matsui 1979, Dundar et al. 2008 and Kim et al. 2012). The descriptions of the geometric and material properties of these test specimens were presented in Chapter 4 and 5. The comparisons are carried out on axial load capacity, axial strain, load versus deflection behaviour and modes of failure obtained from experimental and numerical studies. In addition, the developed FE model was used to predict the individual contributions of steel and concrete to the total load carrying capacity of the FEC column.

#### 6.2 Performance of Finite Element Model

From the finite element analysis for each of these test columns, the predicted load versus deformation response, peak load, peak axial strain and failure mode were obtained and compared with the corresponding experimental results. Moreover, for the eccentrically loaded short columns, comparisons were made with the capacities obtained from numerical analysis, to the experimental investigation both from laboratory tests in current and from published literatures. The axial and transverse stresses in the steel sections of the composite columns at failure were also investigated using the numerical model.

##### 6.2.1 Axial load versus axial deformation

The axial load versus average axial deformation curve for the test specimens of current study and reference test specimens from literatures were constructed from the numerical results and compared to the corresponding experimental results. It was found that the FE models were capable of predicting the load deflection behaviour of experimental results for the 35 FEC columns with good accuracy. A detailed discussion on the results is presented in the following sections.

### **6.2.1.1 Test specimens from current study**

In current research work total thirteen FEC column specimens were tested under concentric and eccentric axial loads. These columns were divided into six groups based on the concrete strength and loading conditions during the test. The experimental loads versus deformation curve were compared to the finite element analysis conducted for each group of specimens. The discussions on the results for each group of specimens are presented below.

#### ***Column Group SCN4A and SCN4B***

Figures 6.1 and 6.2, show the comparisons between the experimental and numerical load versus average axial deformation curves for column group SCN4A (SCN4A1, SCN4A2 and SCN4A3) and SCN4B (SCN4B1, SCN4B2 and SCN4B3). These FEC columns were tested for concentric axial load and constructed with normal strength concrete. Since the three specimens in each group are identical only one numerical simulation is conducted for each group. The experimental load versus axial deformation curves for the three test specimens of each group (SCN4A and SCN4B) were very similar with slight variation in the ultimate capacity. This variation may be attributed to the possibility of the presence of geometric or loading imperfections during the test. The variability in the casting, placement and variation of concrete may also be responsible for the slight variation in the load deformation response of the similar test specimens. The load versus deformation curves obtained from the numerical analysis for columns of group SCN4A and SCN4B was found to be in very good agreement with that obtained from the experimental investigations.

For columns of group SCN4A, the ascending branch of the numerical load versus deformation curves differed from the ascending branch of the load versus deformation curves obtained from the experiments. However, the peak load and the post peak behaviour of the numerical load versus deformation response matched well with that of the experimental curves.

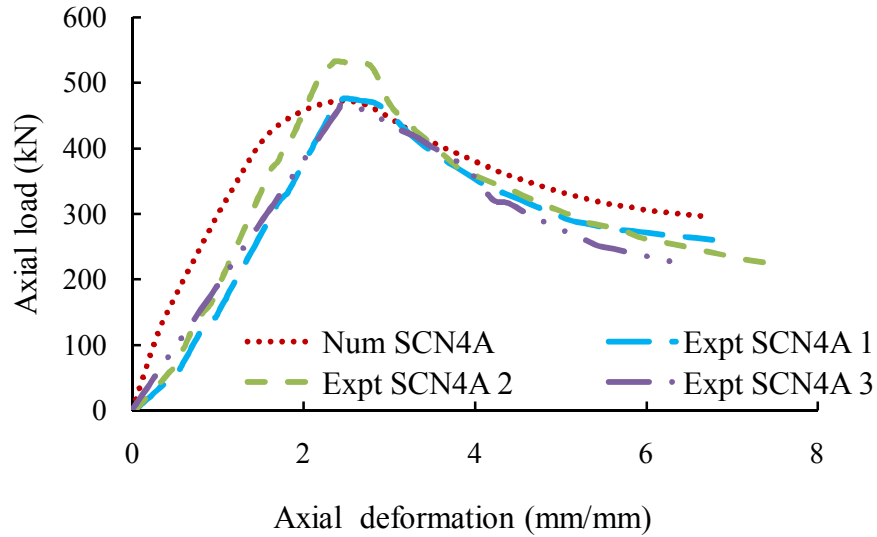


Figure 6.1 Experimental and numerical load versus deformation curve for Group SCN4A

For column group SCN4B, the ascending branch of the numerical load versus deformation curve is similar to the ascending branch of the load versus deformation curves obtained from the experiments. Also the slopes of the ascending branch of the experimental load versus deformation curves were very close to those of numerical load versus deformation curve. However, the peak load and the post peak behaviour of the numerical load versus deformation response matched very well with that of the experimental curves.

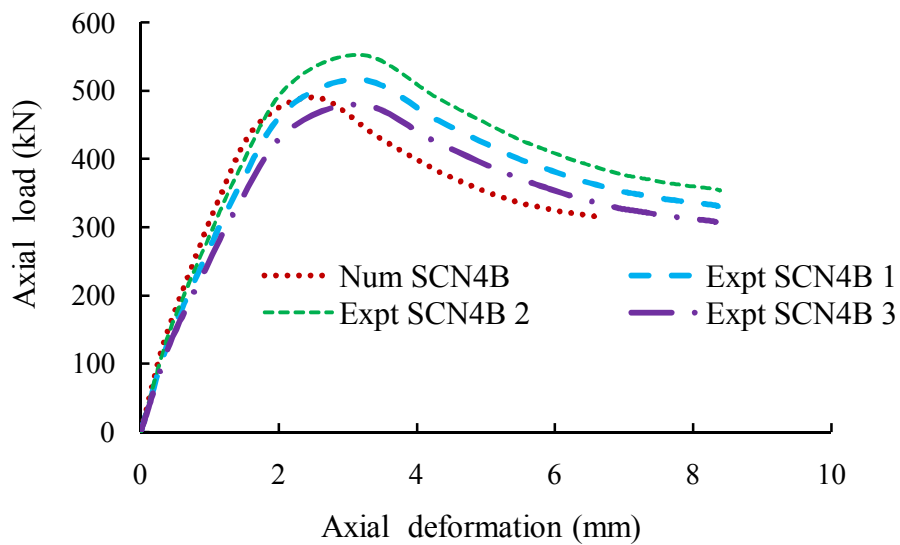


Figure 6.2 Experimental and numerical load versus deformation curve for Group SCN4B

### Column Group SCH6A and SCH6B

The comparison between the experimental and numerical load versus average axial deformation curve for three short columns of group SCH6A (SCH6A1, SCH6A2, SCH6A3) and two columns of group SCH6B (SCH6B1 and SCH6B2) are shown in Figures 6.3 and 6.4, respectively. These groups of column were constructed with high strength of concrete and tested under concentric axial load. For columns of group SCH6A the ascending branch of the numerical load versus deformation curves differ from the ascending branch of the load versus deformation curves obtained from the experiments. However, the peak load and the post peak behaviour of the numerical load versus deformation response matched very well with that of the experimental curves. Similarly, for column group SCH6B the ascending and descending branches of the numerical load versus deformation curves were in excellent agreement with the experimental curves (Figure 6.4).

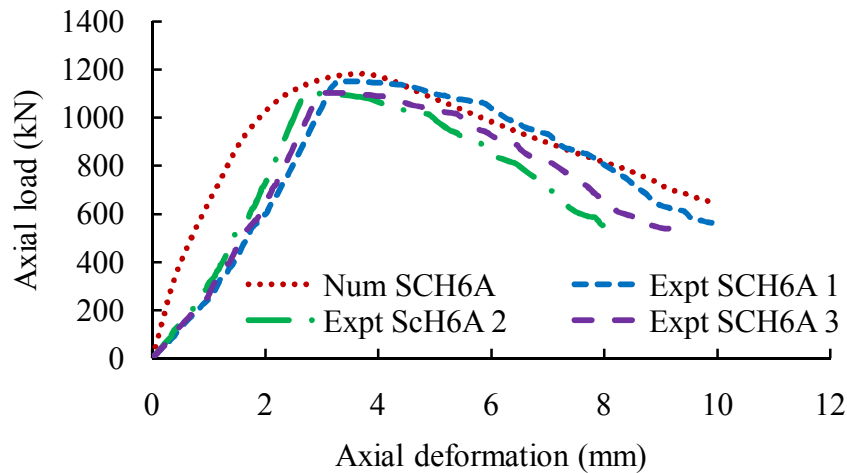


Figure 6.3 Experimental and numerical load versus deformation curve for Group SCH6A

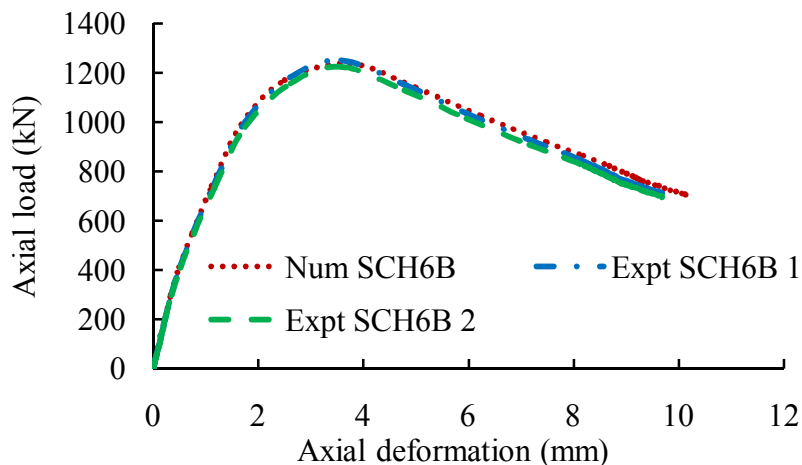


Figure 6.4 Experimental and numerical load versus deformation curve for group SCH6B



### ***Column SCN4E and SCH6E***

The load versus axial deformation curves for the columns SCN4E and SCH6E were shown in Figures 6.5 and 6.6. It was observed that the experimental and numerical load-deformation behaviour of these two FEC columns were very similar. The ascending branch of experimental and numerical load versus deformation curves were very close to each other for these two columns. Numerical ultimate loads of these columns were very close to their experimental capacities. For column SCN4E the numerical load carrying capacity at peak point was about 2% higher than the experimental capacity. For column SCH6E, the experimental ultimate load carrying capacity at peak point was 3% higher than the numerical result. The numerically obtained residual strength of the column after failure matched well with that obtained from the experiments. However, in these columns the axial deformations around and after the peak point of the load versus deformation curves were underestimated (by 8%) by the numerical model. The effects of geometric imperfections and residual stresses were not incorporated in the FE model for FEC columns developed in current study. This may be attributed to the minor variation between the numerical and experimental results.

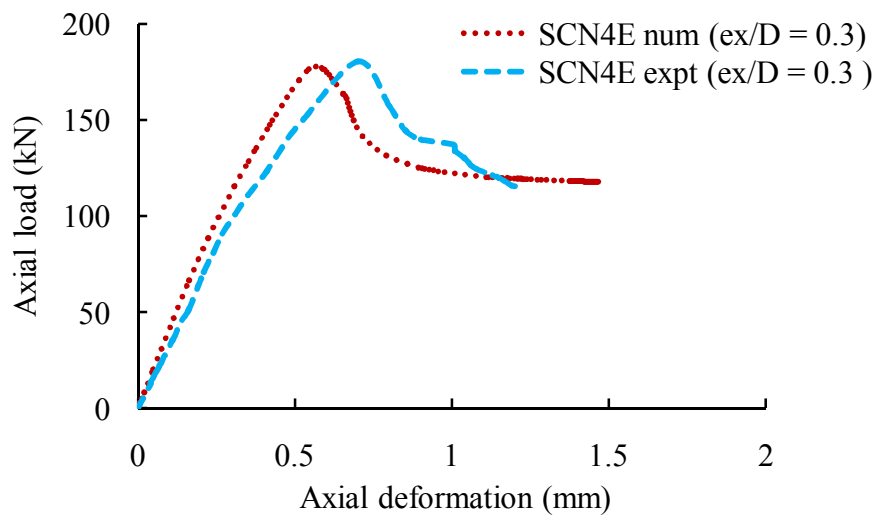


Figure 6.5 Experimental and numerical load versus deformation curve for column SCN4E

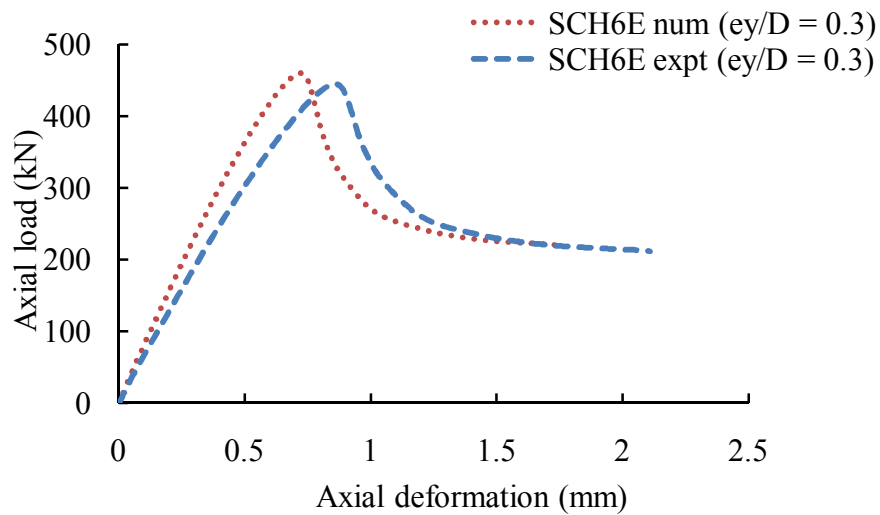


Figure 6.6 Experimental and numerical load versus deformation curve for SCH6E

### 6.2.1.2 Test specimens from published literature

The experimental load versus deformation behaviour of nine (Chen and Yeh 1996 and Kim et al. 2012) FEC columns from published literatures were compared with the numerical results. These specimens were tested for concentric as well as eccentric axial load with normal and high strength concrete. Load versus deflection curve for the reference test columns from published literature were generated numerically. However, the experimental load deflection behaviour for all the reference columns were not available in the literature. The numerical load-deflection behaviour was compared with experimental load versus deformation behavior of seven columns from Chen and Yeh (1996) and two columns from Kim et al. (2012) from the literature.

#### *Chen and Yeh (1996)*

The seven columns tested by Chen and Yeh (1996) were numerically simulated with three different shapes of structural steel sections (H, cross and I-shaped). These columns were constructed with normal strength concrete and were subjected to concentric axial load. The comparison between the experimental and numerical load versus axial deformation responses for three columns constructed with H-shaped structural steel (SRC1, SRC2 and SRC3) are shown in Figures 6.7 to 6.9. Three columns designated as SRC4, SRC5 and SRC6 (Chen and Yeh 1996) were constructed with cross shaped structural steel. The comparison between experimental and numerical load versus axial deformation curves for these columns (SRC4, SRC5 and SRC6) are shown in Figures 6.10 to 6.12. The comparison between the

experimental and numerical load versus axial deformation curve of column SRC7 is shown in Figure 6.13. This column was constructed with I-shaped structural steel section. Normal strength concrete was used in this column and tested for concentric axial load. For all specimens (SRC1 to SRC7), in general, good agreement is obtained between the numerical and the experimental load versus deformation behaviours. For these columns the ascending and descending branches of the numerical load versus axial deformation curves were similar to the experimental load versus axial deformation curves. However, for specimen SRC7 the numerical model is observed to slightly overestimate the axial deformation around and after the peak load point.

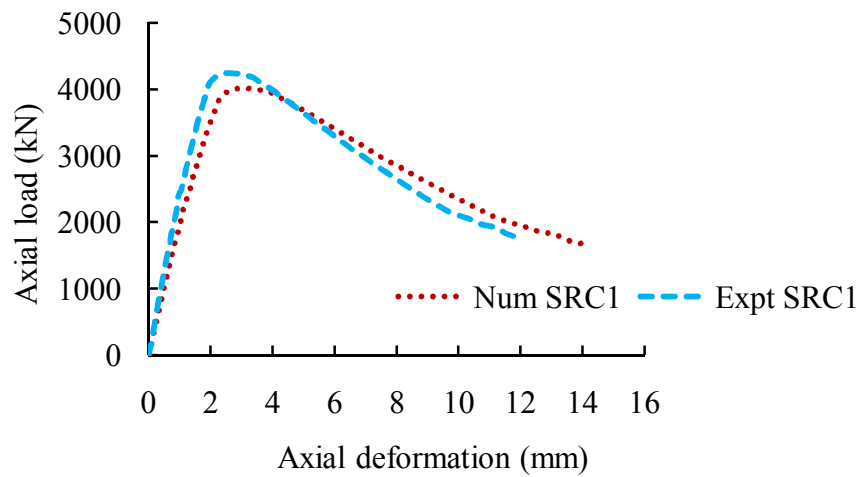


Figure 6.7 Experimental and numerical load versus deformation curve for column SRC1

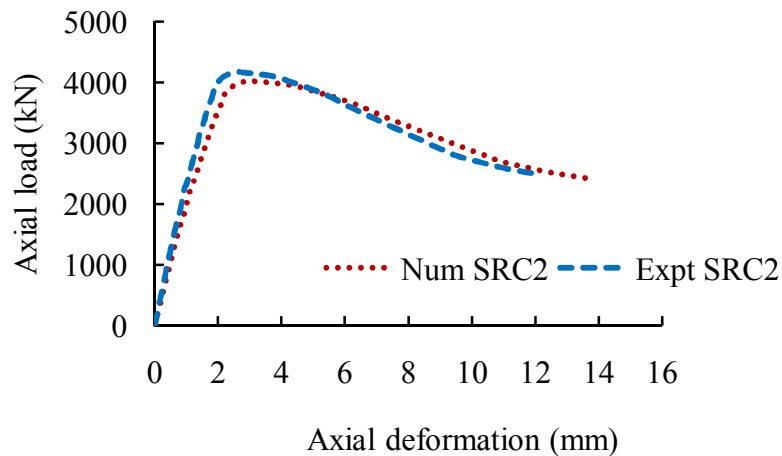


Figure 6.8 Experimental and numerical load versus deformation curve for column SRC2

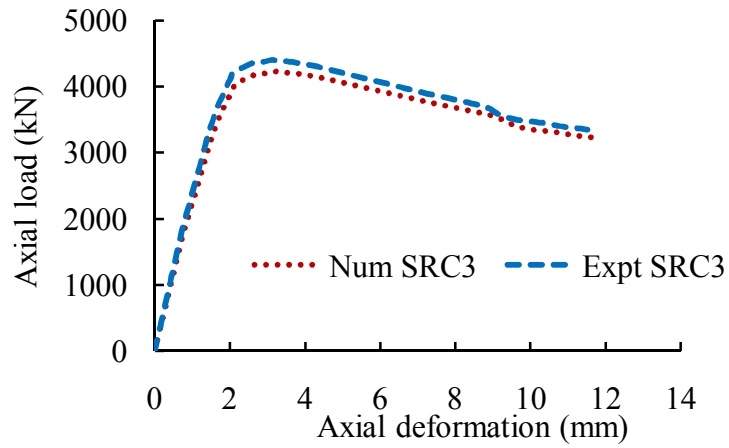


Figure 6.9 Experimental and numerical load versus deformation curve for column SRC3

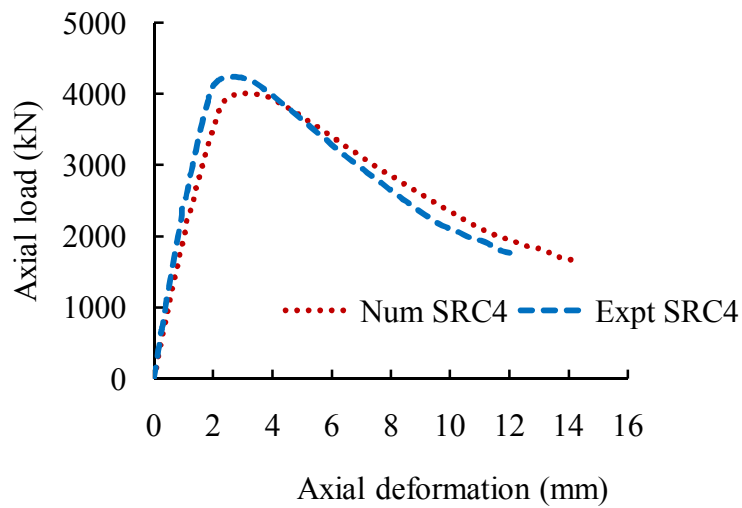


Figure 6.10 Experimental and numerical load versus deformation curve for column SRC4

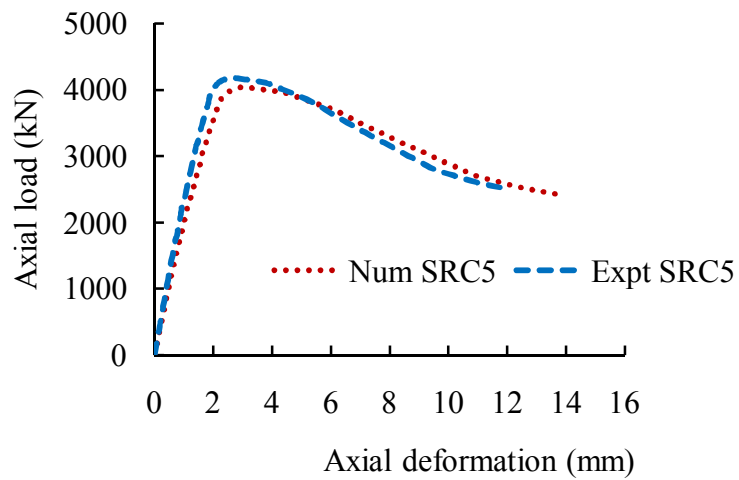


Figure 6.11 Experimental and numerical load versus deformation curve for column SRC5

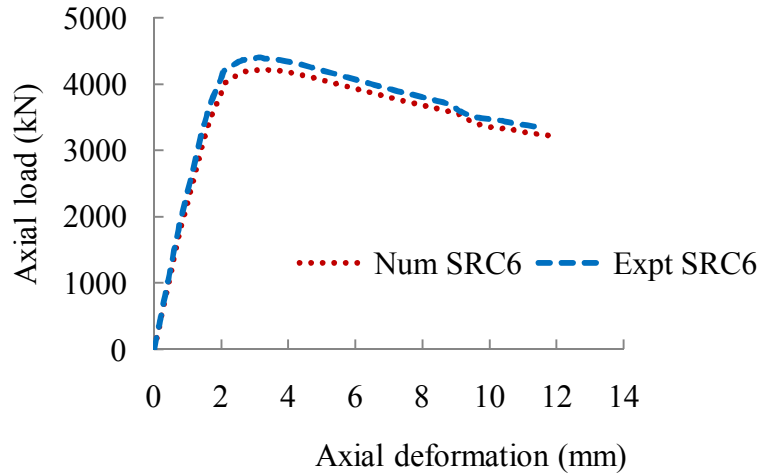


Figure 6.12 Experimental and numerical load versus deformation curve for column SRC6

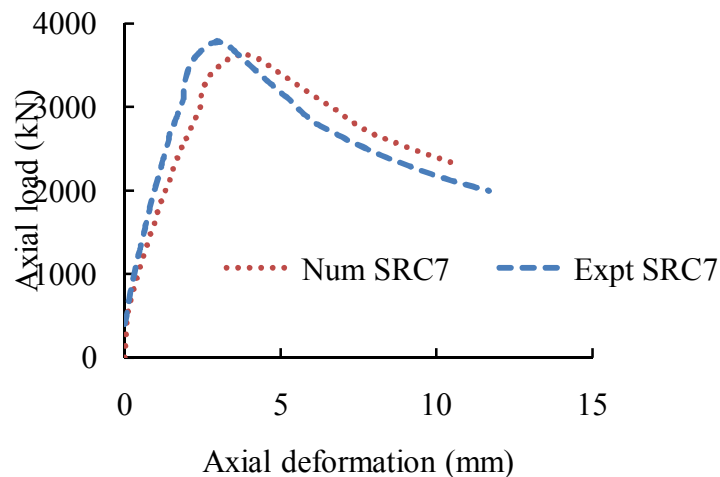


Figure 6.13 Experimental and numerical load versus deformation curve for column SRC7

**Kim et al. (2012)**

Comparisons were carried out between the experimental and numerical load versus axial deformation behaviour for two short, eccentrically loaded FEC columns (C1 and C2) from Kim et al. (2012). These columns were constructed using high-strength structural steel (913 MPa) and high strength concrete (91 MPa). The ascending branch of the numerical load versus axial deformation curves for these specimens C1 and C2 matched well with that of the experimental load versus deformation curves (Figures 6.14 and 6.15). The peak region of the load versus deformation curves obtained from the experiments showed some oscillations which occurred due to the cracking of concrete at the tension side and by spalling of cover concrete at the compression side followed by concrete cover delamination and crushing (Kim et al. 2012). The post peak behaviour of the numerical load versus deformation

response matched well with that of the experimental curve for column C1. For column C2, the descending branch of the numerical load versus deformation curve differed slightly from the descending branch of the load versus deformation curve obtained from the experiment. This may be due to the presence of imperfections in the test specimens which was not included in the numerical simulation. Moreover, in the numerical model the descending branch of the stress versus strain curve for the high strength concrete was generated (based on the cylinder test data from Kim et al. 2012) from the empirical relationships available in published literature. This may be responsible for the differences in the experimental axial deformation values with that obtained from the numerical simulations.

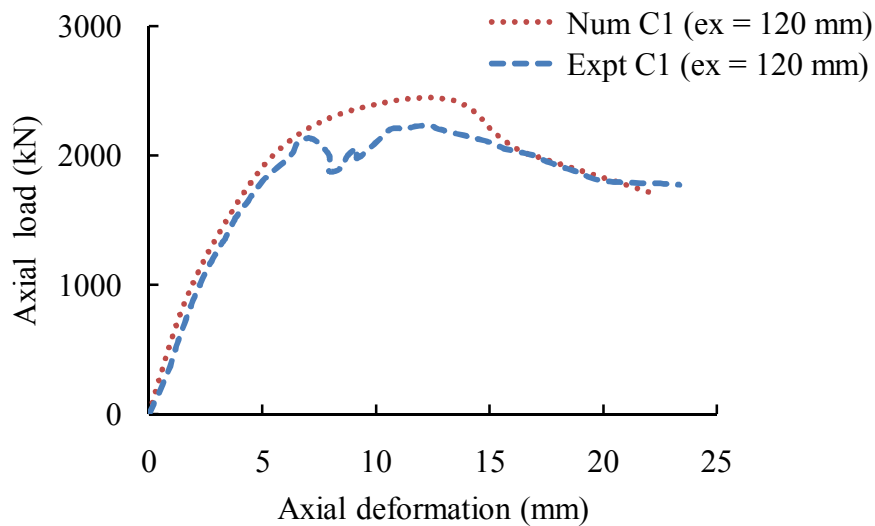


Figure 6.14 Experimental and numerical load versus deformation curve for column C1

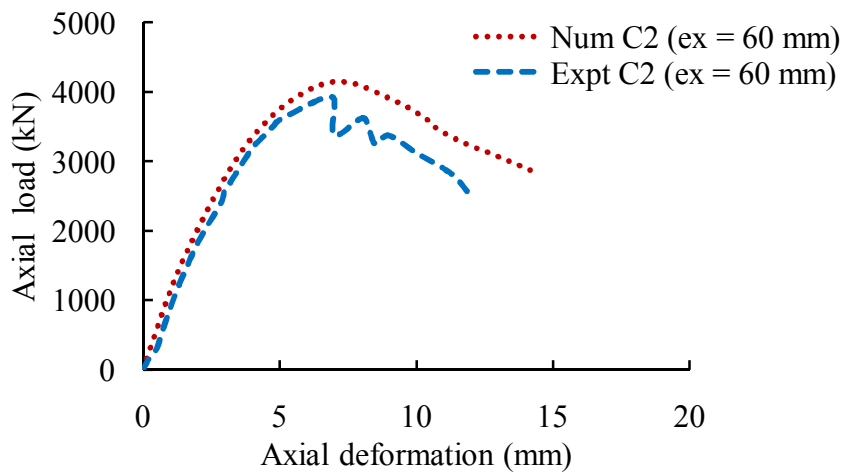


Figure 6.15 Experimental and numerical load versus deformation curve for column C2

## 6.2.2 Axial capacity and axial strain

The ultimate axial load and average axial strain at the ultimate load point for the test specimens of current study and reference test specimens from literature were determined from the numerical results and compared to the corresponding experimental results.

### 6.2.2.1 Test specimens from current study

In current research work total thirteen FEC columns specimens were tested under concentric and eccentric axial load. These columns were divided into six groups (SCN4A, SCN4B, SCH6A, SCH6B, SCN4E and SCH6E) based on the concrete strength and loading conditions during the test. The experimental peak load and corresponding axial strain were compared (as shown in Table 6.1) to the capacity and strains obtained from the finite element analysis conducted for the test specimens. The ratio of the numerical-to-experimental peak load ( $P_{num}/P_{exp}$ ) for the test specimens varied from 0.926 to 1.067 with a mean value of 0.991 and standard deviation of 0.046. This indicates the excellent performance of the finite element model in predicting the ultimate capacity of the test columns.

Table 6.1 shows the mean ratio of the numerical-to-experimental average axial strain at peak load, ( $\epsilon_{num}/\epsilon_{exp}$ ) was 0.874 with a standard deviation of 0.103. Although providing excellent estimates of the peak load, the numerical model is observed to underestimate the axial deformation at peak load. This discrepancy could be due to the presence of imperfections and residual stresses in the test specimens as already mentioned in Section 6.2.1.1. Columns designated as SCN4A (SCN4A1, SCN4A2 and SCN4A3) and SCN4B (SCN4B1, SCN4B2 and SCN4B3) were constructed with normal strength concrete (28 MPa) and tested for concentric axial load. The columns of group SCN4A were constructed with 3% structural steel ratio, whereas this ratio for columns included in group SCN4B was 3.75%. It was observed that axial load carrying capacity was increased by 7% in column SCN4B than SCN4A for the increase in 1% structural steel. This increase in the axial load capacity (for 1% increase in structural steel ratio) was found to be 10% for columns (SCH6A and SCH6B) constructed with high strength concrete (42 MPa).

Table 6:1 Comparison of numerical and experimental results from current study

Ser. no	Specimen designation	Load capacity (kN)		$P_{num}/P_{exp}$	Axial strain at peak load		$\epsilon_{num}/\epsilon_{exp}$
		$P_{num}$	$P_{exp}$		$\epsilon_{num} (\mu\epsilon)$	$\epsilon_{exp} (\mu\epsilon)$	
1	SCN4A 1	471	493	0.955	2550	2707	0.893
2	SCN4A 2	471	502	0.938	2550	2727	0.935
3	SCN4A 3	471	478	0.985	2550	2690	0.948
4	SCN4B 1	490	516	0.950	2541	3241	0.784
5	SCN4B 2	490	503	0.974	2541	3210	0.792
6	SCN4B 2	490	529	0.926	2541	3155	0.805
7	SCH6A 1	1181	1117	1.057	3749	4428	0.847
8	SCH6A 2	1181	1127	1.048	3749	4553	0.823
9	SCH6A 3	1181	1107	1.067	3749	4577	0.819
10	SCH6B 1	1238	1244	0.995	3748	4398	0.852
11	SCH6B 2	1238	1240	0.998	3748	4226	0.887
12	SCN4E	181	178	1.017	1780	1629	1.093
13	SCH6E	445	460	0.967	1945	1793	1.085
<b>Mean</b>				<b>0.991</b>			<b>0.874</b>
<b>SD</b>				<b>0.046</b>			<b>0.103</b>

In Table 6.1, columns designated as SCN4E and SCH6E were constructed with normal strength (28 MPa) and high strength (42 MPa) concrete, respectively. Both the columns were tested for eccentric axial loads. In the test, the axial compressive load in column SCN4E was applied at 33 mm eccentricity about the weak axis of the structural steel I-section of the column. For column SCH6E the load was applied at 50 mm eccentricity about the strong axis of structural steel I section. It was found that the numerical load carrying capacity was 2% higher than the experimental load capacity for column SCN4E. On the other hand, the ultimate capacity obtained from FE analysis for column SCH6E was lower (by 3%) than the capacity obtained from the experiment. The numerical model can satisfactorily predict the axial capacity of the eccentrically loaded columns of current study.

#### 6.2.2.2 Test specimens from published literature

Twenty two columns from published literature were simulated for concentric and eccentric loads. Eighteen columns were constructed with normal strength concrete and four columns with high strength concrete and high strength steel. Ten columns (Chen and Yeh, 1996) out of eighteen were tested for concentric axial load and seven columns (Morino et al. 1984; Matsui 1979 and Dundar et al. 2008) for eccentric loads with uniaxial and biaxial bending. The four FEC columns constructed with high strength steel and high strength concrete, extracted from Kim et al. (2012), were subjected to eccentric axial loads.



***Concentrically Loaded FEC Columns (Chen and Yeh, 1996)***

The comparison between experimental and numerical results of peak load and peak strain of the ten concentrically loaded test specimens from Chen and Yeh (1996) is shown in Table 6.2. Three different shapes of the structural steel section were used in the specimens i.e., H, cross and I-shaped sections. The H-shaped steel section was more alike the wide-flange section, while the I-shaped section had a narrow flange. All of the ten columns were constructed with normal strength concrete (29 MPa). From Table 6.2 it is found that the numerical models for these specimens with various structural steel shapes can satisfactorily predict the experimental peak axial load and corresponding axial strain. The mean ratio and standard deviation of the numerical to experimental capacities, ( $P_{num}/P_{exp}$ ) were 0.981 and 0.046, indicating a very good performance of the numerical model in predicting the capacity of FEC columns with a variety of encased structural steel sections. As shown in Table 6.2, the ratio of the numerical-to-experimental average axial strain at peak load,  $\epsilon_{num}/\epsilon_{exp}$  ranged from 0.971 to 1.283. The average ratio of axial strain at peak load was found to be 1.149 with a standard deviation of 0.093.

Table 6:2 Comparisons of numerical and experimental results for concentric load

References	Specimens designation	Load capacity		$P_{num}/P_{exp}$	Axial strain at peak load		$\epsilon_{num}(\mu\epsilon)/\epsilon_{exp}(\mu\epsilon)$
		Experimental ( $P_{exp}$ ) (kN)	Numerical ( $P_{num}$ ) (kN)		Exp $\epsilon_{exp}$ ( $\mu\epsilon$ )	Num $\epsilon_{num}$ ( $\mu\epsilon$ )	
Chen and Yeh (1996)	SRC1	4220	4013	0.951	2580	2740	1.062
	SRC2	4228	4033	0.954	2200	2530	1.15
	SRC3	4399	4225	0.960	2600	2524	0.971
	SRC4	4441	4642	1.045	2650	3099	1.169
	SRC5	4519	4645	1.028	2850	3300	1.158
	SRC6	4527	4741	1.047	3030	3256	1.075
	SRC7	3788	3636	0.960	2450	3145	1.283
	SRC8	3683	3437	0.933	2550	3030	1.188
	SRC9	3630	3636	1.002	2650	3145	1.186
	SRC10	3893	3621	0.930	2500	3138	1.255
<b>Mean</b>				<b>0.981</b>			<b>1.149</b>
<b>SD</b>				<b>0.046</b>			<b>0.093</b>

### ***Eccentrically loaded FEC Columns***

The finite element results obtained from the simulations of eccentrically loaded columns tested by Morino et al (1984), Dunder et al. (2008) and Matsui (1979) were compared with capacities obtained from the experiments as presented in Table 6.3. These columns were subjected to eccentric load with uniaxial as well as biaxial bending. The average ratio of the numerical load capacity to experimental capacity ( $P_{num}/P_{exp}$ ) was 0.99 with a standard deviation of 0.074. The peak axial load with numerical-to-experimental ratios ranged from 0.901 to 1.11 for these columns. The minor difference between the numerical and experimental results can be attributed to the presence of geometric imperfections or initial out-of-straightness in the test columns. In general, the numerical model is capable of predicting the column capacities under eccentric uniaxial and biaxial loading conditions with very good accuracy.

The values of experimental and numerical peak loads, for two columns are shown in Tables 6.3. The average mean ratio and standard deviation of the numerical to experimental capacities, ( $P_{num}/P_{exp}$ ) were 0.994 and 0.074 for columns CC3 and CC4, respectively (Table 6.3). It was observed that the COV between numerical and experimental load capacity was about 8% for these columns.

Table 6.3 Comparison of numerical and experimental results for eccentrically loaded columns

References	Specimens designation	Location of load		Load capacity (kN)		$P_{num}/P_{exp}$
		$e_x$	$e_y$	Numerical	Experimental	
		(mm)	(mm)	$P_{num}$	$P_{exp}$	
Morino et al. (1984)	A4-00	40	-	474	499	0.950
	A4-45	28.3	28.3	506	518	0.977
	A4-90	-	40	667	740	0.901
Dunder et al. (2008)	CC 3	50	48.5	159	176	0.903
	CC 4	40	39.2	333	319	1.044
Matsui (1979)	1	-	-	1019	996	1.023
	2	-	-	1082	974	1.111
	3	-	-	910	874	1.041
<b>Mean</b>						<b>0.994</b>
<b>SD</b>						<b>0.074</b>

### ***FEC Columns with High Strength Steel and High Strength Concrete***

The values of experimental and numerical peak loads, of four FEC columns (Kim et al. 2012) with high strength steel (913 MPa) and concrete (91 MPa) are given in

Table 6.4. These four columns (C1, C2, C3 to C4) were simulated for eccentric axial load with two different eccentricity ratios about the major axis of the steel I-section.

Table 6.4 Comparison of numerical and experimental results of FEC columns with high strength materials

References	Specimens designation	Location of loads	Load capacity		$P_{num}/P_{exp}$	Axial strain at peak load		$\epsilon_{num}/\epsilon_{expt}$
		$e_x$ (mm)	$P_{exp}$ (kN)	$P_{num}$ (kN)		$\epsilon_{exp}$ ( $\mu\epsilon$ )	$\epsilon_{num}$ ( $\mu\epsilon$ )	
Kim et al. (2012)	C1	120	2203	2449	1.112	4553	4580	1.006
	C2	60	3752	4147	1.105	2508	2874	1.146
	C3	120	2020	2190	1.084	2504	2962	1.183
	C4	120	2211	2440	1.104	5347	4527	0.847
<b>Mean</b>					<b>1.101</b>			<b>1.046</b>
<b>SD</b>					<b>0.012</b>			<b>0.153</b>

The cross sectional geometry of these columns were similar, except the spacing of the transverse ties. All these columns had a square cross-section of  $260 \times 260$  mm. The structural steel ratio and longitudinal rebar ratios were 8.2% and 1.1% respectively. The transverse ties (10 mm diameter) were spaced at a spacing of 50 mm in columns C1, C2 and C3 whereas column C4 had a larger tie spacing of 130 mm. The numerical-to-experimental peak load ratios for these columns varied between 1.08 to 1.11. On an average, the numerically obtained capacities for these eccentrically loaded high strength columns were 10% higher than the experimentally obtained capacities. Possible reasons behind this overestimation of the axial capacities by the numerical model may be due to the variation in the strength of column concrete and cylinder concrete. No strength reduction factors were applied during the simulations of the concrete materials in the FEC columns. Moreover, no geometric imperfections were included in the numerical simulations of the FEC columns. As shown in Table 6.4, the ratio of the numerical-to-experimental average axial strain at peak load point load,  $\epsilon_{num}/\epsilon_{exp}$  was 1.046 and the corresponding standard deviation is 0.153 for these columns. This variation in the axial strain can be attributed to the assumptions in the material behaviour in the numerical simulations.

The experimental ductility indexes of these columns were compared with the numerical results. The ductility index is the ratio of post peak deformation at 80% of ultimate load and deformation at peak load. It was observed from Table 6.5 that the numerical results are very close to experimental results with a mean of 0.974 and a standard deviation of 0.083. The

numerical model was also able to successfully simulate the enhancement in axial capacity and ductility of FEC columns by reducing the spacing of transverse ties. The axial capacity of column C4 which had a tie spacing of 50 mm is increased by 7.8% as compared to the capacity of column C3 with a larger tie spacing of 130 mm.

Table 6.5 Ductility index of FEC columns with high strength materials

Specimen designation	$e_x$ (mm)	Peak load ( $P_0$ ) (kN)		Axial deformation at peak load (mm)		Axial deformation at $0.8P_0$ load(mm)		Ductility Index ( $\mu = \delta_{p0}/0.8\delta_{p0}$ )		$\mu_{num}/\mu_{exp}$
		Exp	Num	Exp	Num	Exp	Num	$\mu_{exp}$	$\mu_{num}$	
		C1	120	2203	2211	7.24	6.301	23.29	19.04	
C2	60	3752	4147	6.57	6.22	10.65	11.25	1.621	1.809	1.116
C3	120	2020	2245	6.56	6.64	19.15	18.08	2.919	2.723	0.933
C4	120	2211	2422	6.66	5.98	23.95	19.5	3.596	3.261	0.907
<b>Mean</b>										<b>0.974</b>
<b>SD</b>										<b>0.083</b>

### 6.2.3 Modes of Failure

Comparisons were carried out between the numerical and experimental modes of failure (current and published research work) of the FEC columns and comments are presented below.

#### 6.2.3.1 Test specimens from current study

In the test columns the primary mode of failure was crushing of concrete. During testing, the column surface was observed in order to follow the development and propagation of cracks. The appearance of cracks was always a sign that the column had reached the failure state. The sequence of damage the test columns started with the formation of the cracks occurring at middle, upper and lower part of the column and with the increase in the applied load, cracks became wider and the cover started to spall off. Finally, crushing of concrete occurred followed by yielding of structural steel and reinforcement.

The failure modes for FEC columns were identified from the finite element analysis and compared with the failure modes in the experiments. The failure modes were concrete crushing (CC), structural yielding (SY), and flexural buckling (F). The three modes were identified by examining the stress of the concrete and structural steel elements at ultimate load point. A comparison between the numerical and experimental failure mode of the test column SCN4A1 is shown in Figure 6.16. In both cases failure was initiated by crushing of concrete followed by yielding of steel and buckling of longitudinal rebars.

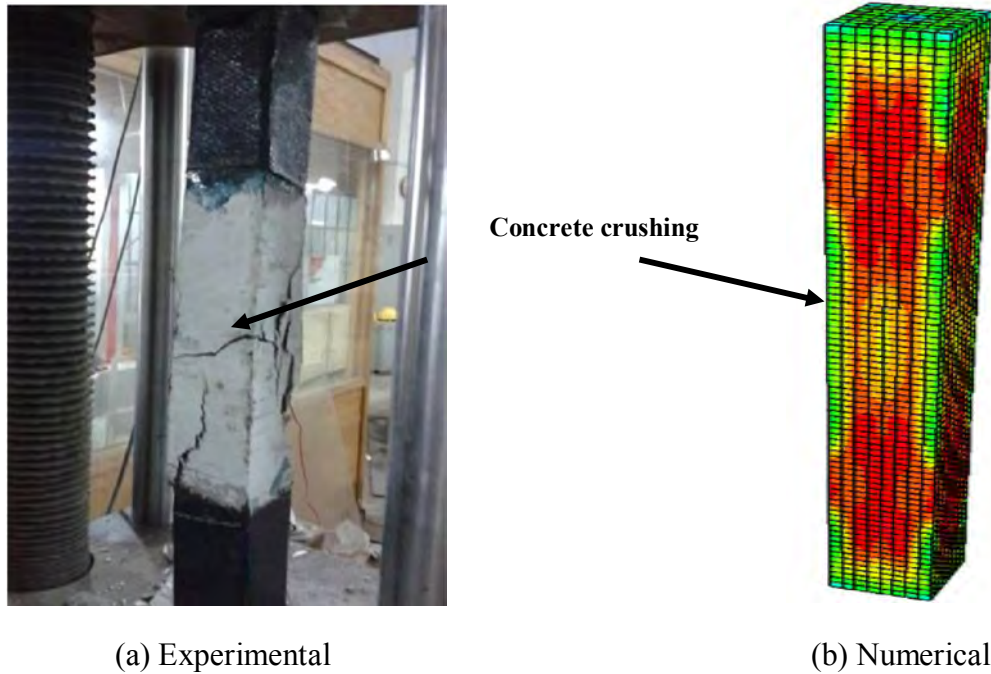


Figure 6.16 Failure of column SCN4B1 (a) Experimental (b) Numerical

The principal stress in steel along Z-Z (3-3) axis is shown in Figure 6.17 for column SCH6B and SCH6E at ultimate load. It was observed from numerical study that the column (SCH6B) failed due to crushing of concrete and followed by structural steel yielding as reported before. The structural steel at top yielded due to eccentric load on column SCH6E. Similar failure behaviour was also observed for this column experimentally, as shown in Chapter 4.

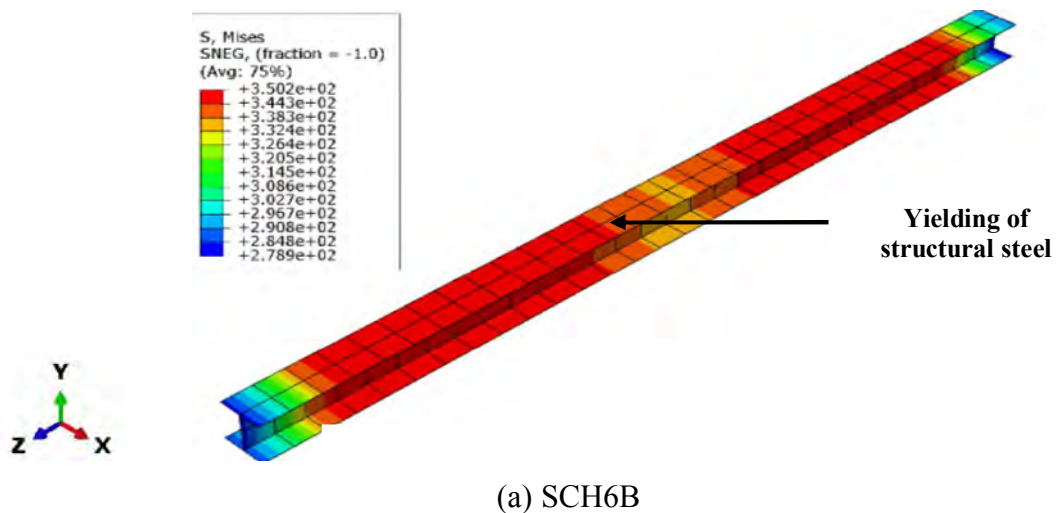


Figure 6.17 Stress contour in structural steel at failure for column

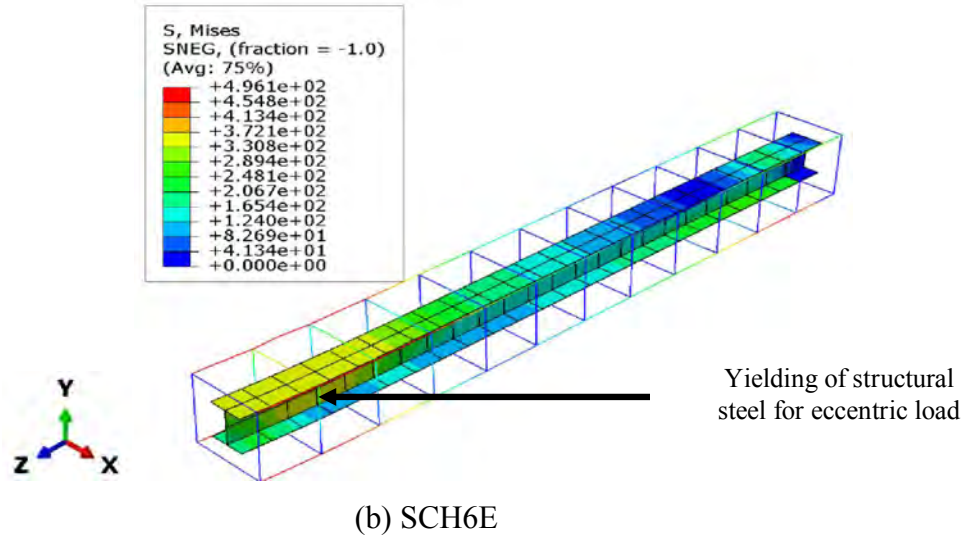


Figure 6.17 (cont.) Stress contour in structural steel at failure for column

(a) SCH6B and (b) SCH6E

### 6.2.3.2 Test specimens from published literature

A comparative study was also carried out between the experimental and numerical failure patterns for the test specimens from published literature.

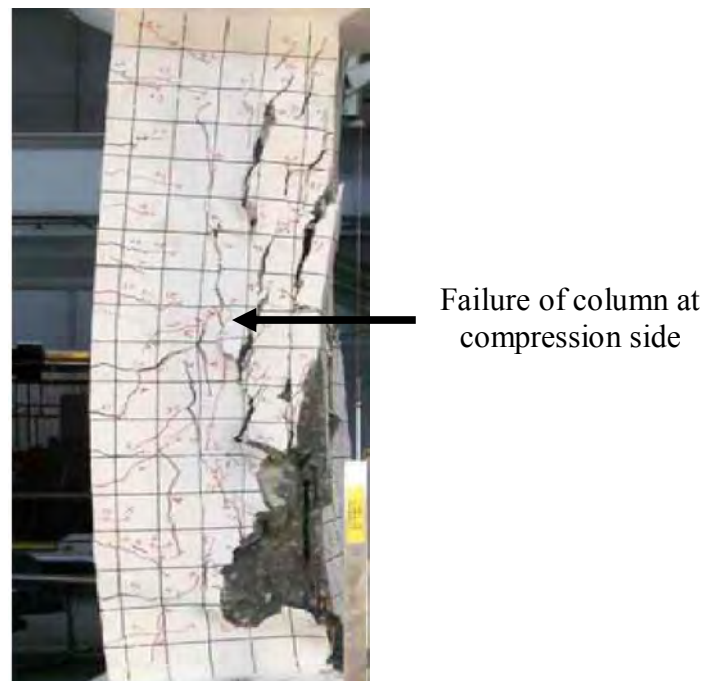


Figure 6.18 Experimental failure of column C1 (Kim et al. 2012)

### *Failure Pattern from Kim et al. (2012)*

Figure 6.18 shows the damage patterns of the specimen C1 at the end of experiments conducted by Kim et al. (2012). The specimen failed because of concrete crushing in the compression side. However, the exact location of the critical section differed in each specimen. After testing, buckling of the longitudinal rebars and crushing of the confined concrete was observed in the fully encased specimens. The measurements by the strain gauges showed that yielding of the ties occurred in C1 and C2. In C3, with relatively large tie spacing, the ties did not yield. In C4 with high-strength ties, the transverse rebars also did not yield. Figure 6.19 shows the numerical failure patterns of the specimens (Kim et al. 2012) at the end of numerical simulation. Numerically, it was observed that the specimen C1 also failed due to concrete crushing in the compression side of the column which is similar to that observed in the tests.

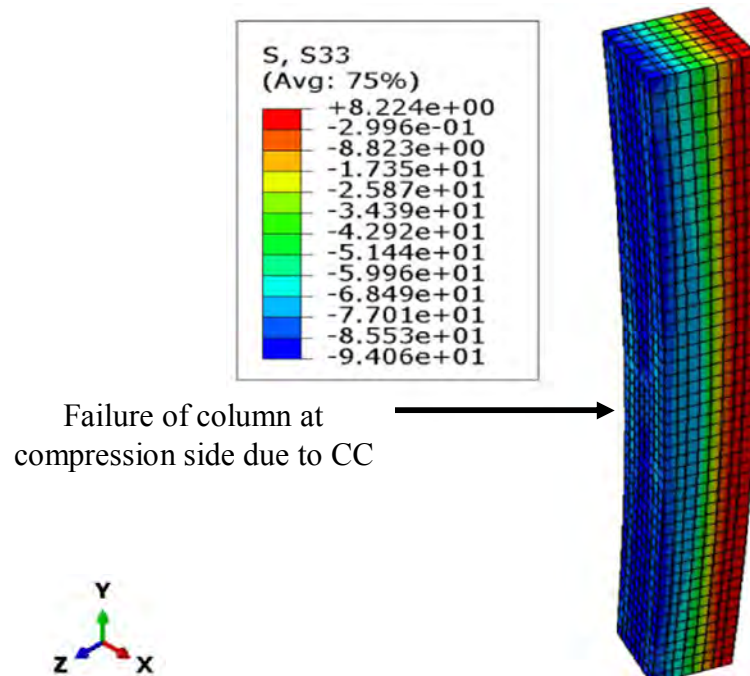
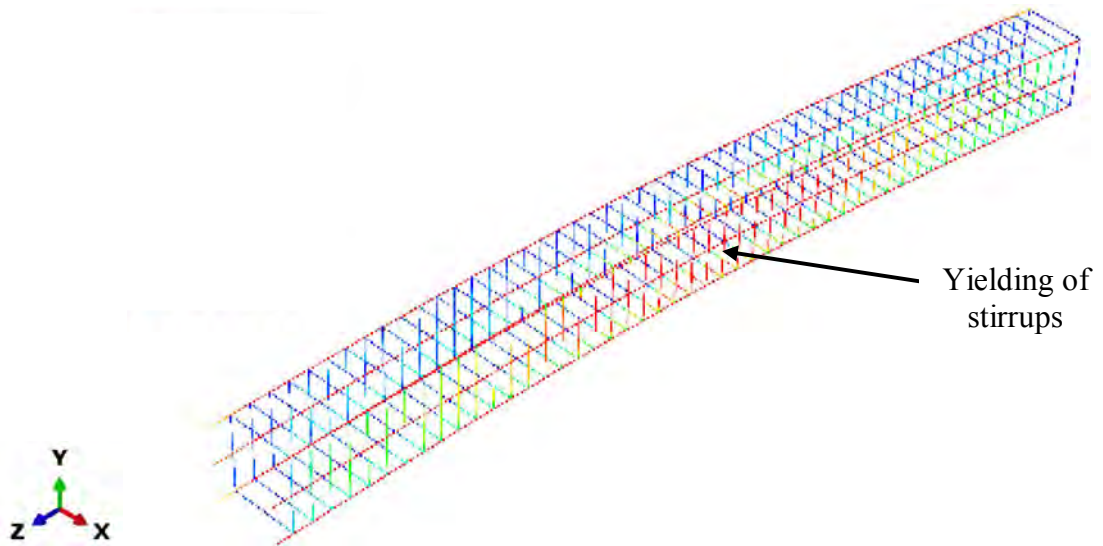
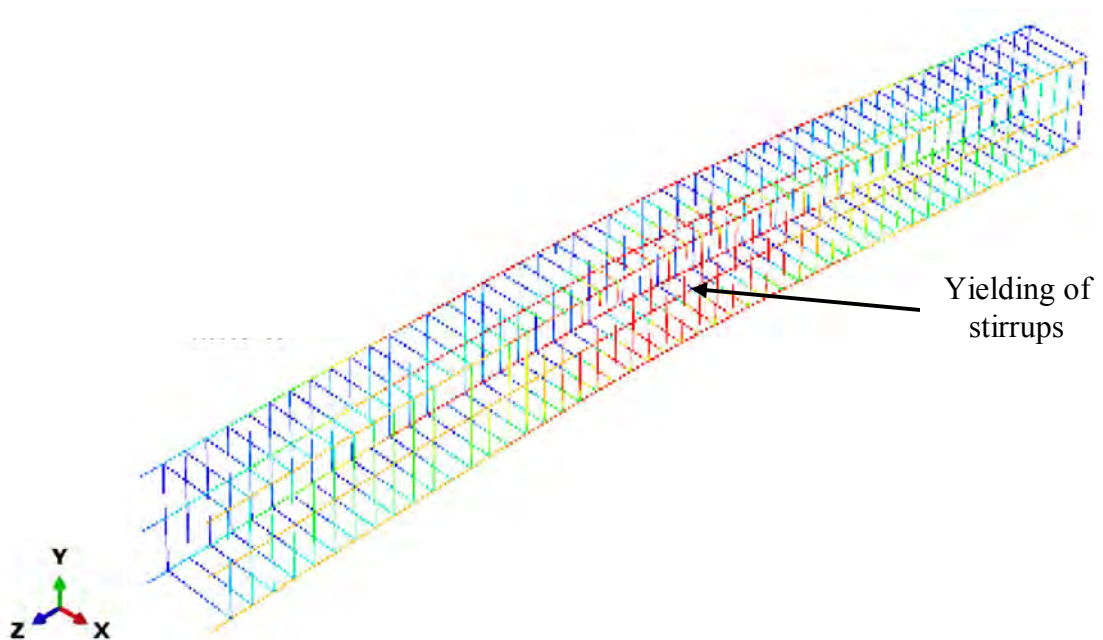


Figure 6.19 Numerical failure of column C1

It was observed from numerical study that the transverse ties ( $f_y = 560$  MPa) of column C1 and C2 also yielded at failure, as shown in Figure 6.20 (a) and (b).



(a) Column C1

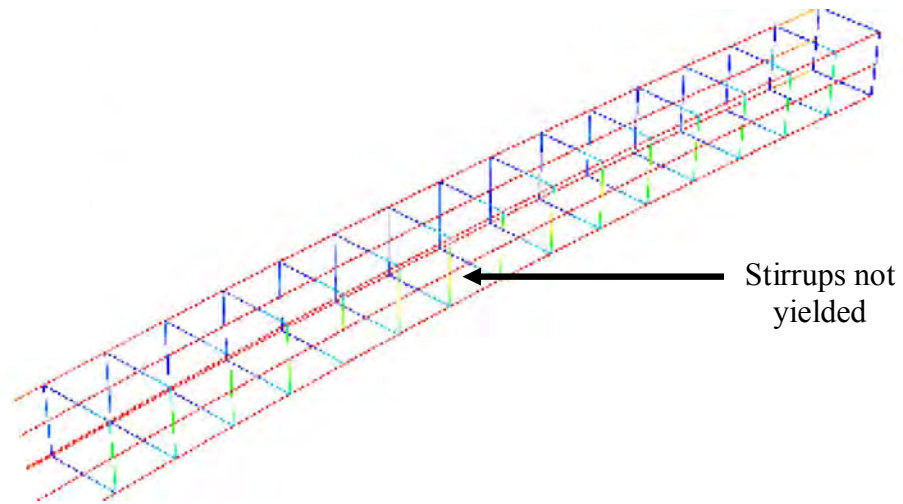


(b) Column C2

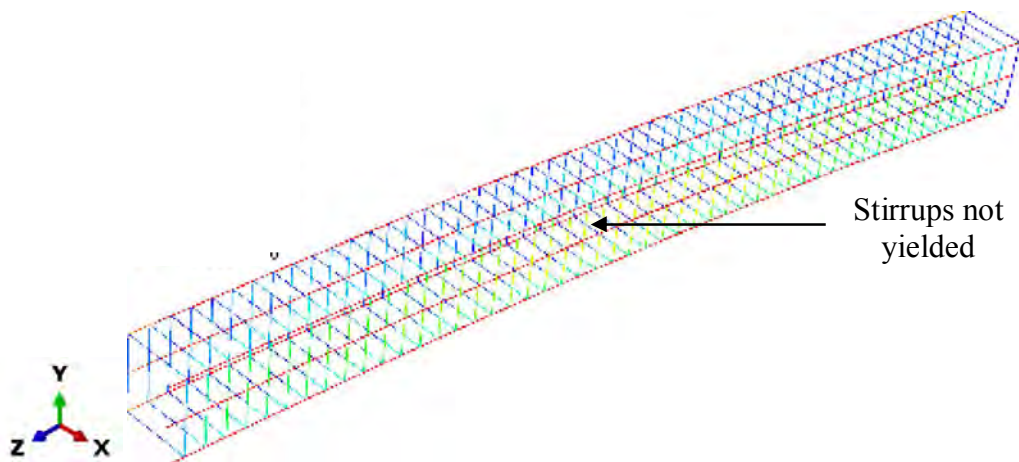
Figure 6.20 Numerically obtained yielding of transverse reinforcement

However, in specimen C3, with a relatively large tie spacing (130 mm) than other column, the ties ( $f_y = 560$  MPa) did not yield, shown in Figure 6.21 (a). The transverse ties in columns C4 also did not yield since these ties were constructed from high strength bars (703 MPa). It is to be mentioned that similar patterns of failure was observed in the experimental study as reported by Kim et al. (2012).





(a) Column C3



(b) Column C4

Figure 6.21 Numerically obtained yielding of transverse reinforcement

***Dundar et al. (2008)***

Figure 6.22 shows the experimental failure patterns of the specimen CC3 and CC4 from Dunder et al. (2008). The specimens were tested for biaxial load and failed due to concrete crushing in the compression side, after concrete cover spalling. At the time of failure the concrete crushed and the longitudinal reinforcing bars buckled in the compression side of the column specimens and then test was terminated. Figure 6.23 shows the numerical damage patterns of the specimens of Dunder et al. (2008) at the end of numerical simulation. Numerically, it was observed that the specimens failed due to concrete crushing at compression side. Similar failure pattern was observed during tests conducted by the authors.

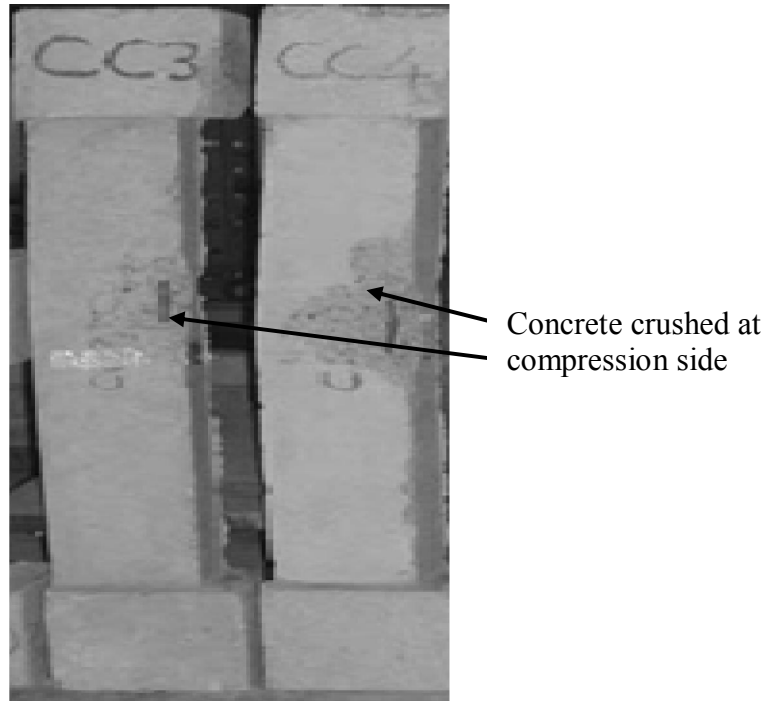


Figure 6.22 Experimental failure of columns CC3 and CC4 (Dundar et al. 2008)

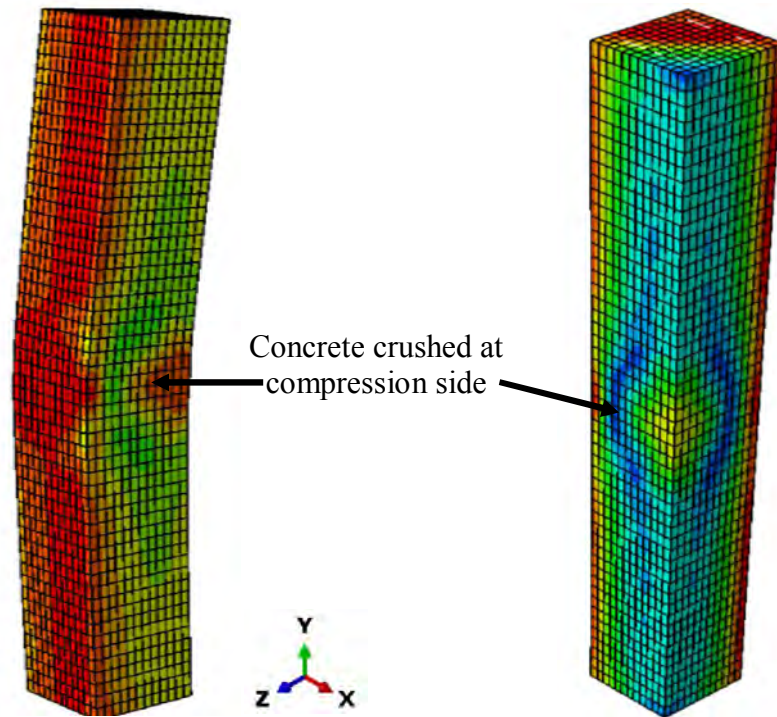
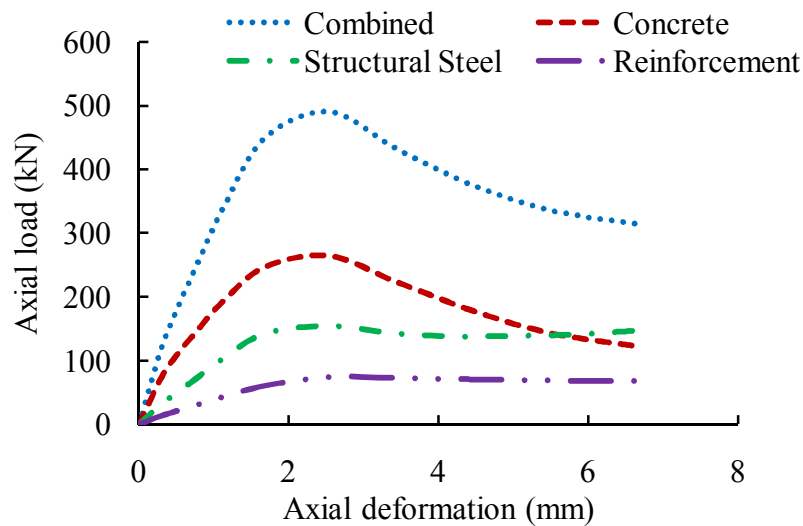


Figure 6.23 Numerical failures for column CC3 and CC4

### 6.3 Contributions of Steel and Concrete in the Capacity of FEC Columns

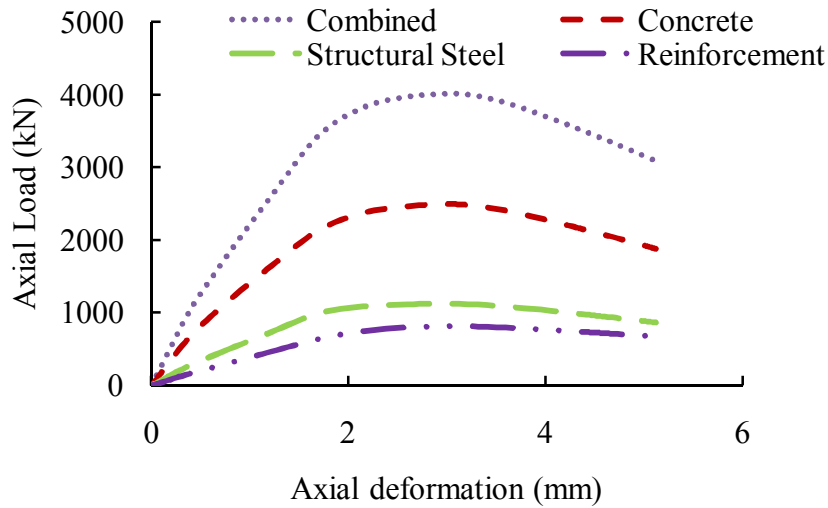
FE model is able to isolate the contribution of the core steel, reinforcement and concrete in the total load carrying capacity of the FEC columns. The axial load and axial deformation of individual elements in the composite section were determined.

Load carrying capacities of different elements of column SCN4B from current study and SRC1 from Chen and Yeh (1996) are shown in Figures 6.24 (a) and (b), respectively. It was observed that in these test columns (SCN4B and SRC1) the contributions by structural steel sections were 30% and 26% and contributions of longitudinal reinforcements were 13% and 18%, respectively on the ultimate capacity of the column. On the other hand, concrete was found to take 57% and 56% of the total load carrying capacity for column SCN4B and SRC1, respectively. The contributions of the individual elements of these FEC columns were very close in both cases.



(a) Column SCN4B from current study

Figure 6.24 Contributions of individual elements of FEC column in the ultimate capacity



(b) Column SRC1 Chen and Yeh (1996)

Figure 6.24 (cont.) Contributions of individual elements of FEC column in the ultimate capacity

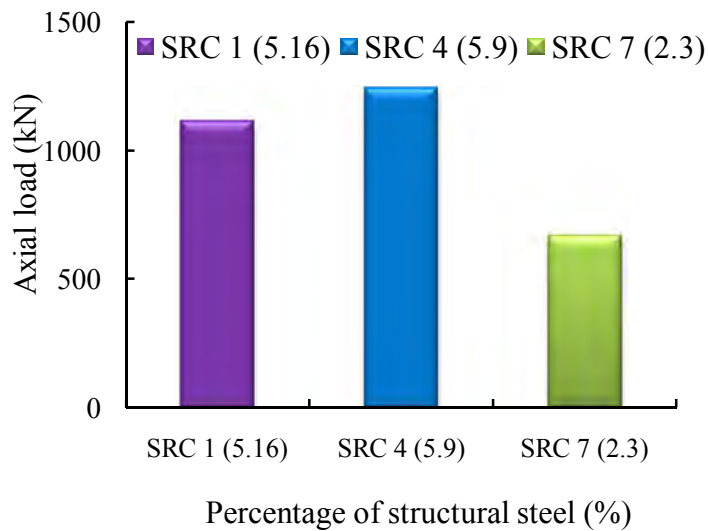


Figure 6.25 Load verse percentage of structural steel in columns

Similarly, a comparison was carried out on varying the percentage of structural steel ratio among the columns SRC1, SRC4 and SRC7. The structural steel ratio in these columns were 5.16%, 5.9% and 2.35% respectively, shown in Figure 6.25. From the nonlinear FE analysis the load carrying capacity of the structural steel of these columns (SRC1, SRC4 and SRC7) under concentric gravity loads were found to be 1114 kN, 1245 kN and 670 kN, respectively. The contributions of the structural steel shape of columns SRC1, SRC4 and SRC7 on the total axial load were 28%, 27% and 19%, respectively. Increasing the structural steel ratio from 2.35% (column SRC7) to 5.9% (Column SRC4) resulted in an increase in

overall axial capacity about 18%. Therefore, structural steel ratio of the composite section has significant effect on the axial strength. A detailed study will be carried out to find the effects of core steel on the overall capacity and ductility of FEC columns in the parametric study to be included in Chapter 7.

#### 6.4 Effect of Concrete Strength on Axial Capacity of FEC Column

Axial load versus deformation curves (as shown in Figure 6.26) of the FEC test columns designated as SCN4B was determined numerically for concrete strength of 27 MPa, 41 MPa, 60 MPa and 70 MPa. The axial capacity of FEC column increased significantly by increasing the strength of concrete. It was observed that the ultimate capacity of FEC column increased by 28%, 65% and 86% by increasing the concrete strength from 27 MPa to 41 MPa, 60 MPa and 70 MPa, respectively. However, the descending branch of the load deflection curves became steep as the concrete strength is increased. This indicated reduction in the overall ductility of the composite column with the increase in the concrete strength. A detailed study will be carried out to find the effect of concrete strength on the overall capacity and ductility of FEC columns to be presented in Chapter 7.

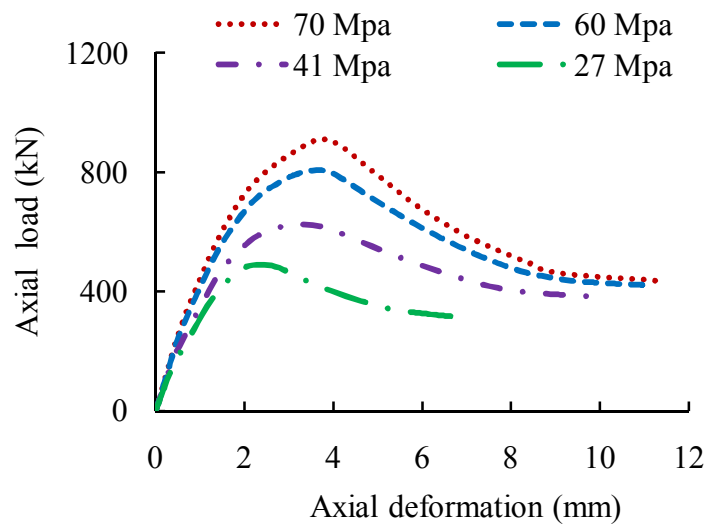


Figure 6.26 Effects of concrete strength on load-deformation of FEC columns.

#### 6.5 Conclusions

The performance of the finite element model developed for FEC column in present study was assessed through the comparison with the FEC column tests. The tests on FEC columns were taken from present study and reference test database from published literatures. The inelastic material properties of structural steel, concrete, longitudinal and transverse reinforcements were incorporated in the FE model. Nonlinear material behaviour for

concrete was simulated using the damage plasticity model in ABAQUS, finite element based software. The FE model was validated for concentric and eccentric loading conditions. The axial capacity and axial shorting of FEC columns were determined from FE analysis. The ratio of the numerical-to-experimental peak load ( $P_{num}/P_{exp}$ ) for current test specimens varied from 0.926 to 1.067 with a mean value of 0.991 and standard deviation of 0.046. The average ratio of the numerical load capacity to experimental capacity ( $P_{num}/P_{exp}$ ) for test specimens from published literature was 0.99 with a standard deviation of 0.074. The peak axial load with numerical-to-experimental ratios ranged from 0.901 to 1.11 for these columns. In general, the FE models can predict the experimental behaviour of FEC columns under concentric and eccentric axial loads with very good accuracy. However, the FE models for FEC columns constructed with high strength concrete and high strength steel were found to overestimate the experimental capacities by 10% (on an average). The difference between the numerical and experimental axial capacity can be attributed to the presence of geometric imperfections or initial out-of-straightness in the test columns and the variation in the strength of column concrete and cylinder concrete. The experimental failure modes and overall load displacement behaviours for FEC test columns were satisfactorily captured in the numerical analysis using the FE model.

The developed FE model was also used to isolate the contributions of concrete and steel section individually for different columns from current study and published literatures for concentric axial load. It was found that concrete carried about 57% and structural steel carried about 28% axial load of the total axial capacity of FEC columns. The effects of structural steel ratio and concrete strength on the behaviour of FEC columns were also studied. These parameters can significantly affect the strength and behaviour of FEC columns. Extensive studies with a wide range of values of these parameters are to be included in the following Chapter.

## CHAPTER 7

### PARAMETRIC STUDY

#### 7.1 Introduction

During the past few decades, steel concrete composite structural systems have been used in many tall buildings all over the world. Most of the early research on fully encased composite (FEC) columns investigated the behaviour of these columns for concentric and eccentric axial load with different steel ratios, concrete strength, shape and size of the core steel section and slenderness ratios. These studies were mainly carried out on FEC columns constructed with normal to high strength of concrete up to 70 MPa and structural steel yield strength up to 415 MPa. Limited studies are available to date on the behaviour of FEC columns with high to ultra-high strength concrete (80 MPa to 200 MPa) and high strength steel ( $F_y > 500$  MPa). Moreover, it was observed from current and published studies that the percentages of I-shaped structural steel in FEC columns of the validated FE models were 2% to 10%. Most of these columns were constructed with structural steel ratio less than 6%. The slenderness ratio of the validated FEC columns ranged from 4 to 10. It was recommended by several researchers that more studies should be done for wide variations of I-shaped structural steel percentage, slenderness ratio, eccentricity and concrete strength.

Studies on numerical simulations of FEC columns are very limited. As experimental studies are costly and time consuming, a numerical study on varying different parameters of FEC columns can be a good alternative. The FE models developed as stated in Chapter 5 were used to assess the influence of important geometric and material parameters on the behaviour of FEC columns. The efficiency and accuracy of the model were demonstrated through comparisons between the experimental and numerical results of a large number of FEC column tests, as presented in Chapter 6. The model was found to be capable of tracing a stable load-strain history up to failure with good accuracy for FEC columns with small and large cross-sections, constructed with normal and high strength concrete, and tested under concentric and eccentric loading conditions. This finite element model was used to simulate the parametric columns to explore the behaviour and strength of FEC columns under concentric and eccentric axial loads.

#### 7.2 Design of Parametric Study

For the parametric study a square column with outer dimensions of 500 mm  $\times$  500 mm was selected. Typical cross section and elevation of FEC column used in the parametric study are

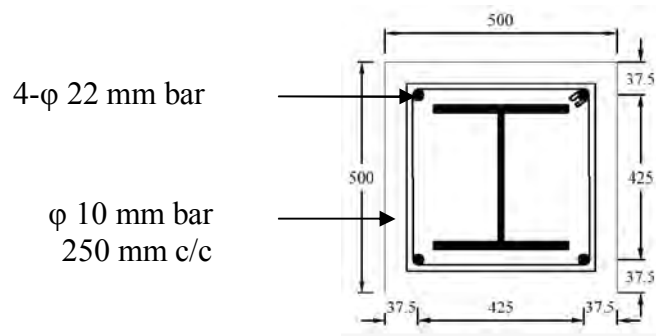
shown in Figure 7.1. This is a moderate size for composite columns and might be suitable in the construction of mid-rise buildings. This column was designed and analysed during the parametric study to incorporate the effects of several geometric and material parameters that can significantly affect the FEC column behaviour. The geometric variables are percentage of I-shaped structural steel, column slenderness and eccentricity of the applied load and spacing of ties. The compressive strength of concrete and grade of steel in FEC column was used as the material variables in the parametric study.

In total, 44 FEC columns were analysed for the parametric study. Details of these columns are given in Tables 7.1 to 7.5. The first letter in the column designation refers to the overall column slenderness ratio. The letters "S", "I" and "L" indicated short ( $L/d = 6$ ), intermediate ( $L/D = 12$ ) and long ( $L/D = 20$ ) columns, respectively. To differentiate between the normal strength (30 MPa), medium strength (60 MPa) and high strength concrete columns (120 MPa), letters "N", "M" and "H" were used in the column designation. The number used in the column designation is simply the serial number as they appeared in the table. Other than above mentioned columns, a group of columns (05) were simulated with concrete having ultimate strength of 120 MPa and structural steel with  $F_y = 913$  MPa to observe the effect of ultra-high strength materials (UHSM). The definition of each parameter, along with its selected range for this study, is presented in turn below.

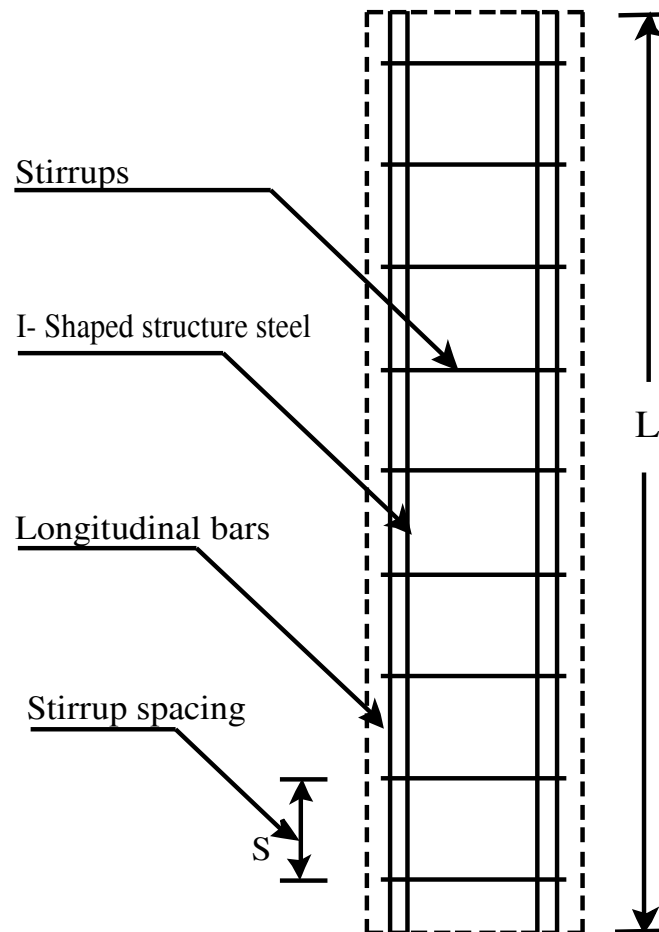
### **7.2.1 Percentage of I-shaped structural steel**

The presence of a large structural steel core provides a beneficial residual strength following concrete crushing that leads to improved ductility. Five different percentages of structural steel 1%, 5%, 10%, 15% and 20% (as shown in Table 7.1) were used in the parametric study with normal, medium and high strength of concrete. These columns are divided into three groups (Table 7.1) depending on the strength of concrete. The slenderness ratio ( $L/D = 6$ ) and the transverse reinforcement spacing of the FEC columns were kept constant in all cases. The load was applied concentrically in these columns.





(a) Cross section



(b) Elevation

Figure 7.1 Typical cross section and elevation of parametric FEC column

(a) Cross section (b) Elevation

### **7.2.2 Column slenderness ratio, $L/D$**

The column slenderness ratio is defined as the ratio of the length ( $L$ ), to the depth of the column cross-section ( $D$ ). The global stability of the column is controlled by the slenderness ( $L/D$ ) ratio. Three different slenderness ratios 6, 12 and 20 were employed in the parametric study (as shown in Table 7.2) to cover the range of short, intermediate and long columns. These parametric studies were carried out on different percentage of structural steel ratios (5% and 10%) and concrete strength (30 MPa and 60 MPa).

### **7.2.3 Load eccentricity ratio, $e/D$**

The behaviour of FEC columns under bending induced by eccentrically applied axial load is greatly affected by the initial load eccentricity ratio. It is obtained by dividing the initial eccentricity, ( $e$ ), of the applied axial load by the depth of the column cross-section, ( $D$ ). Higher  $e/D$  ratios increase flexural compression in the cross-section. It reduced the load carrying capacity of the column as compared to a concentrically loaded column. The load eccentricity ratios used in this study were 0.1, 0.3 and 0.4, as shown in Table 7.3. The load eccentricity ratio of 0.1 was intended to represent an "accidental" eccentricity that might occur in a column that was nominally designed as a gravity column.

### **7.2.4 Concrete compressive strength, $f_{cu}$**

Compressive strength of concrete plays an important role in increasing the load carrying capacity of concrete, thereby reducing the required column size. However, limited experimental and numerical investigations have been performed, to date, on FEC columns with high and ultra-high strength concrete. Thus, in the parametric study the concrete strength were varied as 30 MPa, 60 MPa and 120 MPa (as shown in Table 7.4) to investigate the influence of low, medium and high strength concrete in combination with other parameters.

### **7.2.5 Transverse reinforcement spacing-to-depth ratio, $s/D$**

The primary purpose of transverse reinforcement in concrete-encased composite columns is to provide concrete confinement to prevent spalling around the structural steel core and to properly support longitudinal reinforcement to prevent buckling of the bars. Transverse reinforcement can also provide additional shear capacity. Therefore, transverse reinforcement spacing is an important parameter affecting the ultimate strength and behaviour of columns. The effect of the transverse reinforcement spacing was studied by varying the ratio of transverse tie spacing, ( $s$ ), to the depth of the column cross-section, ( $D$ ).

Three values of the  $s/D$  ratio 0.1, 0.2 and 0.4 (Table 7.5) were used in the parametric study to determine the effect. A constant transverse reinforcement spacing ( $s/D = 0.5$ ) was used to determine the effect of other selected parameters.

Table 7.1 Columns for investigating the effect of structural steel ratio

Groups	specimen	Section (mm)	Length (mm)	L/D	s/D	Structural steel (mm)	Concrete (MPa)	Steel ratio	
								$A_s$ (%)	$A_r$ (%)
Group 1	SN1	500x500	3000	6	0.5	100x100x7x9	30	1	0.6
	SN2	500x500	3000	6	0.5	300x300x13x15	30	5	0.6
	SN3	500x500	3000	6	0.5	300x300x26x28	30	10	0.6
	SN4	500x500	3000	6	0.5	300x300x40x42	30	15	0.6
	SN5	500x500	3000	6	0.5	300x300x54x56	30	20	0.6
Group 2	SM6	500x500	3000	6	0.5	100x100x7x9	60	1	0.6
	SM7	500x500	3000	6	0.5	300x300x13x15	60	5	0.6
	SM8	500x500	3000	6	0.5	300x300x26x28	60	10	0.6
	SM9	500x500	3000	6	0.5	300x300x40x42	60	15	0.6
	SM10	500x500	3000	6	0.5	300x300x54x56	60	20	0.6
Group 3	SH11	500x500	3000	6	0.5	100x100x7x9	120	1	0.6
	SH12	500x500	3000	6	0.5	300x300x13x15	120	5	0.6
	SH13	500x500	3000	6	0.5	300x300x26x28	120	10	0.6
	SH14	500x500	3000	6	0.5	300x300x40x42	120	15	0.6
	SH15	500x500	3000	6	0.5	300x300x54x56	120	20	0.6

Table 7.2 Columns for investigating the effect of slenderness ratio (L/D)

Groups	Specimen	Section (mm)	Length (mm)	L/D	e/D	s/D	Structural steel (mm)	Concrete (MPa)	Steel ratio	
									$A_s$ (%)	$A_r$ (%)
Group 4	SN16	500x500	3000	6	0.2	0.5	300x300x13x15	30	5	0.6
	IN17	500x500	6000	12	0.2	0.5	300x300x13x15	30	5	0.6
	LN18	500x500	10000	20	0.2	0.5	300x300x13x15	30	5	0.6
Group 5	SM19	500x500	3000	6	0.2	0.5	300x300x26x28	60	10	0.6
	IM20	500x500	6000	12	0.2	0.5	300x300x26x28	60	10	0.6
	LM21	500x500	10000	20	0.2	0.5	300x300x26x28	60	10	0.6

Table 7.3 Columns for investigating the effect of eccentricity ratio (e/D)

Groups	Specimen	Section (mm)	Length (mm)	L/D	e/D	s/D	Structural steel (mm)	Concrete (MPa)	Steel ratio	
									$A_s$ (%)	$A_r$ (%)
Group 6	SN25	500x500	3000	6	0.1	0.5	300x300x26x28	30	10	0.6
	SN26	500x500	3000	6	0.3	0.5	300x300x26x28	30	10	0.6
	SN27	500x500	3000	6	0.4	0.5	300x300x26x28	30	10	0.6
Group 7	IN28	500x500	6000	12	0.1	0.5	300x300x26x28	30	10	0.6
	IN29	500x500	6000	12	0.3	0.5	300x300x26x28	30	10	0.6
	IN30	500x500	6000	12	0.4	0.5	300x300x26x28	30	10	0.6

Table 7.4 Columns for investigating the effect of concrete compressive strength ( $f_{cu}$ )

Groups	Specimen	Section (mm)	Length (mm)	L/D	e/D	s/D	Structural steel (mm)	Concrete (MPa)	Steel ratio	
									$A_s$ (%)	$A_r$ (%)
Group 8	SN31	500x500	3000	6	0.1	0.5	300x300x26x28	30	10	0.6
	SM32	500x500	3000	6	0.1	0.5	300x300x26x28	60	10	0.6
	SH33	500x500	3000	6	0.1	0.5	300x300x26x28	120	10	0.6
Group 9	SN34	500x500	3000	6	0.3	0.5	300x300x26x28	30	10	0.6
	SM35	500x500	3000	6	0.3	0.5	300x300x26x28	60	10	0.6
	SH36	500x500	3000	6	0.3	0.5	300x300x26x28	120	10	0.6

Table 7.5 Columns for investigating the effect of transverse reinforcement spacing, (s/D)

Groups	Specimen	Section (mm)	Length (mm)	L/D	s/D	Structural steel (mm)	Concrete (MPa)	Steel ratio	
								$A_s$ (%)	$A_r$ (%)
Group 10	SN37	500x500	3000	6	0.1	300x300x26x28	30	10	0.6
	SM38	500x500	3000	6	0.2	300x300x26x28	30	10	0.6
	SH39	500x500	3000	6	0.4	300x300x26x28	30	10	0.6
Group 11	SN40	500x500	3000	6	0.1	300x300x26x28	60	10	0.6
	SM41	500x500	3000	6	0.2	300x300x26x28	60	10	0.6
	SH42	500x500	3000	6	0.4	300x300x26x28	60	10	0.6

### 7.3 Material Properties of Parametric Columns

Tables 7.1 to 7.5 present the parametric columns used in this study. These FEC columns were assumed to be constructed from 350 W grade steel plates. The nominal yield strength ( $F_y$ ) of structural steel used was 350 MPa, permitted by AISC-LRFD (2010) for FEC columns. The modulus of elasticity and the yield strain ( $\epsilon_y$ ) taken were 200 GPa, and 0.00175 mm/mm. The ultimate strength of the steel plate was taken as 450 MPa and the corresponding strain was assumed to be 100 times the yield strain, i.e., 0.175 mm/mm. The point delineating the onset of strain hardening was also required to define the tri-linear stress-strain curve for steel used in the FE model. This point was defined at a stress value of 350 MPa, with a strain of  $10\epsilon_y$ . Similarly, the nominal yield strength ( $F_y$ ) and the modulus of elasticity of longitudinal and transverse reinforcement used were 450 MPa and 200 GPa, respectively. The Poisson's ratio used for the steel was 0.30.

Three types of concrete, with nominal strengths of 30 MPa, 60 MPa and 120 MPa, were used in the parametric study. To define the concrete stress-strain curves for the FE analyses of these columns, the strain corresponding to the uniaxial compressive strength, the elastic modulus and the Poisson's ratio were required. The strain at the ultimate compressive strength was calculated using the expression proposed by ACI 318-05 as shown in Equation 7.1.

$$\varepsilon_{cu} = (0.71f'_c + 168) \times 10^{-5} \quad (7.1)$$

This equation was developed based on experimental investigations of both normal and high strength concrete. The elastic moduli for the normal and high strength concrete were calculated using the following expression according to ACI 318-05,

$$E_c = 4730\sqrt{f_{cu}} \quad (7.2)$$

In Equations 7.1 and 7.2,  $f_{cu}$  is in MPa. The calculated values of elastic modulus and the strain at the ultimate compressive strength for concrete were used in the parametric columns. The Poisson's ratio for concrete was taken as 0.20.

#### 7.4 Results and Discussion

The columns designed for the parametric study was simulated and analysed using FE model developed in the current study (as presented in Chapter 5). The output parameters extracted from the analysis results were: axial load,  $P_u$ , moment,  $M_u$ , average axial strain,  $\varepsilon_{a,u}$ , and lateral displacement,  $U_{l,u}$ , at failure (i.e., at the peak axial load point). The axial load versus average axial deformation and axial load versus lateral displacement curves were also generated from the numerical analysis for parametric columns. The stiffness and ductility index were also determined to observe the effect for the variation of structural steel percentages.

The lateral displacements of individual columns were determined from numerical study at the middle of the columns. In most cases, concrete crushing (CC) was observed at the middle of compression side in the columns. All the results obtained from the parametric analyses were organized and presented to highlight the individual effect of each parameter. The failure modes in parametric columns were studied using the numerical model. In general the columns reached the peak load by concrete crushing, followed or accompanied by yielding of structural steel. In the following sections, only the significant observations from the parametric study have been reported, along with the relevant Figures.

##### 7.4.1 Effect of structural steel percentages

Fifteen (15) short FEC columns consisted in three groups were considered to observe the effect of structural steel (as shown in Table 7.1). These three groups were divided based on different concrete strength (normal, medium and high). Group 1 consisted of columns SN1, SN2, SN3, SN4 and SN5 and simulated with normal strength concrete (30 MPa). Group 2 consisted of columns SM6, SM7, SM8, SM9 and SM10. These columns were simulated with

medium strength of concrete (60 MPa). Similarly, Group 3 consisted of columns SH11, SH12, SH13, SH14 and SH15 simulated with high strength concrete (120 MPa). The load was applied concentrically at the top centre of the columns. The slenderness ratios ( $L/D$ ) of these columns were 6. Five different percentages of structural steel were used for numerical simulations for each Group of FEC columns. The structural steel percentages used in the columns of each group were 1%, 5%, 10%, 15% and 20%, respectively. The effects of increasing the structural steel ratio from 1% to 20% on the overall behaviour, capacity, ductility and residual strength of FEC columns are presented in the following sections.

#### 7.4.1.1 Load versus axial deformation response

Figures 7.2 to 7.4, show the effects of structural steel percentages on the axial load versus average axial deformation responses for Group 1, Group 2 and Group 3, columns respectively. It is apparent from the figures that as the steel ratio is increased the stiffness and the ultimate capacity of FEC column increases. The residual strength after failure and ductility of the columns were also observed to increase significantly with the increase in the steel ratio. This behaviour is observed within the three groups of columns.

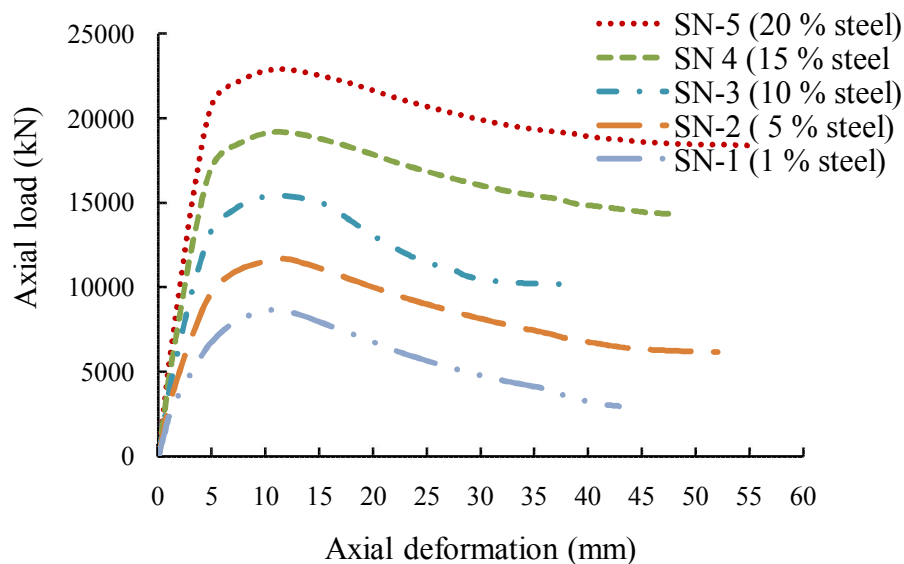


Figure 7.2 Effect of structural steel on load-deformation response curve (Group 1)

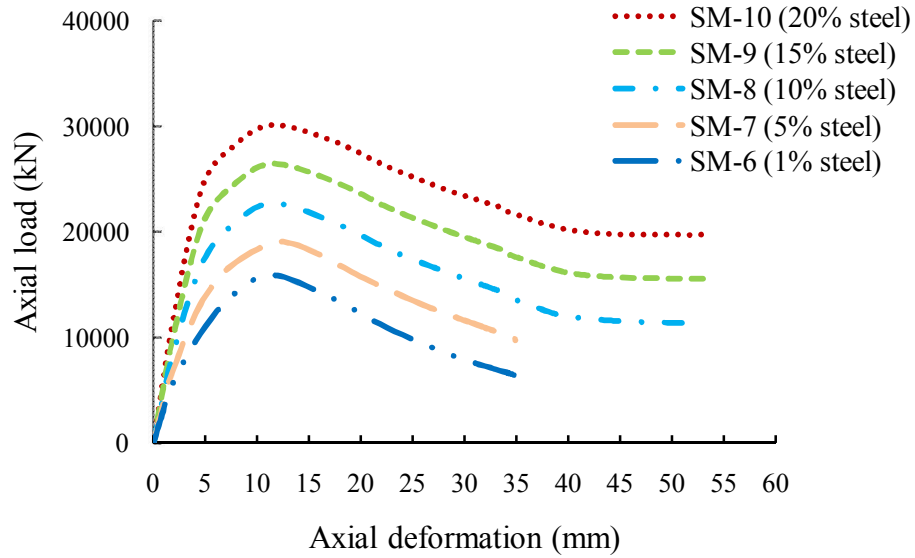


Figure 7.3 Effect of structural steel on load-deformation response curve (Group 2)

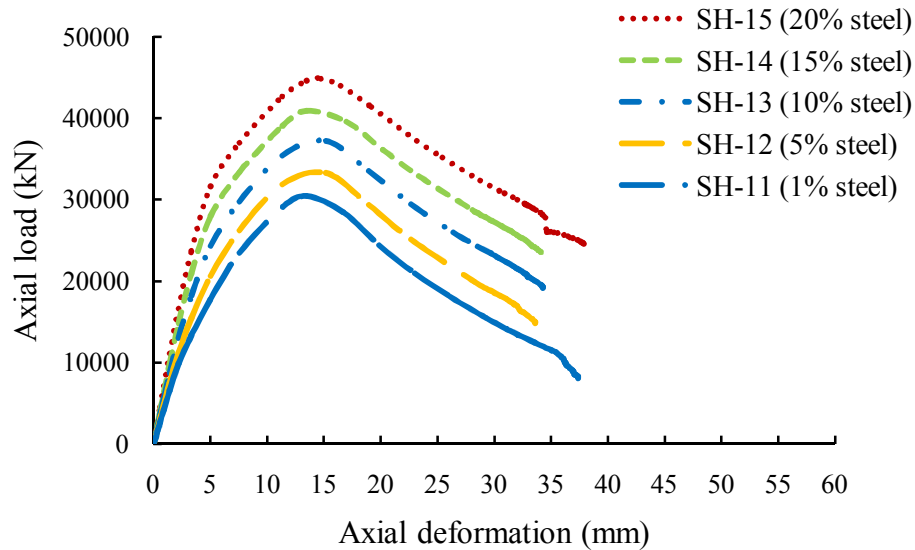


Figure 7.4 Effect of structural steel on load-deformation response curve (Group 3)

#### 7.4.1.2 Axial capacity of FEC columns

Table 7.6 presents the axial capacity of the columns in Group 1, 2 and 3. The numerically obtained capacities for these columns were compared with the theoretical squash load calculated using Equation 7.3 as given below. The theoretical capacities for these columns were found to be 15% lower (on an average) than the numerically obtained capacities. This is due to the strength reduction factor, 0.85 applied on the cylinder strength of concrete to represent the variability in column concrete. The enhancement in the axial capacity of the

$$P_o = 0.85f'_c A_c + A_s f_s + A_{sr} f_{yr} \quad (7.3)$$

columns within each group is also shown in Table 7.6. The increments of numerical loads in percent were determined with respect to the columns with 1% structural steel, i.e. column SN1 for Group 1, SM6 for Group 2 and SH11 for Group 3. The load carrying capacity of columns SN2, SN3, SN4 and SN5 in Group 1 were observed to be 35%, 96%, 122% and 165% higher than column SN1. These columns were short columns and constructed with normal strength concrete (30 MPa). The load carrying capacity of columns SM7, SM8, SM9 and SM10 in Group 2 were 19%, 54%, 67% and 90% higher than column SM6. All the columns of Group 2 were short columns and constructed with concrete strength concrete (60 MPa). Similarly, the load carrying capacity of the columns SH12, SH13, SH14 and SH15 in Group 3 were 9%, 22%, 34% and 48% higher than the column SH11. The columns of Group 3 were constructed with 120 MPa concrete.

Table 7.6 Effect of structural steel ratio on axial load capacity

Group	Column designation	Columns properties				Axial capacity		$P_{u(num)}/P_{u(Theo)}$	Percent of increment	
		L/D	s/D	$A_s$ (%)	$f_{cu}$ (MPa)	$P_{u(num)}$ (kN)	$P_{u(Theo)}$ (kN)		$P_{u(num)}$ (%)	$P_{u(Theo)}$ (%)
Group 1	SN1	6	0.5	1	30	8651	7601	1.14	-	-
	SN2	6	0.5	5	30	11675	10285	1.14	35	35
	SN3	6	0.5	10	30	16989	13744	1.13	96	81
	SN4	6	0.5	15	30	19194	17170	1.12	122	126
	SN5	6	0.5	20	30	22922	20744	1.11	165	172
Group 2	SM6	6	0.5	1	60	15923	13897	1.15	-	-
	SM7	6	0.5	5	60	18977	16306	1.16	19	17
	SM8	6	0.5	10	60	24453	19443	1.17	54	40
	SM9	6	0.5	15	60	26475	24449	1.1	67	76
	SM10	6	0.5	20	60	30183	25964	1.16	90	87
Group 3	SH11	6	0.5	1	120	30435	26490	1.15	-	-
	SH12	6	0.5	5	120	33260	28345	1.17	9	7
	SH13	6	0.5	10	120	37180	30840	1.21	22	17
	SH14	6	0.5	15	120	40886	33310	1.23	34	26
	SH15	6	0.5	20	120	45152	36403	1.24	48	38

The increase in the capacity with respect to 1% structural steel ratio for three different strength of concrete is plotted in Figure 7.5. The increase in the axial capacity of short FEC columns with the variation in the structural steel ratio is greatly affected by the strength of concrete. The rate of increase in the axial capacity for normal strength concrete is higher as compared to high and ultra-high strength concrete. The benefit of using higher percentage of structural steel ratio diminishes as the concrete strength increases.



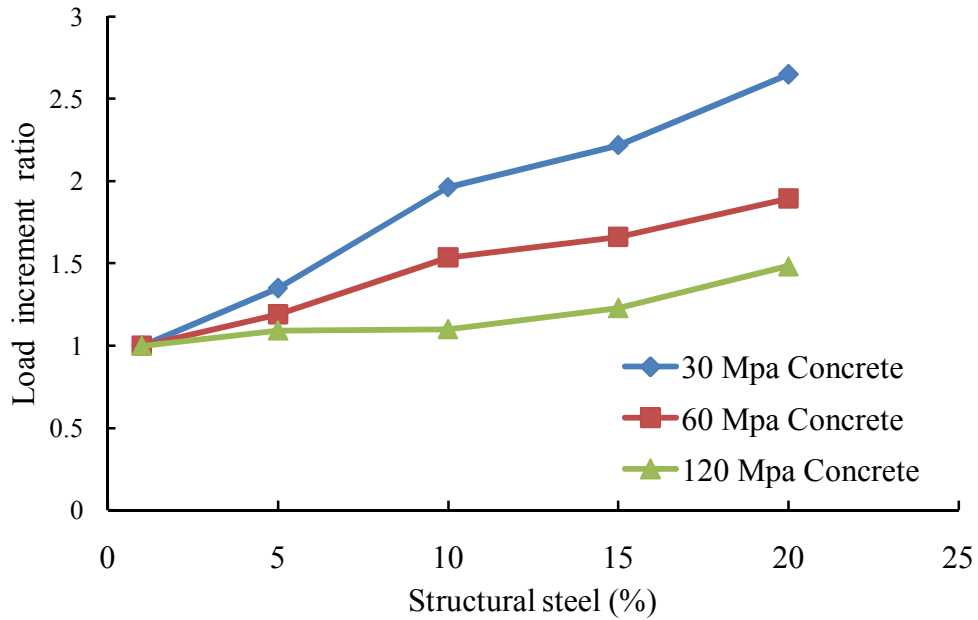


Figure 7.5 Effect of structural steel on axial capacity increment

#### 7.4.1.3 Ductility index for FEC columns

The higher percentages of structural steel usually increase the ductility of FEC columns. Ductility index ( $\mu$ ) is the ratio calculated based on the maximum deformation at ultimate load ( $\delta_{po}$ ) and post peak deformation ( $\delta_{0.7po}$ ) corresponding to 70% of the ultimate load. The ductility index ( $\mu$ ) of these three Groups of columns were determined and presented in Tables 7.7 to 7.9. It was observed from the numerical analysis that column SN4 and SN5 of Group 1 could not reach seventy percent of ultimate capacity ( $0.7P_o$ ) after failure due to numerical instability. These two columns were constructed with higher percentages of steel (15% and 20%) with low strength (30 MPa) of concrete. The ductility index of columns SN1, SN2 and SN3 from Group1 were determined and shown in Table 7.7. The ductility of the columns were increased with the increase of structural steel percentages. The column SN3 was relatively more ductile in Group 1. The ductility index for Group 2 and Group 3 columns are shown in Table 7.8 and Table 7.9, respectively. It was observed that the ductility index increased with the increase of structural steel percentages in the FEC columns. Moreover, it was also found that Group 2 columns showed comparatively higher ductility than Group 3 columns. This is due to the fact that as the concrete strength increases the ductility of the column reduces.

Table 7.7 Ductility index of column Group 1

Specimen designation	Column properties				Axial load (kN)	Axial displacement		Ductility index $\delta_{0.7P_o}/\delta_{P_o}$
	L/D	s/D	$f_{cu}$ (MPa)	$A_s$ (%)		$\delta_{P_o}$ (mm)	$\delta_{0.7P_o}$ (mm)	
SN1	6	0.5	30	1	8651	11.28	22.93	2.03
SN2	6	0.5	30	5	11675	11.27	24.74	2.20
SN3	6	0.5	30	10	15447	10.84	28.01	2.59

Table 7.8 Ductility index of column Group 2

Specimen designation	Column properties				Axial load (kN)	Axial displacement		Ductility index $\delta_{0.7P_o}/\delta_{P_o}$
	L/D	s/D	$f_{cu}$ (MPa)	$A_s$ (%)		$\delta_{P_o}$ (mm)	$\delta_{0.7P_o}$ (mm)	
SM6	6	0.5	60	1	15929	11.32	22.12	1.95
SM7	6	0.5	60	5	18977	11.23	25.55	2.28
SM8	6	0.5	60	10	22750	11.86	29.01	2.45
SM9	6	0.5	60	15	26475	11.98	33.01	2.76
SM10	6	0.5	60	20	30183	12.02	34.02	2.83

Table 7.9 Ductility index of column Group 3

Specimen designation	Column properties				Axial load (kN)	Axial displacement		Ductility index $\delta_{0.7P_o}/\delta_{P_o}$
	L/D	s/D	$f_{cu}$ (MPa)	$A_s$ (%)		$\delta_{P_o}$ (mm)	$\delta_{0.7P_o}$ (mm)	
SH11	6	0.5	120	1	30435	13.5	22.68	1.68
SH12	6	0.5	120	5	33260	14.18	24.62	1.74
SH13	6	0.5	120	10	37180	15.07	26.32	1.75
SH14	6	0.5	120	15	40886	13.49	28.05	2.08
SH15	6	0.5	120	20	45152	13.8	29.2	2.12

#### 7.4.1.4 Modes of failure

The failures in the columns in Group 1, 2 and 3 occurred by crushing of concrete followed by yielding of steel. The crushing of concrete (CC) started near the middle of the columns. The deformed shape with stress contour at failure of concrete was captured as shown in Figure 7.6 of column SN3 (10%). In columns with lower percentages of steel ratio (1% and 5%) yielding of steel occurred shortly after the peak load. However, for columns with steel ratio above 5% the yielding occurred at a later stage as compared to columns with lower steel ratio. Figure 7.7 shows the Von Mises stress for the structural steel of the column and the steel section was observed to yield near the middle of these short columns.

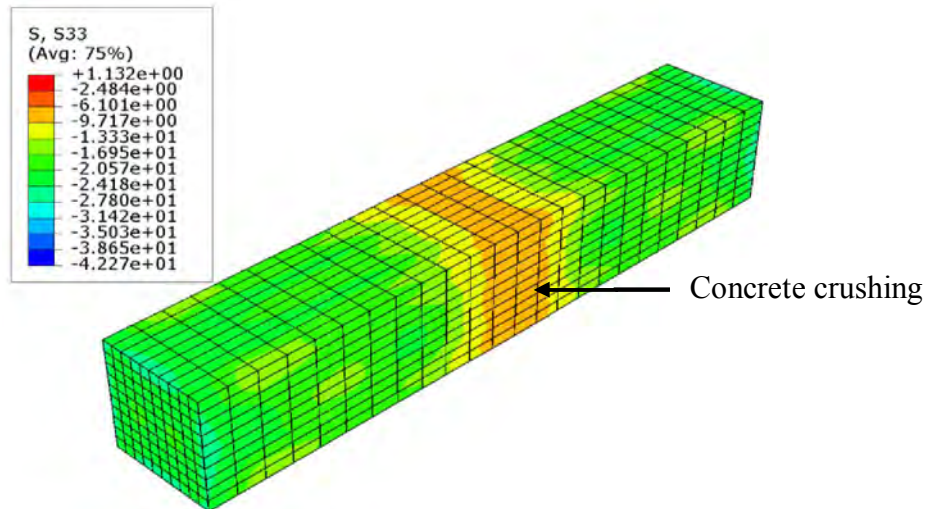


Figure 7.6 Stress contour of concrete at failure

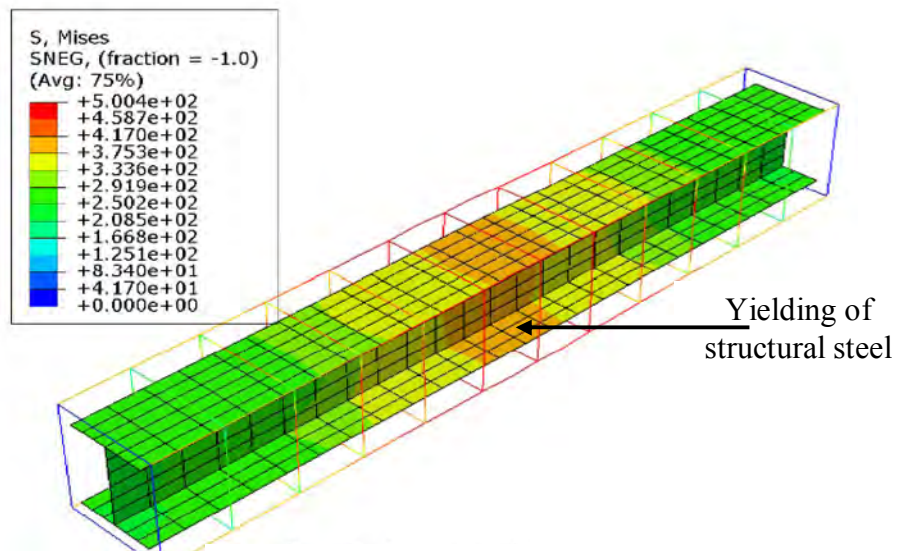


Figure 7.7 Stress contour of structural steel at failure

#### 7.4.2 Effect of overall column slenderness ratio

Six columns (Tables 7.2) divided into two groups (Group 4 and 5) were analysed to observe the effects of overall slenderness ratio. Columns in Group 4 (SN16, IN17 and LN18) was constructed with normal strength concrete (30 MPa) and had a structural steel ratio of 5%. On the other hand, Group 5 columns were constructed using 60 MPa concrete with a steel ratio of 10%. The load was applied eccentrically ( $e/D = 0.2$ ) about major axis of these columns. The slenderness ratios ( $L/D$ ) of these columns were varied as 6, 12 and 20. All the columns were constructed with constant transverse reinforcement spacing of ( $s/D = 0.5$ ) 250 mm. Two different percentages of structural steel were used for the construction of these FEC columns.

#### 7.4.2.1 Load versus axial deformation response

Figures 7.8 and 7.9 show the effects of slenderness ( $L/D$ ) ratios on the axial load versus axial deformation responses for Group 4 and Group 5, respectively. The axial capacity and stiffness of FEC columns were observed to decrease with the increase in slenderness ratio. The ascending part of axial load versus axial deformation curve (Figure 7.8) of column SN16 ( $L/D = 6$ ) was comparatively stiffer than other columns of this Group 4. Similar behaviour was also observed for columns in Group 5. From Figure 7.9, the ascending part of column SM19 was stiffer than other two columns of this Group. Column SN16 and SM19 are short columns of Group 4 and Group 5. As the column gets slender the axial deformation increases accompanied by a decrease in the axial load.

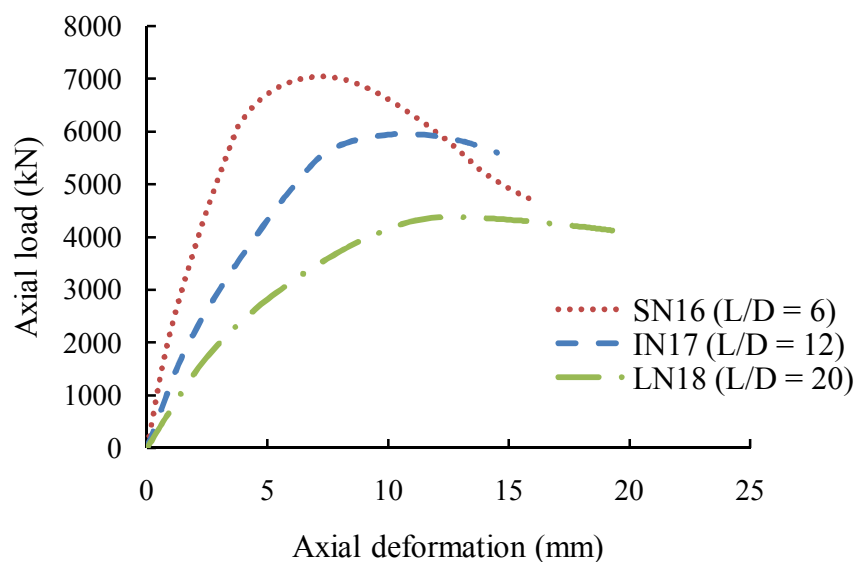


Figure 7.8 Effect of  $L/D$  ratios on axial load versus axial deformation curve (Group 4)

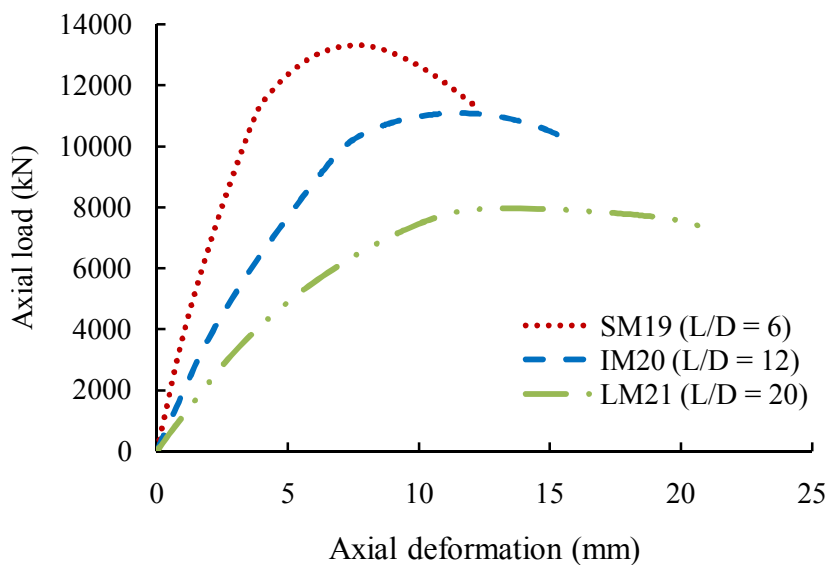


Figure 7.9 Effect of  $L/D$  ratio on axial load versus axial deformation curve (Group 5)

### 7.4.2.2 Peak load and corresponding moment

Table 7.10 shows the effect of the overall column slenderness ( $L/D$ ) ratio on peak load and moment. The columns of Group 4 and Group 5 were constructed with 5% and 10% structural steel. In columns of Group 4, the  $L/D$  ratio was increased from 6 to 12 which resulted in a reduction of ultimate axial load capacity by 18%. On the other hand, increasing the  $L/D$  ratio from 6 to 20 resulted in 37% reduction in the ultimate axial load. The moments at the peak load points for Group 4 increased by 5% and 10% for  $L/D$  ratios of 12 and 20, respectively, with respect to the moment for  $L/D = 6$ . The increase in the bending moment resulted from the increase in second order moment as the column got increasingly slender.

Table 7.10 Effect of structural steel ratio at peak load

Group	Column designation	Column properties				Magnitude of output parameters at peak load point				Percent difference	
		$L/D$	$e/D$	$s/D$	$f_{cu}$ (MPa)	$P_u$ (kN)	$M_u$ (kN-m)	$\epsilon_u$ ( $\mu\epsilon$ )	$U_{1u}$ (mm)	$P_u$ (%)	$M_u$ (%)
Group 4	SN16	6	0.2	0.5	30	7034	805	2452	15	-	-
	IN17	12	0.2	0.5	30	5720	846	1773	48	-18	5
	LN18	20	0.2	0.5	30	4370	879	1241	101	-37	10
Group 5	SM19	6	0.2	0.5	60	13045	1559	2580	17	-	-
	IM20	12	0.2	0.5	60	10807	1633	1937	54	-19	5
	LM21	20	0.2	0.5	60	7962	1673	1400	110	-40	8

Similarly, for columns of Group 5, increasing the slenderness ratio ( $L/D$ ) from 6 to 12 reduced the ultimate capacity by 19%. On the contrary, increasing the  $L/D$  ratio to 20 resulted in 40% reduction in the ultimate axial load. However, the moment at the peak load point is increased by 5% and 8%, respectively, for  $L/D$  ratios of 12 and 20 with respect to that obtained for  $L/D = 6$ . The loads versus slenderness ratio for the columns from these two groups were shown in Figure 7.10. It was found that the ultimate capacity decreased with the increase of slenderness ratio ( $L/D$ ). It was more pronounced when columns were constructed with higher strength concrete. Because, the higher strength concrete columns failed in brittle manner.

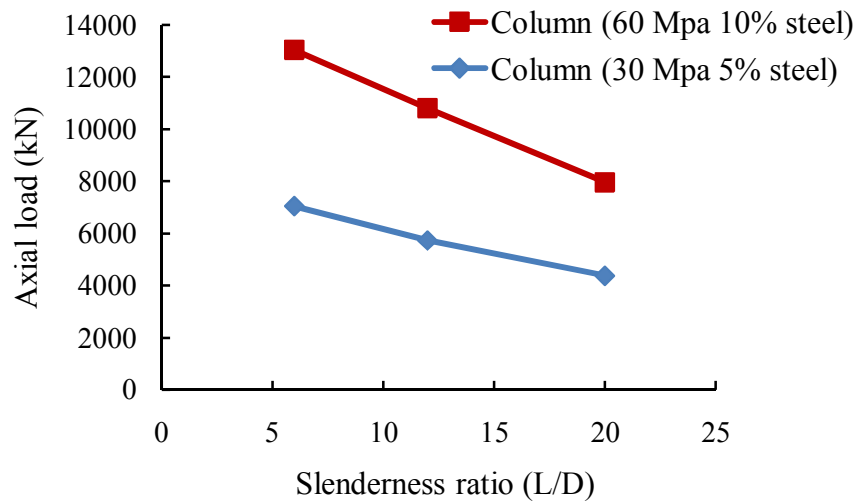


Figure 7.10 Effect of L/D ratios on axial load

#### 7.4.2.3 Load versus lateral displacement response

Axial load versus lateral displacement curve for the columns of Group 4 and Group 5 are showed in the Figures 7.11 and 7.12. From these two figures, the pre-peak region of the load versus lateral displacement curves for the short columns (SN16 and SM19) showed a steep slope and linear behaviour. On the other hand, as the slenderness ratio (L/D) increases, this region of the curve gets nonlinear with reduced initial slope. The nonlinear behaviour occurred due to the increased second order displacement in the slender columns. The short columns also experienced a sharp decline in the post-peak region of the load versus lateral displacement curve, whereas the long columns could withstand the peak axial load over a wide range of lateral displacement.

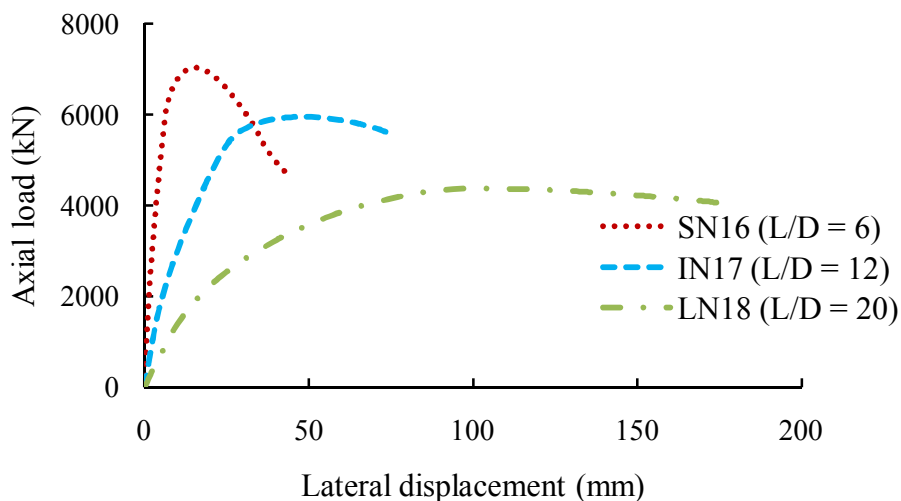


Figure 7.11 Effect of L/D ratios on axial load versus lateral displacement curve (Group 4)

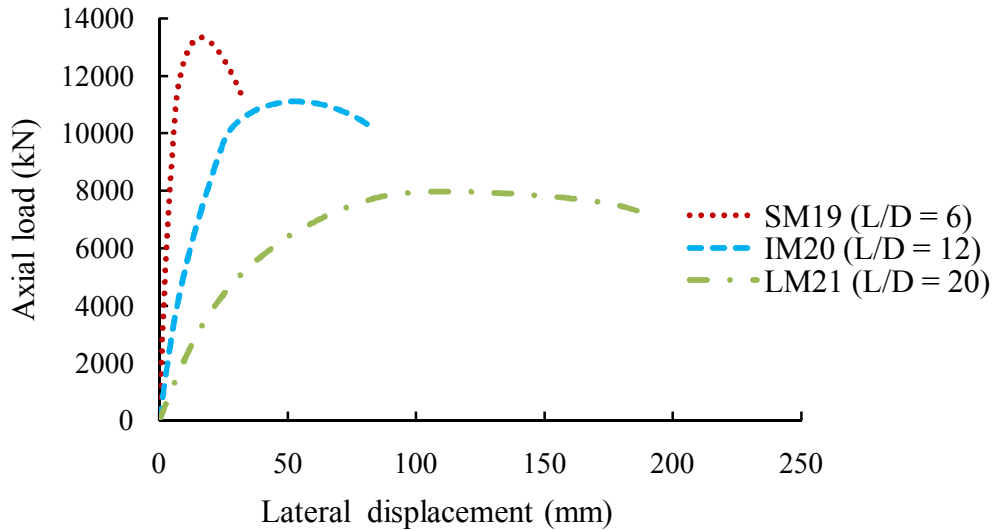


Figure 7.12 Effect of (L/D) ratio on axial load versus lateral displacement curve (Group 5)

#### 7.4.2.4 Load versus moment response

The load versus moment curves for short, intermediate and long columns for Group 4 and 5 are shown in Figure 7.13 and 7.14, respectively. In both cases, the load versus moment curves for the short columns represent more linear behaviour than other columns. However, as the L/D ratio is increased, the curve shows nonlinear behaviour. It was the effect of second order displacement. The effect of column slenderness (L/D) on the load versus moment curve was similar for two Groups.

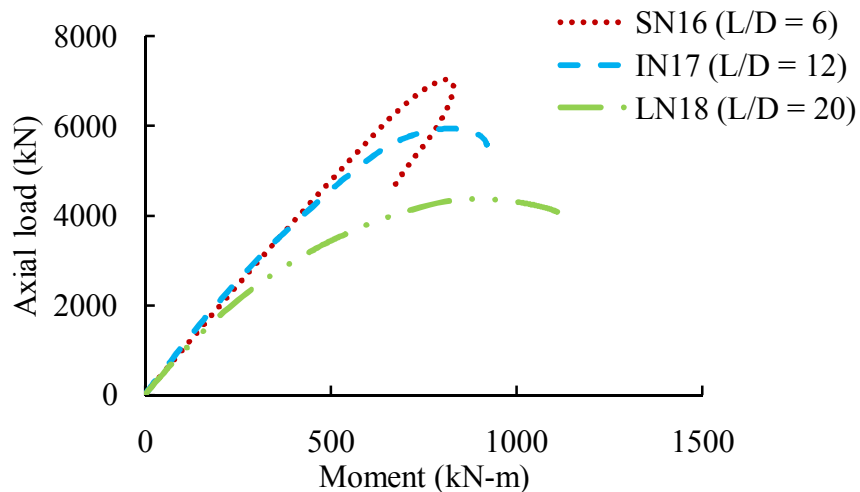


Figure 7.13 Effect of L/D ratio on axial load versus moment curve (Group 4)

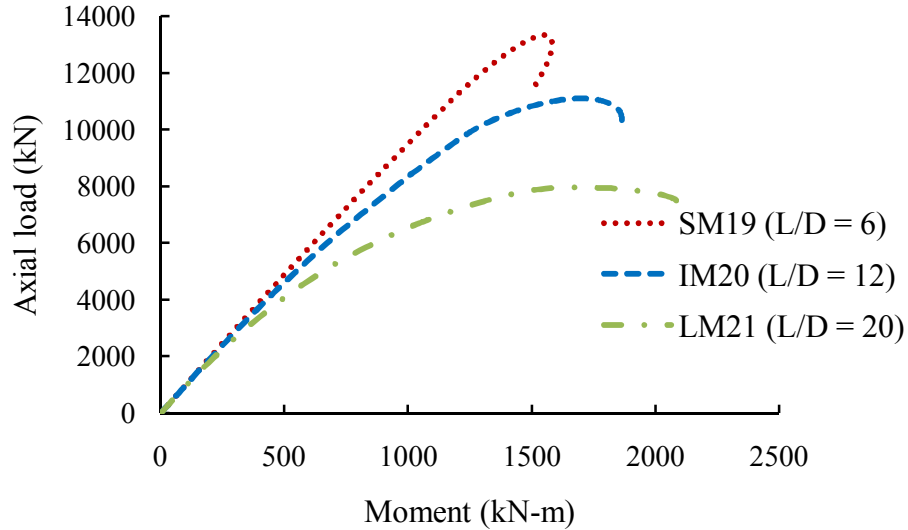
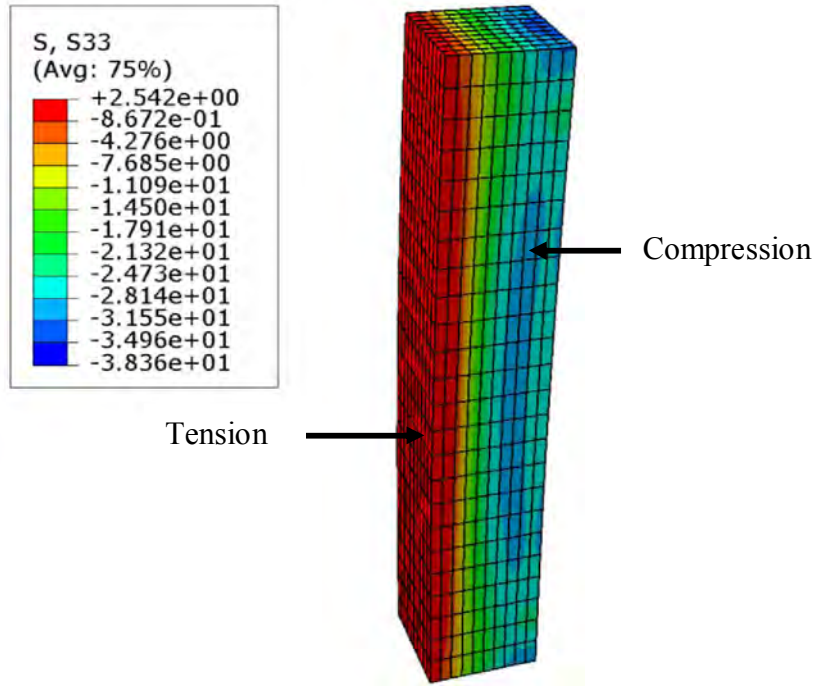


Figure 7.14 Effect of L/D ratio on axial load versus moment curve (Group 5)

#### 7.4.4.5 Modes of failure

The failure in the columns in Group 4 and 5 was attained by crushing of concrete followed by yielding of steel. The crushing of concrete occurred at the compression side of the columns. Figure 7.15 shows the deformed shape along with stress contour at failure for specimens SN16 ( $L/D = 6$ ), IN17 ( $L/D = 12$ ) and LN18 ( $L/D = 20$ ). The failures of the columns were attained mainly due to crushing of concrete at the compression side of the column. It was found that the compressive stress of concrete was comparatively higher at failure of the column with lower slenderness ratio (SN16) than that with higher slenderness ratios. The tensile stress of concrete increased with the increase of slenderness ratio. It was observed from the Figures that the tensile stress of concrete in column LN18 ( $L/D = 20$ ) is comparatively higher than other columns. The data obtained from FE analysis showed that the structural steel reached its yield stress and the flexural buckling failure mode was governed by the concrete elements at the maximum stressed fibers. Figure 7.16 shows the deformed shape of structural steel at failure for specimen IN17 ( $L/D = 12$ ) and LN18 ( $L/D = 20$ ). It was observed that the stress of structural steel decreased with the increase of slenderness ratio ( $L/D$ ).





(a) SN16 (L/D = 6)

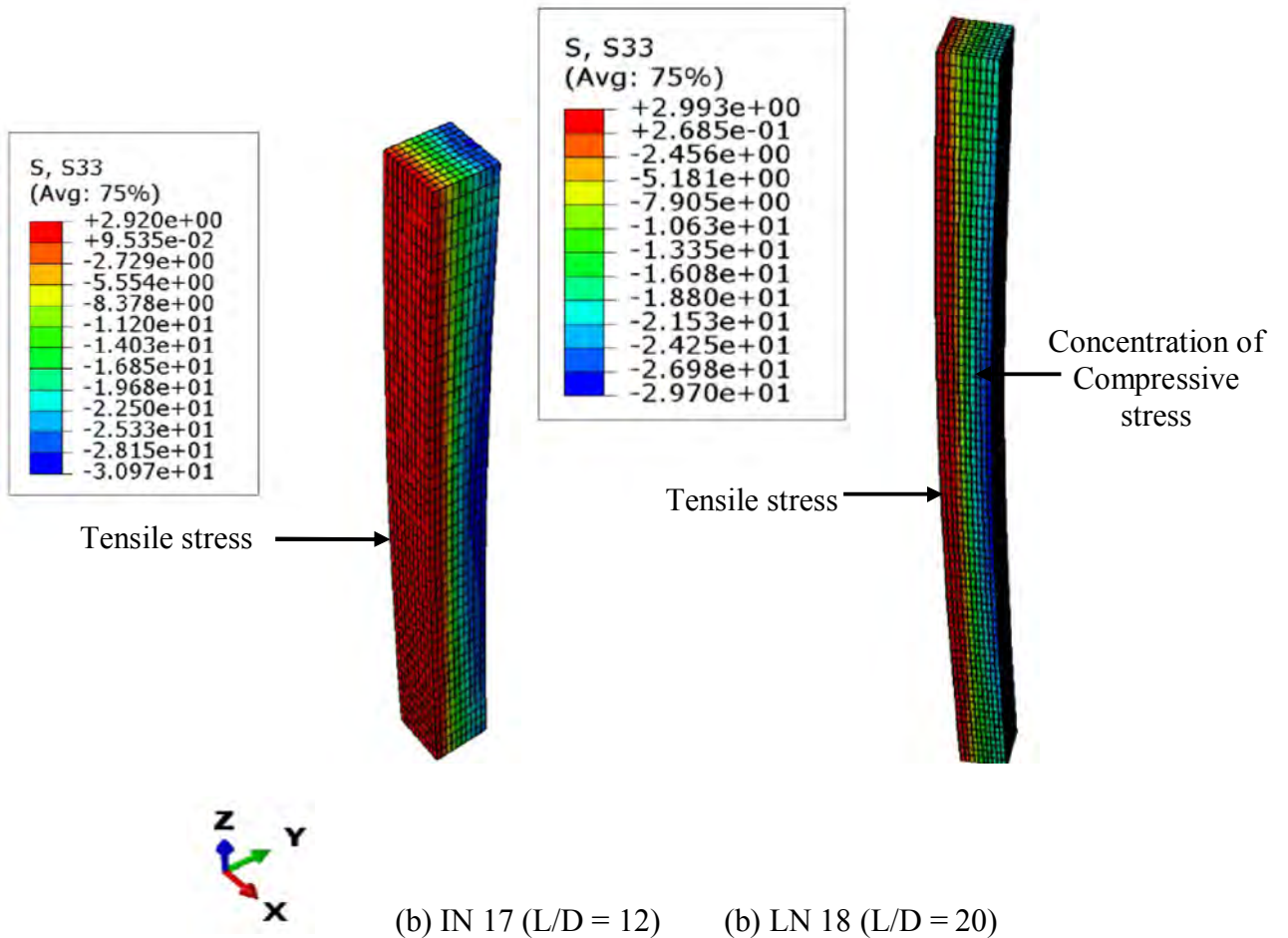


Figure 7.15 Deformed shape and stress contour of concrete at failure

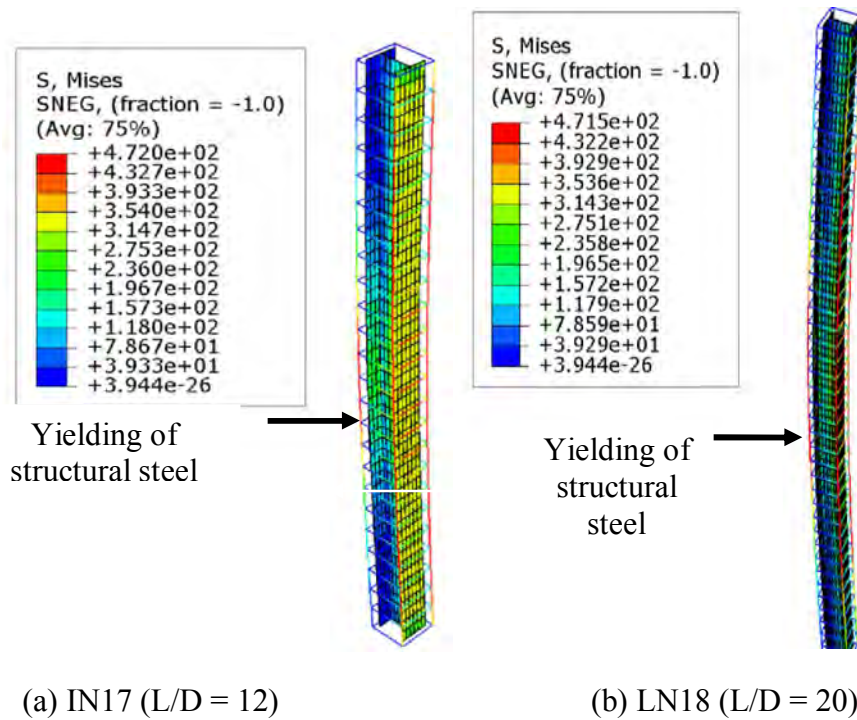


Figure 7.16 Deformed shape and stress contour in structural steel at failure

### 7.4.3 Effect of load eccentricity ratio

Six columns divided into two groups (Group 6 and Group 7) were considered to observe the effects of eccentricity ratio (as shown in Table 7.3). Columns in Group 6 (SN25, SN26 and SN27) were constructed with normal strength concrete (30 MPa) and had a slenderness ratio  $L/D = 6$ . On the other hand, columns in Group 7 (IN28, IN29 and IN30) were also constructed with normal strength concrete and a slenderness ratio of  $L/D = 12$ . The load was applied eccentrically about the major axis of the steel section of the columns. The eccentricity ratios ( $e/D$ ) were 0.1, 0.3 and 0.4, respectively for each Group of columns. All the columns were constructed with structural steel ratio of 10%.

#### 7.4.3.1 Load versus axial deformation response

Figures 7.17 and 7.18 show the effect of the load eccentricity ratio on the axial load versus average axial deformation curve for the two Groups of columns. From the Figures it was observed that increase in the load eccentricity ratio ( $e/D$ ) resulted in significant decrease in axial capacity and initial stiffness of the FEC column. It was observed from the Figures that the reduction in stiffness was more pronounced in columns with higher slenderness ratio ( $L/D = 12$ ). A flatter peak followed by gradual post-peak strength decline was observed with the increase of  $e/D$  ratios in the columns of Group 6 and Group 7. On the other hand, the columns in Group 6 experienced a comparatively steeper slope in the ascending region

than Group 7. This is due to the fact that column with higher slenderness ratio experiences larger axial deformation resulting in lower stiffness as compared to short columns.

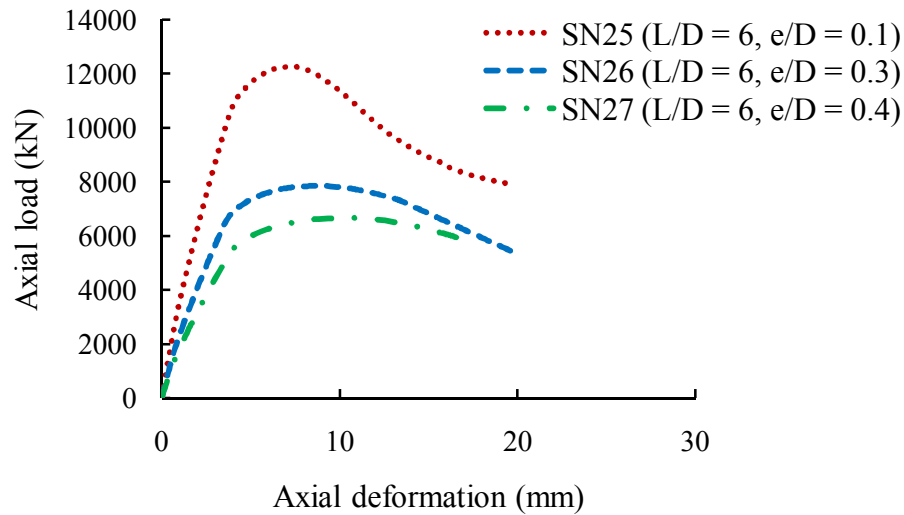


Figure 7.17 Effect of  $e/D$  ratio on load versus axial deformation curve (Group 6)

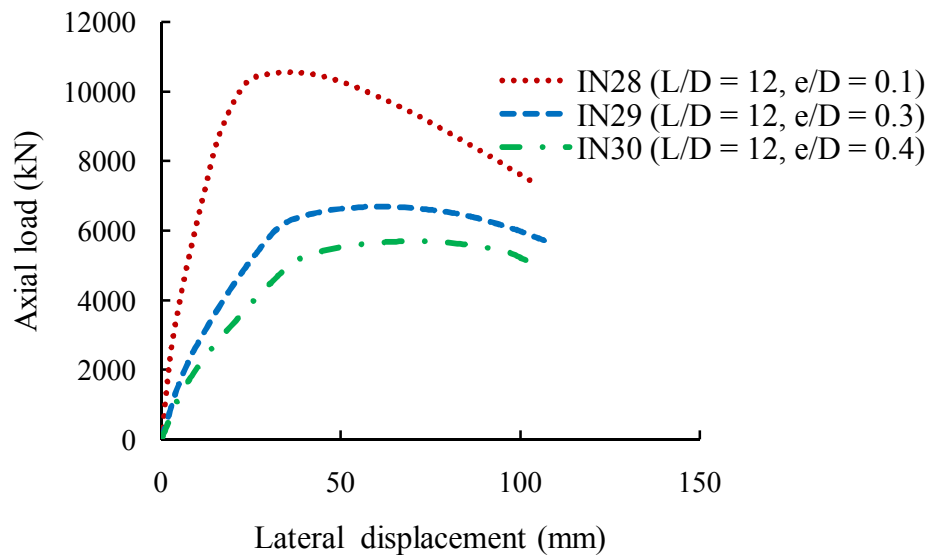


Figure 7.18 Effect of  $(e/D)$  ratio on axial load versus axial deformation curve (Group 7)

#### 7.4.3.2 Peak load and corresponding moment

Table 7.11 shows the influence of the eccentricity ratio on the axial load capacity and corresponding moment of the FEC columns. For columns in Group 6, the peak axial loads corresponding to  $e/D = 0.1$  were reduced by 36% and 46% when  $e/d$  ratios were increased to 0.30 and 0.40, respectively. Similarly, for the columns of Group 7, the capacity was decreased, by 37% and 47% for  $e/D = 0.30$  and 0.40, respectively. For columns in Group 6, the moment corresponding to  $e/D = 0.1$  were increased by 73% and 91% when  $e/D$  ratios

were increased to 0.30 and 0.40, respectively. Similarly, for the columns of Group 7, the moment was increased, by 54% and 58% for  $e/D = 0.30$  and  $0.40$ , respectively.

Table 7.11 Effect of eccentricity ratio on peak load and moment

Group	Column designation	Column properties				Magnitude of output parameters at peak load point				Percent difference	
		L/D	e/D	s/D	$f_{cu}$ (MPa)	$P_u$ (kN)	$M_u$ (kN-m)	$\epsilon_u$ ( $\mu\epsilon$ )	$U_{1u}$ (mm)	$P_u$ (%)	$M_u$ (%)
Group 6	SN25	6	0.1	0.5	30	12260	776	2481	13	-	-
	SN26	6	0.3	0.5	30	7846	1337	3330	21	-36	73
	SN27	6	0.4	0.5	30	6652	1476	3394	24	-46	91
Group 7	IM28	12	0.1	0.5	30	10560	903	1992	35	-	-
	IM29	12	0.3	0.5	30	6683	1387	2054	54	-37	54
	IM30	12	0.4	0.5	30	5591	1420	2109	55	-47	58

It is to be highlighted here that the column SN3 was constructed with similar properties of Group 6. This column (SN3) was analysed for concentrically loaded condition and the obtained axial capacity was 16989 kN (Table 7.6). The load carrying capacities of all the columns in Group 6 were less than the column SN3. The capacity was reduced by 27%, 54% and 61% for columns SN25 ( $e/D = 0.1$ ), SN26 ( $e/D = 0.3$ ) and SN27 ( $e/D = 0.4$ ), respectively than column SN3 ( $e/D = 0$ ).

#### 7.4.3.3 Load versus lateral displacement responses

The effects of eccentricity ratio ( $e/D$ ) on the load versus lateral displacement response were presented in Figures 7.19 and 7.20 for the columns of Group 6 and Group 7. In these two groups, the lateral displacement at a particular load increases with an increase in the  $e/D$  ratio, as expected. The increase of lateral displacement was more pronounced in case of intermediate (Figure 7.20) than short columns (Figure 7.19). It was due to the lower flexural stiffness of the intermediate columns (Figure 7.20). These Figures also showed that the peak region of the curve becomes relatively flat with a gradual drop in axial load capacity in the descending branch as the  $e/D$  ratio increases.

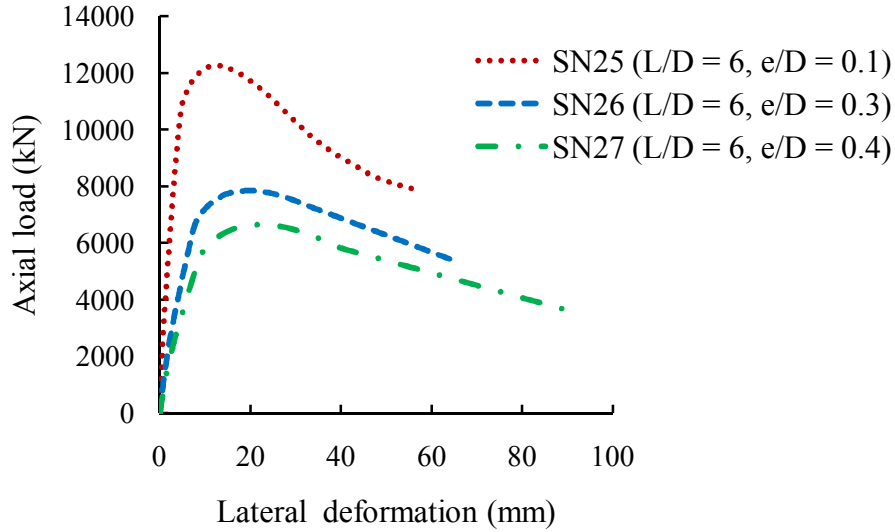


Figure 7.19 Effect of ( $e/D$ ) ratio on axial load versus lateral displacement curve (Group 6)

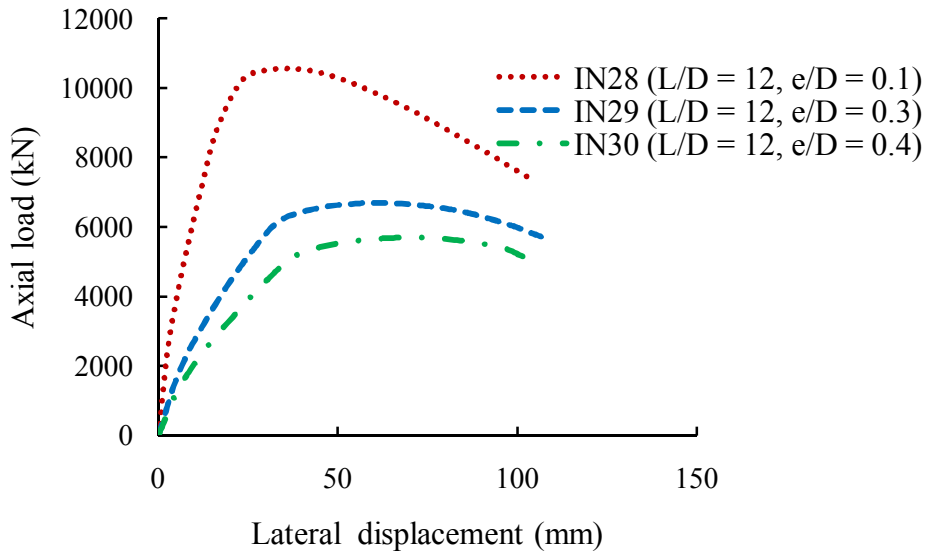


Figure 7.20 Effect of ( $e/D$ ) ratio on axial load versus lateral displacement curve (Group 7)

#### 7.4.3.4 Axial load versus moment

Figures 7.21 and 7.22 show the axial load versus moment curves for short and intermediate columns in each Group. The load versus moment curve for the short columns expressed essentially linear behaviour. However, as the  $e/D$  ratio is increased, the curve showed nonlinear behaviour. It was the effect of second order displacement. The effects of eccentricity ratio on the load versus moment curves were similar for the columns in both groups (Groups 6 and 7).

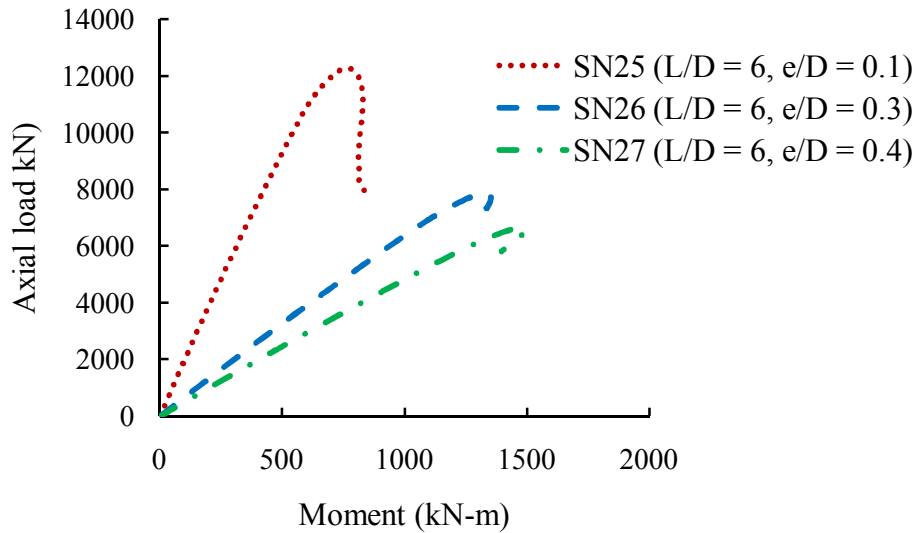


Figure 7.21 Effect of  $e/D$  ratio on axial load versus moment curve (Group 6)

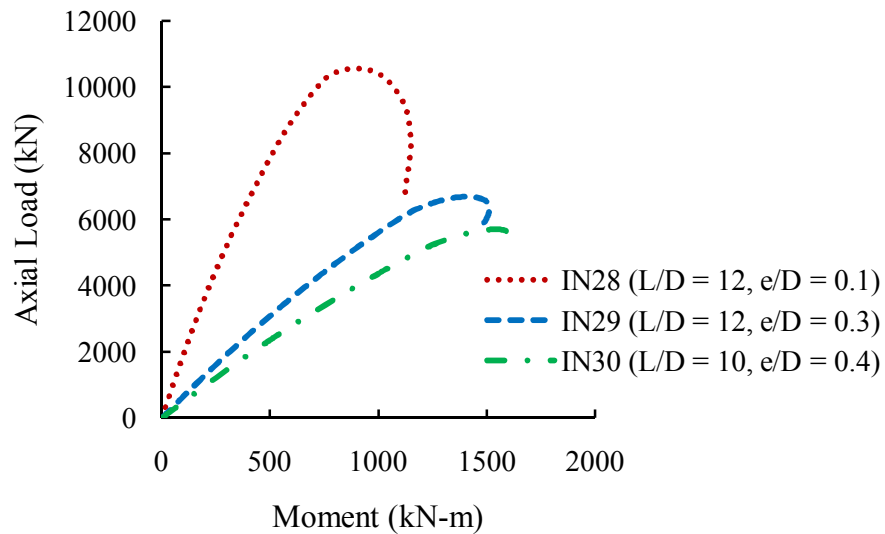


Figure 7.22 Effect of  $e/D$  ratio on axial load versus moment curve (Group 7)

#### 7.4.4 Effect of concrete compressive strength

Six columns divided into two groups (Group 8 and Group 9) were considered to observe the effect of concrete compressive strength as shown in Table 7.4. Within each group the strength of concrete was varied from 30 MPa, 60 MPa and 120 MPa. The eccentricity ratio ( $e/D$ ) of all the columns in Group 8 and Group 9 were 0.1 and 0.3, respectively. The load was applied eccentrically about major axis of the columns. The slenderness ratios ( $L/D$ ) for all columns in Group 8 and 9 were 6. The structural steel ratio used for the FEC columns was 10%.

#### 7.4.4.1 Load versus average axial deformation

Figures 7.23 and 7.24 represent the axial load versus deformation curves of the columns in Group 8 and Group 9. It was observed from these Figures that the ultimate axial load and stiffness of the short FEC column is greatly affected by the strength of concrete. The axial load versus axial deformation responses of FEC columns with higher strength concrete show steeper slopes at the ascending portions of the curves due to the higher modulus of elasticity. Columns (SH33 and SH36) constructed with 120 MPa concrete also demonstrate sharp post-peak strength declines as compared to other columns. However, the columns constructed with higher strength concrete showed brittle failure manner as compared to column with medium and lower strength of concrete.

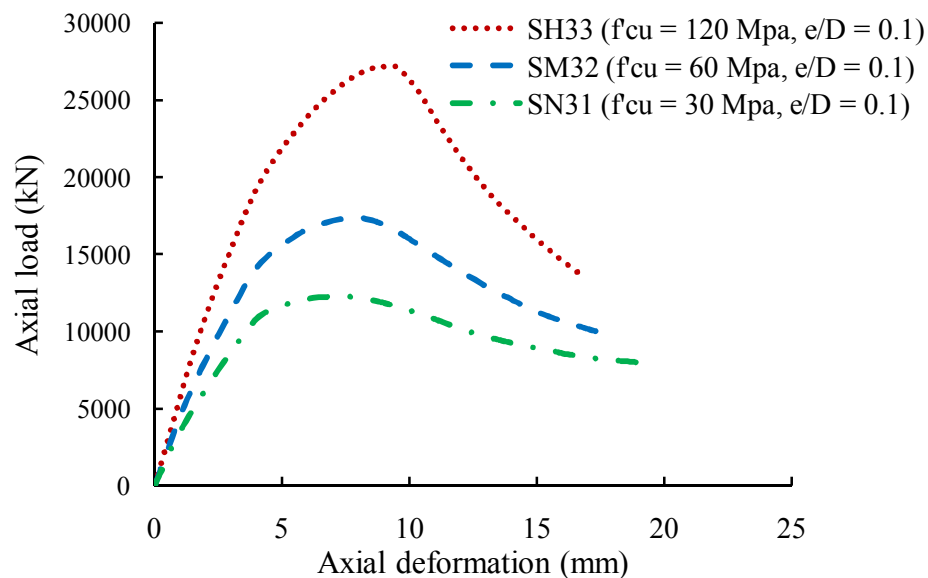


Figure 7.23 Effect of concrete compressive strength on axial load vs deformation curve (Group 8)

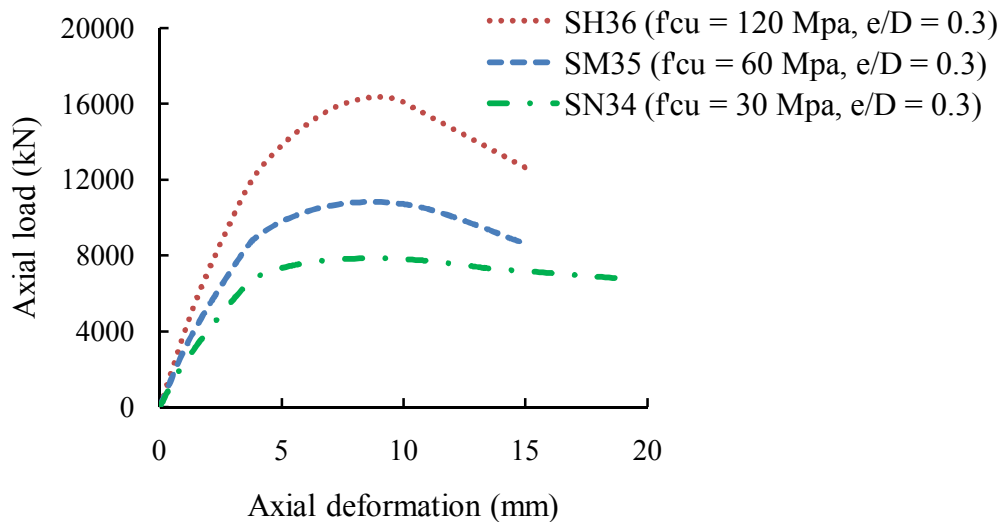


Figure 7.24 Effect of concrete compressive strength on axial load vs deformation curve (Group 9)

#### 7.4.4.2 Peak load and corresponding moment

The effects of normal (30 MPa), medium (60 MPa) and high (120 MPa) strength concrete in the ultimate capacity of FEC columns are shown in Table 7.12. The capacity increment from low to medium and medium to high strength of concrete columns were calculated. The columns of Group 8 and Group 9 were simulated with  $e/D$  ratios of 0.1 and 0.3, respectively. The ultimate axial load capacity of column SM32 was increased by 42% with respect to column SN31 when the concrete strength was increased from 30 MPa to 60 MPa. On the other hand, the ultimate load capacity of column SH33 increased by 56% when the concrete strength was increased from 60 MPa to 120 MPa. Similarly, the ultimate capacity of columns SM35 is increased by 38% with respect to column SN34 ( $f_{cu} = 60$  MPa). The ultimate load capacity of column SH36 is increased by 51% when concrete strength is increased from 60 MPa to 120 MPa. The effect of concrete compressive strength on the bending moment at the peak (ultimate) load point was also presented in Table 7.12. The bending moment was observed to be increased by 44% and 39% respectively for Group 8 and Group 9 with the increase of concrete strength from 30 MPa to 60 MPa. Again, increasing the concrete strength from 60 MPa to 120 MPa resulted in 61% increase in moment capacity for Group 8 and 53% increase in moment for Group 9 columns. The average increase in the peak axial load and corresponding moment for two Groups (with different  $e/D$  ratios) were 40% and 42%, respectively when the concrete strength is increased from 30 MPa to 60 MPa. Similarly, the average ultimate axial load capacity and moment of columns were increased by 54% and 57% respectively, when concrete strength was increased from 60 MPa to 120 MPa. However the ductility of the columns decreased significantly as the concrete strength increased Figures 7.23 and 7.24.

Table 7.12 Effect of concrete compressive strength on peak load moment

Group	Column designation	Column properties				Magnitude of output parameters at peak load point				Percent difference	
		L/D	e/D	s/D	$f_{cu}$ (MPa)	$P_u$ (kN)	$M_u$ (kN-m)	$\epsilon_u$ ( $\mu\epsilon$ )	$U_{1u}$ (mm)	$P_u$ (%)	$M_u$ (%)
Group 8	SN31	6	0.1	0.5	30	12260	772	2333	13	-	-
	SM32	6	0.1	0.5	60	17390	1113	2667	14	42	44
	SH33	6	0.1	0.5	120	27213	1796	3117	16	56	61
Group 9	SN34	6	0.3	0.5	30	7847	1334	2933	20	-	-
	SM35	6	0.3	0.5	60	10818	1850	3027	21	38	39
	SH36	6	0.3	0.5	120	16359	2830	3082	23	51	53



#### 7.4.4.3 Behaviour of FEC columns with UHSM

Strength of individual material plays a vital role on the overall capacity of FEC columns. To maximize the advantage of the concrete-encased steel columns, the majority of recent studies were focused on the use of high strength materials. Recently, high strength structural steel having yield stresses exceeding 800 MPa is developed and is becoming popular with 100 MPa concrete (Kim et al. 2012). Thus, in order to maximize the strength of concrete encased steel columns, the combination of high-strength steel and high strength concrete needs to be considered (Kim et al 2014). However, the use of high strength steel might cause difficulty in the design of the composite columns, since, the yield strain of the high strength steel is greater than the ultimate axial compressive strain of concrete (Figure 7.25). The steel section may not develop its full plastic strength at failure of the composite section because of the early crushing of the concrete. This degrades capacity ductility and economy of composite column with ultra-high strength materials (Kim et al. 2012). Limited research has been performed to address these effects of ultra-high strength materials on the behaviour of composite columns. For this reason code guidelines have imposed restrictions on material strength (i.e.  $f_y \leq 525$  MPa and  $f_{cu} \leq 70$  MPa as per AISC 2010).

In this research the behaviour of FEC columns with ultra-high strength material (UHSM) has been numerically studied using the developed FE model. The structural steel yield strength and concrete compressive strength were considered to be 913 MPa and 120 MPa, respectively. Ductility and failure behaviour of FEC columns were observed with various spacing of transverse reinforcement. The ultimate axial capacity of five (05) FEC columns were determined from the numerical analysis as presented in Table 7.13.

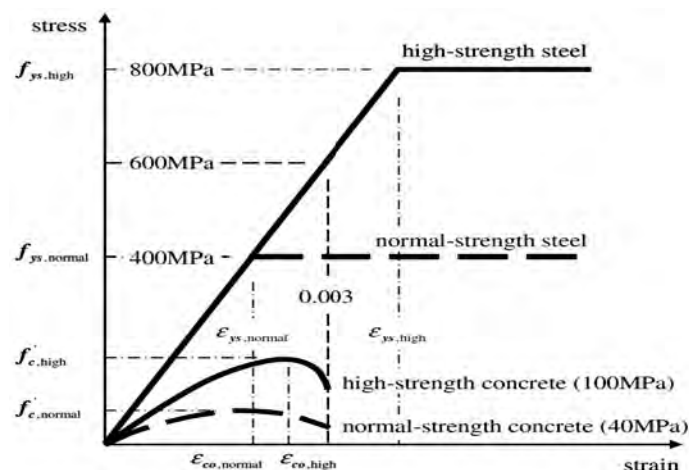


Figure 7.25 Stress-strain relationships of high-strength steel and concrete (Kim et al. 2012)

Five specimens short and square in section (500 mm × 500 mm), designated as SHH11, SHH12, SHH13, SHH14, and SHH15 were considered for this study. The structural steel percentages of these five FEC columns were 1%, 5%, 10%, 15% and 20%, respectively. The transverse reinforcement spacing of these columns were 250 mm. Table 7.13 represents the axial capacity of these columns constructed with UHSM. The numerically obtained capacities for these columns were compared with the theoretical squash load calculated using Equation 7.1. The increments of numerical loads in percent were determined with respect to the column with 1% structural steel, i.e. column SHH11. The load carrying capacity of the columns SHH12, SHH13, SHH14 and SHH15 were observed to be 30%, 66%, 103% and 134% higher than column SHH11. The percent of load increments of these FEC columns were higher than the columns constructed with normal strength concrete and structural steel (Table 7.6).

Table 7.13 Effect of UHSM on peak load of FEC columns

Group	Column designation	Columns properties				Axial capacity		$P_{u(num)}/P_{u(Theo)}$	Percent of increment	
		L/D	Structural steel ( $f_y$ )	$f_{cu}$ (MPa)	$A_s$ (%)	$P_{u(num)}$ (kN)	$P_{u(Theo)}$ (kN)		$P_{u(num)}$ (%)	$P_{u(Theo)}$ (%)
UHSM	SHH11	6	931	120	1	31439	29843	1.15	-	-
	SHH12	6	931	120	5	40847	38805	1.17	30	30
	SHH13	6	931	120	10	52384	48886	1.21	66	63
	SHH14	6	931	120	15	63967	59743	1.23	103	100
	SHH15	6	931	120	20	73683	70601	1.24	134	136

#### 7.4.5 Effect of transverse reinforcement spacing

The effect of transverse reinforcement spacing was studied on FEC columns constructed with normal and UHSM. It plays vital role on the ductility, confinement and early crushing of concrete. Seven FEC columns were numerically simulated to observe the effect of transverse reinforcement. Of the seven, six FEC columns (Table 7.5) included in two Groups (Group 10 and Group 11) were constructed with normal strength of structural steel and concrete. Group 10 (SN37, SN38 and SN39) and Group 11 (SM40, SM41 and SM42) were constructed with normal (30 MPa) and medium (60 MPa) strength concrete. Another, FEC column (SHH13) with UHSM was also considered in this study. All the columns were analysed for concentric axial load. The transverse reinforcement spacing ( $s/D$ ) used were 0.1, 0.2 and 0.4. The structural steel ratio used for the simulations of these FEC columns was 10%.

### 7.4.5.1 Load versus axial deformation

Figure 7.26 shows the axial load versus axial deformation for the columns in Group 10. The ascending branch of all the columns in this Group showed similar behaviour. On the other hand, the failure behaviour was influenced by the spacing of transverse reinforcement. It was observed from the Figure that the post-peak failures of the columns were influenced by the spacing of transverse reinforcement. Column SN37 showed flattened peak than column SN39. The columns SN37, SN38 and SN39 were simulated with transverse reinforcement spacing to depth ratio,  $s/D = 0.1$ ,  $s/D = 0.2$  and  $s/D = 0.4$ , respectively. The ductility index of the columns in Group 10 was increased with the decrease of transverse reinforcement spacing as shown in Table 7.14. The percent increase in ductility with respect to column SN39 were 11% and 22% respectively in column SN38 and SN37. Ductility index ( $\mu$ ) is the ratio calculated based on the maximum deformation at ultimate load ( $\delta_{po}$ ) and post peak deformation ( $\delta_{0.7po}$ ) corresponding to 70% of the ultimate load.

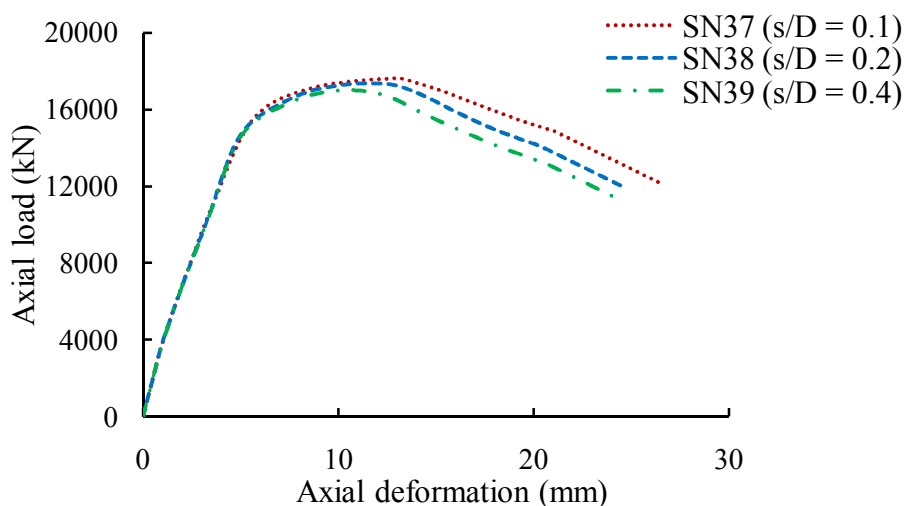


Figure 7.26 Effect of transverse reinforcement spacing on load-deformation response (Group 10)

Table 7.14 Ductility index of column Group 10

Specimen designation	Column properties				Axial load (kN)	Axial displacement		Ductility index $\frac{\delta_{0.7Po}}{\delta_{Po}}$
	L/D	s/D	$f_{cu}$	$A_s$		$\delta_{po}$	$\delta_{0.7po}$	
			(MPa)	(%)		(mm)	(mm)	
SN37	6	0.1	30	10	17661	12.87	27.83	2.2
SN38	6	0.2	30	10	17328	12.37	24.21	2
SN39	6	0.4	30	10	16988	12.25	22.1	1.8

#### 7.4.5.2 Peak load for different tie spacing

The effect of transverse reinforcement spacing on the ultimate capacity of FEC columns were studied and shown in Table 7.15. The increase in ultimate capacity was calculated in percent for the selected s/D ratios of 0.1, 0.2 and 0.3. The ultimate axial load capacity of columns SN38 (s/D = 0.2) and SN37 (s/D = 0.1) were increased by 2% and 4% compared to column SN39 (s/D = 0.4). Similarly, the ultimate axial load capacity of columns SM41 (s/D = 0.2) and SM40 (s/D = 0.1) were increased about 3% and 4% with respect to column SM42 (s/D = 0.4).

Table 7.15 Effect of transverse reinforcement spacing on peak load

Groups	Column designation	Column properties				Peak load	Percent difference
		L/D	A <sub>s</sub> (%)	s/D	f <sub>cu</sub> (MPa)	P <sub>u</sub> (kN)	P <sub>u</sub> (%)
Group 10	SN37	6	10	0.1 (50mm)	30	17661	4
	SN38	6	10	0.2(100mm)	30	17328	2
	SN39	6	10	0.4 (200mm)	30	16988	0
Group 11	SM40	6	10	0.1 (50mm)	60	25173	4
	SM41	6	10	0.2 (100mm)	60	24936	3
	SM42	6	10	0.4 (200mm)	60	24173	0

#### 7.4.5.3 Effect of tie spacing with UHSM

The higher strength steel and concrete is characterized by extraordinary mechanical and durability properties. It has a very brittle material behaviour. In the case of FEC columns, it is necessary to allow for relatively large ductility and avoid brittle failure. It was well established (Kim et al. 2012) that high ductility can be achieved in FEC columns by furnishing a large amount of lateral confinement steel. It was observed that properly detailed lateral transverse reinforcement can provide higher ductility, prevent premature buckling of main reinforcement and early crushing of concrete. In this study a comparison was carried out to simulate a column (SH13) with ultra-high strength structural steel and different transverse reinforcement spacing, as shown in Table 7.16. Initially, column SH13 was considered with ultra-high strength concrete (120 MPa) and normal strength structural steel (350 MPa) and tie spacing of 250 mm. Again, this column (SH13) was simulated with ultra-high strength concrete (120 MPa) and ultra-high strength structural steel (913 MPa), and designated as column SHH13. The column SHH13 was simulated for tie spacing of 250 mm and 125 mm. Figure 7.27 presents the axial load versus deformation curves for column SH13 and SHH13 (s = 125 mm and s = 250 mm). It was observed from Figure 7.27 that the

column SHH13 failed in a brittle manner when considered with a larger tie spacing (250 mm). On the other hand, this column showed ductile behaviour at failure (i.e. a flatter peak followed by gradual post peak decline) considering tie spacing of 125 mm. Sudden crushing of concrete at failure was prevented in the columns with closely spaced lateral ties due to the confinement effect. This will result in improved ductility of the columns with ultra high strength materials. The increase in ductility in columns SHH13 was about 41% when the tie spacing is reduced from 250 mm to 125 mm (Table 7.16). However, the ultimate axial load capacity of FEC column was not affected significantly by the confinement effect of reduced tie spacing. From Table 7.16, it is clear that use of ultra-high strength structural steel resulted in 40% increase in strength in FEC column (SHH13,  $s = 250$  mm) as compared to FEC column (SH13,  $s = 250$  mm) while sacrificing the ductility by 17%. However, the ductility was regained when the tie spacing in column SHH13 was reduced by 50% (i.e.  $s = 125$  mm).

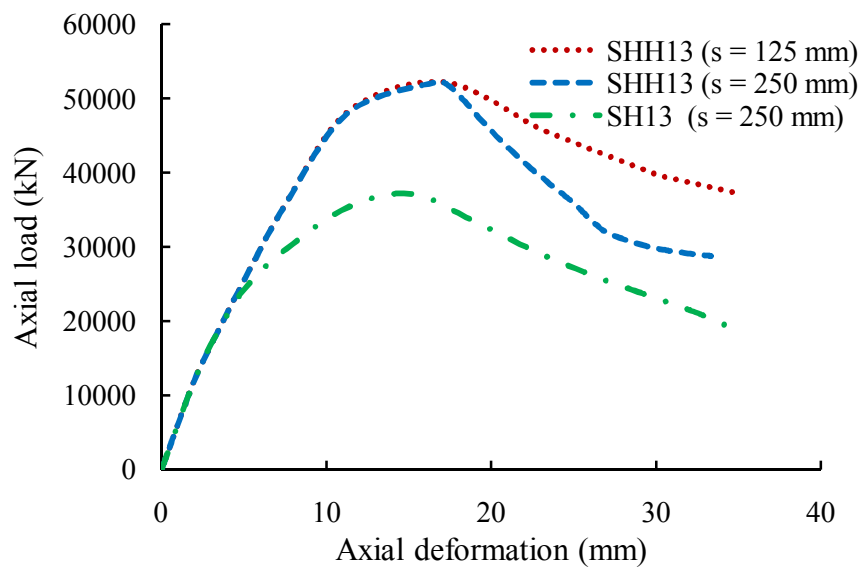


Figure 7.27 Effect of transverse reinforcement spacing on load-deformation response curve

Table 7.16 Ductility index of column with normal and high strength of materials

Column designation	Structural steel $F_y$ (MPa)	Concrete $f_{cu}$ (MPa)	Column properties			Peak load $P_u$ (kN)	Axial displacement		Ductility index $\frac{\delta_{0.7po}}{\delta_{po}}$
			$A_s$ (%)	s/D	L/D		$\delta_{po}$	$\delta_{0.7po}$	
SH13	350	120	10	0.5 (250 mm)	6	37180	15.07	26.32	1.75
SHH13	913	120	10	0.5 (250 mm)	6	52384	16.94	24.64	1.45
SHH13	913	120	10	0.25 (125 mm)	6	53187	17.12	34.99	2.05

## 7.5 Conclusions

A detailed parametric analysis was performed to study the behaviour of FEC columns subjected to concentric and eccentric axial loads. The geometric and material properties were varied and their influences were observed with respect to the peak axial load and corresponding moment, failure mode and overall column load-deformation responses. The important findings of the study are presented below:

- (a) The structural steel ratio has significant effect on the strength and failure behaviour of FEC columns. The axial capacity of FEC columns constructed with 30 MPa, 60 MPa and 120 MPa concrete has increased by 96%, 54% and 22% respectively, when the structural steel ratio is increased from 1% to 10%. The percent of load increase was higher with the increment of structural steel ratio for normal strength concrete (30 MPa) and structural steel strength 350 MPa. On the contrary, it was comparatively less for columns with higher strength concrete (120 MPa) and structural steel strength 350 MPa.
- (b) The residual strength after failure and ductility of the columns were also observed to increase significantly with the increase in the structural steel ratio.
- (c) The rate of load increment was comparatively higher when the columns were constructed from 5% to 10% structural steel.
- (d) The axial load capacity of short FEC columns with normal strength concrete (30 MPa) was observed to be reduced by 18% and 37%, when the L/D ratio was increased from 6 to 12 and 20, respectively. Similarly, the axial load capacity of short FEC column with medium strength concrete (60 MPa) was reduced by 19% and 40%, when the L/D ratio was increased from 6 to 12 and 20, respectively.
- (e) The short FEC columns shows steep slope and linear behaviour in the pre-peak region of the load versus lateral displacement response curve. On the other hand, as the slenderness ratio (L/D) increase, the region of the curve gets nonlinear with reduced initial slope.
- (f) The axial load carrying capacity of FEC column reduces significantly when the position of the load changes from concentric to eccentric. The load carrying capacity of a column (SN3) was observed to reduce by 27%, 54% and 61% when the e/D ratios were increased from e/D = 0 to 0.1, 0.3 and 0.4, respectively.
- (g) The average ultimate axial load capacity and moment of columns was observed to be increased by 40% and 42% respectively, when concrete strength increased from 30 MPa

to 60 MPa. Similarly, the average ultimate axial load capacity and moment of columns were increased by 54% and 57% respectively, when concrete strength increased from 60 MPa to 120 MPa. However, the ductility of FEC column was reduced as the concrete strength is increased.

- (h) The axial capacity of the FEC column remains nearly unaffected by the spacing of the transverse reinforcement. However, the loads versus axial deformation curves demonstrate a more ductile response for closes spacing of the transverse rebars. The ductility of the column increased by 22% when the transverse rebar spacing is reduced by 50%.
- (i) FEC columns made with ultra-high strength concrete of 120 MPa and ultra high strength steel with yield strength of 913 MPa has shown ultra high axial capacities compared to columns with normal strength concrete (30 MPa) and normal strength structural steel (350 MPa). Use of ultra high strength structural steel in FEC column, increased overall capacity by 40% accompanied by a reduction in the ductility by 17%. However the ductility may be regained if the tie spacing is reduced by 50% i.e. tie spacing halved.

## CHAPTER 8

### COMPARISONS OF FEC COLUMN STRENGTH WITH DESIGN CODES

#### 8.1 Introduction

The formulation of design equations for composite column started from early twentieth century. American Concrete Institute (ACI), American Institute for Steel Construction (AISC) and Euro code 4 are being widely used around the world for the design of composite structure. The ACI-318 treated the design of concrete encased composite columns through the extension of the design provisions for ordinary reinforced concrete columns. On the other hand, the AISC-LRFD approach treated the design of concrete-encased composite columns by extending the provisions recommended for bare steel columns. In AISC code, the design of an encased composite column proceeded by transforming the reinforced concrete portion into an equivalent contribution of structural steel shape. On the contrary, in European standard (Euro Code 4) the full interaction between the steel and concrete sections are considered until the failure occurs.

In this chapter a comparison is carried out between the experimental, numerical and the above mentioned (three) codes with respect to the strength of FEC columns. This comparative study compares the safety factors of the different codes (ACI-318, AISC-LRFD and Euro code 4) and the applicability of the equations given by codes for ultra-high strength materials (UHSM). The code specified design equations for composite columns have some restrictions regarding the material strength. These equations are applicable for concrete strength not greater than 70 MPa and structural steel strength up to 525 MPa. The applicability of these equations for FEC columns constructed with ultra-high strength concrete (strength greater than 100 MPa) and ultra-high strength structural steel (strength greater than 525 MPa) is also investigated and relevant difference highlighted. Forty nine (49) FEC columns were selected from current and published literature for this comparative study with different strength of materials for concentric and eccentric axial loads.

#### 8.2 Ultimate Axial Capacity for Concentrically Loaded Columns

Ultimate capacity of forty one (41) concentrically loaded FEC columns (current study and published literatures) were determined and compared with the un-factored strength predicted by the ACI 318 (2014), AISC-LRFD (2010) and Euro Code 4 (2005). Out of forty one, five FEC columns were considered with UHSM (concrete strength 120 MPa and structural steel strength 913 MPa). Another five columns were constructed with high strength concrete



120 MPa and normal strength of structural steel ( $F_y = 350$  MPa). Rest of the columns were constructed with concrete and steel having strength within the code specified limits. The code specified equations used for predicting the strength of the FEC columns are given in Chapter 3. Ratio of code predicted capacities with respect to experimental or numerical results are given in Tables 8.1 through 8.9. In these tables,  $P_{exp}$  represents the ultimate column capacity obtained from the test results done in current study and published literatures. Numerical capacities of these columns are also determined in this current study and represented as  $P_{num}$  in the Tables.  $P_{ACI}$ ,  $P_{AISC}$  and  $P_{EC}$  were the predicted nominal capacities using ACI-318 (2014), AISC LRFD (2010) and Euro code 4 (2005) guidelines, respectively.

### **8.2.1 Test specimens from current experimental study**

The ultimate capacity of the 11 (eleven) FEC columns from four different groups (SCN4A, SCN4B, SCH6A and SCH6B) were determined experimentally in the laboratory and numerically using FE models. These columns were constructed with structural steel strength 350 MPa and was subjected to concentric axial load. The experimental and numerical capacities of these columns are given in Chapter 4 and Chapter 6, respectively. The experimental and numerical capacities are compared with the unfactored strength predicted by the ACI 318 (2014), AISC-LRFD (2010) and Euro code 4 (2005) of these columns and shown in Table 8.1.

The mean values of ACI-318 (2014), AISC-LRFD (2010) and Euro code 4 (2005) with respect to experimental capacities are 0.756, 0.842 and 0.89, respectively. Similarly, the standard deviation of ACI-318, AISC-LRFD and Euro code 4 with respect to experimental were 0.025, 0.045 and 0.048, respectively. It revealed that all the predicted capacities based on the ACI-318 (2014) approach were conservative (by 25%) as compared to the test results. The predicted capacities based on the AISC-LRFD (2010) approach are found to be conservative by 16%. Similarly, the predicted capacities based on the Euro code 4 (2005) approach are found to be 11% conservative compared to the test results.

Table 8.1 Comparison between test results and predicted values using code guidelines

Specimen designation	Concrete $f_{cu}$ (Mpa)	Height (mm)	BxD (mm)	$P_{num}$ (kN)	$P_{exp}$ (kN)	$P_{ACI}$ (kN)	$P_{AISC}$ (kN)	$P_{EC}$ (kN)	$P_{num}/P_{exp}$	$P_{ACI}/P_{exp}$	$P_{AISC}/P_{exp}$	$P_{EC}/P_{exp}$
SCN4A1	28	900	100×100	471	493	369	402	428	0.955	0.748	0.815	0.868
SCN4A2	28	900	100×100	471	502	369	402	428	0.938	0.735	0.801	0.853
SCN4A3	28	900	100×100	471	478	369	402	428	0.985	0.772	0.841	0.895
SCN4B1	28	900	100×100	490	516	376	409	436	0.950	0.729	0.793	0.845
SCN4B2	28	900	100×100	490	503	376	409	436	0.974	0.748	0.813	0.867
SCN4B3	28	900	100×100	490	529	376	409	436	0.926	0.711	0.773	0.824
SCH6A1	42	900	150×150	1181	1117	878	1000	1067	1.057	0.786	0.895	0.955
SCH6A2	42	900	150×150	1181	1127	878	1000	1067	1.048	0.779	0.887	0.947
SCH6A3	42	900	150×150	1181	1107	878	1000	1067	1.067	0.793	0.903	0.964
SCH6B1	42	900	150×150	1238	1244	938	1079	1137	0.995	0.754	0.867	0.914
SCH6B2	42	900	150×150	1238	1240	938	1079	1065	0.998	0.756	0.870	0.859
<b>Mean</b>									<b>0.990</b>	<b>0.756</b>	<b>0.842</b>	<b>0.890</b>
<b>SD</b>									<b>0.048</b>	<b>0.025</b>	<b>0.045</b>	<b>0.048</b>
<b>COV (%)</b>									<b>4.8</b>	<b>3.3</b>	<b>5.3</b>	<b>5.4</b>

### 8.2.2 Test specimens from published literature

The ultimate axial capacity of the ten (10) FEC columns from Chen and Yeh (1996) are compared with the unfactored design strength predicted by the ACI 318 (2014), AISC-LRFD (2010) and Euro code 4 (2005). Numerical capacities of these columns are also determined in this study as shown in Chapter 6. These columns are constructed with different shapes of structural steel and normal strength concrete.

Table 8.2 Comparison between test results and code predicted results

Specimen designation	Concrete $f_{cu}$ (Mpa)	Height (mm)	BxD (mm)	$P_{num}$ (kN)	$P_{exp}$ (kN)	$P_{ACI}$ (kN)	$P_{AISC}$ (kN)	$P_{EC}$ (kN)	$P_{num}/P_{exp}$	$P_{ACI}/P_{exp}$	$P_{AISC}/P_{exp}$	$P_{EC}/P_{exp}$
SRC1	29.5	1200	280×280	4113	4220	3258	3809	4072	0.975	0.7921	0.903	0.990
SRC2	28.1	1200	280×280	4033	4228	3185	3725	3983	0.954	0.7897	0.881	0.988
SRC3	29.8	1200	280×280	4225	4399	3273	3828	3983	0.960	0.7747	0.870	0.943
SRC4	29.8	1200	280×280	4642	4441	3586	4193	4451	1.045	0.7725	0.944	0.959
SRC5	29.8	1200	280×280	4645	4519	3586	4193	4451	1.028	0.772	0.928	0.958
SRC6	29.5	1200	280×280	4741	4527	3586	4175	4432	1.047	0.7564	0.922	0.935
SRC7	28.1	1200	280×280	3636	3788	2584	3005	3212	0.960	0.7107	0.793	0.883
SRC8	26.4	1200	280×280	3437	3683	2493	2900	3101	0.933	0.7253	0.787	0.902
SRC9	28.1	1200	280×280	3636	3630	2584	3005	3212	1.002	0.7107	0.828	0.883
SRC10	29.8	1200	280×280	3621	3893	2675	3111	3323	0.930	0.7387	0.799	0.918
<b>Mean</b>									<b>0.983</b>	<b>0.754</b>	<b>0.865</b>	<b>0.934</b>
<b>SD</b>									<b>0.042</b>	<b>0.031</b>	<b>0.059</b>	<b>0.039</b>
<b>COV (%)</b>									<b>4.2</b>	<b>4.1</b>	<b>6.8</b>	<b>4.1</b>

In Table 8.2 experimental results of Chen and Yeh (1996) are compared with the predicted capacities using ACI 318, AISC-LRFD and Euro code 4, approaches. The mean values of ACI 318, AISC-LRFD and Euro code 4 with respect to experimental capacity were 0.754, 0.865 and 0.934, respectively. Similarly, the standard deviation of ACI 318, AISC-LRFD

and Euro code 4 with respect to experimental results are 0.031, 0.059, and 0.039, respectively. The predicted capacities using these three approaches are found to be conservative by 25% (ACI 318), 13% (AISC 2010) and 7% (EC 4) as compared to the test results.

### 8.2.3 Specimens of parametric study

The ultimate axial capacity of the fifteen (15) FEC columns from parametric study are compared with the unfactored strength predicted by the ACI 318 (2014), AISC-LRFD (2010) and Euro code 4 (2005) as shown from Tables 8.3 to 8.5. These columns were constructed with normal (30 MPa), medium (60 MPa) and high strength (120 MPa) concrete. Numerical capacity of these columns were determined in current study shown in Chapter 7. The structural steel percentages of these columns were 1%, 5%, 10 %, 15 % and 20%. It was observed that the predicted capacities for normal strength concrete using these three approaches ACI 318, AISC-LRFD and Euro code 4 are 19%, 7% and 3% conservative as compared to the numerical results.

Table 8.3 Comparison between numerical results and code predicted results  
(Normal concrete and normal strength structural steel)

Specimen designation	Concrete $f_{cu}$ (Mpa)	Height (mm)	B×D (mm)	$P_{num}$ (kN)	$P_{ACI}$ (kN)	$P_{AISC}$ (kN)	$P_{EC}$ (kN)	$P_{ACI}/P_{num}$	$P_{AISC}/P_{num}$	$P_{EC}/P_{num}$
SN1	30	3000	500×500	8651	6683	7615	8159	0.773	0.880	0.943
SN2	30	3000	500×500	11675	9552	10985	11547	0.818	0.941	0.989
SN3	30	3000	500×500	16989	12779	14727	15306	0.752	0.867	0.901
SN4	30	3000	500×500	19194	16255	18692	19308	0.847	0.974	1.006
SN5	30	3000	500×500	22922	19730	22648	23670	0.861	0.988	1.033
<b>Mean</b>								<b>0.810</b>	<b>0.930</b>	<b>0.974</b>
<b>SD</b>								<b>0.047</b>	<b>0.054</b>	<b>0.052</b>
<b>COV (%)</b>								<b>5.8</b>	<b>5.8</b>	<b>5.3</b>

Comparisons of the numerical results obtained from current study on medium strength concrete (60 MPa) FEC columns with the predicted capacities using ACI 318, AISC-LRFD, Euro code 4 are shown in Table 8.4. These columns are constructed with medium strength concrete (60 MPa) and normal strength structural steel (350 MPa). It was observed that the predicted capacities using these three approaches ACI 318, AISC-LRFD and Euro code 4 were 24%, 13% and 9% conservative compared to the numerical results.

Table 8.4 Comparison between numerical results and code predicted results  
(Medium strength concrete and normal strength structural steel)

Specimen	Concrete	Height	BxD	$P_{num}$	$P_{ACI}$	$P_{AISC}$	$P_{EC}$	$P_{ACI}/$	$P_{AISC}/$	$P_{EC}/$
designation	$f_{cu}$ (Mpa)	(mm)	(mm)	(kN)	(kN)	(kN)	(kN)	$P_{num}$	$P_{num}$	$P_{num}$
SM6	60	3000	500x500	15923	12015	13524	14453	0.755	0.849	0.908
SM7	60	3000	500x500	18977	14658	16768	17828	0.772	0.884	0.939
SM8	60	3000	500x500	24453	17632	20268	20951	0.721	0.829	0.857
SM9	60	3000	500x500	26475	20834	23914	24603	0.787	0.903	0.929
SM10	60	3000	500x500	30183	24036	27551	28223	0.796	0.913	0.935
<b>Mean</b>								<b>0.766</b>	<b>0.876</b>	<b>0.914</b>
<b>SD</b>								<b>0.030</b>	<b>0.036</b>	<b>0.034</b>
<b>COV (%)</b>								<b>3.9</b>	<b>4</b>	<b>3.7</b>

Comparisons between the numerical results on high strength concrete with the predicted capacities using ACI 318, AISC-LRFD and Euro code 4 approaches are shown in Table 8.5. These columns are constructed with higher strength concrete (120 MPa) and normal strength structural steel (350 MPa). It was observed that the predicted capacities using these three codes ACI 318 (2014), AISC-LRFD (2010) and Euro code 4 (2005) are 27%, 17% and 14% conservative than the numerical results. It reveals that the equations given by the codes are safe for concrete strength up to 120 MPa and structural steel strength up to 525 MPa (this is the upper limit for steel yield stress in AISC 2010 code).

Table 8.5 Comparison between numerical results and code predicted results  
(High strength concrete and normal strength steel)

Specimen	Concrete	Height	BxD	$P_{num}$	$P_{ACI}$	$P_{AISC}$	$P_{EC}$	$P_{ACI}/$	$P_{AISC}/$	$P_{EC}/$
designation	$f_{cu}$ (Mpa)	(mm)	(mm)	(kN)	(kN)	(kN)	(kN)	$P_{num}$	$P_{num}$	$P_{num}$
SH11	120	3000	500x500	30435	22678	25057	26749	0.745	0.823	0.879
SH12	120	3000	500x500	33260	24870	28187	29254	0.748	0.847	0.880
SH13	120	3000	500x500	37180	27337	31258	32040	0.735	0.841	0.862
SH14	120	3000	500x500	40886	29993	34275	35017	0.734	0.838	0.856
SH15	120	3000	500x500	45152	32449	37282	37969	0.719	0.826	0.841
<b>Mean</b>								<b>0.736</b>	<b>0.835</b>	<b>0.864</b>
<b>SD</b>								<b>0.011</b>	<b>0.010</b>	<b>0.016</b>
<b>COV(%)</b>								<b>1.3</b>	<b>1.2</b>	<b>1.8</b>

#### 8.2.4. Specimens with UHSM

The ultimate axial capacity of five FEC columns simulated with ultra high strength materials were determined numerically. These columns were constructed with high strength concrete 120 MPa and high strength structural steel ( $F_y = 913$  MPa). These specimens were short and square in section (500 mm  $\times$  500 mm) and designated as SHH11, SHH12, SHH13, SHH14 and SHH15. The structural steel percentages of these five FEC columns were 1%, 5%, 10%,

15% and 20% respectively. The transverse reinforcement spacing in these columns were 250 mm. The numerical capacities for these columns were compared with the unfactored design strengths predicted by the ACI 318, AISC-LRFD and Euro code 4 as shown in Table 8.6. It was observed that the predicted capacities using these three code approaches ACI 318, AISC-LRFD and Euro code 4 (2005) are 25%, 16% and 14% conservative than the numerical results. Therefore, the code specified methodology for axial capacity prediction equation can safely be used for FEC columns constructed with ultra-high strength materials subjected to concrete axial load only.

Table 8.6 Comparison between numerical results and code predicted results  
(High strength structural steel and concrete)

Specimen designation	Materials strength		Height (mm)	B×D (mm)	P <sub>exp</sub> (kN)	P <sub>ACI</sub> (kN)	P <sub>AISC</sub> (kN)	P <sub>EC</sub> (kN)	P <sub>ACI</sub> /	P <sub>AISC</sub> /	P <sub>EC</sub> /
	concrete f <sub>cu</sub> (MPa)	steel f <sub>ys</sub> (MPa)							P <sub>num</sub>	P <sub>num</sub>	P <sub>num</sub>
SHH11	120	913	3000	500×500	31439	23875	26291	28087	0.759	0.836	0.893
SHH12	120	913	3000	500×500	40847	31044	35055	36078	0.760	0.858	0.883
SHH13	120	913	3000	500×500	52384	39109	44174	44886	0.747	0.843	0.857
SHH14	120	913	3000	500×500	63967	47795	53722	54231	0.747	0.840	0.848
SHH15	120	913	3000	500×500	73683	56481	63105	63134	0.767	0.856	0.857
<b>Mean</b>									<b>0.756</b>	<b>0.847</b>	<b>0.868</b>
<b>SD</b>									<b>0.01</b>	<b>0.01</b>	<b>0.02</b>
<b>COV (%)</b>									<b>1.3</b>	<b>1.1</b>	<b>2</b>

The results of comparison for forty one FEC columns are summarized in Table 8.7. From this table it is found that the ACI-to-numerical capacity ratio has a mean value of 0.762 with standard deviation of 0.052 and COV of 6.8%. Similarly, the AISC-to numerical capacity ratio has a mean value of 0.864 with standard deviation of 0.058 and COV of 6.7%. On the other hand, Euro code 4-to numerical capacity ratio has a mean value of 0.907 with standard deviation of 0.064 and COV of 7%. It was observed that the predicted capacities using these three approaches ACI 318 (2014), AISC-LRFD (2010) and Euro code 4 (2005) are 24%, 14% and 10% conservative compared to the numerical results for concentrically loaded columns.

This observation reveals that the Euro code 4 approach generally provides closer estimate in predicting the capacities of FEC columns subjected to axial compression only. This is due to the fact that Euro code 4 (2005) considers the full interaction between the steel and concrete sections until the failure occurs. It is seen that the strength predicted by ACI 318 is relatively, more conservative among the three specifications, since this code considers the

effect of accidental eccentricity in the capacity prediction equation. It is also clear from Table 8.7 that the equations given by the three codes can safely predict the capacity of FEC columns constructed with UHSM (concrete 120 MPa and structural steel 913 MPa) for concentric axial load. Therefore, for concentrically loaded FEC columns the material strength limits specified in these codes can be extended to cover the high and ultra-high strength materials.

Table 8.7 Statistical results for the 41 FEC columns listed in Tables (8.1–8.6) for concentric axial load

References columns	Numbers of tested specimens	$P_{ACI}/$ $P_{num}$	$P_{AISC}/$ $P_{num}$	$P_{EC}/$ $P_{num}$
Current Study (28 to 42 MPa)	11	0.763	0.85	0.899
Published literature (30 MPa)	10	0.754	0.866	0.934
Parametric study (30 MPa)	5	0.81	0.93	0.974
Parametric study (60 MPa)	5	0.766	0.876	0.914
Parametric study (120 MPa)	5	0.736	0.835	0.841
Parametric study (120 MPa and 913 MPa)	5	0.756	0.847	0.866
<b>Mean</b>		<b>0.762</b>	<b>0.864</b>	<b>0.907</b>
<b>SD</b>		<b>0.052</b>	<b>0.058</b>	<b>0.064</b>
<b>COV(%)</b>		<b>6.8</b>	<b>6.7</b>	<b>7</b>

### 8.3 Eccentrically Loaded FEC Columns

The numerical capacities of eccentrically loaded FEC columns were compared with the unfactored design strength predicted by the AISC-LRFD (2010) code only. The load versus moment (P-M interaction) curves for bending about major axis of the steel section were developed using the plastic stress distribution method in AISC-LRFD (2010). The applicability of this design code for eccentric axial load with various strength of constituent materials were evaluated. Eight FEC columns constructed with different strength of concrete and structural steel were considered for this comparative study. Three columns from Group 6 (SN25, SN26 and SN27 from parametric study) were constructed with normal strength of structural steel (350 MPa) and concrete (30 MPa). Another, two columns were SH33 and SH36 from Group 8 and Group 9, respectively. These two columns were constructed with normal strength of structural steel ( $F_y = 350$  MPa) and high strength concrete ( $f_{cu} = 120$  MPa). Three columns constructed with UHSM (structural steel of 913 MPa and concrete strength 120 MPa) were also included in this code comparison. These columns were designated as SHH13E1, SHH13E2 and SHH13E3. These eight eccentrically loaded FEC columns were simulated with different eccentricity ratios ( $e/D$ ). The specimens had a cross-section of 500 mm  $\times$  500 mm and a constant length of 3000 mm. All the columns were

constructed with 10% structural steel. Typical cross-section of the columns were shown in Figure 7.1 in Chapter 7.

### 8.3.1 Load versus moment (P-M) curves

The interaction diagram (P-M curve) for major axis bending was constructed based on the plastic stress distribution equations given by AISC-LRFD (2010) specification as presented in Chapter 3. The strength reduction factor and slenderness effect were not considered in the development of these curves. P-M curves were generated for normal strength of material (SN25, SN26 and SN27), high strength of concrete columns (SH33 and SH36) and for columns with UHSM (SHH13E1, SHH13E2 and SHH13E3). The ultimate load capacities of these columns were determined from numerical analysis. Flexural moment was determined considering the second-order effect of the columns using Equation 8.1. The maximum flexural moment occurred at the mid-height of the FEC columns.

$$M_m = P(e_x + \Delta_m) \quad (8.1)$$

Where,

$P$  is the peak load

$e_x$  is the eccentricity

$\Delta_m$  is the second order displacement at mid-height level.

Figure 8.1 presents the load versus moment (P–M) diagrams according to the AISC-LRFD (2010) guidelines and the numerical results for the columns SN25, SN26 and SN27. These three columns were constructed with normal strength concrete (30 MPa) and structural steel of 350 MPa yield strength. The numerical load versus bending moment curves were plotted for these three columns SN25, SN26 and SN27 with  $e/D$  ratios 0.1, 0.3 and 0.4, respectively. It was observed from Figure 8.1 that the numerical capacities of these FEC columns were higher than the code predicted capacities by 3% to 9% for different eccentricities.

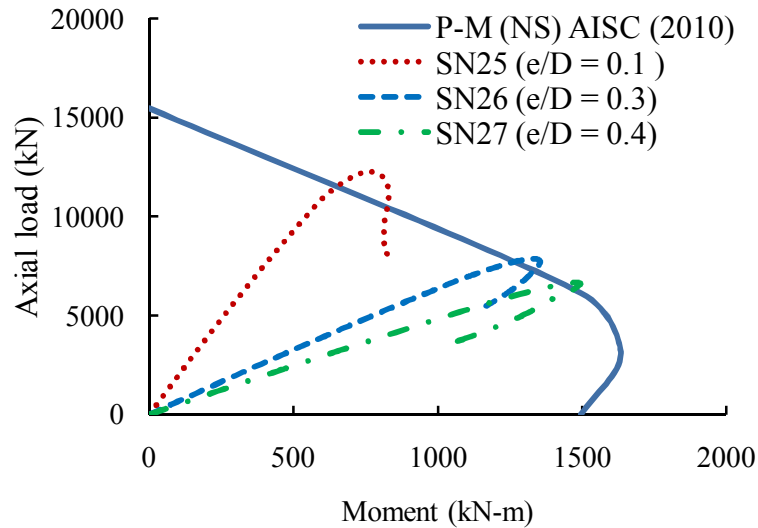


Figure 8.1 Load-moment curves for FEC columns with normal strength material

The numerical load versus moment (P-M) diagrams for the FEC column SH33 and SH36 along with the code (AISC-LRFD 2010) predicted failure envelope are presented in Figure 8.2. These two columns were constructed with higher strength concrete (120 MPa) and normal strength structural steel (350 MPa). Column SH33 had an initial load eccentricities ratio 0.1 where as column SH36 had an  $e/D$  ratio of 0.3. It was observed from Figure 8.2 that the numerical capacities of these FEC columns were higher (5% to 9%) than the code predicted capacities for different eccentricity ratios. It revealed that the equations given by AISC-LRFD (2010) can safely be used for high strength concrete up to 120 MPa and structural steel yield strength up to 500 MPa. The maximum limit for concrete strength as provided in AISC-LRFD (2010) can be extended up to 120 MPa from the existing value of 70 MPa. Numerical load and moment capacities of these columns were compared with the code predicted capacities as shown in Tables 8.8 and 8.9.



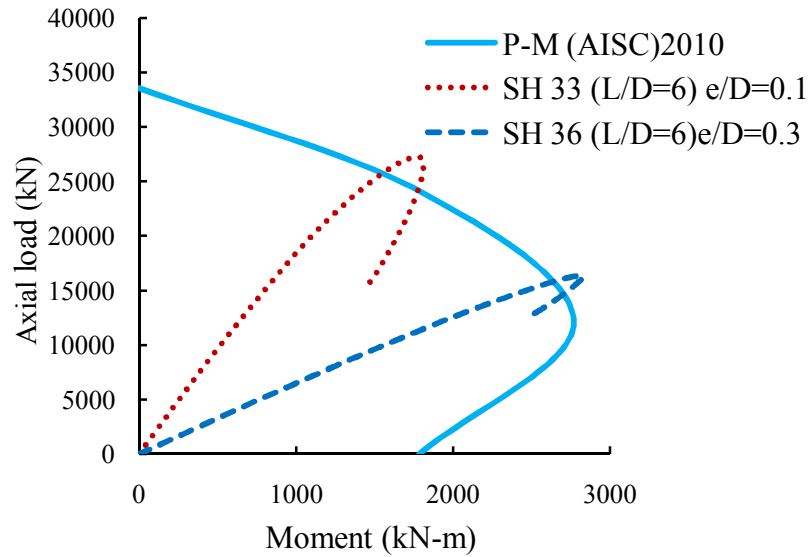


Figure 8.2 Load-moment curves for FEC columns with high strength concrete

The plastic stress distribution method in AISC-LRFD (2010) code for the prediction of the P-M diagram has material strength limitation. As specified in the code this method can be applied for composite columns constructed with concrete strength not exceeding 70 MPa and steel yield strength not greater than 525 MPa. To assess the applicability of this method for the prediction of the load and moment capacities for FEC columns with material strength exceeding the specified limits. Columns SHH13E1, SHH13E2 and SHH13E3 were analysed, for various  $e/D$  ratios. The load versus moment curves obtained numerically are compared with interaction diagram computed following AISC-LRFD guidelines, as shown in Figure 8.3.

For column SHH13E1 which had an initial load eccentricity of 10% the numerical load and moment capacities matched very well with the code predicted capacities. However, as the eccentricity ratio  $e/D$  increases the numerical capacities became lower (by 12%) as compared to the code predicted capacities (column SHH13E2 and SHH13E3). This is due to the fact that the P-M interaction diagrams plotted using AISC-LRFD (2010) method is based on plastic strength of structural steel. It is assumed that steel has reached its yield stress ( $F_y$ ) at the ultimate point. On the contrary, in FEC columns with ultra-high strength steel the load carrying capacity is limited by the early crushing of concrete before yielding of the structural steel section.

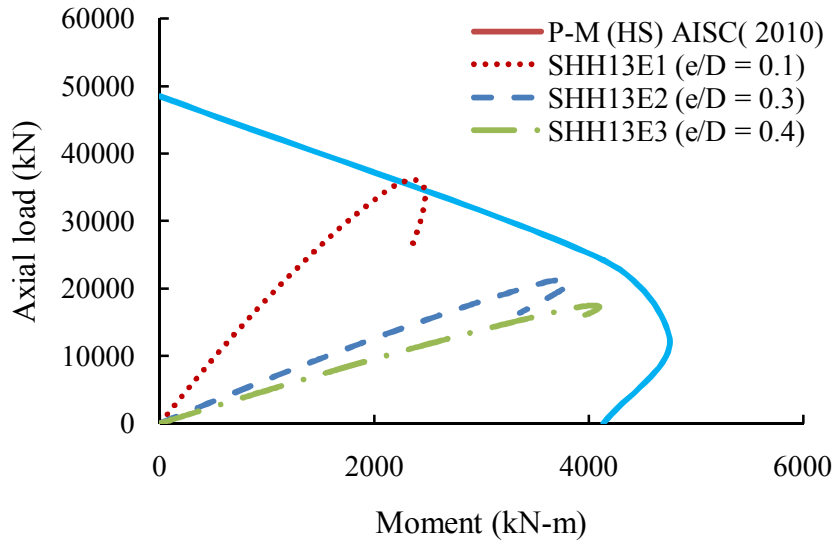


Figure 8.3 Load-moment curve for FEC columns with UHSM

### 8.3.2 Comparison between numerical and code predicted capacities

The numerical capacities of the FEC columns were compared with the code predicted capacities as shown in Tables 8.8 and 8.9. The numerical capacities were higher than the code predicted capacities when the columns were constructed with code specified values for material strength. On the other hand, the numerical capacities were lower than the code predicted capacities when the columns are constructed with UHSM and larger eccentricity. The safety factors decreased with the increase of eccentricity ratio irrespective of materials strength. It is obvious that the equations given by AISC-LRFD (2010) can be safely used for concrete strength up to 120 MPa and structural steel yield strength of 525 MPa. However, these equations need to be modified for the FEC columns constructed with UHSM ( $f_{cu} = 120$  MPa and  $F_y = 913$  MPa).

Table 8.8 Comparison between numerical and code predicted axial loads

Group based on material	Specimen designation	Eccentricity (e/D)	Structural steel		B × D (mm)	$P_{num}$ (kN)	$P_{AISC}$ (kN)	$P_{AISC}$ / $P_{num}$
			$F_y$ (MPa)	$f_{cu}$ (MPa)				
$F_y \leq 525$	NSC SN25	0.1	350	30	500×500	12260	11200	0.914
	SN26	0.3	350	30	500×500	7846	7500	0.956
	SN27	0.4	350	30	500×500	6653	6500	0.977
$F_y \leq 525$	HSC SH33	0.1	350	120	500×500	27214	25000	0.919
	SH36	0.3	350	120	500×500	16128	15300	0.949
$f_{cu} = 120$ MPa $F_y = 913$ MPa	UHSM SHH13E1	0.1	913	120	500×500	36026	35000	0.972
	SHH13E2	0.3	913	120	500×500	21279	24000	1.128
	SHH13E3	0.4	913	120	500×500	17485	19500	1.116

Table 8.9 Comparison between numerical and code predicted bending moments

Group based on material	Specimen designation	Eccentricity (e/D)	Structural steel		Concrete $f_{cu}$ (MPa)	$B \times D$ (mm)	$M_{num}$ (kN-m)	$M_{AISC}$ (kN-m)	$M_{AISC}/M_{num}$
			$F_y$ (MPa)						
NSC $F_y \leq 525$	SN25	0.1	350		30	500×500	776	706	0.91
	SN26	0.3	350		30	500×500	1337	1283	0.96
	SN27	0.4	350		30	500×500	1476	1456	0.986
HSC $F_y \leq 525$	SH33	0.1	350		120	500×500	1686	1650	0.979
	SH36	0.3	350		120	500×500	2713	2632	0.970
UHSM $f_{cu} = 120$ MPa $F_y = 913$ MPa	SHH13E1	0.1	913		120	500×500	2461	2400	0.975
	SHH13E2	0.3	913		120	500×500	3743	4200	1.122
	SHH13E3	0.4	913		120	500×500	4047	4578	1.131

#### 8.4 Conclusions

Experimental and numerical results of forty one FEC columns done by previous researchers and current study were considered for the evaluation of the accuracy of strength provisions in the ACI 318 (2014), AISC-LRFD (2010) specification and Euro code 4 (2005). It was observed that the overall predicted capacities using these three approaches ACI 318, AISC-LRFD and Euro code 4 were 24%, 14% and 10% conservative (safety margins) than the numerical and experimental results. The safety margins are observed to be increased with the increase of concrete strength. The equations given by the codes can be used safely for the FEC columns constructed with normal and high strength materials for concentric axial load. However, the brittle behaviour of columns with UHSM must be taken into consideration. To ensure sufficient ductility closely spaced transverse reinforcement must be used in FEC column.

The applicability of AISC-LRFD (2010) guidelines for eccentrically loaded columns or columns subjected to axial compression and bending has been also assessed for high strength materials. The simplified plastic stress distribution proposed in AISC-LRFD (2010) was found to be unsafe for predicting the load and moment capacities of eccentrically load FEC columns with ultra-high strength structural steel and concrete. AISC-LRFD (2010) using full plastic capacity of the structural steel section overestimated the theoretical results (P-M curve) when constructed with higher strength of the materials. Experimental and numerical capacity of the FEC columns could not reach the plastic capacity due to early crushing of ultra-high strength concrete. The current design provisions can be extended for predicting the load-carrying capacity of the composite columns constructed with ultra-high strength structural steel and ultra-high strength concrete for eccentric axial load.

## CHAPTER 9

### CONCLUSIONS AND RECOMMENDATIONS

#### 9.1 Summary

Extensive experimental and numerical investigations were conducted to study the behaviour and strength of fully encased composite (FEC) columns. The experimental program consisted of thirteen (13) FEC columns of two different sizes with various percentages of I-shaped structural steel and concrete strength. These FEC columns were square in size and constructed with normal (28 MPa) and high strength (42 MPa) concrete. The columns were tested for concentric and eccentric axial loads to observe the failure behaviour and the ultimate load carrying capacity of FEC columns. The ABAQUS/Standard, finite element code was used to construct the numerical model for FEC columns. To validate the model, simulations were conducted for both concentrically and eccentrically loaded FEC column. The finite element analysis was conducted on thirteen short FEC columns from current study and twenty two FEC column specimens from published literature. The finite element model was also used to predict the individual contributions of the steel and concrete to the total load carrying capacity of the composite column. A parametric study was conducted using the finite element model to investigate the influence of geometric and material properties of FEC columns subjected to concentric load and eccentric load with strong axis bending and with variable load eccentricities. The geometric variables were percentage of structural steel, column slenderness ( $L/D$ ) ratio, eccentricity ratio ( $e/D$ ) and spacing of ties ( $s/D$ ). The compressive strength of concrete and yield strength of structural steel section in FEC columns were considered as the material variables. The numerical model was also used to investigate the effects of ultra-high strength concrete (120 MPa) and high strength steel ( $F_y = 913$  MPa) on strength and ductility of FEC columns. Finally, the load capacities obtained from experimental and numerical studies were compared with the predicted values using the guidelines given by the ACI-318 (2014), AISC-LRFD (2010) and Euro code 4 (2005) for concentric and eccentric axial load with various strength of materials.

#### 9.2 Conclusions

Within the limited scope of the study, the following conclusions may be drawn. These conclusions are grouped under three sub-headings (Experimental and Numerical Study, Parametric study and comparison with code predicted capacities) are listed below.

### 9.2.1 Experimental and numerical study

- (i) Steel ratio, concrete strength and eccentricity of applied loading has noticeable influence on the axial capacity and failure behaviour of FEC columns. For 1% increase in the structural steel ratio the axial capacities increased by 7% and 10% for columns constructed with 28 MPa and 42 MPa concrete, respectively. Axial capacity of concentrically loaded ( $e/D = 0$ ) FEC column reduces significantly (by 62%) when subjected to eccentric load ( $e/D = 0.3$ ) producing bending about strong axis of the steel section.
- (ii) Failure occurred due to crushing of concrete near the middle region and compression side of the columns for concentric and eccentric axial load, respectively. Columns constructed with 42 MPa concrete showed brittle failure as compared to the columns constructed with 28 MPa concrete.
- (iii) The numerical model developed in this study was found to be capable of tracing a stable load-strain history with good accuracy for FEC columns with small and large cross-sections, constructed with normal and high strength concrete, and tested under concentric and eccentric loading conditions. Moreover, the model was able to simulate the experimental failure mode well.
- (iv) The numerical model can predict the peak load quite well with a mean value of  $P_{num}/P_{exp}$  of 0.99 for test specimens from current study and published literatures. It indicates a good performance of the finite element model in predicting the ultimate capacity of the test columns.
- (v) From the numerical simulations, the individual contributions of concrete and structural steel to the total load carrying capacity of the composite section were 57% and 28%, respectively.

### 9.2.2 Parametric study

- (ii) The structural steel ratio has significant effect on the strength and failure behaviour of FEC columns. The axial capacity of FEC columns constructed with 30 MPa, 60 MPa and 120 MPa concrete was increased by 96%, 54% and 22% respectively, when the structural steel ratio is increased from 1% to 10%. The benefits of using higher percentage of structural steel ratio diminishes as the concrete strength increases. The

residual strength after failure and ductility of the columns were also observed to increase significantly with the increase in the steel ratio.

- (iii) The axial capacity and stiffness of FEC columns were decreased with the increase in the slenderness ratio. As the slenderness ratio is increased from 6 to 20 the axial capacity of FEC columns were reduced by 37% for 30 MPa concrete and 40% for 60 MPa concrete. The higher strength concrete columns failed in a brittle manner as the slenderness ratio is increased.
- (iv) The peak axial load was affected significantly by the  $e/D$  ratio. The average reduction in the axial capacity was 36% and 46% for  $e/D$  ratios of 0.15 and 0.30, respectively, with respect to the capacity with  $e/D = 0.1$ . These results include the effects of various  $L/D$  ratios and are also applicable for normal strength (30 MPa) as well as medium strength (60 MPa) concrete FEC columns.
- (v) The ultimate axial capacity and corresponding moment of FEC columns were affected significantly by the strength of concrete. The average increase in the peak axial load and corresponding moment for FEC columns (with different  $e/D$  ratios) were 40% and 42%, respectively when the concrete strength is increased from 30 MPa to 60 MPa. Similarly, the average ultimate axial load capacity and moment of FEC columns were increased by 54% and 57% respectively, when concrete strength was increased from 60 MPa to 120 MPa. However, the columns constructed with higher strength concrete showed brittle failure behaviour as compared to FEC columns with normal strength concrete.
- (vi) The axial capacity of the FEC column was unaffected by the spacing of the transverse reinforcement. However, the load versus axial deformation curves demonstrated a more ductile response for lower values of the spacing of transverse rebars. The ductility of the column was increased by 22% when the transverse rebar spacing is reduced by 50%.
- (vii) FEC columns constructed with ultra-high strength concrete of 120 MPa and ultra-high strength structural steel of 913 MPa showed ultra-high axial capacities as compared to columns with normal strength concrete (30 MPa) and normal strength steel (350 MPa). Use of ultra-high strength structural steel in FEC column increased the overall capacity by 40% accompanied by a reduction in the ductility by 17%. However the ductility was regained when the tie spacing was reduced by 50%.

### **9.2.3 Review of code provisions**

- (i) The overall predicted capacities for FEC columns using the guidelines in ACI 318 (2014), AISC-LRFD (2010) and Euro code 4 (2005) were 24%, 14% and 10% conservative (safety margins) than the numerical results for FEC columns with normal to ultra-high strength materials (UHSM) subjected to concentric axial load only.
- (ii) The equations given by the three codes can safely predict the capacity of FEC columns constructed with UHSM (concrete 120 MPa and structural steel 913 MPa) for concentric axial load. Therefore, for concentrically loaded FEC columns the material limits specified in these codes may be extended to cover the ultra-high strength materials.
- (iii) The simplified plastic stress distribution proposed in AISC-LRFD (2010) was found to be unsafe for predicting the load and moment capacities of eccentrically loaded FEC columns with ultra-high strength structural steel and concrete. The current design provisions need to be extended to incorporate the effect of UHSM (ultra-high strength structural steel and ultra-high strength concrete) on FEC columns for eccentric axial load.

### **9.3 Recommendations for Future Research**

The following recommendations are made for future investigations.

- (i) Further experimental investigations on FEC columns with high and ultra-high strength materials are required to have complete understanding of the effects of these materials on strength and failure behaviour of these columns.
- (ii) The current numerical model was developed for monotonic loading conditions only. Effects of cyclic loadings may be addressed in future research work.
- (iii) The numerical model may be extended to incorporate the effects of geometric imperfections and residual stresses on the behaviour of FEC columns.
- (iv) The effects of the dynamic loading on the behaviour of composite columns with high strength materials may be investigated.
- (v) Further improvement to the finite model can be done by simulating the interface between steel and concrete using contact algorithms in ABAQUS.
- (vi) Further numerical investigations are required to study the effect of high strength materials on slender FEC columns.

- (vii) Future research work is required to propose modifications to the code provided guidelines for the construction of P-M diagram for composite columns with high and ultra-high strength materials.



## REFERENCES

- Almusallam, T.H., and Alsayed, S. H. (1995). "Stress-strain relationship of normal, high strength and light weight concrete." *Magazine of Concrete Research*, 47 (107), 39-44.
- American Concrete Institute. (2014). "Building code requirements for structural concrete (ACI 318-14) and commentary." *ACI 318-14*, Farmington Hills, MI.
- American Institute of Steel Construction. (2010). "Specification for structural steel buildings." *An American National Standard, ANSI/AISC 360-10*, Chicago.
- Amin, A. M. M., Fadel, A. M., Gaawan, S. M., and Darwish, R. A. (2016). "Assessment the limit of steel core area in the encased composite column." *Int. Journal of Engineering Research and Applications*, 6(1- 3), 72-78.
- Bangladesh National Building Code (1993). *BNBC*, Dhaka, Bangladesh.
- Barr, B., and Lee, M. K. (2003). "Modelling the strain-softening behaviour of plain concrete using a double-exponential model." *Magazine of Concrete Research*, 55 (4), 343-353.
- Begum, M., Driver, R. G. and Elwi, A. E. (2007). "Finite element modeling of partially encased composite columns using the dynamic explicit solution method" *Journal of Structural Engineering, ASCE*, 133(3), 326-334.
- Bridge, R. Q., and Roderick, J. W. (1978). "Behavior of built-up composite columns." *Journal of Structural Division, ASCE*, 104(7), 1141-1155.
- British Standard (BS.5400-5): Steel, Concrete and Composite Bridges (2002) Part 5, code of practice for design of composite Bridges.
- Burr, W.H. (1912). "Composite columns of concrete and steel." *Proc, The Institution of Civil Engineers* 188 (1912), 114-126.
- Carreira, D. J., and Chu, K. H. (1985). "Stress strain relationship for plain concrete in compression." *ACI Journal*, 82 (6), 796-804.
- Carreira, D. J., and Chu, K. H. (1985). "Stress-Strain relationship for reinforced concrete in tension." *ACI Journal*, 83 (3), 21-28.
- Chen, C. C., and Yeh, S.nC. (1996). "Ultimate strength of concrete encased steel composite columns." *Proc of the Third National Conference on Structural Engineering, China*, 2197–206.

- Chen, C. C., Weng, C.C., Lin, I. M., and Li, J. M. (1999). "Seismic behavior and strength of concrete encased steel stub columns and beam columns." Report no. MOIS 881012-1. *Architecture and Building Research Institute, China*.
- Chen, C. C., and Lin, N. J. (2006). "Analytical model for predicting axial capacity and behavior of concrete encased steel composite stub columns." *Journal of Constructional Steel Research*, 62, 424–433.
- Cristina, C., Alina, H. K., Pop, M., Nicolae, C., Gabriel, U., and Paul, P. (2014). "Behavior of fully encased steel-concrete composite columns subjected to monotonic and cyclic loading." *Journal of Applied Engineering Science*, 12 (280), 81-88.
- CSA (2009). "Design of steel structures." Published by Canadian Standards Association 5060 Spectrum Way, Suite 100, Mississauga, Ontario, Canada.
- Dundar, C., Tokgoz, S., Tanrikulu, A. K., and Baran, T. (2007). "Behaviour of reinforced and concrete-encased composite columns subjected to biaxial bending and axial load." *Building and Environment*, I (III) III-III.
- Eggemann, H. (2003). "Development of composite columns. Emperger's effort." *Proceedings of the First International Congress on Construction History*, Madrid, 20<sup>th</sup> -24<sup>th</sup> January.
- Ellobody, E., Young, B., and Lam, D. (2011). "Eccentrically loaded concrete encased steel composite columns." *Thin-walled structures*, 49, 53-65.
- Ellobody, E., and Young, B. (2011). "Numerical simulation of concrete encased steel composite columns." *Journal of Constructional Steel Research*, 67, 211–222.
- European Committee for Standardization (CEN). (2005). "Design of composite steel and concrete structures–Part 4-2: General rules and rules for bridges." *Euro code 4*, Brussels, Belgium.
- Furlong, R.W. (1976). "AISC Column design logic makes sense for composite columns too." *Engineering Journal, ASCE*, 13 (1), 1-7.
- Furlong, R.W. (1977). "Composite Columns - A Bridge between AISC and ACI Regulations." *International Colloquium on Stability of Structures under Static and Dynamic Loads*. Washington, D.C., May 17-19, National Science Foundation and ASCE 709-717.

- Furlong, R.W. (1978). "A recommendation composite column design rules consistent with specifications of the American Institute of Steel Construction." *Structural Stability Research Council*. Boston, Massachusetts.
- Gajanan, M., Sabnis. (1979). "Hand book of composite construction engineering." Van Nostr and Reinhold Company, New York, N.Y. 10020 (Ch.1).
- Gysel, V. A., and Taerwe, L. (1996). "Analytical formulation of the complete stress- strain curve for high strength concrete." *Materials and structures*, 29 (1996), 529-533.
- Hibbitt, Karlsson and Sorensen, Inc. (HKS) (2013). *ABAQUS/ Explicit User's Manual*, Version 6.13.
- Hsu, C. T. T. (1974). "Behavior of structural concrete subjected to biaxial flexure and axial compression," *PhD thesis*, Mc. Gill University, Montreal, Canada.
- Hsu, L. S. and Hsu, T. C. T. (1994). "Stress-strain behaviour of steel fiber high strength concrete under compression." *ACI Materials Journal*, 91(4), 448-457.
- Iu, C. K. (2015). "Nonlinear analysis for the pre-and post-yield behaviour of a composite structure with the refined plastic hinge approach." *Journal of Constructional Steel Research*, 119 (2015), 1–16
- Kim, C. S., Park, H. G., Chung, K. S., and Choi, I. R. (2012). "Eccentric axial load testing for concrete-encased steel columns using 800 MPa steel and 100 MPa concrete." *Journal of Structural Engineering, ASCE*, 138(8), 1019-1031.
- Kim, C. S., Park, H. G., Chung, K. S., and Choi, I. R. (2013). "Eccentric Axial Load capacity of high-strength steel-concrete composite columns of various sectional shapes." *Journal of Structural Engineering, ASCE*, 10.1061/(ASCE)ST. 1943-541X. 0000879, 04013091-12.
- Lubliner, J., Oliver, J., Oller, S., and Onate, E. (1989). "A plastic-damage model for concrete." *International Journal of solids and structures*, 25(3), 229-326.
- Lu, H. Z., and Zhao, Y. G. (2010). "Empirical stress-strain model for unconfined high-strength concrete under uniaxial compression." *Journal of Materials in Civil Engineering, ASCE*, 22(11), 1181-1186.
- Marzouk, H., and Chen, Z. (1995). "Fracture energy and tension properties of high-strength concrete." *Journal of Materials in Civil Engineering*, 7(2), 108-116.

- Matsui C. (1979). "Study on elasto-plastic behaviour of concrete-encased columns subjected to eccentric axial thrust." *Annual Assembly of Architectural Institute of Japan*, 1627–8.
- Mirza, S. A., and Skrabek, B. W. (1992). "Statistical analysis of slender composite beam–column strength." *Journal of Structural Engineering, ASCE*, 118(5), 1312–31.
- Mohammad, R. B., Grondin, G. Y. and Elwi, A. E. (2003). "Experimental and numerical investigation of steel plate shear wall," *Ph D dissertation*, University of Alberta, Department of Civil Engineering, Canada.
- Morino, S., Matsui C., and Watanabe H. (1984). "Strength of biaxially loaded SRC columns." *Proceedings of the US/Japan joint seminar on composite and mixed construction*. New York, NY, ASCE, 185–94.
- Mote, A. N., and Vijay, B. (2013). "Experimental and simulation of columns of steel section encased in reinforced concrete." *International Journal of Science and Engineering*, 1(2), 105-108.
- Munoz, P. R. (1994). "Behavior of biaxially loaded concrete-encased composite columns," *Ph D dissertation*, New Jersey Institute of Technology, Newark, N. J.
- Munoz, P.R., and Hsu, C. T. T. (1997). "Behavior of biaxial loaded concrete- encased composite columns." *Journal of Structural Engineering, ASCE*, 123 (9), 1163-1171.
- Ramm, E., (1981). "Strategies for Tracing the Nonlinear Response near Limit Points." *In: Nonlinear Finite Element Analysis in Structural Mechanics*. Springer, New York.
- Riks, E., (1979). "An incremental approach to the solution of snapping and buckling problems." *International Journal of Solids and Structures*, 15, 529-551.
- SSRC Task group 20. (1979). "A specification for the design of steel-concrete composite columns." *AISC Engineering Journal Fourth Quarter*.
- Samanta, A. K., and Paul A. (2013). "Evaluation of current design practices on estimation of axial capacity of concrete encased steel composite stub columns: A Review." *Journal of Civil Engineering and Architecture*, 7 (9), 1080-1091.
- Sfer, D., Carol, I., Gettu, R., and Etse, G. (2002). "Study on the behaviour of concrete under triaxial compression." *Journal of the Engineering and Mechanics, ASCE*, 128 (2), 156-162.
- Shanmugam, N. E., and Lakshmi, B. (2001). "State of art report on steel composite columns." *Journal of Constructional Steel Research*, 57(10), 1041-1080.

- Shih, T. H., Chen, C. C., Weng, C. C., Yin, S.Y. L., and Wang, J. C. (2013). "Axial strength and ductility of square composite columns with two interlocking spirals." *Journal of Constructional Steel Research*, 90 (2013), 184–192.
- Soliman, K. Z., Arafa, A. I., and Elrakib, T. M. (2013). "Review of design codes of concrete encased steel short columns under axial compression." *Journal House and Building National Research Center*, Cairo, Egypt, 19 (2013), 134-143.
- Tawil, S. E., and Deierlein, G. G. (1999). "Strength and ductility of concrete encased composite columns." *Journal of Structural Engineering, ASCE*, 125(9), 1009–1019.
- Taylor, R., Khalil, H. S., and Yee, K. M. (1983). "Some tests on a new type of composite column." *Proc., Inst. of Civil. Engrs., Part 2, Technical Note 355*, 283-296.
- Tokgoz, S., and Dundar, C., (2008). "Experimental tests on biaxial loaded concrete encased composite columns." *Journal on Steel and Composite Structure*, 8 (5), 423-438.
- Tsai, K. C., Lien, Y., and Chen, C. C. (1996). "Behavior of axially loaded steel reinforced concrete columns." *Journal of the Chinese Institute of Civil and Hydraulic Engineering*, 8(4), 535–545.
- Tsai, W. T. (1988). "Uniaxial compression stress-relation of concrete." *Journal of Structural Engineering, ASCE*, 114 (9), 2133-2136.
- Tsao, W. H., and Hsu, C. T. T. (1993). "A non-linear computer analysis of biaxially loaded L-shaped slender reinforced concrete columns." *Journal of Structural Engineering, ASCE*, 49 (4), 579-588.
- Virdi, K. S., and Dowling, P. J. (1973). "The ultimate strength of composite columns in biaxial bending." *Proceedings of the Institution of Civil Engineers*, Part 2, 251-272.
- Wang, G., and Hsu, C. T. T. (1992). "Complete biaxial load-deformation behavior of reinforced concrete columns." *Journal on Structural Engineering, ASCE*, 118(9), 2590-2609.
- Wang, P. T., Shah, S. P. and Naaman, A. E. (1978). "Stress-strain curves of normal and lightweight concrete in compression." *ACI Journal*, 75 (11), 603-611.
- Wee, T. H., Chin, M. S. and Mansur, M. A. (1996). "Stress-strain relationship of high strength concrete in compression." *Journal of Materials in Civil Engineering, ASCE*, 8(2), 70-76.

Weng, C. C., and Yen, S. I. (2002). "Comparison of concrete-encased composite column strength provisions of ACI code and AISC specification." *Journal on Engineering Structures*, 24, 59-72.

Yang, Z., and Chen, M. (2015). "Analysis on the impact behavior of super high strength concrete filled steel tube columns." *Metal Journal, Metallurgical Mining Industry, Fujian, China*, 12, 1-11.